TECTONIC SIGNIFICANCE OF THE ATNARKO COMPLEX, COAST MOUNTAINS, BRITISH COLUMBIA

by

STEVE A. ISRAEL

B.Sc. (*Hons*.), Memorial University of Newfoundland, 1998
M.Sc., The University of British Columbia, 2001

A THESIS SUBMITTED IN PARTIAL FULFILLMENT OF
THE REQUIREMENTS FOR THE DEGREE OF

DOCTOR OF PHILOSOPHY

in

THE FACULTY OF GRADUATE STUDIES
(Geological Sciences)

THE UNIVERSITY OF BRITISH COLUMBIA

(Vancouver)

May, 2008

ABSTRACT

The Atnarko complex located in west-central British Columbia comprises pre-Early Jurassic metavolcanic and metasedimentary rocks, termed the Atnarko assemblage, which is structurally interleaved with Late Triassic to Early Cretaceous orthogneiss. The Atnarko assemblage correlates with continental margin assemblages found within the Coast plutonic complex. Tectonic interaction between the Insular and Intermontane superterranes resulted in several phases of deformation including; 1) poorly preserved Jurassic deformation, 2) Early to mid-Cretaceous, southwest to west directed, compression, 3) mid-Cretaceous, north to northeast directed, compression, 4) mid- to Late Cretaceous dextral and sinistral ductile/brittle shearing, and 5) post latest Cretaceous brittle faulting. Peak metamorphism coincides with generation of migmatite in the Early Cretaceous (~117-115 Ma) and is contemporaneous with penetrative ductile fabrics. The Atnarko complex had cooled below 350^{o}C by the Late Cretaceous and ductile fabrics are cross-cut by latest Cretaceous to Paleocene plutons.

Comparison of the Atnarko complex to equivalent portions of the orogen along strike, indicates a post mid-Cretaceous change in structural style. To the northwest the orogen records continued southwest-directed compression which dominates the deformation style; while to the southeast large dextral strike-slip faults dominate. Relative plate motions between ca. 70-60 Ma indicate that dextral transpression occurred between the Kula and North American plates. Strain during this transpressive deformation was partitioned into compressive and translational regions. The Atnarko complex area is situated at the transition between translation and compression.

The conditions of the lower and middle crust within the orogen were established by how strain was partitioned across the orogen. The distributed strain also shaped how the orogen responded to Tertiary extension. Continued compression to the northwest of the Atnarko complex led to increased crustal thickness and partial melting of lower and middle crust in the Tertiary. Conversely, the cessation of compression in the southeast lead to a more stable (i.e. cooler) crustal lithosphere. A change in relative plate motions in the early Tertiary triggered full-scale, orogen-perpendicular, collapse in the northwest facilitated by decoupling between the middle and lower crusts along thermally weakened layers. Localized orogen-parallel extension occurred in the southeast which was kinematically linked to large dextral strike-slip faults where the upper crust remained coupled to the middle and lower crust.

TABLE OF CONTENTS

CHAPTER THREE

Decoupling of the lower crust within the western Canadian Cordillera: Evidence from the Atnarko complex

CHAPTER FOUR

The Nature of superterrane boundaries from Alaska to southwestern British Columbia

CHAPTER FIVE

APPENDIX I

APPENDIX II

APPENDIX III

LIST OF TABLES

LIST OF FIGURES

ACKNOWLEDGEMENTS

First and foremost I thank my supervisor Lori Kennedy, who first proposed this project and for taking on a student with more thoughts of the field than of the lab. I am truly thankful for all her help and support throughout the course of the project from discussions on Cordilleran tectonics to prospects of jobs in the Yukon.

The rest of my supervisory committee, Rich Friedman, Jim Mortensen and Kelly Russell are all owed a huge amount of gratitude for rising to the occasion of last minute reviews and suggestions and for answering emails and phone messages from the far north, usually at odd hours. Rich Friedman is owed a special thanks for going way above the call of duty in the geochron lab without his help there is no way this thesis would have been finished.

I must also thank colleagues at the Yukon Geological Survey, especially Grant Abbott and Don Murphy, for allowing me to work on British Columbia geology while mapping in the southwest Yukon. Discussions on Cordilleran geology with Maurice Colpron, Don Murphy, Craig Hart and Lee Pigage were invaluable. The YGS is a great place to work and all of those who I share a building with are great friends who in their own way helped me complete this thesis.

Support for field studies, especially one as remote as the Atnarko, is a hard thing to come by these days. Field logistics and map production support provided by the Geological Survey of Canada and the British Columbia Geological Survey is greatly appreciated. Geological discussions with Jim Haggart, Brian Mahoney, Glenn Woodsworth, Larry Diakow and Bert Struik helped tremendously. Getting field assistants to work in such a spectacular place is not hard, but finding some that are a great help and make the tough days fun is more difficult. Thanks to Tim Barry and Ken Glover for making field work even more enjoyable.

Friends at UBC who kept life entertaining and continue to do so, what can I say? I guess just thanks for everything, there are so many of you that helped me keep my perspective through the years. In particular, Scott Heffernan, Steve Quane, Martin Stewart, Justin Stockwell, Mike

Henrichsen, Dave Smithson, Lawrence Winter and Simon Haynes for so many memories and more to come. Bradshaw, it is a real drag you can’t be around to see this thing done, we all miss you.

Finally, a huge amount of thanks to my wife Olwyn for her unwavering support and dedication to someone whose thoughts have been more on rocks than anything else.

CO-AUTHORSHIP STATEMENT

This PhD thesis comprises field mapping, collection of laboratory data, analysis of field and lab data and synthesis and development of tectonic models. All work was performed by me (Steve Israel), except where noted otherwise. In all cases my supervisor, Dr. L. Kennedy was responsible for securing support, discussing and refining ideas and providing editorial advice. On that basis she is a co-author to each paper.

Chapter 2 is a version of a paper to be submitted to the Geological Society of America *Bulletin*. My co-authors include Dr. Lori Kennedy and Mr. Tom Ulrich. T. Ulrich analyzed samples for Ar-Ar geochronology and provided interpretations of ages.

Chapter 3 is a version of a paper to be submitted to *Tectonics*. My co-authors include Drs. Lori Kennedy, Rich Friedman and Jim Mortensen and Mr. Tom Ulrich. R. Friedman performed dilution chemistry on all U-Pb TIMS analyses as well as analyzing samples and providing discussion on interpretation of TIMS ages. R. Friedman also ran samples for LA-ICPMS and discussion on age interpretation. J. Mortensen helped with LA-ICPMS data capture and interpretation of some TIMS data. T. Ulrich performed Ar-Ar analyses and interpretation of argon ages.

Chapter 4 is a synthesis paper and I intend it for publication in the Canadian Journal of Earth Sciences.

Lastly my thesis includes two 1:50 000-scale bedrock geology maps. The first is co-authored by Dr. Peter van der Heyden, who was involved in reconnaissance mapping of the Atnarko complex. All additional mapping and compilation is the result of my thesis research. The second map is co-authored by Drs. Peter van der Heyden, Jim Haggart and Glenn Woodsworth. P. van der Heyden provided reconnaissance mapping of the Atnarko complex and Drs. J. Haggart and G. Woodsworth mapped an area outside of this study area.

CHAPTER ONE

INTRODUCTION

Preamble

Mountain belts (orogens) are complex geologic systems formed in response to plate tectonic processes. Exhumed orogens are, therefore, critical parts of the Earth that allow for field and laboratory studies of middle to lower crustal rocks that support continent scale mountain belts. Specifically they provide insight into the construction of crustal roots to arcs and to the processes responsible for continental accretion.

On a global scale the evolution of orogenic belts can be ascribed to the interaction of two or more tectonic plates at convergent margins. A cycle develops where by lithospheric scale deformation leads to crustal thickening and a concomitant increase in topography. This constructional event is commonly followed by collapse and exhumation of middle and lower crustal rocks (Dewey, 1988). How the orogen evolves through time is a function of: 1) large-scale plate dynamics; 2) rheological properties of the crustal lithosphere; and 3) the rates of input of new or recycled magmatic material (e.g. magma).

Transpression refers to a situation in which strain is partitioned between orogen parallel translation and orogen normal compression (Fossen and Tikoff, 1998; Saint Blanquat et al., 1998). The consequence is the compartmentalization of strain across the orogen to form discrete zones that deform differently. How strain is partitioned and the styles of deformation featured by each zone reflect relative plate motions and rheological properties of the lithosphere. Differences in deformation styles are manifest at both the Earth's surface and at depth. In some instances, the crust becomes stratified in terms of styles of deformation. This occurs, for example, where upper crustal layers become decoupled from lower portions of the crust, allowing the layers to deform independently (Grocott et al., 2004). In actively deforming magmatic arcs the presence of melt enhances deformation by promoting strain softening and strain localization. It also increases the likelihood of extreme strain partitioning to the point that portions of the crust become decoupled (Vanderhaeghe and Teyssier, 2001; Brown, 2004).

Orogens that coincide with magmatic arcs are associated with enormous amounts of heat and melt. The initial crustal thickening stages of orogenesis can potentially lead to the generation of partially melted lower crust (Thompson and Connolly, 1995; Ducea, 2001). Overthickening combined with thermal weakening of the crust by partial melting create gravitational instabilities in the crust and can cause decoupling of the upper crust from the lower crust. These events greatly facilitate collapse of the orogen.

The orogen represented by the western Canadian and southeast Alaskan Cordillera hosts the Coast plutonic complex, a belt of plutonic and metamorphic rocks extending for more than 1800 km and recording over 150 My of magmatism and deformation (Fig. 1.1). The complex is part of an accretionary orogen that is characterized by a collage of tectonic terranes amalgamated over time to the western margin of North America (Monger and Nokelberg, 1996; Dickinson, 2000). The Coast plutonic complex is the product of the interaction between two large composite terranes, the Insular and Intermontane superterranes. The most widely accepted view is that initial interaction between the two superterranes began by Middle Jurassic time or possibly earlier (van der Heyden, 1992; Saleeby, 2000; Gehrels, 2001). Once the two superterranes docked the relative plate motions at the boundary changed several times causing the margin to undergo periods of transpression, transtension, extension and predominantly strike slip motion. How the orogen reacted to the changes in plate motions is captured in the magmatic, structural

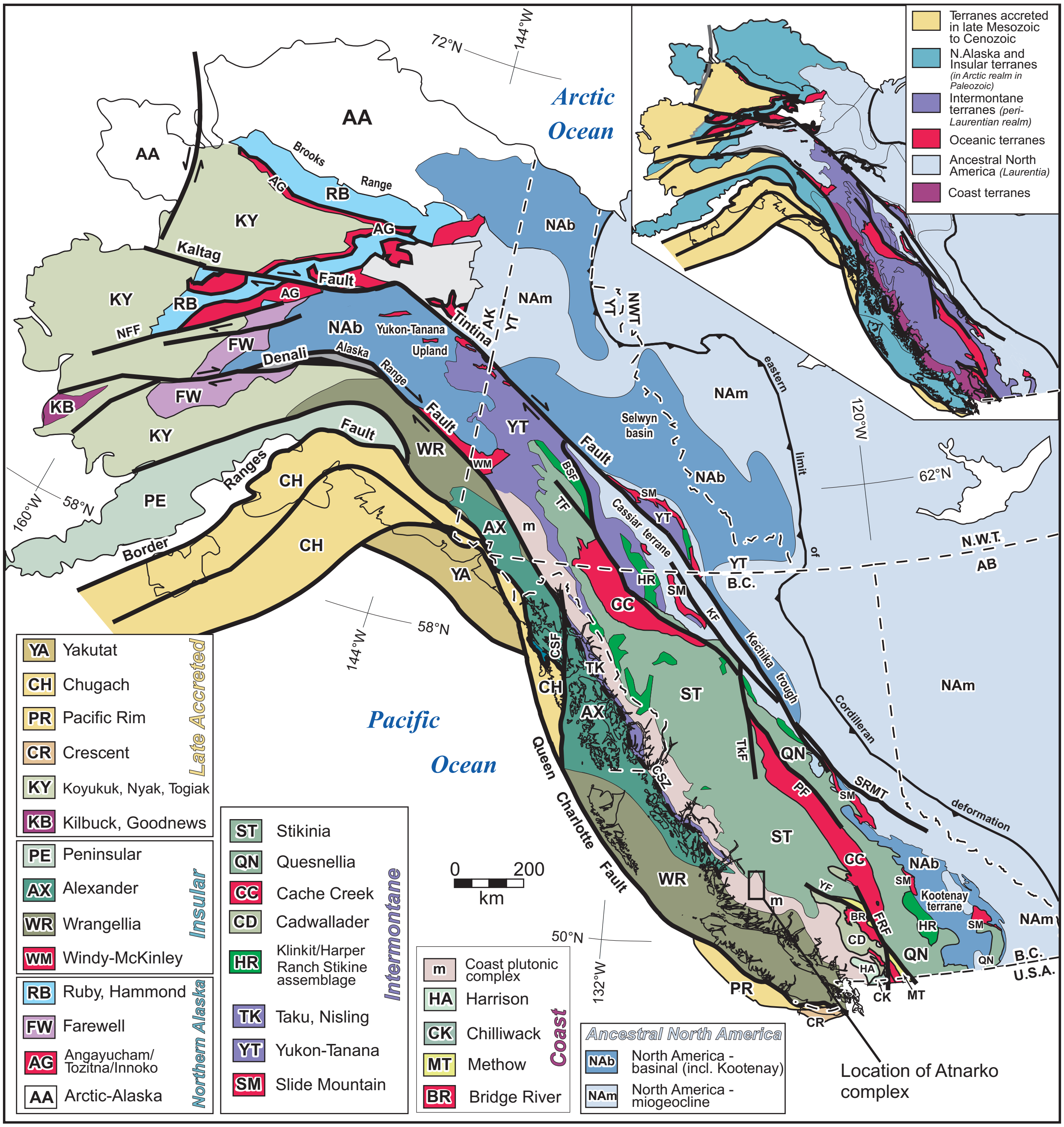

Figure 1.1 Terranes of the Alaska-Canadian Cordillera. Inset showing the tectonic realms as defined by Colpron et al., (2007). Location of the Atnarko complex indicated by box. Faults: BSF-Big Salmon fault; CSF-Chatham Strait fault; CSZ-Coast shear zone; FRF-Fraser River fault; KF-Kechika fault; NFF-Nixon Fork-Iditarod fault; PF-Pinchi fault; SMRT-southern Rocky Mountain trench; TkF-Takla-Finlay-Ingenika fault system; YK-Yalakom fault. Modified from Colpron et al., (2007).

and metamorphic history of middle and lower crustal rocks now exposed within the Coast plutonic complex.

The Atnarko complex, located within the Coast plutonic complex, near the boundary between the Insular and Intermontane superterranes, is composed of middle and lower crustal rocks that represent part of the over 150 My evolution of the orogen (Fig. 1.1). This thesis is based on detailed field based study of the rocks exposed in the Atnarko complex and dating of the deformation and metamorphism.

Previous Work

The Atnarko complex and surrounding terrain was previously mapped at only reconnaissance level. Tipper (1969) first mapped the Anahim map sheet at 1:250 000 scale and identified strongly deformed metaigneous, metavolcanic and metasedimentary rocks intruded by deformed plutonic bodies. His study was regional in context and provided no detailed understanding of the complex. The Mount Waddington map sheet to the south of the Atnarko complex (Tipper, 1968) and to the west in the Bella Coola map area (Baer, 1973) were also mapped at this time. The last geological work in the Atnarko area is that of van der Heyden (1990; 1991) who undertook reconnaissance 1:50 000 scale mapping and preliminary geochronological studies of the area. This thesis represents the first comprehensive study of the Atnarko complex.

In 2001 the Geological Survey of Canada and the British Columbia Geological Survey initiated a Targeted Geoscience Initiative (TGI) project centred on the Bella Coola area, west of the Atnarko complex. The aim of the TGI was to remap the region and assess the mineral potential of the area (Haggart et al., 2006). This provided an opportunity for detailed study in the Atnarko complex. The region of the Atnarko complex is characterized by rugged, steep to gently rounded glaciated mountains of the British Columbia Coast Mountain chain. The field area is remote and accessible only by helicopter.

Objectives of Thesis

The objectives of this research are to: 1) provide a field based geological model for the Atnarko complex, a relatively unknown region within the Coast Mountains of British Columbia; 2) determine the relationships between structure, metamorphism and plutonism within the Atnarko complex; 3) establish a connection between the events recorded by the Atnarko complex and the formation of the Coast Mountains orogen; and to 4) relate the events recorded in the Atnarko complex to the existing framework for the Cordillera.

Organization of Thesis

The thesis is divided into three chapters, each of which focuses on different aspects of the Atnarko complex. The individual chapters are written as manuscripts for submission as publications in international scientific journals.

Chapter 2 establishes the geologic foundation of the Atnarko complex on the basis of the structural, metamorphic and lithologic characteristics of the complex. Detailed 1:50 000 scale bedrock mapping coupled with structural analysis and $^{40}Ar/^{39}Ar$ geochronology of metamorphic minerals provide the framework for this research. This work is written as a manuscript: "*Early Cretaceous to Tertiary history of the Atnarko complex, southwest British Columbia,*" to be submitted to the *Geological Society of America Bulletin*.

Chapter 3 presents the results of thermochronology applied to the Atnarko complex which are used to establish the structural and magmatic history of the complex. This manuscript provides a detailed look into the processes associated with convergent margins and shows how orogens respond to relative plate motions. This manuscript "*Coupling and decoupling between the lower* *and middle crust within the western Canadian Cordillera: Evidence from the Atnarko complex,*" is to be submitted to the journal *Tectonics*.

Chapter 4 provides a regional context for the lithologies of the Atnarko complex. Furthermore it establishes relationships between terranes within the orogen by comparing and contrasting the tectonostratigraphic relationships across the Insular superterrane-Coast plutonic complex-Intermontane superterrane boundaries along strike from southeast Alaska to southwestern British Columbia. This manuscript "*A comparative analysis of superterrane boundaries from Alaska to southwestern British Columbia,*" is to be submitted to the *Canadian Journal of Earth Science*.

Chapter 5 summarizes the conclusions drawn from the previous chapters and presents a set of recommendations for future work in the Atnarko area.

Included in the thesis are two 1:50 000 scale bedrock maps that depict the geologic relationships of the Atnarko complex and surrounding region. The maps are the result of the interpretation of data collected over a total of seven months of field work by the author with a compilation of older mapping. These maps have been published by the Geological Survey of Canada and include: 1) Israel, S and van der Heyden, P. (2006). *Geology, Atnarko (93C/05), British Columbia*; Geological Survey of Canada, Open File 5389, scale 1:50 000*;* 2) Israel, S., van der Heyden, P., Haggart, J.W., and Woodsworth, G.J. (2006). *Geology, Junker Lake and part of Knot Lakes (93C/04 and 92N/13), British Columbia*; Geological Survey of Canada Open File 5388, scale 1:50 000.

Coast belt-Coast plutonic complex definitions

Any geologic study in the North American Cordillera is rife with terminology. Not the least of which is the difference between the Coast belt and the Coast plutonic complex. Both of these terms have been used over the years to describe rocks of the outermost mountainous terrain of the Canadian and Alaskan portions of the North American Cordillera. This thesis deals extensively with these terms and I have tried to use the two terms effectively. Chapters two and three of this thesis are largely concerned with the Coast plutonic complex, whereas Chapter four deals with the complex and how it fits within the wider Coast belt scheme of Cordilleran tectonics. Because of this, I feel it necessary to give brief definitions of each term such that the reader is clear as to what I mean when using the terms.

Coast Belt

The Coast belt is defined in terms of morphogeological characteristics and includes the topographically high (mountainous) region along the western coast of British Columbia and portions of southeast Alaska (Fig. 1.2; Wheeler and McFeely (1991). It includes all the rocks of the Coast plutonic complex as well as rocks that belong to Stikinia, Wrangellia, the Alexander terrane and various late Mesozoic and Cenozoic overlap assemblages. Boundaries are defined on morphology and to some extent geology.

Coast plutonic complex

The term Coast plutonic complex has been used for decades in Cordilleran geology. The definition of the term is somewhat subjective but it is considered an entity within the Coast belt. Woodsworth et al., (1991) provide a definition that is adhered to in this thesis. Their definition states, "…the Coast plutonic complex of the Coast belt, a long and narrow zone of plutonic and lesser metamorphic rocks extending from southern British Columbia into the Yukon Territory." The boundaries are somewhat arbitrary as many of the plutons included in the complex intrude into adjacent Intermontane and Insular superterranes; however, it is possible in places to draw a line on a map between higher grade metamorphic rocks and lower-grade to unmetamorphosed rocks. These lines are almost always faults, separating true Coast plutonic complex from clearly

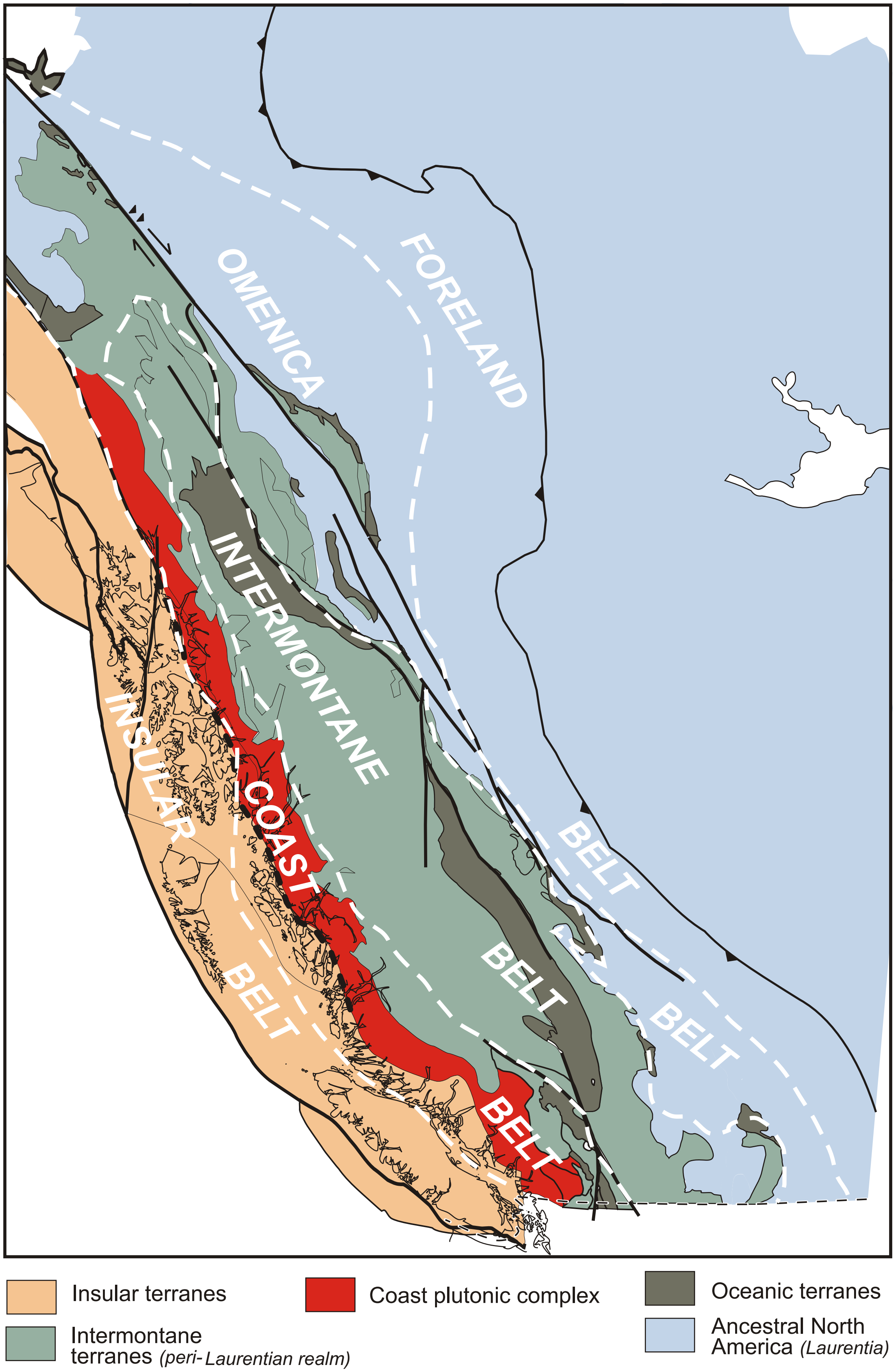

Figure 1.2. Map of parts of the Alaskan and Canadian Cordillera illustrating difference between tectonic terranes and morphogeological belts. Terrane boundaries modified from Colpron et al. (2007). Morphogeological belt boundaries from Wheeler and McFeely (1991).

identifiable rocks belonging to the adjacent superterranes (Fig. 1.2). The plutons and much of the metamorphism of the country rocks are the result of tectonic interaction between the Insular and Intermontane superterranes and therefore I believe the Coast plutonic complex can be considered as a tectonic entity unto itself.

REFERENCES

Baer, A. J., 1973, Bella Coola-Laredo Sound map areas: British Columbia, Geological Survey of Canada Memoir 372, 122 p.

Brown, M., 2004, The mechanism of melt extraction from lower continental crust of orogens: Transactions of the Royal Society of Edinburgh: Earth Sciences, v. 95, p. 35-48.

Dewey, J. F., 1988, Extensional collapse of orogens: Tectonics, v. 7, p. 1123-1139.

Dickinson, W. R., 2000, Geodynamic interpretation of Paleozoic tectonic trends oriented oblique to the Mesozoic Klamath-Sierran continental margin in California, *in* Soreghan, M. J., and Gehrels, G. E., eds., Paleozoic and Triassic paleogeography and tectonics of western Nevada and northern California: Boulder, Colorado, Geological Society of America, p. 209-245.

Ducea, M., 2001, The California arc: thick granitic batholiths, ecologitic residues, lithospheric-scale thrusting, and magmatic flare-ups: GSA Today, v. 11, no. 11, p. 4-10.

Fossen, H., and Tikoff, B., 1998, Extended models of transpression and transtension, and application to tectonic settings, *in* Holdsworth, R. E., Strachan, R. A., and Dewey, J. F., eds., Transpressional and Transtensional Tectonics, Geological Society, London, Special Publications, 135, p. 15-33.

Gehrels, G. E., 2001, Geology of the Chatham Sound region, southeast Alaska and coastal British Columbia: Canadian Journal of Earth Sciences, v. 38, p. 1579-1599.

Grocott, J., McCaffrey, K. J. W., Taylor, G. K., and Tikoff, B., 2004, Vertical coupling and decoupling in the lithosphere, *in* Grocott, J., McCaffrey, K. J. W., Taylor, G. K., and Tikoff, B., eds., Vertical Coupling and Decoupling in the Lithosphere, Geological Society, London, Special Publications, 227, p. 1-7.

Haggart, J. W., Diakow, L. J., Mahoney, J. B., Woodsworth, G. J., Struik, L. C., Gordee, S. M., and Rusmore, M. E., 2006, Geology, Bella Coola region (93D/01,/07,/08,/10,/15 and parts of 93D/02,/03,/06,/09,/11,/14,/16 and 92M/15 and /16), British Columbia: Geological Survey of Canada, Open File 5385, scale 1:100 000.

Monger, J. W. H., and Nokelberg, W. J., 1996, Evolution of the North America Cordillera: generation, fragmentation, displacement and accretion of successive North American plate-margin arcs, *in* Coyner, A. R., and Fahey, P. L., eds., Geology and ore deposits of the North American Cordillera: Symposium Proceedings: Reno-Sparks, Nevada, Geological Society of Nevada, p. 1133-1152.

Saint Blanquat, M., Tikoff, B., Teyssier, C., and Vigneresse, J. L., 1998, Transpressional kinematics and magmatic arcs, *in* Holdsworth, R. E., Strachan, R. A., and Dewey, J. F., eds., Transpressional and Transtensional Tectonics, Geological Society, London, Special Publications, 135, p. 327-340.

Saleeby, J. B., 2000, Geochronologic investigations along the Alexander-Taku terrane boundary, southern Revillagigedo Island to Cape Fox areas, southeast Alaska, *in* Stowell, H. H., and McClelland, W. C., eds., Tectonics of the Coast Mountains in southeast Alaska and British Columbia, Geological Society of America, p. 107-143.

Thompson, A. B., and Connolly, J. A. D., 1995, Melting of the continental crust: some thermal and petrological constraints on anatexis in continental collision zones and other tectonic settings: Journal of Geophysical Research, v. 100, p. 15556-15579.

Tipper, H. W., 1968, Geology, Mount Waddington: Geological Survey of Canada, Preliminary Map, 5-1968.

Tipper, H. W., 1969, Geology of the Anahim map area: Geological Survey of Canada Map 1202A, scale, scale 1:250,000, 1 sheet.
van der Heyden, P., 1990, Eastern margin of the Coast Belt in west-central British Columbia, Current Research, Part E, Geological Survey of Canada, p. 171-182.
van der Heyden, P., 1991, Preliminary U-Pb dates and field observations from the eastern Coast Belt near 52^{o}N, British Columbia, Current Research, Part A, Geological Survey of Canada, p. 79-84.
van der Heyden, P., 1992, A Middle Jurassic to early Tertiary Andean-Sierran arc model for the Coast Belt of British Columbia: Tectonics, v. 11, p. 82-97.
Vanderhaeghe, O., and Teyssier, C., 2001, Partial melting and flow of orogens: Tectonophysics, v. 342, p. 451-472.
Wheeler, J. O., and McFeely, P., 1991, Tectonic assemblage map of the Canadian Cordillera and adjacent parts of the United States of America: Geological Survey of Canada, scale 1:2,000,000.
Woodsworth, G. J., Anderson, R. G., and Armstrong, R. L., 1991, Plutonic Regimes, Chapter 15, *in* Gabrielse, H., and Yorath, C. J., eds., Geology of the Cordilleran Orogen in Canada, Geological Survey of Canada, p. 491-531.

CHAPTER 2

EARLY CRETACEOUS TO TERTIARY HISTORY OF THE ATNARKO COMPLEX, SOUTHWEST BRITISH COLUMBIA

INTRODUCTION

The present day crustal structure is a record of how the crust responds to plate interactions. The main driving mechanisms behind the various stages of orogenic construction are a combination of relative motions along the plate margins and the addition of magmatic material during crustal anatexis and/or the introduction of melt from mantle sources (Dewey, 1980, 1988; Vanderhaeghe and Teyssier, 2001). The western North American Cordilleran orogen of Canada, Alaska and Washington records at least 150 My of orogenic construction and collapse during terrane accretion. The Coast plutonic complex of the western North American Cordillera is a belt of plutonic and metamorphic rocks in excess of 1800 km long. It stretches from Alaska, through British Columbia and into northern Washington (Fig. 2.1). The exact boundaries of the Coast plutonic complex are somewhat arbitrary, coinciding with the limit of metamorphic rocks that were originally part of the bounding Insular and Intermontane superterranes (Woodsworth et al., 1991)

The formation of the Coast plutonic complex is attributed to the accretion of the Insular superterrane to the western margin of the Intermontane superterrane. The accretion began by the Middle Jurassic (or before) and continued into the Tertiary (Monger et al., 1982; McClelland et al., 1992a; van der Heyden, 1992). Studies of the Coast plutonic complex have identified several phases of deformation linked to orogen development involving crustal thickening followed by extension and exhumation of middle and lower crustal rocks (Andronicos et al., 1999; Crawford et al., 1999; Rusmore et al., 2005; Hollister and Andronicos, 2006). Plate reconstruction models for the western North American Cordillera indicate changes in plate vectors between the North American and outboard Pacific plates (Farallon and Kula plates) from earliest Cretaceous relative sinistral movement to dextral motion by Late Cretaceous with varying amounts of compression orthogonal to the strike of the orogen (Engebretson et al., 1985; Lonsdale, 1988).

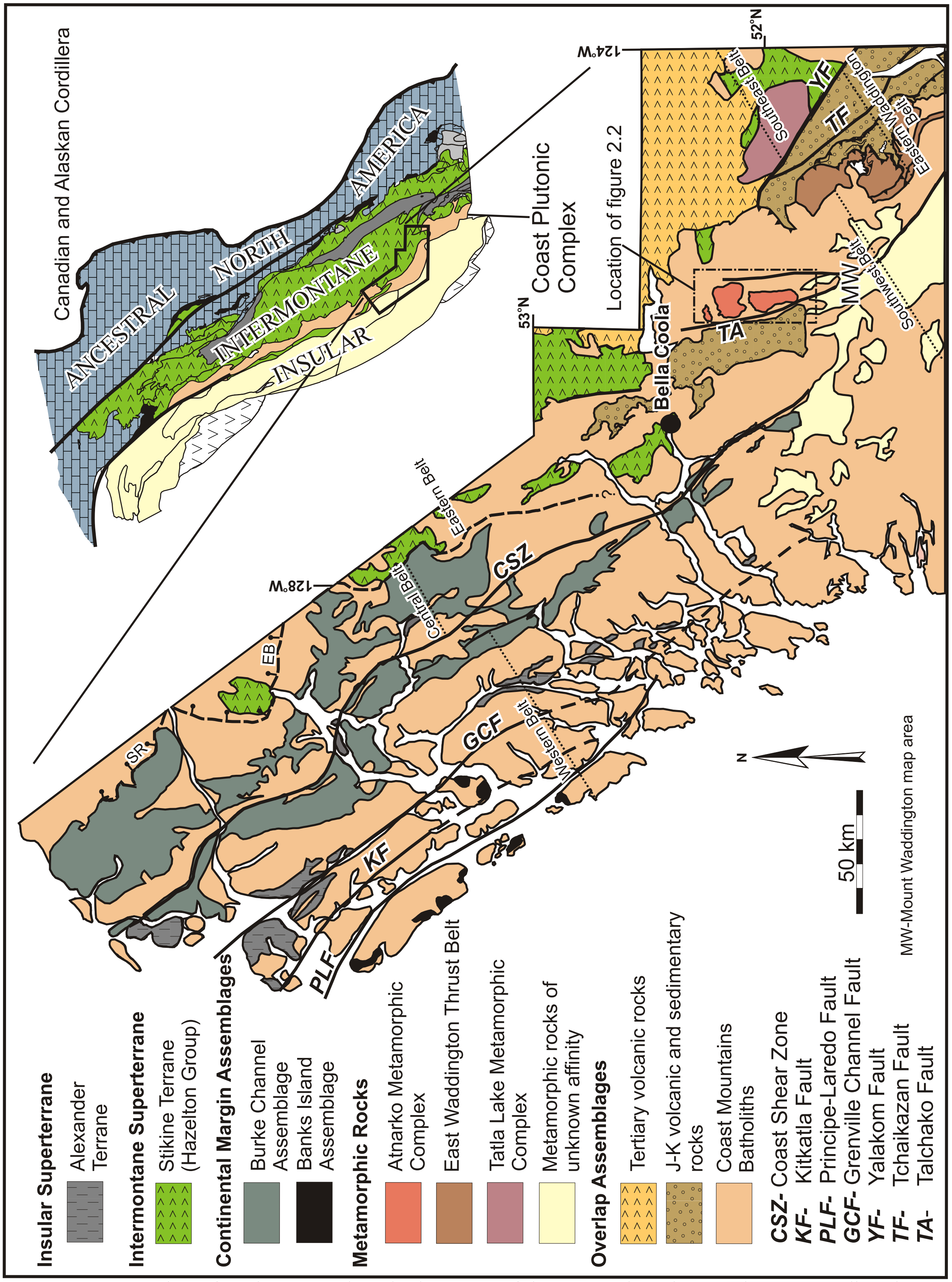

Figure 2.1. Location of study area and geologic nature of the Coast Plutonic complex surrounding the Atnarko complex. SR, EB-Shames River and Eastern Boundary detachment systems, respectively. MW-Mount Waddington Map area. Modified from Boghossian et al., [2000]; Chardon et al., [1999]; Rusmore and Woodsworth [1994]; Rusmore et al., [2005] and van der Heyden et al., [1994].

The Insular superterrane, Coast plutonic complex and Intermontane superterrane all form northwest trending belts separated from each other by crustal-scale zones of deformation (Fig. 2.1). Near Bella Coola, west-central British Columbia (Fig. 2.1), the post crustal thickening history of the orogen is markedly different from areas to the northwest and southeast along strike. This difference is manifest by substantial Eocene extension which exhumed middle and lower crustal rocks northwest of the Bella Coola area. In contrast, to the southeast, the orogen features small, localized extensional complexes within a dominantly dextral strike-slip regime (Friedman and Armstrong, 1988; Coleman and Parrish, 1991; Andronicos et al., 2003; Rusmore et al., 2005). Polydeformed metamorphic rocks of the Atnarko complex are located at the latitude where this transition in structural style occurs. Previous work suggested that the metamorphic rocks in the Atnarko complex had the same history as rocks to the northwest; namely that they recorded Cretaceous compression followed by Eocene extension and exhumation. Work presented here shows this not to be the case.

In this chapter results from bedrock mapping within the Atnarko complex and structural and chronologic data are used to establish a geologic history for the complex. The data and observations from this work do not support Eocene extension as the main mechanism of exhumation within the Atnarko complex. Rather the data suggest that deformation and subsequent exhumation of metamorphic rocks relates to compression in Early to Late Cretaceous time. The fundamental differences in structural style observed along the strike of the orogen can be explained by strain partitioning during Late Cretaceous dextral transpression such that compression occurred northwest of the study area and dextral translation occurred to the southeast. This led to dramatically different late Mesozoic and Early Tertiary histories, in particular the style and amount of extension varies along strike within the orogen.

GEOLOGIC SETTING

Insular Superterrane

The Insular superterrane includes the Alexander and Wrangell (Wrangellia) terranes (Fig. 2.1). The Alexander terrane comprises latest Proterozoic to Triassic volcanic, clastic sedimentary and carbonate rocks (Jones et al., 1977). Wrangellia is composed of Middle and Late Paleozoic arc sequences and scattered Middle Triassic sedimentary rocks overlain by voluminous Late Triassic flood basalts and carbonates. The two terranes have different Early Paleozoic histories but are believed to have been amalgamated by the Carboniferous and accreted to the western edge of the Intermontane terrane as a single coherent crustal block (Jones et al., 1977; Gardner et al., 1988; Monger and Journeay, 1994; Dickinson, 2004). At the latitude of the study area, Alexander terrane rocks are the only component of the Insular superterrane (Gehrels, 2001). These crop out on islands along the BC and Alaska coasts west of the study area (Fig. 2.1).

Intermontane Superterrane

The Intermontane superterrane includes the Stikine (Stikinia), Cache Creek and Quesnel (Quesnellia) terranes. The discussion in this chapter considers only Stikinia, the westernmost portion of the Intermontane superterrane (Fig. 2.1). Stikinia, as represented at the eastern margin of the Coast plutonic complex, is composed of the Hazelton Group, an Early to Middle Jurassic volcanic and sedimentary arc sequence that is widespread from Bella Coola north to 58^{o}N latitude (Marsden and Thorkelson, 1992; Gordee, 2005).

The Hazelton Group is unconformably to disconformably overlain by Early to mid-Cretaceous volcanic and sedimentary rocks of the Monarch assemblage (van der Heyden et al., 1994; Haggart et al., 2003). The older volcanic portion of the Monarch assemblage is correlated with the Gambier Group which is interpreted to be an Early Cretaceous volcanic arc sequence built on Wrangellia and the Insular superterrane. The Gambier Group and the Monarch assemblage are thought by some workers to represent one Early to mid-Cretaceous volcanic arc built across the Intermontane and Insular superterrane boundary (Monger et al., 1994b; Israel et al., 2006a).

Coast plutonic complex

The Coast plutonic complex is a magmatic and metamorphic belt that stretches from Alaska to southernmost British Columbia and northwest Washington. The complex is attributed to tectonic interaction between the Insular and Intermontane superterranes and the subduction of intervening oceanic crust (Fig. 2.1; Monger et al., 1982; van der Heyden, 1992; Dickinson, 2000). Mesozoic to Tertiary plutonic rocks intrude variably deformed and metamorphosed supracrustal rocks of both the Intermontane and Insular superterranes, as well as rocks believed to be part of the Yukon-Tanana terrane, a terrane comprised of metamorphosed and deformed rocks of continental margin affinity (Armstrong, 1988; van der Heyden, 1989; Mortensen, 1992; Monger and Journeay, 1994; Gehrels, 2001; Colpron et al., 2007). For this study the Coast plutonic complex is defined as consisting of Mesozoic plutons and the metamorphic rocks found within and at the edges of the plutons. The eastern and western boundaries are somewhat variable, but often coincide with structures that place higher-grade metamorphic rocks over lower-grade rocks that belong demonstrably to either the Insular or Intermontane superterrane (Fig. 2.1).

Tectonic and structural relationships

The timing of accretion of the Insular superterrane to the western margin of the Intermontane superterrane is a subject of debate. Early models suggested a mid-Cretaceous age for initial accretion (Berg et al., 1972; Monger et al., 1982). Subsequent studies suggested that the accretion began in the latest Triassic to Middle Jurassic (McClelland et al., 1992a; van der Heyden, 1992; Monger et al., 1994a; Monger and Nokelberg, 1996; Dickinson, 2000; Saleeby, 2000). A third model suggests that the Insular and Intermontane superterranes were located well to the south relative to their present day position until mid-Cretaceous time and were translated northward to present day latitudes in the latest Cretaceous to Tertiary (Irving et al., 1995; Wynne et al., 1995; Cowan et al., 1997), the so-called 'Baja-B.C. model". Some of the proposed displacement for the latter model is thought to have occurred on the Coast shear zone. The Coast shear zone is a ~1200 km structure located within the Coast plutonic complex (Hollister and Andronicos, 1997). The evidence for substantial post mid-Cretaceous orogen parallel motion on the Coast shear zone is questionable for two reasons: 1) most of the latest Cretaceous to Tertiary movement along the Coast shear zone is top to the west compression overprinted in places by top to the east normal displacement (Rusmore et al., 2000; Rusmore et al., 2001; Andronicos et al., 2003); and, 2) continuous pre-Cretaceous geologic units have been traced across the main strand of the shear zone in southeast Alaska that suggests no significant lateral movement since at least mid-Cretaceous (Gehrels, 2001).

As much as 800 km of relative sinistral motion is believed to have occurred between the Intermontane and Insular superterranes between earliest Cretaceous (possibly older) and Late Cretaceous time (Monger et al., 1994b; Evenchick, 2001; Umhoefer et al., 2002; Israel et al., 2006a). Several large sinistral strike-slip faults, located at the margins of the Coast plutonic complex, such as the Grenville Channel shear zone and the Tchaikazan fault were active during the Early to mid-Cretaceous (Chardon et al., 1999; Israel et al., 2006a). Coeval compressional structures with a component of sinistral shear are reported from throughout the Coast plutonic complex and adjacent terranes and are thought to have been active during the Early to mid-Cretaceous (Schiarizza et al., 1997; Evenchick, 2001).

Mid-Cretaceous compression affected the entire outboard margin of the orogen and resulted in a southwest-west directed thrust belt formed on the western margin of the Coast plutonic complex and a temporally overlapping northeast-north directed belt formed on the eastern margin (Crawford et al., 1987; Journeay and Friedman, 1993; Rusmore and Woodsworth, 1994). Dextral transpression followed compression beginning at ~70 Ma with partitioned strain accommodated by compression along the Coast shear zone and translation along the Yalakom and other fault systems (Umhoefer and Schiarizza, 1996; Andronicos et al., 1999; Rusmore et al., 2001). Relative plate motions are believed to have changed such that the orogen underwent dextral transtension beginning at ~ 59 Ma (Engebretson et al., 1985; Engebretson and Blake, 2002; Andronicos et al., 2003; Rusmore et al., 2005).

ATNARKO COMPLEX

The Atnarko complex is located at the eastern margin of the Coast plutonic complex, near the boundary with the Intermontane superterrane, east-southeast of the town of Bella Coola, British Columbia (Fig. 2.1). The Atnarko complex is composed of polydeformed, metavolcanic and metasedimentary rocks, gneisses and migmatites of varying ages and Earliest Jurassic to Paleocene plutons. It was first described by Tipper (1969) and later by van der Heyden (van der Heyden, 1990, 1991). Although both studies were reconnaissance in nature, they served to establish the general geology and preliminary age estimates for the complex.

The Atnarko complex is bound to the west by the steeply dipping Talchako fault zone that juxtaposes low grade Jurassic to Cretaceous volcanic and sedimentary rocks against the higher grade metamorphic rocks of the Atnarko complex (Haggart et al., 2006; Israel and van der Heyden, 2006; Israel et al., 2006b). The low grade volcanic and sedimentary rocks are assigned to the Hazelton Group (part of Stikinia) and the Monarch assemblage an Early Cretaceous volcanic and sedimentary overlap assemblage. To the north the Atnarko complex is thrust to the north along a series of well defined mylonite zones and closely spaced northeast striking faults, over relatively undeformed Early Cretaceous plutons (van der Heyden, 1991, 2004; Israel and van der Heyden, 2006). The eastern and southern boundaries of the Atnarko complex are not as well constrained. To the east the boundary of Atnarko complex is obscured by undeformed Eocene plutons and thick accumulations of Miocene volcanic rocks and Quaternary sedimentary deposits. The eastern boundary coincides with a variably deformed and metamorphosed Late Jurassic pluton that is thrust to the east over Triassic volcanic rocks correlated with the Stikine terrane (van der Heyden et al., 1994). van der Heyden et al. (1994) suggest this thrust is part of the northeast verging East Waddington fold and thrust belt which occurs at the eastern boundary of the Coast plutonic complex (Fig. 2.1). The eastern boundary of the Atnarko complex may, therefore, be a continuation of the zone of thrust faults along its northern boundary. To the south the Atnarko complex passes into the northern Mount Waddington map area (Fig. 2.1), where amphibolite and greenschist facies metavolcanic and metasedimentary rocks of unknown affinity dominate (Roddick and Tipper, 1985).

Lithology

Atnarko assemblage

Supracrustal rocks found within the Atnarko complex, here referred to as the Atnarko assemblage, consist of mafic and minor felsic metavolcanic rocks intercalated with metasedimentary rocks. In the southern and northern portions of the complex the assemblage forms thrust sheets within an imbricate zone that involves Late Jurassic to mid-Cretaceous plutons and gneisses and migmatites (Fig. 2.2). The Atnarko assemblage is mainly upper greenschist facies but reaches lower amphibolite facies where in thrust contact with overlying gneisses and migmatites (see below). Transposition of primary layering has obscured original depositional relationships making estimates of stratigraphic thickness for the Atnarko assemblage suspect. Determination of stratigraphic relationships between volcanic and sedimentary rocks is also made difficult.

Metavolcanic rocks occur as thick sequences of massive metabasalt and are by far the most abundant rock type within the Atnarko assemblage (Fig. 2.3A). Metabasalts are fine-grained, dark green to black, are altered and host numerous chlorite and epidote veins. No primary volcanic textures were observed; however, locally preserved relict layering of metabasalt and metasedimentary rocks suggest an original package of basaltic lava and volcaniclastic deposits.

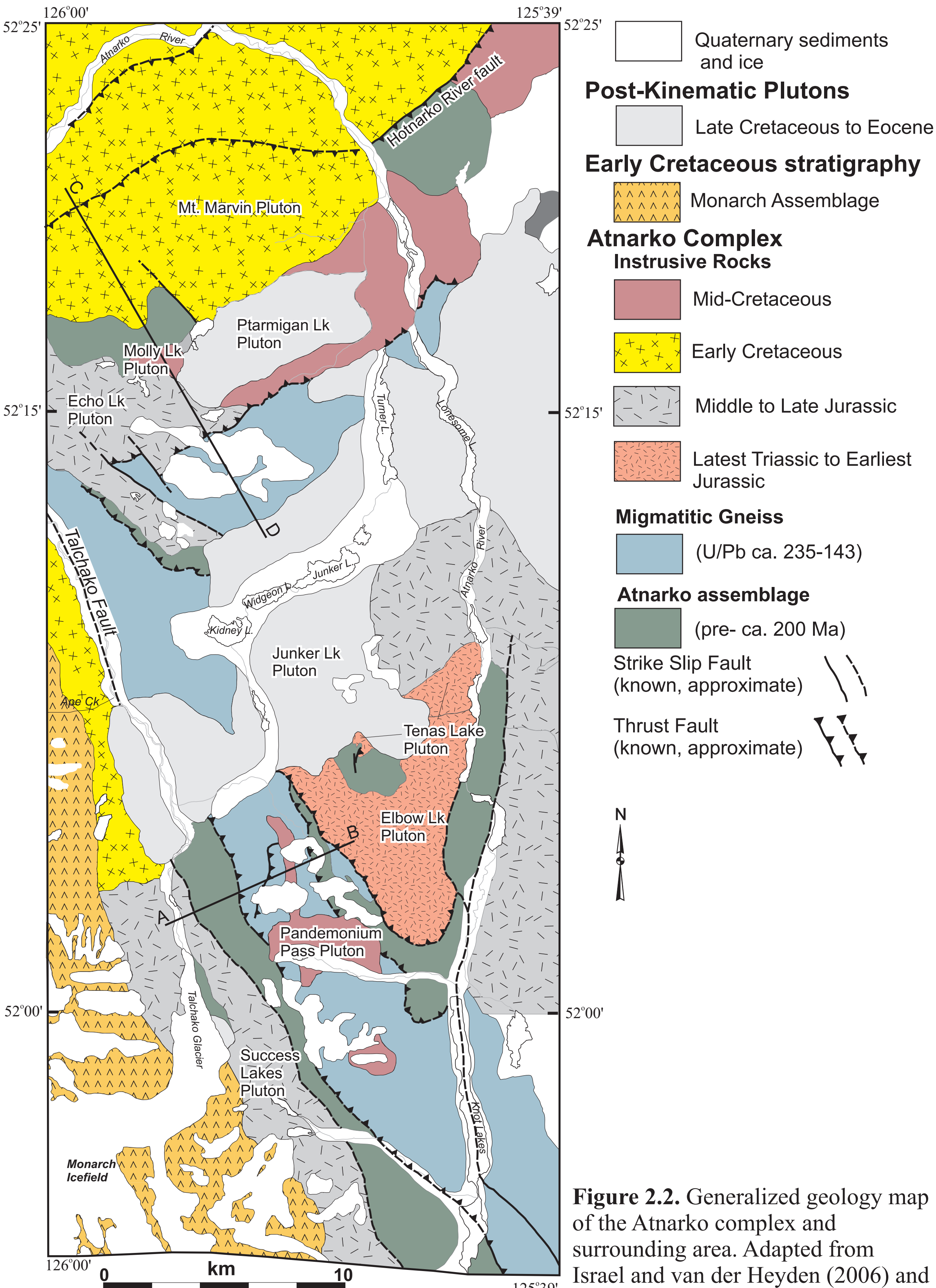

Figure 2.2. Generalized geology map of the Atnarko complex and surrounding area. Adapted from Israel and van der Heyden (2006) and Israel et al., (2006b).

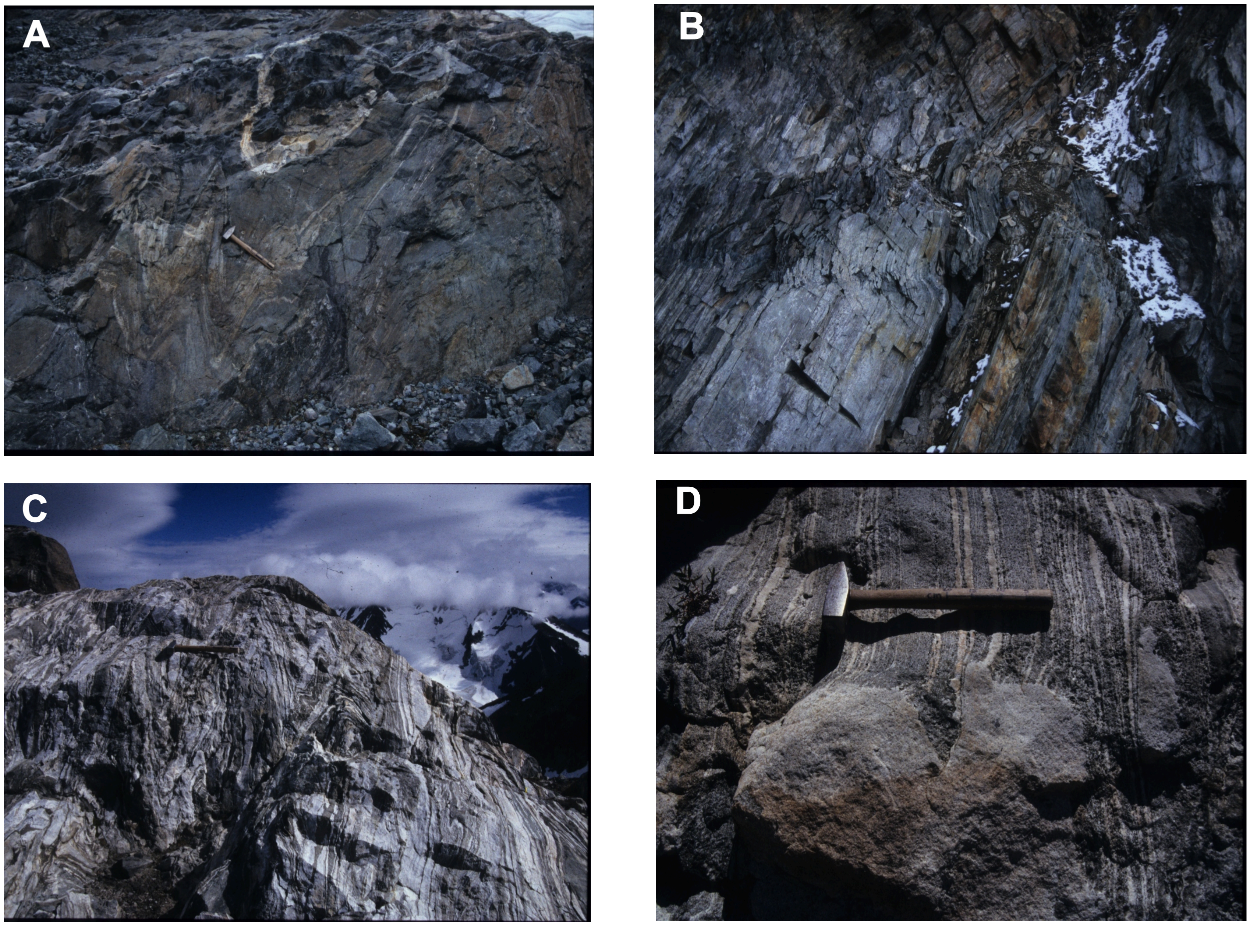

Figure 2.3. (A) Strongly folded metabasalt from the Atnarko assemblage. (B) Interbedded quartzite and psammitic metasediments from the Atnarko assemblage. Field of view ~10 m. (C) Compositionally layered gneiss from the southern Atnarko complex. (D) Stromatic migmatite cross-cut by felsic dyke similar to leucosomes defining layering in migmatite.

Felsic metavolcanic rocks are rare and occur as very fine-grained, light grey layers up to a meter thick within metasedimentary rocks.

Metasedimentary rocks are quartz rich and fine-grained and contain little pelitic material. The majority of metasedimentary outcrops consist of psammite to quartzite (Fig. 2.3B). Outcrops of biotite schist are rare. The metasediments outcrop as beige to light green and grey layers commonly intercalated with metabasalts. Rare pebble to cobble conglomerate is interlayered with metabasalt and finer-grained quartz rich metasediments. Clasts are flattened, elongated and consist of fine-grained psammite, quartzite and rare metabasalt. At one locality in the central Atnarko complex, thin bands of metacarbonate are interlayered with fine-grained metasediments.

The age of the assemblage is not well constrained. The assemblage must be older than the ca. 200 Ma Tenas Lake pluton which intrudes metavolcanic and metasedimentary rock in the central part of the complex. van der Heyden (2004) reports a ca.155 Ma age for zircons collected from a metarhyolite within the Atnarko assemblage that he interpreted as a metamorphic age.

Gneisses and Migmatites

Gneisses and migmatites occur throughout the Atnarko complex where they are structurally interleaved with the Atnarko assemblage and intruded by post-kinematic plutons (Fig. 2.2). Orthogneiss has variable compositions, the most common being quartz-diorite. These are generally coarse- to medium-grained and consist of plagioclase, quartz, hornblende, biotite ± potassium feldspar. The hornblende:biotite ratios vary. Orthogneisses in the north of the mapped area are more muscovite-rich than gneisses in the south. The aluminosilicates phases kyanite, sillimanite, and andalusite are everywhere absent and garnet is only rarely observed. The absence of these key index metamorphic minerals makes it difficult to determine the physical conditions (e.g., pressure-temperature) attending deformation. Thin, coarse-grained amphibolite layers within the orthogneiss represent either mafic dykes or enclaves of mafic volcanic rocks derived from the Atnarko assemblage. Thick, massive, fine-grained amphibolite layers occur locally within larger gneiss bodies. Compositional layering is defined by hornblende- and biotite-rich bands within more leucocratic material (Fig. 2.3C). Locally, melt occurs within amphibolitic layers and areas of migmatization occur throughout the gneiss packages. The migmatites are mainly stromatic in form with leucosomes of plagioclase, quartz, muscovite ± garnet. Individual leucosomes range in thickness from less than one centimeter to greater than a meter. For the most part leucosomes are parallel to the main foliation but locally cross-cut the foliation at high angles (Fig. 2.3D). Feldspar-rich layers composed of coarse-grained plagioclase crystals and porphyroclasts are common near migmatite zones. Gneisses and migmatite are tight to isoclinally folded and refolded and sheared along ductile shear zones.

U-Pb age determinations of zircon from the orthogneiss bodies in the south and north produced ages of ca.143 and 235 Ma, respectively. These are interpreted as the crystallization ages of the protoliths.

Intrusive rocks

A number of plutons of diverse ages and displaying various states of deformation intrude the Atnarko complex (Figure 2.2) and range in age from latest Triassic to Paleocene. Several weakly deformed plutons, that preserve some original igneous textures, appear to overlap in time with the gneisses.

The Tenas Lake pluton is the oldest recognized pluton (ca. 200 Ma) and comprises fine- to coarse-grained hornblende ± pyroxene diorite, quartz diorite and biotite-hornblende tonalite. It is restricted to the central part of the complex where it intrudes rocks of the Atnarko assemblage. It is strongly deformed and locally gneissic in texture. Deformation features such as lobate contacts and strung out dyklets that lie along the main foliation in the host rocks suggest that the pluton is syn-tectonic (Fig. 2.4A).

The next oldest body is the Elbow Lake pluton comprising quartz-diorite and tonalite. It is located in the southern Atnarko complex where it is thrust over the Atnarko assemblage and

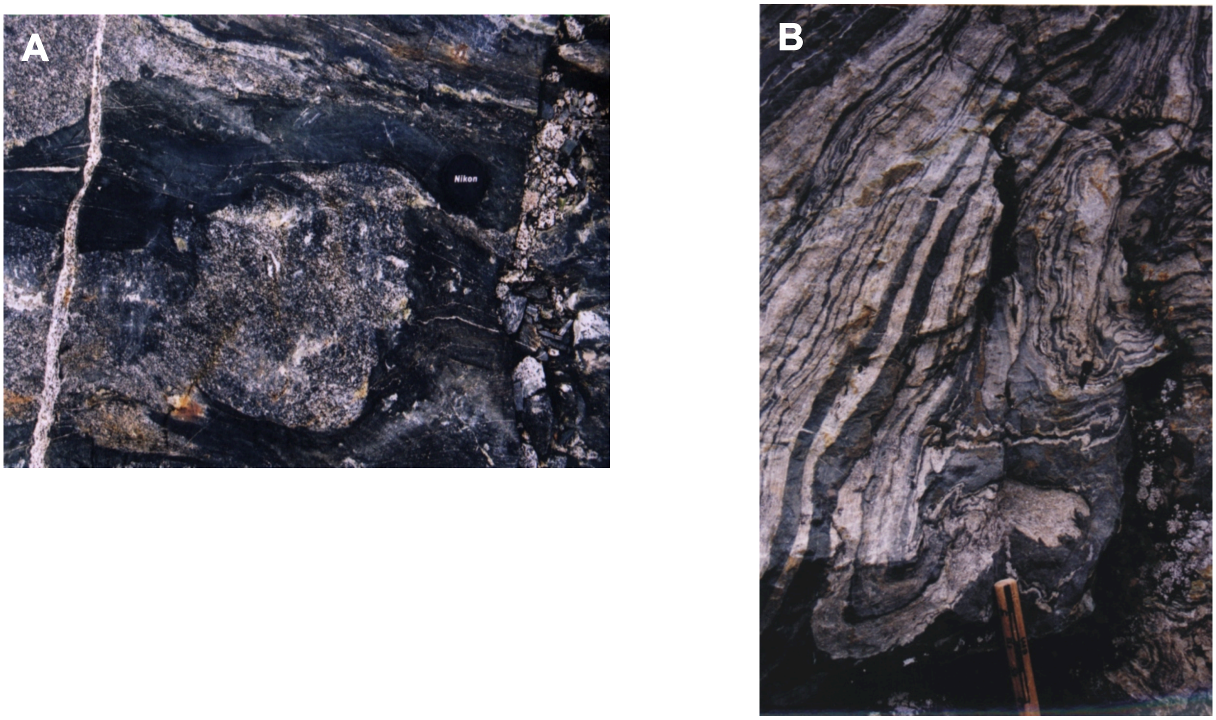

Figure 2.4. A) Lobate and cuspate margins exhibited by the syn-tectonic Tenas Lake pluton. Pluton cross-cuts foliation and is also drawn into and deformed along foliation planes. B) D_2 northeast verging folds developed in dykes that can be traced into the syn-tectonic Pandemonium Pass pluton. Note the lobate and cuspate morphology of the dyke suggesting it was still very hot when folded. View looking west.

gneisses and migmatites that make up the core of the complex (Fig. 2.2). A several meter thick mylonite defines the structural base of the pluton. Deformation within the Elbow Lake pluton decreases upwards away from the mylonite zone. Analyses of zircons from the Elbow Lake pluton result in an interpreted crystallization U-Pb age of approximately 185 Ma.

The Success Lakes pluton is located in the southwestern part of the study area where it is separated from the Atnarko complex by the Talchako fault (Fig. 2.2). The pluton is a variably deformed hornblende-biotite-quartz-diorite that is cut by numerous mafic dykes and epidote veins. van der Heyden (1991, 2004) reports a U-Pb zircon age of 157 ± 11 Ma interpreted to be the crystallization age of the Success Lakes pluton.

The Echo Lake pluton crops out in the northern portion of the Atnarko complex where it is in faulted contact with gneisses and the Atnarko assemblage and in intrusive contact with metavolcanic and metasedimentary rocks of the Atnarko assemblage (Fig. 2.2). Locally the pluton contains large xenoliths of gneissic and mylonitic country rock. The Echo Lake pluton is variably deformed, displaying intense deformation along its faulted margins. An approximate crystallization age of 143 Ma for the pluton is based on U-Pb analyses of zircon (see Chapter 3).

The Mount Marvin pluton forms the northern extent of the Atnarko complex (Fig. 2.2). It is a strongly foliated to gneissic tonalite to granodiorite that is thrust northward over similar rocks that are less deformed (van der Heyden, 1991). A U-Pb zircon age of 129 Ma reported by van der Heyden (1991, 2004) is interpreted to be the crystallization age of the Mount Marvin pluton.

The Molly Lake pluton is similar to the Mount Marvin pluton and it is difficult to distinguish between the two in the field. The Molly Lake pluton is a small body found in the northern portion of the complex; however it is likely part of a much larger body found to the east described by van der Heyden (1994) and Tipper (Tipper, 1969). van der Heyden (1991; 2004) describes the structures within the pluton as syn-intrusive. Although physically similar and spatially associated with the Mount Marvin pluton, the Molly Lake pluton is significantly younger with an age of ca. 115 Ma (van der Heyden, 1991; 2004).

The Pandemonium Pass pluton is located in the southern part of the Atnarko complex. It crops out as tongues several hundred meters wide that are topographically higher, yet continuous with, a much larger exposure in the valley bottom suggesting the pluton is quite large at depth. The Pandemonium Pass pluton is syn-tectonic with respect to north-northeast verging folds and thrusts (Fig. 2.4). A foliation is developed along the margins of the pluton but is absent only a short distance away from the country rock. Dykes and sills off the main body intrude along the foliation developed in the country rock and are folded along with the foliation. Brecciation of the wall rock at the contact with the Pandemonium Pass pluton is common. The age of the pluton is ca. 80 Ma based on U-Pb and Ar/Ar analyses of zircon and biotite respectively (see Chapter 3).

Latest Cretaceous to Paleocene medium-to fine-grained hornblende-biotite tonalites to granodiorites that crop out throughout the Atnarko complex include the Junker Lake pluton (65.2 ± 0.3 Ma (van der Heyden, 2004), the Ptarmigan Lake pluton, 58 Ma (see Chapter 3) and an unnamed 63.3 ± 0.3 Ma (van der Heyden, 2004) pluton near the Talchako glacier in the south part of the study area (Fig. 2.2). These plutons show no evidence of ductile deformation and cross-cut all ductile features in the host rocks. Each body contains some evidence of brittle deformation ranging from small micro-fractures to large brittle shears.

Structural Geology

In the south the Atnarko complex is characterized by northwest striking, moderately to steeply east-northeast dipping, foliations. In the north, foliations strike northeast and dip to the north-northwest and south-southeast. The main structural geometries and data are displayed in figures 2.2, 2.5 and 2.6.

Several deformation events affected the Atnarko complex. The style and intensity of these events varies from south to north and are discussed below from oldest to youngest, beginning

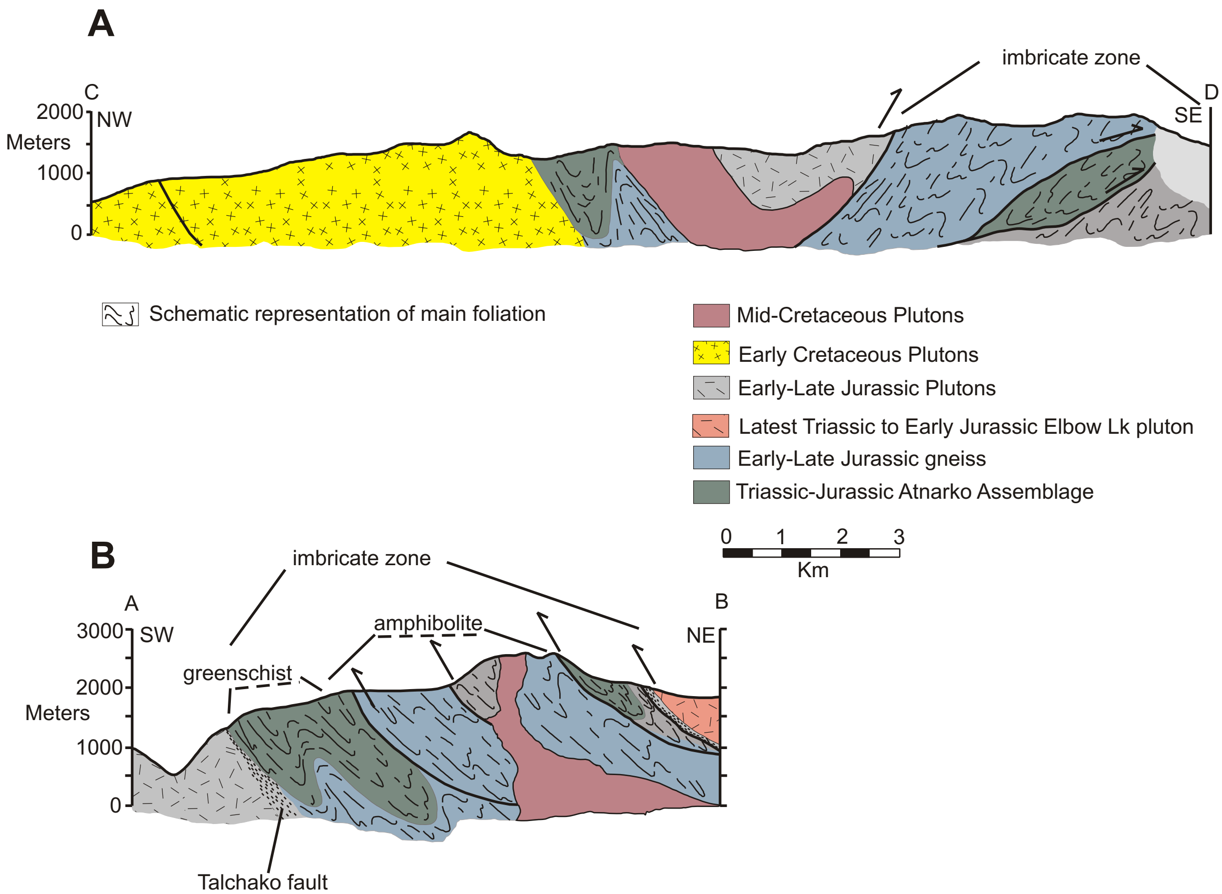

Figure 2.5. Schematic geologic cross-sections from the Atnarko complex. (A) The southern Atnarko and (B) the northern Atnarko. Location of cross-section lines shown on Figure 2.

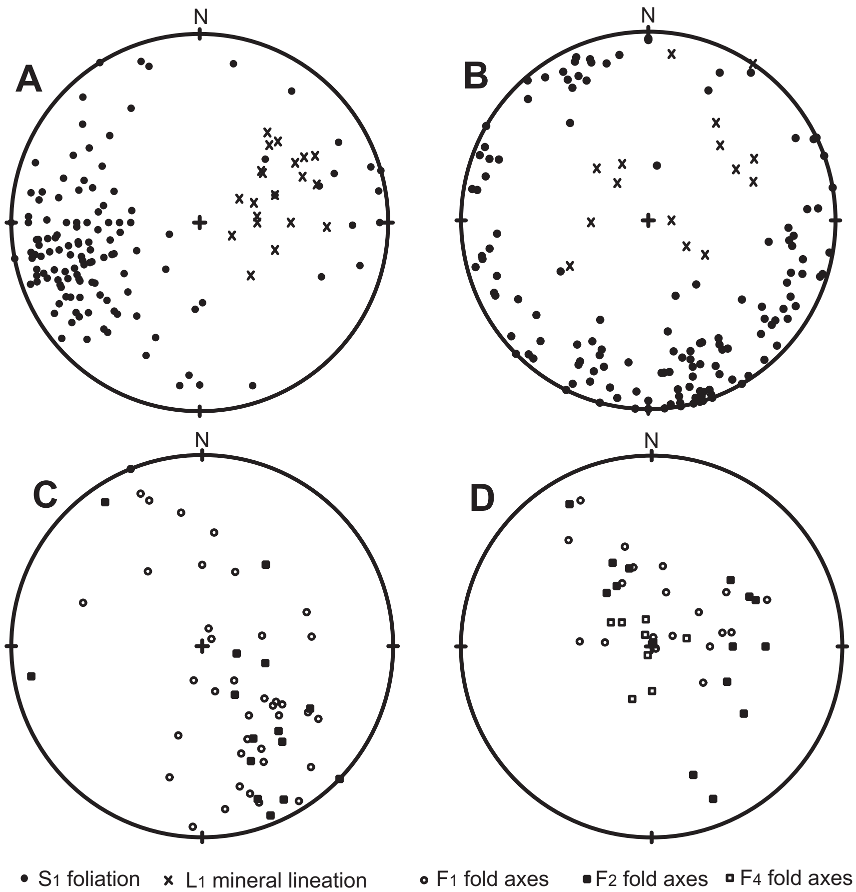

Figure 2.6. Equal area, lower hemisphere stereoplots of (A) S_1 foliations and L_1 mineral lineations in the southern Atnarko complex. (B) S_1 foliations and L_1 mineral lineations in the northern Atnarko complex. (C) F_1 and F_2 fold axes in the southern Atnarko complex. (D) F_1 to F_4 fold axes in the northern Atnarko complex.

with Early Cretaceous deformation. An older, poorly defined pre-Early Cretaceous deformation event is recognized but not discussed here. Evidence for this older event includes apparent syn-tectonic features in the earliest Jurassic Tenas Lake pluton and xenoliths of strongly deformed rock within the ca. 143 Ma Echo Lake pluton.

Phase 1 (D_1) southwest directed compression

Compositional layering and transposed layering define the main foliation within the Atnarko assemblage. This foliation is termed S_1 and strikes northwest in the south and east-northeast in the north (Fig. 2.6A, B). In the south, a structural stack of units within a 5 km wide imbricate zone that has gneisses and migmatites thrust over rocks of the Atnarko assemblage is interpreted as resulting from the D_1 event (Fig. 2.5). Northwest striking mylonitic shear zones within the imbricate stack are moderately to steeply dipping and separate underlying rocks of the Atnarko assemblage from hangingwall gneisses and migmatites. This arrangement defines an inversion of metamorphic grade across the imbricate zone (Fig. 2.5). Microstructures from mylonites were examined in thin-sections cut parallel to the lineation and perpendicular to the foliation from samples near the top of the imbricate zone and indicate top to the southwest movement (Fig. 2.7A). Structures attributed to D_1 deformation in the north are not as easily discernable as in the south. Structural stacking involving the Atnarko assemblage, gneisses and migmatites is present; however, contacts between the units are obscured by younger plutonic bodies. D_1 shear zones are northwest and west striking with moderate to steep dips to the northeast and north respectively.

D_1 deformation includes folding and formation of the transposed S_1 foliation. Refolding of S_1 during D_1 progressive deformation resulted in Type III interference patterns (Fig. 2.7D). F_1 folds in the southern Atnarko plunge northwest and southeast and are overturned to the west-southwest. Overturned limbs are commonly sheared off indicating tops to the west-southwest. In the northern Atnarko complex F_1 folds plunge moderately to steeply northeast and northwest, are

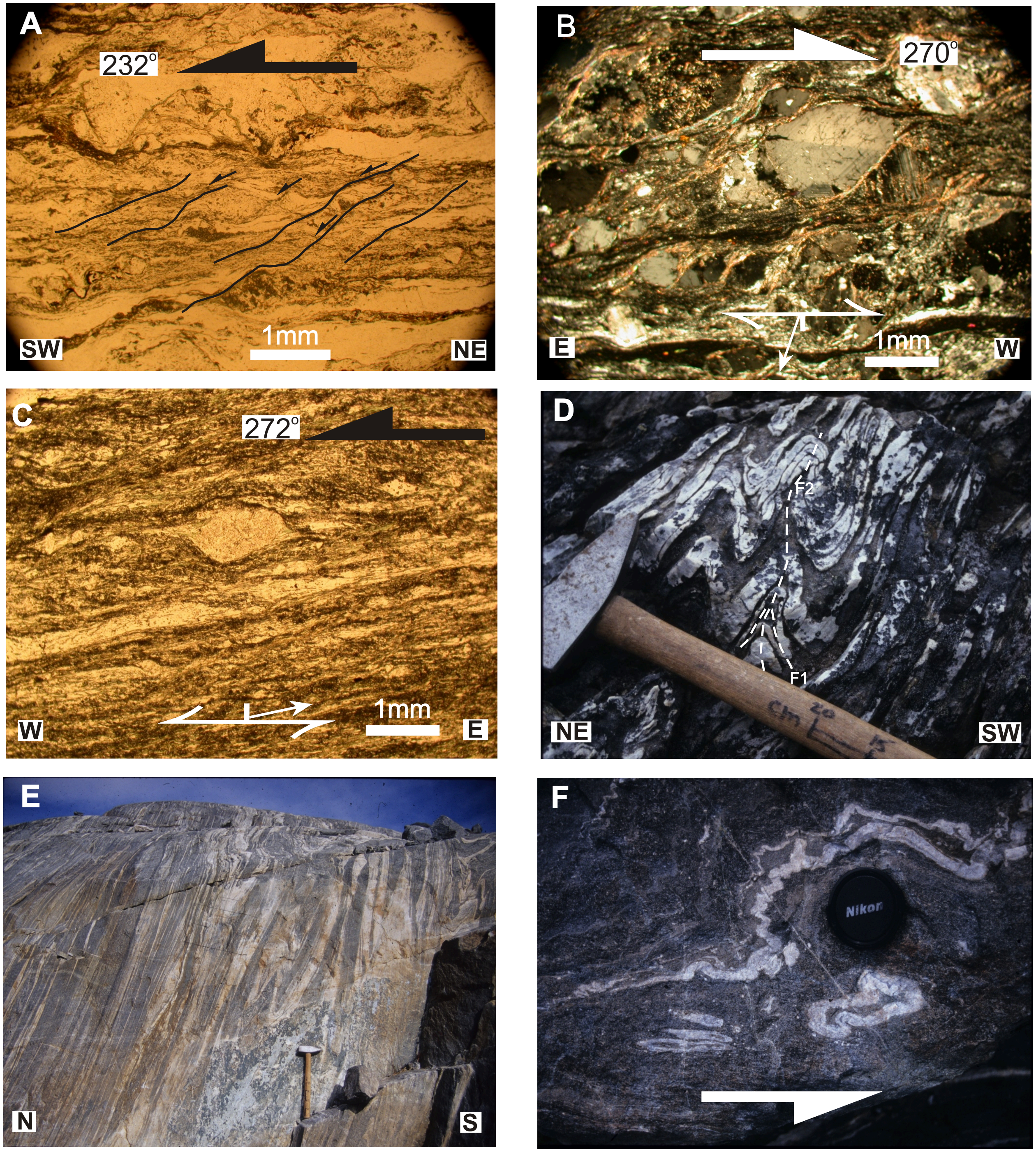

Figure 2.7. (A) Mylonite within the Elbow Lake pluton, fabrics within indicate tops to the west sense of shear. (B) σ-type porphyroclast indicating tops to the west from northwest striking S_1 foliation in the northern Atnarko complex. (C) West-northwest striking S_1 fabric in the northern Atnarko complex with winged porphyroclasts exhibiting tops to the west oblique motion. Foliation and lineation symbols within B and C represent the amount of oblique vs. orthogonal movement. (D) F_1 folds in the southern Atnarko complex, Type III interference patterns visible just above hammer in center of photo. (E) F_1 south verging tight folds in gneissic rocks in the northern Atnarko complex. (F) Sheath folds from the southern Atnarko complex exhibiting a component of sinistral shearing with most movement out of the page (towards southwest). All thin sections are shown parallel to L_1 lineation and perpendicular to S_1 foliation.

tight to isoclinal and verge to the south and southeast (Fig. 2.6D, 2.7E). Rare sheath folds developed in areas of high strain show a component of sinistral shear (Fig. 2.7F).

L_1 mineral lineations are rare (likely due to recrystallization related to flattening during younger deformation) except where preserved within and near large D_1 shear zones. In plutonic bodies L_1 is defined by stretched quartz aggregates; whereas in metavolcanic rocks L_1 is defined by aligned hornblende and/or biotite grains. L_1 lineations in the south trend northeast with shallow to moderate plunges (Fig. 2.6A). In the north the orientation of L_1 lineations plunge shallowly to steeply toward the northeast and southwest with significant scatter (Fig. 2.6B). On northwest to north striking foliations, L_1 plunge down dip. Kinematics indicators imply movement towards the west-southwest. On northeast-southwest striking S_1 foliations, L_1 is shallowly to moderate plunging and related kinematic indicator imply more oblique movement towards the west (Fig. 2.7B, C; Fig. 2.8).

Phase 2 (D_2) north-northeast directed compression

The second phase of deformation in the southern domain is responsible for the development of open, slightly asymmetric north-northeast verging folds and southwest and northeast moderately dipping shear zones that cut across and deform D_1 structures. The majority of D_2 shear zones strike southeast with moderate southwest dips. A subordinate number of shear zones are northwest striking and northeast dipping. These zones are interpreted as D_1 structures that were reactivated as back thrusts during D_2 north-northeast compression. The southwest dipping shear zones range in size from <10 cm to several meters in thickness. Many of the shear zones fold older D_1 fabrics indicating tops to the northeast movement (Fig. 2.9A).

S_2 is locally developed within and near D_2 shear zones and is not a regionally developed foliation. Crenulation of S_1 by F_2 is observed at one locality and the crenulation lineation plunges moderately towards the east-southeast. Locally, cataclastic shear zones characterized by foliated and brecciated gouge define D_2 faults. The fault surfaces contain slickenside fibers and the

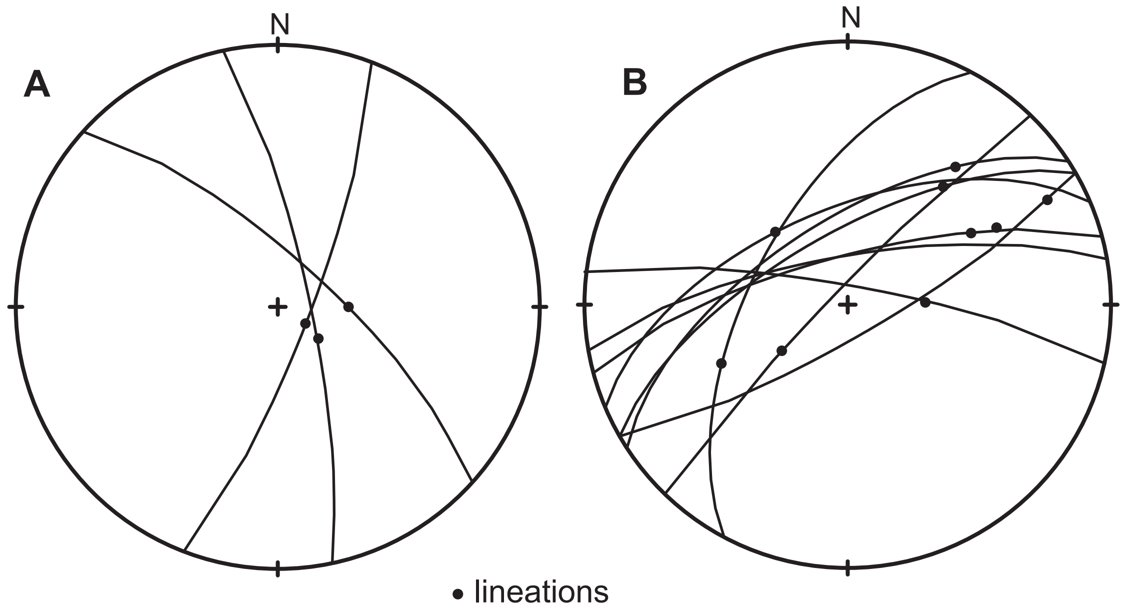

Figure 2.8. Equal area, lower hemisphere stereoplots of (A) Northwest-Northeast S_T foliation with steep down dip L_1 lineations and (B) Northeast-Southwest striking S_T foliations with moderately to shallowly plunging L_1 lineations.

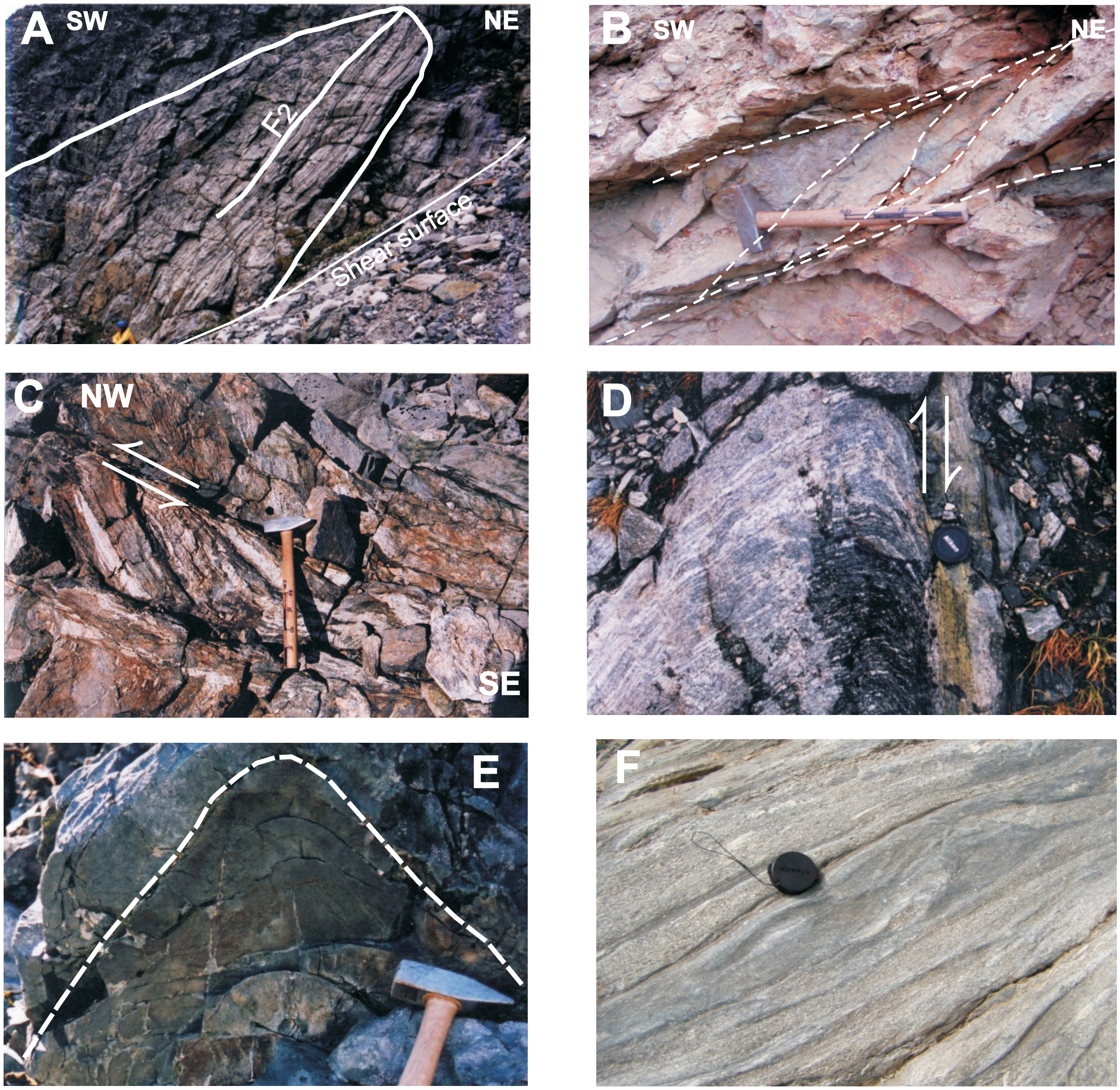

Figure 2.9. (A) Northeast verging D_2 fault with F_2 fold in the hangingwall with lower limb sheared off. (B) Shear fabric developed within the Hotnarko River fault. (C) D_3 sinistral shear zone striking northwest exhibiting ductile/brittle features. (D) D_3 dextral mylonite developed in gneisses, S_1 being folded into mylonite zone, top of photo towards north. (E) Steeply plunging F_4 folds developed in metavolcanic rocks in the northern Atnarko complex. (F) Mylonitic foliation within quartz diorite defining the Talchako fault zone.

geometry of horses developed within the damage zones suggest top to the northeast movement. F_2 folds developed during D_2 trend southeast and northwest with moderate to shallow plunges (Fig. 2.6C). These folds are open and have wavelengths less than one metre. Folds near D_2 shear zones are tighter, verge northeast to north, and commonly have sheared off overturned limbs. In the northern Atnarko complex, F_2 folds are open to closed with shallow to moderate plunges towards the northwest and southeast (Fig. 2.6D). The difference in orientation in F_2 folds from south to north is attributed to overprinting younger deformation. The largest of the D_2 structures, here named the Hotnarko River thrust, located in the northern most Atnarko complex, is a zone several meters wide that strikes to the east-southeast and dips shallowly to moderately to the south-southwest with well developed shear fabrics indicating top to the northeast shear (Figs. 2.2; 2.9B). The fault places strongly metamorphosed and deformed Atnarko assemblage over moderately deformed and metamorphosed plutonic rocks (Fig. 2.2). van der Heyden (1991) infers this fault to continue towards the west across the northern extent of the Atnarko complex (Fig. 2.2).

L_2 lineations, typically composed of stretched quartz grains or aligned hornblende, are only developed within D_2 shear zones, and are oblique to down dip plunging.

Phase 3 (D_3) high angle ductile/brittle shearing

Mylonitic shear zones cross-cut and deform S_1 foliation. The mylonites range in width from less than 10 cm to over several meters. Kinematic indicators such as drag folds of S_1, intrafolial folds and winged σ-type porphyroclasts indicate sinistral and dextral motion (Fig. 2.9C, D). Sinistral shear zones are vertical to steeply dipping and strike west-northwest. Dextral shear zones are steeply-to-moderately dipping and strike north-northwest. Some of the observed shear zones have features that are ductile/brittle in nature (Fig. 2.9C).

F_3 folds are restricted to areas near D_3 shear zones, are vertical to steeply plunging and affect S_1 foliation (i.e. drag folds). In the north regional folding of the S_1 foliation occurs as the result of large D_3 shear zones that strike nearly perpendicular to main fabric.

L_3 lineations are rare; however, where observed indicate oblique slip along S_3 foliations. Orientation of lineations coupled with fold vergence, indicate hanging wall up towards the west within sinistral zones and hanging wall up towards the south within dextral shear zones. Several D_3 shear zones that deform S_1 were identified without kinematic indicators.

D4 (D_4) dextral brittle faulting

D_4 four brittle faults and buckle folds cut across all other structures, deform the youngest intrusive rocks in the area and are locally developed. Sheer fabrics along fault zones and folds associated with these fault zones comprise D_3. Faults include large, up to 100 m wide, zones of fractured and altered country rock and smaller fractured and gouge filled zones less than 10 cm wide. The largest observed D_4 faults are dextral and strike northwest with near vertical dips. Numerous smaller faults have been identified with apparent sinistral offset as were several moderately dipping reverse and normal faults. No significant offsets were observed along any of the D_4 faults identified. Discrete fractures are ubiquitous in the north and are locally filled with quartz and epidote. Ductile shear zone fabrics are commonly overprinted by fractures and fault gouge indicating earlier formed ductile shear zones have been reactivated during brittle deformation. F_4 folds are steeply plunging towards the north-northwest, are open to closed in form and are only locally developed (Figs. 2.6D, 2.9E).

The Talchako Fault

The Talchako fault is located along the Talchako River valley and defines the western margin of the Atnarko complex (Fig. 2.2). The fault is defined by a mylonitized diorite containing a north-northwest striking foliation (Fig. 2.9F). The fault follows the Talchako River valley from the Bella Coola River, south to Ape Creek where it is intruded by a latest Cretaceous pluton.

South of the pluton the fault is mapped as a moderately to steeply dipping mylonite zone that separates the Success Lakes pluton and metavolcanic and metasedimentary rocks of the Atnarko assemblage (Fig. 2.2). The Talchako fault remained active as a mylonitic, ductile shear zone until at least the onset of D4 brittle deformation (see discussion). van der Heyden (1991; 1990) interpreted the Talchako fault as a major brittle feature that accommodated both dextral strike-slip and top to the west normal motion. A multitude of brittle faults that splay off the northern portion of the fault (Israel and van der Heyden, 2006), are interpreted as reactivation features that occurred in Tertiary. Timing and kinematics of movement along the Talchako are discussed later in the chapter in the context of regional geologic relationships.

Metamorphism

Metasedimentary and mafic metavolcanic rocks of the Atnarko assemblage and associated gneisses lack the critical metamorphic minerals (e.g. aluminosilicates) needed to assess the metamorphic conditions. Peak metamorphic conditions (M_1) coincide with D_1 deformation on the basis of the following observations: 1) S_1 foliations within the highest-grade portions of the complex are defined by hornblende and plagioclase with stringers of recrystalized quartz (Fig. 2.10A); 2) the main foliation in gneisses is generally characterized by hornblende, biotite, plagioclase, quartz ± muscovite and recrystallization of feldspar is common (Fig. 2.10B); and 3) partial melt structures are common in the amphibolites (Fig. 2.10C). These characteristics indicate relatively high temperatures during D_1 deformation. Recrystallization of feldspar occurs at temperatures above 500^{o}C (Passchier and Trouw, 1996) and although partial melting of amphibolite occurs over a wide range of temperatures and pressures, at least 650^{o}C is needed to produce even the smallest percentage of melt (Rushmer, 1991).

Pressure within the Atnarko complex during M_1 metamorphism is also not well constrained. Assuming an average geothermal gradient within active arcs of ~30^{o}C/km (Rothstein and

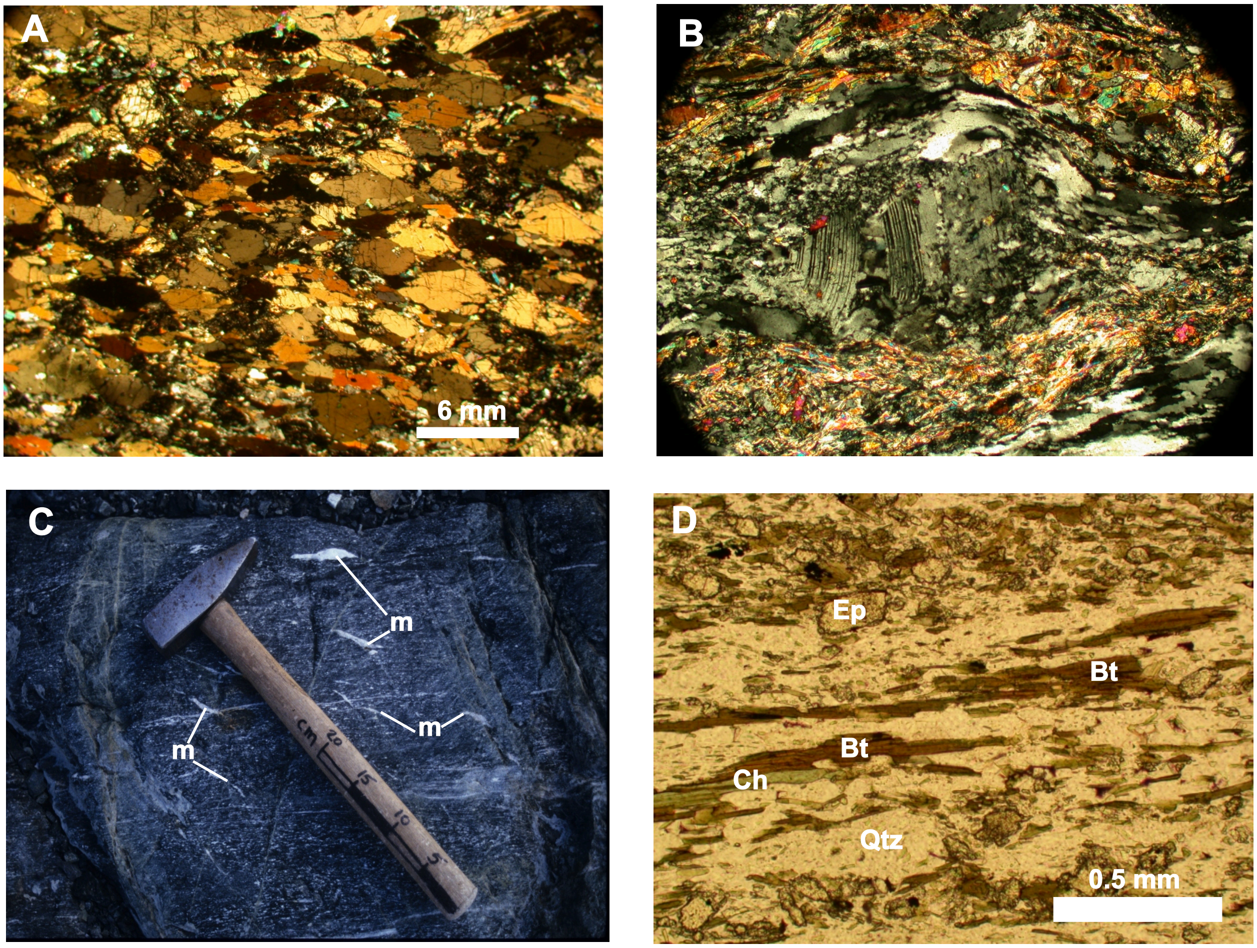

Figure 2.10. (A) S_1 fabric defined by hornblende in sample from imbricate zone in the southern domain. (B) Recrystallized quartz (ribbons) and plagioclase (small crystals surrounding relict grain in middle of image). (C) Leucocratic pockets interpreted as previous melt (m) within amphibolite from the southern Atnarko complex. (D) Greenschist facies metasedimentary rock from the Atnarko complex. Ep-Epidote, Bt-Biotite, Ch-Chlorite.

Manning, 2003) then the pressure associated with a peak metamorphic temperature of 650^{o}C would have been on the order of 7-8 kbars.

Within the lower grade rocks, foliations are defined by biotite, epidote and chlorite (Fig. 2.10D). Minor amounts of hornblende occur nearest to structurally overlying gneisses. The presence of hornblende implies the lower grade rocks reached a metamorphic grade of upper greenschist to lower amphibolite during D_1 where juxtaposed with structurally overlying higher grade metamorphic rocks.

All younger structural events are interpreted to have occurred under lower metamorphic conditions. Replacement of hornblende by biotite and biotite by chlorite occurs throughout the complex, and is interpreted as passive replacement during slow exhumation which accompanied thrusting and uplift due to erosion.

TIMING OF STRUCTURES AND METAMORPHISM

Absolute and relative ages of syn-kinematic and post-kinematic plutons and cooling ages from hornblende and biotite are used to constrain timing of structural and metamorphic events (Figure 2.11).

Timing of D_1

In the south, the hanging wall of the uppermost D_1 thrust sheet consists of the ca. 200 Ma Elbow Lake pluton (Figure 2.2). S_1 foliations are developed along the margin of the pluton where it is thrust over rocks of the Atnarko assemblage. $^{40}Ar/^{39}Ar$ analyses of the hornblende that defines the foliation indicate that cooling through ~560^{o}C occurred at 117.5 ± 1.7 Ma (sample 01-SIS-46; Fig. 2.12; Table 2.1). In the north, D_1 foliations and faults are developed within the 129 Ma Mount Marvin pluton and the 115 Ma Molly Lake pluton. Cooling of hornblende, which defines the foliation within the Mount Marvin pluton, occurred at 117.8 ± 0.8 Ma (sample 01-SIS-20c; Fig. 2.12; Table 2.1). This age overlaps with the cooling age of hornblende in the south, indicating that D_1 deformation was well underway by 117 Ma. van der Heyden (1990, 2004)

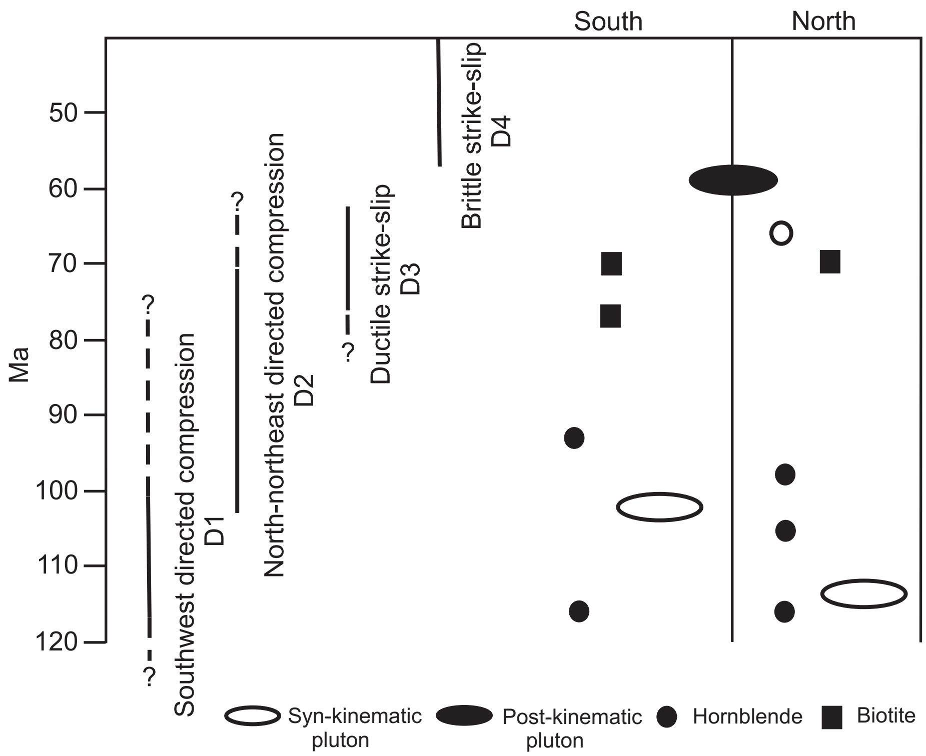

Figure 2.11. Relative timing of structural events within the Atnarko complex. Hornblende and biotite cooling ages record uplift of the northern and southern portions of the complex and syn- to post-kinematic plutons indicate upper and lower ages of deformation. See text for details.

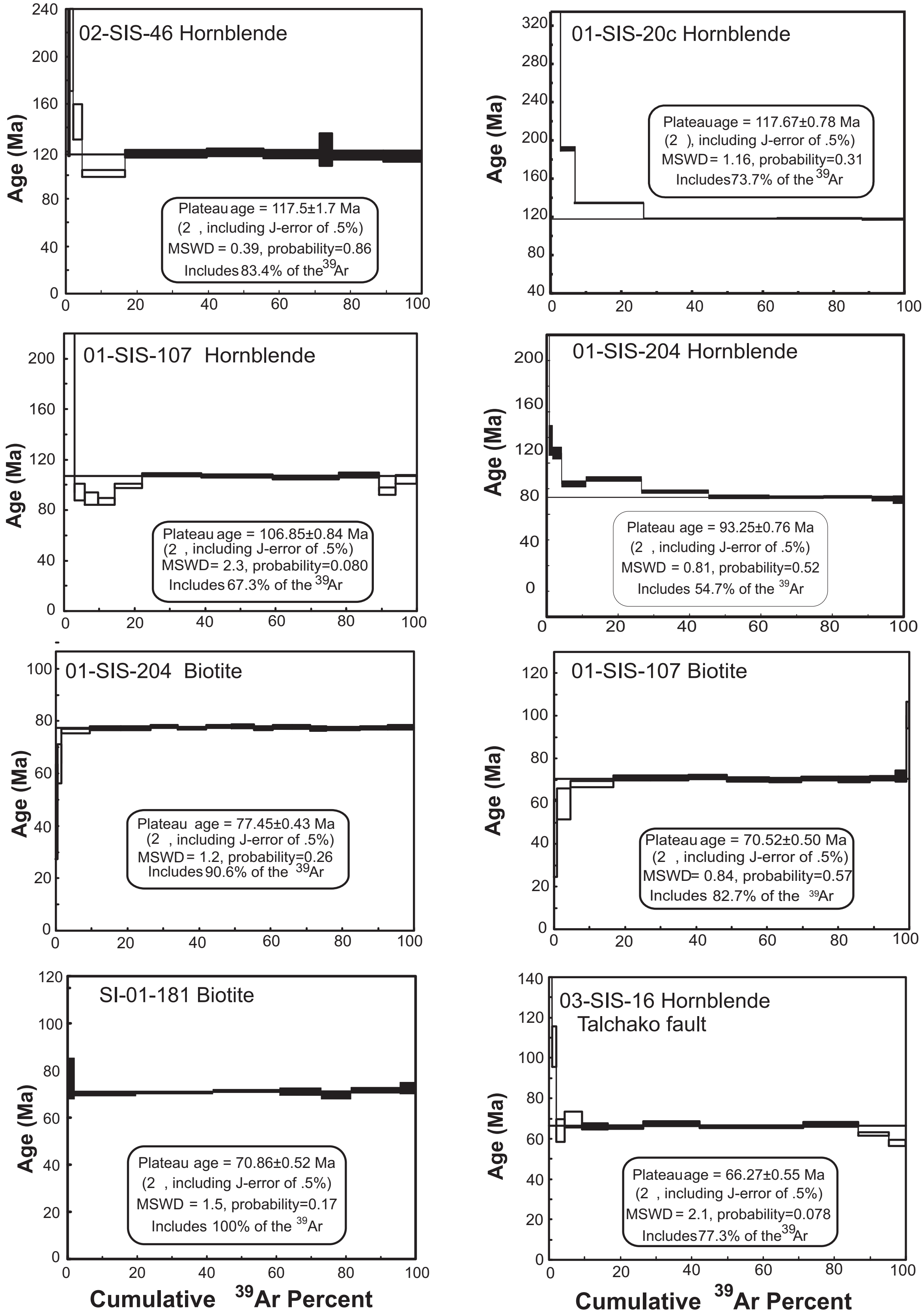

Figure 2.12. Ar release spectra for step-heating analyses of biotite and hornblende from the Atnarko complex. Box heights represent 2σ errors. Plateau steps are filled, rejected steps are open. Ar-Ar data are presented in Table 2.1

Table 2.1 ^{40}Ar-^{39}Ar age data for hornblende and biotite from the Atnarko complex.

Laser[1] Power (%)	Isotope Ratios									
	$^{40}Ar/^{39}Ar$	$^{38}Ar/^{39}Ar$	$^{37}Ar/^{39}Ar$	$^{36}Ar/^{39}Ar$	Ca/K	Cl/K	%^{40}Ar	%^{39}Ar	$^{40}Ar^*/^{39}Ar_K$	Age±2σ
02-SIS-46, hornblende, J = 0.009734±0.000018; volume ^{39}ArK = 274.29 x 10^{-10} cm^3, integrated age 125.33±1.81 Ma (2σ)										
2	349.826±0.028	0.196±0.143	2.884±0.041	0.768±0.058	25.278	0.009	63.91	0.31	126.906±12.149	1451.17±95.44
2.4	132.114 0.032	0.082 0.215	3.872 0.049	0.325 0.084	33.964	0.002	71.16	0.3	38.332 7.739	572.06 98.97
2.6	72.504 0.042	0.060 0.285	3.294 0.047	0.214 0.076	28.88	0.001	85.14	0.49	10.833 4.082	180.86 64.85
2.9	55.582 0.029	0.046 0.242	2.597 0.035	0.144 0.100	22.757	0.001	74.49	0.94	14.245 4.133	234.27 63.74
3.2	26.458 0.014	0.028 0.207	4.040 0.025	0.065 0.047	35.446	0	67.79	2.54	8.572 0.906	144.58 14.69
3.5	9.730 0.012	0.019 0.046	4.505 0.016	0.017 0.032	39.542	0	39.51	12.02	5.921 0.180	101.09 2.98
3.8	8.095 0.016	0.019 0.041	7.191 0.017	0.011 0.049	63.266	0.001	15.02	23.11	6.938 0.198	117.89 3.25
4.1	8.395 0.016	0.021 0.063	8.167 0.018	0.012 0.041	71.91	0.001	17.52	15.81	6.988 0.189	118.73 3.12
4.4	7.472 0.011	0.020 0.049	7.636 0.015	0.009 0.074	67.206	0.001	8.31	15.71	6.911 0.209	117.46 3.44
4.7	12.355 0.017	0.024 0.123	6.058 0.020	0.023 0.119	53.24	0.001	42.72	3.61	7.130 0.836	121.05 13.74
5	7.814 0.010	0.020 0.053	7.126 0.016	0.010 0.072	62.686	0.001	13.05	14.46	6.851 0.222	116.47 3.65
5.3	7.721 0.014	0.020 0.052	7.238 0.018	0.010 0.088	63.681	0.001	12.67	10.69	6.800 0.273	115.63 4.50
01-SIS-20c,hornblende, J =0.005390±0.000006, volume ^{39}ArK = 428.73 x 10^{-10} cm^3, intergrated age 147.16±0.57 Ma (2σ)										
2	303.704±0.014	0.359±0.065	0.409±0.068	0.447±0.039	2.698	0.06	38.59	0.23	188.072±5.730	1262.82±27.67
2.4	264.010 0.011	0.287 0.033	0.280 0.048	0.292 0.024	2.016	0.05	30.75	0.74	182.992 2.831	1238.12 13.86
2.8	88.422 0.009	0.128 0.039	0.178 0.032	0.095 0.023	1.315	0.022	29.39	1.85	61.928 0.850	519.62 6.19
3.2	29.776 0.005	0.190 0.015	0.649 0.019	0.034 0.026	5.045	0.039	29.57	4.08	20.679 0.287	190.65 2.51
3.6	17.116 0.005	0.295 0.011	1.196 0.015	0.011 0.024	9.351	0.065	15.99	19.4	14.308 0.108	134.03 0.98
4	14.312 0.005	0.312 0.011	1.221 0.013	0.008 0.024	9.546	0.069	12.38	37.71	12.501 0.082	117.64 0.75
4.4	14.241 0.006	0.324 0.011	1.192 0.013	0.008 0.020	9.502	0.071	11.5	24.02	12.540 0.088	118.00 0.80
4.8	14.052 0.010	0.299 0.015	1.141 0.019	0.008 0.037	9.094	0.065	10.77	11.97	12.407 0.152	116.79 1.38
02-SIS-107, hornblende, J = 0.009736±0.000020, volume ^{39}ArK = 794.97 x 10^{-10} cm^3, intergrated age 113.51±0.78 (2σ)										
2	164.678±0.021	0.091±0.087	0.354±0.047	0.269±0.062	3.246	0.006	47.68	0.42	86.419±4.989	1101.42±47.59
2.2	42.389 0.013	0.032 0.177	0.195 0.049	0.082 0.059	1.792	0.001	56.3	0.78	18.574 1.427	299.88 21.23
2.4	16.407 0.007	0.022 0.148	0.139 0.036	-0.000 5.668	1.279	0.002	-0.24	1.7	16.488 0.522	268.59 7.91
2.6	11.267 0.013	0.018 0.094	0.138 0.027	0.020 0.068	1.265	0	51.34	2.9	5.494 0.402	94.01 6.70
2.8	9.110 0.011	0.018 0.090	0.199 0.017	0.014 0.068	1.83	0	43.12	3.84	5.193 0.280	88.98 4.68
3	7.688 0.008	0.015 0.058	0.469 0.018	0.009 0.051	4.313	0	34.28	4.67	5.064 0.148	86.83 2.48
3.2	7.425 0.007	0.015 0.026	1.198 0.016	0.007 0.048	11.021	0	22.29	7.86	5.788 0.106	98.90 1.77
3.4	7.053 0.006	0.015 0.034	1.880 0.014	0.004 0.051	17.301	0	10.55	16.71	6.333 0.078	107.94 1.29
3.6	6.931 0.005	0.015 0.034	1.543 0.013	0.004 0.046	14.204	0	9.97	20.29	6.262 0.061	106.77 1.01
3.8	6.829 0.005	0.015 0.038	1.423 0.013	0.004 0.066	12.956	0	9.58	18.71	6.195 0.077	105.66 1.28
4	7.223 0.006	0.015 0.036	1.681 0.014	0.005 0.084	15.312	0	12.98	11.54	6.307 0.125	107.52 2.07
4.2	6.170 0.008	0.014 0.046	1.256 0.015	0.003 0.178	11.435	0	10.34	4.61	5.549 0.183	94.92 3.04
4.6	6.630 0.007	0.015 0.050	1.811 0.014	0.004 0.184	16.5	0	8.44	5.98	6.092 0.201	103.96 3.33
01-SIS-204,hornblende, J =0.009734±0.000018, volume ^{39}ArK = 1283.4 x 10^{-10} cm^3, intergrated age 107.62±0.71 Ma (2σ)										
2	310.868±0.018	0.132±0.057	0.356±0.043	0.497±0.040	3.116	0.006	46.7	0.21	166.197±6.147	1736.11±41.24
2.3	155.701 0.020	0.071 0.122	0.341 0.046	0.244 0.051	2.98	0.003	45.69	0.22	84.812 3.798	1085.86 36.53
2.6	39.979 0.015	0.032 0.154	0.252 0.051	0.082 0.084	2.206	0	59.98	0.44	16.044 2.034	261.80 30.90
2.9	17.319 0.013	0.021 0.078	0.220 0.031	0.032 0.076	1.924	0	53.09	0.97	8.143 0.717	137.62 11.67
3.2	13.633 0.010	0.018 0.104	0.612 0.019	0.021 0.044	5.351	0	44.88	2.45	7.535 0.287	127.70 4.69
3.5	8.573 0.006	0.017 0.028	1.185 0.014	0.010 0.049	10.372	0	29.37	6.77	6.074 0.145	103.62 2.41
3.8	7.205 0.013	0.016 0.034	1.802 0.019	0.005 0.051	15.78	0	12.75	15.61	6.308 0.115	107.52 1.91
4.1	6.150 0.012	0.017 0.033	2.110 0.017	0.003 0.051	18.482	0	7.53	18.66	5.709 0.089	97.57 1.49
4.4	5.696 0.012	0.017 0.026	2.206 0.017	0.003 0.068	19.324	0	4.37	16.98	5.469 0.088	93.56 1.47
4.7	5.704 0.009	0.016 0.033	1.842 0.015	0.003 0.044	16.131	0	4.73	15.07	5.453 0.061	93.31 1.01
5	5.853 0.006	0.016 0.024	1.524 0.013	0.003 0.067	13.45	0	6.87	13.55	5.468 0.063	93.56 1.05
5.3	5.802 0.007	0.016 0.020	1.882 0.014	0.003 0.116	16.625	0	7.5	5.89	5.386 0.117	92.20 1.95
5.6	5.903 0.007	0.015 0.067	1.697 0.015	0.004 0.171	14.992	0	9.9	3.19	5.337 0.183	91.36 3.05
01-SIS-204,biotite, J =0.009729±0.000016, volume ^{39}ArK = 3296.04 x 10^{-10} cm^3, intergrated age 77.01±0.27 Ma (2σ)										
2	52.604±0.012	0.045±0.098	0.036±0.062	0.171±0.024	0.321	0	95.03	0.44	2.619±1.054	45.39±18.04
2.2	10.094 0.006	0.018 0.072	0.010 0.065	0.022 0.068	0.091	0	63.54	1.02	3.685 0.443	63.55 7.50
2.4	5.443 0.006	0.014 0.028	0.005 0.041	0.004 0.042	0.043	0	18.84	7.92	4.425 0.053	76.05 0.88
2.6	5.092 0.008	0.013 0.026	0.004 0.046	0.002 0.044	0.036	0	11.88	8.72	4.494 0.045	77.21 0.76
2.7	4.882 0.006	0.013 0.039	0.003 0.042	0.001 0.073	0.031	0	8.18	8.27	4.491 0.039	77.15 0.66
2.8	4.817 0.005	0.013 0.033	0.004 0.027	0.001 0.077	0.035	0	6.11	7.68	4.530 0.032	77.82 0.54
2.9	4.753 0.005	0.013 0.023	0.004 0.051	0.001 0.084	0.039	0	5.7	7.93	4.490 0.032	77.13 0.53
3	4.799 0.004	0.013 0.035	0.005 0.062	0.001 0.088	0.043	0	5.61	7.08	4.538 0.032	77.94 0.53
3.1	4.801 0.005	0.013 0.019	0.006 0.059	0.001 0.110	0.049	0	5.69	6.3	4.535 0.039	77.90 0.66
3.2	4.787 0.007	0.013 0.031	0.007 0.042	0.001 0.105	0.061	0	6.4	5.33	4.488 0.045	77.11 0.76
3.3	4.824 0.006	0.013 0.023	0.007 0.032	0.001 0.107	0.066	0	6.38	5.29	4.524 0.045	77.71 0.75
3.4	4.810 0.007	0.013 0.031	0.009 0.045	0.001 0.095	0.08	0	6.29	5.08	4.515 0.043	77.56 0.73

continuation of Table 2.1. ^{40}Ar-^{39}Ar age data for hornblende and biotite from the Atnarko complex

3.5	4.788 0.007	0.013 0.017	0.010 0.028	0.001 0.098	0.091	0	6.51	4.52	4.484 0.045	77.03 0.76
3.6	4.750 0.008	0.013 0.023	0.011 0.023	0.001 0.047	0.098	0	5.8	9.43	4.482 0.039	77.00 0.66
3.8	4.760 0.006	0.013 0.026	0.014 0.025	0.001 0.103	0.125	0	5.66	7.68	4.498 0.040	77.27 0.68
4	4.784 0.008	0.013 0.022	0.025 0.031	0.001 0.104	0.222	0	5.83	7.3	4.513 0.048	77.53 0.81
01-SIS-107,biotite, J =0.009734±0.000018, volume ^{39}ArK = 1413.64 x 10^{-10} cm^3, intergrated age69.82±0.50 Ma (2σ)										
2	31.179±0.010	0.030±0.146	0.092±0.029	0.098±0.037	0.828	-0.001	92.15	0.67	2.451±1.057	42.54±18.13
2.3	11.115 0.005	0.018 0.068	0.033 0.039	0.027 0.054	0.296	0	69.54	3.88	3.390 0.427	58.58 7.26
2.6	7.111 0.005	0.015 0.029	0.022 0.021	0.011 0.024	0.2	0	44.72	12.04	3.938 0.081	67.86 1.37
2.8	5.860 0.006	0.014 0.037	0.027 0.029	0.006 0.036	0.239	0	29.93	10.66	4.113 0.069	70.83 1.16
3	5.176 0.006	0.014 0.037	0.030 0.032	0.004 0.060	0.27	0	20.66	10.63	4.114 0.071	70.83 1.20
3.2	5.019 0.006	0.014 0.026	0.026 0.033	0.003 0.059	0.232	0	17.63	10.87	4.141 0.059	71.29 0.99
3.4	4.725 0.006	0.013 0.040	0.025 0.025	0.002 0.076	0.223	0	13.99	11.86	4.071 0.058	70.11 0.98
3.6	4.640 0.006	0.013 0.033	0.026 0.033	0.002 0.082	0.231	0	12.71	8.94	4.057 0.056	69.88 0.94
3.8	4.679 0.006	0.013 0.042	0.029 0.019	0.002 0.074	0.262	0	12.75	10.64	4.090 0.052	70.43 0.89
4.1	4.610 0.005	0.014 0.033	0.046 0.021	0.002 0.127	0.412	0	11.78	8.67	4.073 0.074	70.15 1.26
4.4	4.680 0.007	0.013 0.049	0.070 0.030	0.002 0.082	0.626	0	12.53	7.32	4.101 0.059	70.62 0.99
4.7	4.991 0.009	0.014 0.065	0.131 0.017	0.003 0.167	1.168	0	16.76	3.08	4.162 0.153	71.64 2.58
5	5.912 0.014	0.016 0.109	0.233 0.035	0.000 3.105	2.081	0	0.9	0.73	5.871 0.371	100.27 6.17
01-SIS-181, biotite, J = 0.005386±0.000006, volume ^{39}ArK = 173.71 x 10^{-10} cm^3, intergrated age 70.95±0.47 Ma (2σ)										
2	17.295±0.011	0.054±0.117	0.058±0.099	0.045±0.068	0.094	0.006	49.38	2.14	8.048±0.947	76.55±8.82
2.3	8.646 0.005	0.054 0.028	0.016 0.075	0.006 0.061	0.081	0.009	12.3	17.61	7.365 0.116	70.18 1.08
2.6	8.171 0.005	0.074 0.022	0.018 0.062	0.004 0.051	0.106	0.014	7	21.98	7.406 0.070	70.56 0.65
2.9	7.905 0.005	0.026 0.038	0.016 0.063	0.003 0.073	0.084	0.003	2.49	19.11	7.481 0.075	71.27 0.70
3.2	7.868 0.006	0.026 0.040	0.019 0.066	0.004 0.144	0.086	0.002	0.92	11.91	7.451 0.174	70.99 1.63
3.5	7.872 0.006	0.028 0.051	0.024 0.079	0.005 0.114	0.101	0.003	1.37	8.56	7.303 0.191	69.60 1.79
4	8.071 0.006	0.026 0.048	0.018 0.076	0.004 0.104	0.087	0.002	3.32	14.03	7.512 0.132	71.56 1.24
4.5	8.623 0.007	0.028 0.115	0.035 0.106	0.010 0.087	0.108	0.002	2.58	4.66	7.607 0.268	72.44 2.50
03-SIS-16, biotite, J = 0.009729±0.000016, volume ^{39}ArK = 881.3 x 10^{-10} cm^3, intergrated age 69.86±0.54 Ma (2σ)										
1.8	125.654±0.027	0.074±0.076	0.653±0.048	0.280±0.056	4.508	0.002	65	0.13	44.125±4.242	644.38±52.09
2	86.528 0.011	0.054 0.121	0.710 0.021	0.178 0.054	4.901	0.002	59.83	0.27	34.866 2.838	526.94 37.20
2.2	35.204 0.014	0.023 0.192	0.572 0.036	0.068 0.077	3.948	-0.001	55.91	0.6	15.566 1.534	254.40 23.39
2.4	14.432 0.014	0.018 0.085	0.625 0.027	0.029 0.072	4.312	0	57.17	1.25	6.196 0.605	105.61 10.01
2.6	7.180 0.008	0.014 0.103	0.877 0.016	0.012 0.089	6.052	-0.001	48.35	2.36	3.717 0.330	64.08 5.58
2.8	5.727 0.008	0.015 0.063	1.751 0.016	0.007 0.110	12.092	0	29.67	4.8	4.040 0.231	69.55 3.91
3	4.754 0.005	0.015 0.036	2.115 0.013	0.005 0.068	14.607	0	19.56	7.28	3.836 0.097	66.10 1.64
3.2	4.530 0.005	0.015 0.020	2.424 0.013	0.004 0.038	16.747	0	16	9.87	3.818 0.052	65.80 0.88
3.4	4.316 0.005	0.016 0.029	2.924 0.013	0.003 0.069	20.214	0	9.49	15.94	3.921 0.073	67.54 1.24
3.6	4.154 0.004	0.015 0.019	2.854 0.013	0.003 0.038	19.727	0	8.22	28.97	3.826 0.040	65.94 0.67
3.8	4.367 0.005	0.016 0.046	3.172 0.013	0.004 0.062	22.116	0	11.05	15.26	3.899 0.074	67.17 1.26
4	3.966 0.006	0.014 0.051	1.927 0.013	0.003 0.062	13.422	0	9.04	8.71	3.618 0.052	62.41 0.89
4.2	3.993 0.006	0.015 0.055	2.003 0.013	0.004 0.078	13.96	0	16.2	4.55	3.356 0.087	57.96 1.48

[1] "<" indicates step used in plateau age calculations, ">'" indicates step used in inverse correlation calculations.

Neutron flux monitors: 24.36 Ma MAC-83 biotite (Sandeman et al. 1999); 28.02 Ma FCs (Renne et al., 1998)

Isotope production ratios: $(^{40}Ar/^{39}Ar)_K$=0.0302, $(^{37}Ar/^{39}Ar)_{Ca}$=1416.4306, $(^{36}Ar/^{39}Ar)_{Ca}$=0.3952, Ca/K=1.83($^{37}Ar_{Ca}/^{39}Ar_K$).

describes the Molly Lake pluton as syn-intrusive with respect to northeast striking foliations, suggesting that deformation related to D_1 continued through 115 Ma. Hornblende that defines S_1 foliation in gneiss in the central portion of the complex has a cooling age of 106.9 ± 0.9 Ma (sample 01-SIS-107; Fig. 2.12; Table 2.1). This age may indicate either continued D_1 uplift of deeper parts of the complex or a resetting of the hornblende by unidentified pluton. Similarly the cooling age of hornblende from the imbricate zone in the southern Atnarko complex at 93.3 ± 0.8 Ma (sample 01-SIS-204; Fig. 2.12; Table 2.1) may indicate resetting of the hornblende or continued deformation. D_1 fabrics and structures are cut by the ca. 80 Ma Pandemonium Pass pluton that is syn-kinematic with respect to D_2.

Timing of D_2

D_2 deformation records a change from southwest to north-northeast directed compression. D_2 folds and north to northeast verging shear zones observed within the ca. 80 Ma syn-tectonic Pandemonium Pass pluton indicate that north-northeast directed compression occurred during the Late Cretaceous. $^{40}Ar/^{39}Ar$ biotite cooling ages of 77.5 ± 0.4 Ma (sample 01-SIS-204, Fig. 2.12, Table 2.1) and 70.5 ± 0.5 Ma (sample 01-SIS-107; Fig. 2.12, Table 2.1) from the southern and northern domains respectively, indicate the entire Atnarko complex was cooled below ~350^{o}C by the Late Cretaceous and that any significant uplift associated with D_2 deformation had ended by this time. These ages also suggest that uplift and cooling in the north-central Atnarko lagged behind the south by at least 7 My.

Timing of D_3

D_3 high strain zones cross-cut D_1 fabrics, occur within the Pandemonium Pass pluton, and are intruded by Late Cretaceous to Eocene plutons. Therefore D_3 is constrained to between 80 and 64 Ma. Biotite collected from foliation within a high strain D_3 shear zone in the southern Atnarko resulted in an $^{40}Ar/^{39}Ar$ cooling age of 70.9 ± 0.5 Ma (sample 01-SIS-181; Fig. 2.12; Table 2.1) indicating cooling of the fabric within the shear zone below 350^{o}C occurred in the latest Cretaceous. The overlap of timing between D2 and D3 is discussed below in more detail.

Timing of D_4

Phase four deformation is post early Paleocene as D4 structures cross-cut 58 Ma dykes of the Ptarmigan Lake pluton. Similar structures cross-cut the ca. 65 Ma Junker Lake pluton (van der Heyden, 2004). The duration of D_4 deformation is not clear, but the deformation must be older than undeformed Miocene basalts that overlie the northeastern most portions of the Atnarko complex.

Timing of M_1

Peak metamorphic conditions (M_1) within the Atnarko complex cannot be directly dated; however, cooling through 560^{o}C in the south and the north occurred by 117 Ma, suggesting that regional amphibolite grade metamorphism ended by this time. Local resetting of hornblende occurs near intruding plutons and within specific sites of deformation (i.e., along the Talchako fault). Cooling through biotite closure temperature (~330^{o}C) occurred by ~30 My later, suggesting slow cooling of the complex throughout Late Cretaceous to Tertiary. Slow cooling is also suggested by the replacement of hornblende by biotite and subsequent chlorite overgrowth. This slow cooling is interpreted as the result of uplift due mainly to compressional tectonics and associated denudation of the orogen.

DISCUSSION

Summary of Atnarko structural evolution

Figure 2.13 illustrates the structural characteristics of the Atnarko complex. Structures related to southwest-west directed thrusting dominate the Atnarko complex. Crystallization ages of syn-tectonic plutons and cooling ages of hornblende indicate that southwest-west directed thrusting began sometime after 129 Ma and continued no later than 80 Ma. A component of sinistral shear is associated with southwest-west directed thrusting indicated by oblique, mainly sinistral,

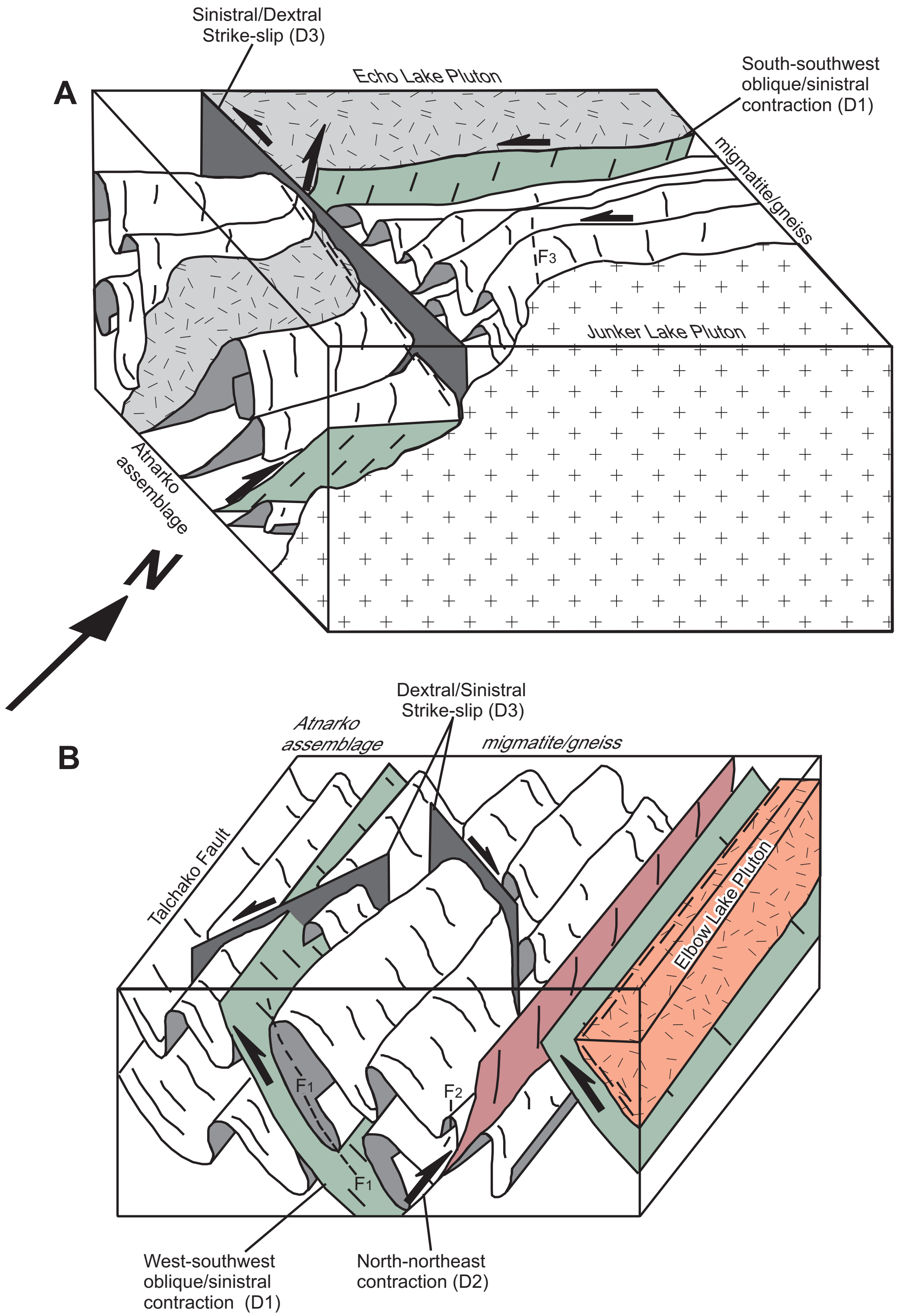

Figure 2.13. Schematic block diagrams illustrating the Early to Late Cretaceous structural relationships of the A) northern Atnarko complex, and B) the southern Atnarko complex. D_4 brittle deformation is not shown on diagrams. North arrow for both diagrams. Note diagrams are meant to show the structures present in the Atnarko complex and their relationships with one another. Some structures shown here are not of sufficient scale to be shown on Figure 2.2.

shearing in the northern Atnarko complex and sinistrally deformed sheath folds and sinistral shear fabrics from the south.

North-northeast directed compression partially overlaps and overprints the southwest-west directed event. North-northeast compression began by at least 80 Ma, as indicated by syn-tectonic plutons (e.g., the Pandemonium Pass pluton), possibly earlier. Uplift and exhumation of the complex through the biotite cooling temperature ended by ~70 Ma. Replacement of higher grade metamorphic minerals by lower grade minerals without appreciable deformation suggests that the exhumation related to thrusting was slow, and, because the compressional deformation appears to be over by ~70 Ma, was likely aided by erosion of the thrust belt.

The overlap in timing of D_3 and D_2 structures is interpreted as being the result of flattening across the Atnarko complex during the waning stages of D_2 compression. Fabrics developed during D_1 and D_2 deformation are steepened during deformation and as a result compression was transferred into almost conjugate steeply-dipping sinistral and dextral D_3 shear zones (Fig. 2.13).

The change in the orientation of S_1 in the north with respect to the south is attributed to three main factors; 1) a stronger development of sinistral shear in the north rather than direct west-southwest compression, as indicated by oblique L_1; 2) intrusion of the Junker Lake pluton (Fig. 2.2) is interpreted to have re-orientated foliations in the country rock (the elongate west-east strike of the pluton may have rotated a portion of the northern complex); and 3) the apparently stronger overprinting of younger deformation found in the north exemplified by more obvious F_3 and F_4 development in the north with respect to the south. It is likely that all these factors played roles in the orientation of structures in the north.

Finally, after the Atnarko complex had cooled below biotite cooling temperatures and intrusion of Late Cretaceous to Early Tertiary plutons, brittle deformation affected the entire area.

Movement on the Talchako fault

Determining the motion along the Talchako fault is key in characterizing the overall tectonic framework of the Atnarko complex. Movement along the Talchako fault occurred between ~70 Ma (or earlier) and ~65 Ma. At least 45 km of sinistral offset is interpreted to have occurred on the Talchako fault prior to ~65 Ma on the following six lines of evidence (Fig. 2.14A, B).

1) The Talchako fault has ductile fabrics defined by hornblende and biotite and has kinematics representative of apparent sinistral shear (Fig. 2.14B).

2) The Echo Lake and Success Lakes plutons are on opposite sides of the Talchako fault and have the same latest Jurassic-Earliest Cretaceous age, composition and deformation features and are interpreted to be offset equivalents (Fig. 2.14A).

3) Dykes of unfoliated biotite-hornblende-diorite intrude the Success Lakes pluton west of the Talchako fault and have reported K-Ar hornblende and biotite ages of 128 ± 8 Ma and 96.8 ± 7.2 (van der Heyden, 2004). East of the Talchako fault adjacent to the Success Lake pluton, ages from metamorphic and igneous rocks range from 117 to 93 Ma for hornblende and 81 to 70 Ma for biotite. The discrepancy in ages suggests a significantly different pre-70 Ma history for the two plutonic bodies. Proposed restoration along the Talchako fault (Fig. 2.14) juxtaposes the dykes (128 Ma) within the Success Lakes pluton next to the Mt. Marvin pluton which is equivalent in age (129 Ma). Hornblende and biotite cooling ages from the Mt. Marvin pluton overlap with those from the dykes from within the Success Lakes pluton and are an anomaly in the north (van der Heyden, 2004). This data suggests that dykes within the Success Lakes pluton have the same crystallization and cooling history as the Mt. Marvin pluton in the north and represent offset equivalents.

4) Figure 2.14C illustrates the known metamorphic cooling ages of hornblende and biotite from 51^{o} to 54.5^{o} north latitude. Cooling ages for both minerals have a continuous southwest trend until the latitude of the Atnarko complex where an apparent offset translates rocks with older

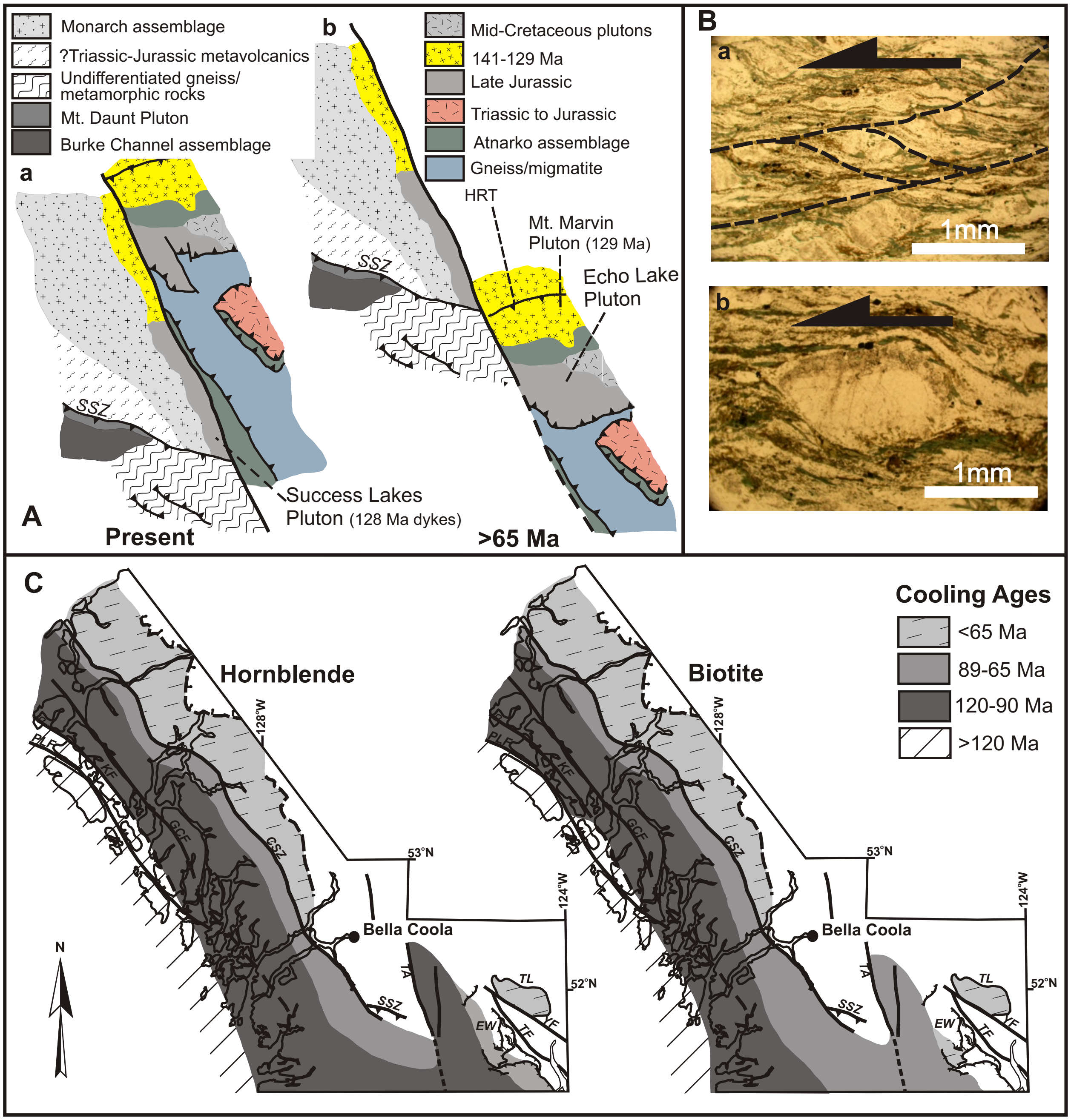

Figure 2.14. (A) Restoration of ~45 km of sinistral offset along the Talchako fault. Simplified geology with Tertiary plutons removed. (a) Present day distribution of units, (b) pre-65 Ma distribution of units. Note the apparent abrupt termination of the Sheemahant shear zone-*SSZ* and the possible continuation of the shear zone along the Hotnarko River thrust (HTR) north of the Mt. Marvin pluton. (B) Photomicrographs from samples collected within the Talchako fault zone. (a) Shear bands indicating top to the left, sinistral motion. (b) σ-type porphyroclasts indicating top to the left, sinistral motion. PPL 2.5x. Samples cut perpendicular to foliation. (C) Known Early Cretaceous to Eocene metamorphic cooling ages from the Coast Belt orogen between latitudes 51° to 54.5° for hornblende and biotite. Area depicted same as Fig. 1. Data from Andronicos et al., [2003]; Chardon et al., [1999]; Friedman and Armstrong [1988]; Roddick [1996]; Rusmore and Woodsworth [1994]; Rusmore et al., [2003]; van der Heyden [1989] and this study. CSZ-Coast shear zone, PLF-Principe-Laredo fault, GCF- Grenville Channel fault, KF- Kitkatla fault, SSZ-Sheemahant shear zone, TA-Talchako fault, YF-Yalakom fault, TF-Tchaikazan fault, EW-East Waddington thrust belt, TL-Tatla Lake metamorphic complex.

cooling ages to the north. Sinistral offset along the Talchako fault can explain this northward migration of cooling ages.

5) East of the Atnarko complex the East Waddington thrust belt appears to end abruptly (Sheemahant shear zone; Fig. 2.14A). Evidence for north to northeast directed compression in the Atnarko area extends the East Waddington structures to the west. Restoration of the proposed sinistral motion juxtaposes the Hotnarko River thrust next to the Sheemahant shear zone, suggesting a possible continuation of the north-northeast directed system.

6) Undifferentiated gneisses and metamorphic rocks west of the Talchako fault and south of the Sheemahant shear zone are lithologically similar to rocks in the Atnarko complex (Roddick and Tipper, 1985; Roddick, 1996) and restore to a position next to the complex. Northwest striking, southwest verging thrust faults within these gneisses are very similar to D_1 structures in the Atnarko complex and restore into a position just west of the Atnarko (Fig. 2.14A).

Along strike variation in orogen development

The geology along strike to northwest and southeast of the Atnarko complex is discussed here to highlight the differences and similarities in the orogenic system represented by the Coast plutonic complex. The evolution of the system as a whole is then discussed in the light of new data presented from the Atnarko complex.

Northwest of the Atnarko complex

The Coast plutonic complex can be divided into three separate structural and lithologic belts: A) the Western belt; B) the Central belt and C) the Eastern belt, with their boundaries defined by crustal-scale shear zones (Crawford et al., 1987; Andronicos et al., 2003; Rusmore et al., 2005).

The Western belt includes rocks west of the Coast shear zone to the British Columbia and Alaska coast lines, and extends from south of the Atnarko complex northwest into southeast Alaska (Fig. 2.1). This area is characterized by highly metamorphosed and strongly deformed gneisses and schists of continental margin affinity and lower grade volcanic and sedimentary rocks of the Insular superterrane (Crawford et al., 1987; Klepeis and Crawford, 1999; Boghossian and Gehrels, 2000; Gehrels and Boghossian, 2000). These rocks are intruded by Jurassic to mid-Cretaceous plutons (van der Heyden, 1992; Chardon et al., 1999). Lower grade Insular superterrane rocks form the footwall to higher grade gneisses and migmatites across a southwest to west verging thrust system referred to as the western thrust belt (Fig. 2.1; Crawford et al., 1987; McClelland et al., 1992b). The onset of thrusting in the Western belt is not well constrained but may have started by 110 Ma (Crawford et al., 1987). Cooling of the belt below 350^{o}C occurred by ~85 Ma suggesting deformation and metamorphism had mainly ceased by this time, but may have continued to 70 Ma (Crawford et al., 1987; Rusmore et al., 2000). Several large-scale, high-angle strike-slip faults that exhibit sinistral offset are found in the western belt and were active during the mid-Cretaceous (Chardon et al., 1999). These include the Grenville Channel, Kitkatla and Principe-Laredo fault systems (Fig. 2.1). These faults appear to merge west of the Bella Coola region and are not found south of the Atnarko complex (Fig. 2.1). Chardon et al. (1999) suggest these faults are part of a sinistral transpressional regime that affected the Coast plutonic complex during mid-Cretaceous time.

The Central belt consists of strongly deformed and metamorphosed supracrustal rocks and orthogneiss intruded by Late Cretaceous to Eocene plutons. The belt is bound to the west by the Coast shear zone and to the east the Shames River shear zone and eastern boundary detachment systems (Heah, 1991; Andronicos et al., 2003; Rusmore et al., 2005). The high-grade core of the Central belt is referred to as the Central Gneiss Complex (Hollister, 1982; Hutchison, 1982; Hollister and Andronicos, 2000). Plutons intruded between ~90 and 42 Ma form an elongate northwest trending batholithic complex that extends from north of Bella Coola into southeast Alaska (Hollister and Andronicos, 2000; Andronicos et al., 2003). Metamorphic grade in the Central belt is predominantly amphibolite with local development of granulite facies (Hollister and Andronicos, 2000). Deformation includes Late Cretaceous dextral transpression followed by two stages of exhumation ending in the Eocene. Cooling of the Central belt below 560^{o}C is recorded at ~51 Ma with temperatures at or below ~350^{o}C by 48 Ma (Crawford et al., 1987; Andronicos et al., 2003; Rusmore et al., 2005). The dominant structural feature of the central belt is the Coast shear zone, a more than 1200 km long deformation zone that is defined by northeast side up (to the southwest) between ~65 and 50 Ma, locally with subsequent southwest side up deformation (Klepeis et al., 1998; Rusmore et al., 2001; Andronicos et al., 2003). Rusmore et al. (2001) have traced the Coast shear zone south of Bella Coola to the edge of the Mount Waddington map sheet (Fig. 2.1). There is no obvious continuation of the structure along strike through the Mount Waddington area (Roddick and Tipper, 1985).

The Eastern belt is characterized by unmetamorphosed to subgreenschist facies volcanic, sedimentary and plutonic rocks of the Stikine terrane (Crawford et al., 1987; van der Heyden, 1992; Andronicos et al., 1999; Rusmore et al., 2005). Where exposed the contact between the Central and Eastern belts is marked by the Shames River shear zone and East Side detachment (Fig. 2.1; Heah, 1991; Andronicos et al., 2003; Rusmore et al., 2005). Low grade rocks of the Eastern belt merge with the trace of the Coast shear zone west of Bella Coola (Fig. 2.1). Northeast directed compressional features in the lower grade rocks located west of the Atnarko complex include southwest dipping thrust faults and mountain scale overturned folds (Mahoney et al., 2002; Haggart et al., 2003). Similar structures are also found in the Stikine terrane east of the Shames River and eastern boundary shear zones (van der Heyden, 1989). These structures have been related to mid-Cretaceous deformation associated with the East Waddington Thrust Belt. Extensional movement on the Shames River shear zone and East Side detachment is related to exhumation of the Central belt during Paleocene through Eocene extension (Klepeis and Crawford, 1999; Andronicos et al., 2003; Rusmore et al., 2005).

Southeast of the Atnarko complex

Dividing the rocks to the southeast of the Atnarko complex is not as straightforward as in the northwest. The rocks are dramatically different in structural style, metamorphic history and age from those in the northwest. The area to the southeast of the Atnarko complex is divided into three belts; the Southwest belt, the Eastern Waddington belt and the Southeast belt (Fig. 2.1).

The Southwest belt comprises the area from the eastern extent of structural and intrusive contacts between the Coast plutonic complex and the Intermontane superterrane (i.e., the eastern extent of the Coast belt) to the western British Columbia shoreline (Fig. 2.1). The Southwest belt is characterized by Jurassic to Tertiary plutons enclosing large pendants of amphibolite to greenschist grade metamorphic rocks of uncertain affinity and lower grade volcanic and sedimentary rocks of the Insular superterrane (Roddick and Tipper, 1985). Southwest to west directed compression of the Coast Belt thrust system place high grade metamorphic rocks over the lower grade Insular rocks (Journeay and Friedman, 1993). Timing, kinematics and structural architecture of the thrust belt has led to correlation between the Coast Belt thrust system and the western thrust belt found northwest of the Atnarko complex (Crawford et al., 1987; Journeay and Friedman, 1993). There is little difference between the Western belt and the Southwestern belt and the two regions exhibit the same broad structural, lithologic and metamorphic characteristics.

The Eastern Waddington belt is bound to the west by intrusions of the Coast plutonic complex and the uppermost thrust sheet of the East Waddington thrust belt and to the east by the Yalakom fault (Fig. 2.1). Within the Eastern Waddington belt, Triassic volcanic and sedimentary rocks of the Stikine terrane structurally overly Jura-Cretaceous sedimentary and volcanic rocks across a northeast verging system of thrusts (Rusmore and Woodsworth, 1994; Umhoefer et al., 1994). Thrusting is characterized by an inverted metamorphic gradient with a decrease in grade down structural section. Syn-kinematic Late Cretaceous (87 Ma) orthogneiss of the uppermost thrust sheet is thrust over low grade volcanic and sedimentary rocks. Thrust faulting had begun by at least 87 Ma and possibly as early as 110 Ma, based on an interpreted syn-thrust setting for the deposition of mid-Cretaceous basinal marine deposits in the foreland of the thrust system (Rusmore and Woodsworth, 1994; Umhoefer et al., 1994). Data from the thrust belt suggest deformation related to thrusting ended shortly after 84 Ma but may have continued to 68 Ma when the belt was intruded by post-kinematic plutons (Rusmore and Woodsworth, 1994). The thrust belt has been traced as far west as the northeastern most margin of the Atnarko complex where Early Cretaceous plutons are thrust over rocks of the Stikine terrane (van der Heyden et al., 1994). The foreland of the thrust system is dissected by latest Cretaceous to Eocene dextral strike-slip faults, the most notable of these are the Tchaikazan and Yalakom faults. These faults are part of a system of dextral strike-slip faults that are found along the length of the western North American Cordillera (Struik, 1993; Umhoefer and Schiarizza, 1996). The Yalakom fault has as much as 115 km of accumulated dextral offset between ~69 Ma to 34 Ma and was associated with regional extension during the last 10 My of movement (Umhoefer and Kleinspehn, 1995; Umhoefer and Schiarizza, 1996). The Tchaikazan fault has a protracted history that includes at least 40 km of Early Cretaceous sinistral slip overprinted by 7 to 8 km of early Tertiary dextral slip (Mustard and van der Heyden, 1994; Schiarizza et al., 1997; Israel et al., 2006a). Interaction between the two large faults resulted in numerous related structures including a series of left-stepping dextral faults and related folds (Schiarizza et al., 1997).

The Southeastern belt is bound on the southwest by the Yalakom fault system and continues east into the Intermontane superterrane (Fig. 2.1). Rocks within this belt are mostly volcanic and sedimentary rocks of the Stikine terrane overlain by Miocene volcanic rocks. The most striking feature of this belt is the Tatla Lake metamorphic complex formed during Eocene extension (Friedman and Armstrong, 1988). The complex is truncated to the southwest by the Yalakom fault and is bound to the north and southeast by normal faults that separate low grade cover rocks from the high grade metamorphic core (Friedman and Armstrong, 1988). Rocks within the core are gneisses and migmatites with latest Jurassic to Cretaceous crystallization ages. The gneisses and migmatites have undergone a series of deformational events, culminating with early Eocene uplift of the complex. The uplift was likely kinematically linked to movement on the Yalakom system (Friedman and Armstrong, 1988). Several similar metamorphic core complexes are found on the eastern side of the Yalakom fault system along strike to the southeast (Parrish et al., 1988; Coleman and Parrish, 1991; Paterson et al., 2004).

Plate motions, strain partitioning and tectonic implications

~120-80 Ma (Sinistral transpression)

Deformation between 120 and 80 Ma affected the entire Coast plutonic complex. Two oppositely verging thrust systems have been identified flanking the Coast plutonic complex. The first is a southwest directed thrust belt that places rocks of continental margin assemblages and metamorphosed rocks of Wrangellia and the Alexander terrane over lower grade overlap assemblages (Crawford et al., 1987; Journeay and Friedman, 1993; Morozov et al., 1998; Hollister and Andronicos, 2006). A second northeast verging thrust belt places metamorphic and plutonic rocks of the Coast plutonic complex over lower grade rocks of the Intermontane superterrane (Rusmore and Woodsworth, 1994; Umhoefer et al., 1994; Umhoefer and Miller, 1996).

The southwest verging system marks the western boundary of the Coast plutonic complex and represents the response to underthrusting of the Insular superterrane under the Intermontane superterrane from ~120-80 Ma (Fig. 2.15A; Journeay and Friedman, 1993; Crawford et al., 2000; Hollister and Andronicos, 2006). In the Atnarko complex thrusting was well underway by ~117 Ma with the cooling of amphibolite signaling uplift of the high-grade imbricate zone. Elsewhere thrusting began by at least 110 Ma (Crawford et al., 1987).

The northeast boundary of the Coast plutonic complex is defined by the north-northeast verging thrusts, from the Atnarko complex eastward (Fig. 2.15A). Northeast compression began

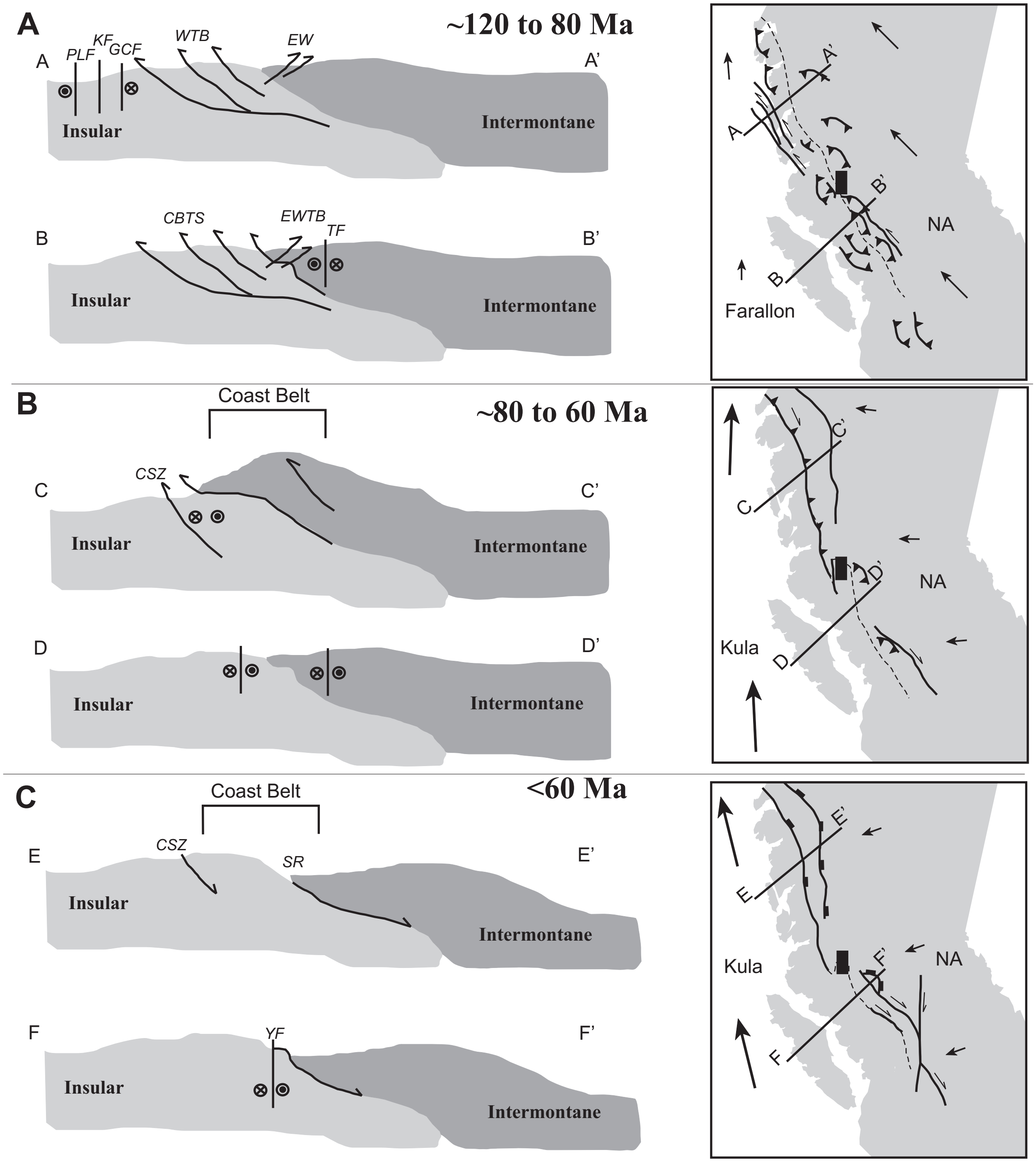

Figure 2.15. Tectonic evolution of the western Cordilleran margin from the Early Cretaceous to Tertiary. Arrows within insets indicate approximate plate motion vectors of North America, Farallon and Kula plates (Engebretson, 1985; Lonsdale, 1988), black box show location of Atnarko complex. (A) Early to mid-Cretaceous sinistral transpression along the entire Coast orogen similar styles of deformation from the north to south. (B) mid-Cretaceous dextral transpression where strain is partitioned into compression and continued crustal thickening in the north and dextral translation with some minor compression in the south. (C) Tertiary dextral transtension leads to large-scale orogen perpendicular extension in the north and minor orogen parallel extension in the south that is kinematically linked to extensive dextral translation. See text for more detail. Dashed line in plan view insets depicts the approximate boundary between the Insular and Intermontane superterranes. CSZ-Coast shear zone, PLF-Principe-Laredo fault, GCF- Grenville Channel fault, KF- Kitkatla fault, SR-Shames River and eastern boundary detachment, YF-Yalakom fault, TF-Tchaikazan fault, WTB-Western thrust belt, EW-East Waddington thrust belt, CBTS-Coast belt thrust system.

by at least 80 Ma, and likely earlier, in the Atnarko complex and overprints and partially overlaps spatially and temporally with southwest directed thrusting. Northwest of the Atnarko complex northeast verging thrusts have been documented within the Sheemahant shear zone and within low grade cover rocks in the Bella Coola region (Rusmore et al., 2000; Mahoney et al., 2002).

Sinistral oblique thrusting in the northern part of the Atnarko complex reflects sinistral transpression active along the orogen margin during the Early to mid-Cretaceous, which is consistent with plate motions at this time (Fig. 2.15A; Engebretson et al., 1985). Several large high angle sinistral strike-slip faults were active during this time located at the inboard and outboard margins of the Coast plutonic complex (Fig. 2.15A; Schiarizza et al., 1997; Chardon et al., 1999; Israel et al., 2006a).

80-60 Ma (Dextral transpression)

The structural response of the orogen to the onset of dextral transpression changes along strike. To the northwest and southeast of the Atnarko complex the expression of post-70 Ma deformation is strikingly different. To the northwest, southwest directed compression is clearly expressed. Shear patterns within the Central Gneiss complex and syn-deformation plutons suggest dextral transpression from ~70 to 60 Ma (Crawford et al., 1999; Andronicos et al., 2003; Rusmore et al., 2005). Here, the Coast shear zone accommodated southwest directed compression from ~67 to 60 Ma.

To the southeast, major dextral strike-slip displacement began by latest Cretaceous as indicated by movement on a left stepping dextral compressional fault system (Umhoefer and Kleinspehn, 1995; Umhoefer and Schiarizza, 1996). The system extends southward to the Northern Cascades belt where major fault systems having similar structural styles record ductile deformation between 68-65 Ma (Miller and Bowring, 1990; Miller, 1994; Umhoefer and Schiarizza, 1996).

These fault systems comprise a large, dominantly dextral strike-slip system active to the east and southeast of the Atnarko complex (Fig. 2.15B).

Plate reconstruction models for the latest Cretaceous suggest that the orogen was undergoing oblique dextral convergence (Fig. 2.15B; Engebretson et al., 1985). The Talchako fault zone at this time records sinistral displacement. The Talchako fault separates two systems that were undergoing dextral transpression that was expressed by dominantly compressional deformation in the northwest and dextral translation in the southeast (Fig. 2.15B). In this model the Talchako fault acted as a tear fault that formed at the boundary between areas of more pronounced compression from those with dominantly lateral motion.

Post 60 Ma (Dextral transtension)

Structures within the rocks of the Coast plutonic complex record a change from dextral transpressive to a transtensive setting (Friedman and Armstrong, 1988; Andronicos et al., 2003; Rusmore et al., 2005; Hollister and Andronicos, 2006). During this time Hollister and Andronicos (2006) suggest the area to the northwest of the Atnarko complex was a topographic high and was unstable during the changed plate interactions. Large-scale orogenic collapse was accommodated by movement along the Shames River shear zone and the eastern boundary detachment under ductile normal mylonitic shearing (Fig. 2.15C). Brittle deformation dominated to the southeast of the Atnarko complex with both dextral transpressional and transtensional strike slip deformation along the Yalakom fault system (Umhoefer and Kleinspehn, 1995; Umhoefer and Schiarizza, 1996). Extension occurred along, and was kinematically linked to, the Yalakom fault system, and led to unroofing of metamorphic core complexes along the strike-slip fault system (Friedman and Armstrong, 1988; Coleman and Parrish, 1991; Smith, 1998).

CONCLUSIONS

The Atnarko metamorphic complex is located at the boundary between the Insular and Intermontane superterranes and records Early Jurassic to Tertiary deformation within the Coast plutonic complex. Southwest to west directed compression occurred along the western boundary of the Coast plutonic complex followed by, and slightly overlapping with, northeast to north directed compression. This occurred during sinistral transpression that affected much of the Cordilleran margin at this latitude.

After a change in plate motions, dextral transpression was partitioned into strike-slip-dominated areas southeast of the Atnarko complex, and compression-dominated areas northwest of the complex, potentially separated by the Talchako fault. Southwest compression continued with associated uplift and crustal thickening to the northwest of the Atnarko complex while areas to the southeast were dominated by dextral translation. Plate motions continued to change and dextral transtension contributed to mass exhumation to the northwest and local extension and exhumation in the southeast.

REFERENCES

Andronicos, C. L., Chardon, D. H., and Hollister, L. S., 2003, Strain partitioning in an obliquely convergent orogen, plutonism, and synorogenic collapse: Coast Mountains Batholiths, British Columbia, Canada: Tectonics, v. 22, no. 2, doi:10.1029/2001TC001312.

Andronicos, C. L., Hollister, L. S., Davidson, C., and Chardon, D., 1999, Kinematics and tectonic significance of transpressive structures within the Coast Plutonic Complex, British Columbia: Journal of Structural Geology, v. 21, p. 229-243.

Armstrong, R. L., 1988, Mesozoic and early Cenozoic magmatic evolution of the Canadian Cordillera, *in* Clark, S. P., Jr., Burchfield, B. C., and Suppe, J., eds., Processes in continental lithospheric deformation, Geological Society of America, p. 55-91.

Berg, H. C., Jones, D. L., and Richter, D. H., 1972, Gravina-Nutzotin belt-tectonic significance of an upper Mesozoic sedimentary and volcanic sequence in southern and southeastern Alaska: USGS Professional paper 800-D.

Boghossian, N. D., and Gehrels, G. E., 2000, Nd isotopic signature of metasedimentary pendants in the Coast Mountains between Prince Rupert and Bella Coola, British Columbia, *in* Stowell, H. H., and McClelland, W. C., eds., Tectonics of the Coast Mountains, southeastern Alaska and British Columbia: Boulder, Colorado, Geological Society of America Special Paper 343, p. 77-87.

Chardon, D., Andronicos, C. L., and Hollister, L. S., 1999, Large-scale transpressive shear zone patterns and displacements within magmatic arcs: The Coast Plutonic Complex, British Columbia: Tectonics, v. 18, no. 2, p. 278-292.

Coleman, M. E., and Parrish, R. R., 1991, Eocene dextral strike-slip and extensional faulting in the Bridge River terrane, southwest British Columbia: Tectonics, v. 10, p. 1222-1238.

Colpron, M., Nelson, J. L., and Murphy, D. C., 2007, Northern Cordilleran terranes and their interactions through time: GSA Today, v. 17, no. 4/5, p. 1-10.

Cowan, D. S., Brandon, M. T., and Garver, J. I., 1997, Geologic tests of hypotheses for large coastwise displacements-a critique illustrated by the Baja British Columbia controversy: American Journal of Science, v. 297, p. 117-173.

Crawford, M. L., Crawford, W. A., and Gehrels, G. E., 2000, Terrane assembly and structural relationships in the eastern Prince Rupert quadrangle, British Columbia, *in* Stowell, H. H., and McClelland, W. C., eds., Tectonics of the Coast Mountains, southeastern Alaska and British Columbia: Boulder, Colorado, Geological Society of America Special Paper 343, p. 1-21.

Crawford, M. L., Hollister, L. S., and Woodsworth, G. J., 1987, Crustal deformation and regional metamorphism across a terrane boundary, Coast Plutonic Complex, British Columbia: Tectonics, v. 6, no. 3, p. 343-361.

Crawford, M. L., Klepeis, K. A., Gehrels, G. E., and Isachsen, C., 1999, Batholith emplacement at mid-crustal levels and its exhumation within an obliquely convergent margin: Tectonophysics, v. 312, p. 57-78.

Dewey, J. F., 1980, Episodicity, sequence and style at convergent plate boundaries, *in* Strangway, D. W., ed., The continental crust and its mineral deposits, Geological Association of Canada, Special Paper 20, p. 553-557.

Dewey, J. F., 1988, Extensional collapse of orogens: Tectonics, v. 7, p. 1123-1139.

Dickinson, W. R., 2000, Geodynamic interpretation of Paleozoic tectonic trends oriented oblique to the Mesozoic Klamath-Sierran continental margin in California, *in* Soreghan, M. J., and Gehrels, G. E., eds., Paleozoic and Triassic paleogeography and tectonics of western Nevada and northern California: Boulder, Colorado, Geological Society of America, p. 209-245.

Dickinson, W. R., 2004, Evolution of the North American Cordillera: Annual Reviews of Earth and Planetary Science, v. 32, p. 13-45.
Engebretson, D. C., and Blake, M. C., 2002, Alternatives to Mesozoic plate configurations and terrane displacements within the Pacific Basin and along western North America: Geological Society of America *Abstracts with Programs*, v. Cordilleran Section meeting, Session 42.
Engebretson, D. C., Cox, A., and Gordon, R. G., 1985, Relative motions between oceanic and continental plates in the Pacific basin: Geological Society of America Special Paper 206, p. 58.
Evenchick, C. A., 2001, Northeast-trending folds in the western Skeena Fold Belt, northern Canadian Cordillera: a record of Early Cretaceous sinistral plate convergence: Journal of Structural Geology, v. 23, no. 6-7, p. 1123-1140.
Friedman, R. M., and Armstrong, R. L., 1988, Tatla Lake metamorphic complex: An Eocene metamorphic core complex on the southwestern edge of the Intermontane Belt of British Columbia: Tectonics, v. 7, no. 6, p. 1141-1166.
Gardner, M. C., Bergman, S. C., Cushing, G. W., MacKevett, E. M., Plafker, G., Campbell, R. B., Dodds, C. J., McClelland, W. C., and Mueller, P. A., 1988, Pennsylvanian pluton stitching of Wrangellia and the Alexander Terrane, Wrangell Mountains, Alaska: Geology, v. 16, no. 11, p. 967-971.
Gehrels, G. E., 2001, Geology of the Chatham Sound region, southeast Alaska and coastal British Columbia: Canadian Journal of Earth Sciences, v. 38, p. 1579-1599.
Gehrels, G. E., and Boghossian, N. D., 2000, Reconnaissance geology and U-Pb geochronology of the west flank of the Coast Mountains between Bella Coola and Prince Rupert, coastal British Columbia, *in* Stowell, H. H., and McClelland, W. C., eds., Tectonics of the Coast Mountains, SE Alaska and Coastal British Columbia, Geological Society of America, p. 61-76.
Gordee, S. M., 2005, Volcanostratigraphy, age and geologic setting of the Lower-Middle Jurassic upper Hazelton Group, west-central British Columbia [MSc thesis]: University of British Columbia, 173 p.
Haggart, J. W., Diakow, L. J., Mahoney, J. B., Woodsworth, G. J., Struik, L. C., Gordee, S. M., and Rusmore, M. E., 2006, Geology, Bella Coola region (93D/01,/07,/08,/10,/15 and parts of 93D/02,/03,/06,/09,/11,/14,/16 and 92M/15 and /16), British Columbia: Geological Survey of Canada, Open File 5385, scale 1:100 000.,Geological Survey of Canada, Open File 5385, scale.
Haggart, J. W., Mahoney, J. B., Daikow, L. J., Woodsworth, G. J., Gordee, S. M., Snyder, L. D., Poulton, T. P., Friedman, R. M., and Villeneuve, M. E., 2003, Geological setting of the eastern Bella Coola map area, west-central British Columbia, Current Research 2003-A4, Geological Survey of Canada, p. 9.
Heah, T. S. T., 1991, Mesozoic ductile shear and Paleogene extension along the eastern margin of the Central Gneiss Complex, Coast Belt, Shames River area, near Terrace, British Columbia [MSc thesis]: University of British Columbia, 155 p.
Hollister, L. S., 1982, Metamorphic evidence for rapid (2mm/yr) uplift of a portion of the Central Gneiss Complex, Coast Mountains, B.C.: Canadian Mineralogist, v. 20, p. 319-332.
Hollister, L. S., and Andronicos, C. L., 1997, A candidate for the Baja British Columbia fault system in the Coast Plutonic complex: GSA Today, v. 7(11), p. 1-7.
Hollister, L. S., and Andronicos, C. L., 2000, The Central Gneiss Complex, Coast Mountains, British Columbia, *in* Stowell, H. H., and McClelland, W. C., eds., Tectonics of the Coast Mountains, southeastern Alaska and British Columbia: Boulder, Colorado, Geological Society of America Special Paper 343, p. 45-59.

Hollister, L. S., and Andronicos, C. L., 2006, Formation of new continental crust in Western British Columbia during transpression and transtension: Earth and Planetary Science Letters, v. 249, p. 29-38.
Hutchison, W. W., 1982, Geology of the Prince Rupert-Skeena map area, British Columbia, Memoir, Geological Survey of Canada, p. 116.
Irving, E., Thorkelson, D., Wheadon, P. M., and Enkin, R., 1995, Paleomagmatism of the Spences Bridge Group and northward displacement of the Intermontane Belt, British Columbia: A second look: Journal of Geophysical Research, v. 100, no. B4, p. 6057-6071.
Israel, S., Schiarizza, P., Kennedy, L. A., Friedman, R. M., and Villeneuve, M. E., 2006a, Evidence for Early to Late Cretaceous, sinistral deformation in the Tchaikazan River area, southwestern British Columbia: Implications for the tectonic evolution of the southern Coast Belt, *in* Haggart, J., Enkin, R., and Monger, J. W. H., eds., Paleogeography of the western North American Cordillera, Geological Association of Canada, Special Paper 46, p. 331-350.
Israel, S., and van der Heyden, P., 2006, Geology, Atnarko (93C/05), British Columbia: Geological Survey of Canada, Open File 9999, scale 1:50,000.
Israel, S., van der Heyden, P., Haggart, J., and Woodsworth, G. J., 2006b, Geology, Junker Lake and part of Knot Lakes (93C/04 and 92N/13), British Columbia: Geological Survey of Canada, Open File 9999, scale 1:50,000.
Jones, D. L., Silberling, N. J., and Hillhouse, J., 1977, Wrangellia-A displaced terrane in northwestern North America: Canadian Journal of Earth Sciences, v. 14, p. 2565-2577.
Journeay, J. M., and Friedman, R. M., 1993, The Coast Belt thrust system: evidence of late Cretaceous shortening in southwest British Columbia: Tectonics, v. 12, no. June 1993, p. 756-775.
Klepeis, K. A., and Crawford, M. L., 1999, High-temperature arc-parallel normal faulting and transtension at the roots of an obliquely convergent orogen: Geology, v. 27, no. 1, p. 7-10.
Klepeis, K. A., Crawford, M. L., and Gehrels, G. E., 1998, Structural history of the crustal-scale Coast shear zone north of Portland Canal, southeast Alaska and British Columbia: Journal of Structural Geology, v. 20, no. 7, p. 883-904.
Lonsdale, P., 1988, Paleogene history of the Kula plate: Offshore evidence and onshore implications: Geological Society of America Bulletin, v. 109, p. 733-754.
Mahoney, J. B., Struik, L. C., Daikow, L. J., Hrudey, M. G., and Woodsworth, G. J., 2002, Structural geology of the eastern Bella Coola map area, southwest British Columbia: Geological Survey of Canada Current Research, v. A10, p. 9.
Marsden, H., and Thorkelson, D., 1992, Geology of the Hazelton volcanic belt in British Columbia: Implications for the Early to Middle Jurassic evolution of Stikinia: Tectonics, v. 11, no. 6, p. 1266-1287.
McClelland, W. C., Gehrels, G. E., and Saleeby, J. B., 1992a, Upper Jurassic-Lower Cretaceous basinal strata along Cordilleran margin: Implications for the accretionary history of the Alexander-Wrangellia-Peninsular terrane: Tectonics, v. 11, p. 823-835.
McClelland, W. C., Gehrels, G. E., Samson, S. D., and Patchett, P. J., 1992b, Structural and geochronologic relationships along the western flank of the Coast Mountains batholith: Stikine River to Cape Fanshaw, central southeastern Alaska: Journal of Structural Geology, v. 14, no. 4, p. 475-489.
Miller, R. B., 1994, A mid-crustal contractional zone in a major strike-slip system, North Cascades, Washington: Journal of Structural Geology, v. 16, p. 47-60.

Miller, R. B., and Bowring, S. A., 1990, Structure and chronology of the Oval Peak batholith and adjacent rocks: Implications for the Ross Lake fault zone, North Cascades, Washington: Geological Society of America Bulletin, v. 102, p. 1361-1377.

Monger, J. W. H., Clowes, R. M., Cowan, D. S., Potter, C. J., Price, R. A., and Yorath, C. J., 1994a, Continent-ocean transitions in western North America between latitudes 46 and 56 degrees: transects B1, B2, B3, *in* Speed, R. C., ed., Phanerozoic evolution of North American continent-ocean transitions: Boulder, Colorado, Geological Society of America, p. 357-397.

Monger, J. W. H., and Journeay, J. M., 1994, Guide to the geology and tectonic evolution of the southern Coast Mountains: Geological Survey of Canada Open File 2490.

Monger, J. W. H., and Nokelberg, W. J., 1996, Evolution of the North America Cordillera: generation, fragmentation, displacement and accretion of successive North American plate-margin arcs, *in* Coyner, A. R., and Fahey, P. L., eds., Geology and ore deposits of the North American Cordillera: Sypmposium Proceedings: Reno-Sparks, Nevada, Geological Society of Nevada, p. 1133-1152.

Monger, J. W. H., Price, R. A., and Templeman-Kluit, D. J., 1982, Tectonic accretion and the origin of two metamorphic and plutonic welts in the Canadian Cordillera: Geology, v. 10, p. 70-75.

Monger, J. W. H., van der Heyden, P., Journeay, J. M., Evenchick, C. A., and Mahoney, J. B., 1994b, Jurassic-Cretaceous basins along the Canadian Coast belt: Their bearing on pre-mid-Cretaceous sinistral displacements: Geology, v. 22, p. 175-178.

Morozov, I. B., Smithson, S. B., Hollister, L. S., and Diebold, J. B., 1998, Wide-angle seismic imaging across accreted terranes, southeastern Alaska and western British Columbia: Tectonophysics, v. 299, p. 281-296.

Mortensen, J. K., 1992, Pre-Mid-Mesozoic tectonic evolution of the Yukon-Tanana terrane, Yukon and Alaska: Tectonics, v. 11, no. August 1992, p. 836-853.

Mustard, P. S., and van der Heyden, P., 1994, Stratigraphy and sedimentology of the Tatla Lake-Bussel Creek map areas, west-central British Columbia, Current Research, 1994-A, Geological Survey of Canada, p. 95-104.

Parrish, R. R., Carr, S. D., and Parkinson, D. L., 1988, Eocene extensional tectonics and geochronology of the southern Omineca Belt, British Columbia and Washington: Tectonics, v. 7, p. 181-212.

Passchier, C. W., and Trouw, R. A. J., 1996, Micro-tectonics, Springer, 289 p.

Paterson, S., R, Miller, R. B., Alsleben, H., Whitney, D. L., Valley, P. M., and Hurlow, H., 2004, Driving mechanism for >40 km of exhumation during contraction and extension in a continental arc, Cascades core, Washington: Tectonics, v. 23.

Roddick, J. A., 1996, Geology, Rivers Inlet-Queens Sound, British Columbia (92M), (102P): Geological Survey of Canada.

Roddick, J. A., and Tipper, H. W., 1985, Geology, Mount Waddington (92N) map area: Geological Survey of Canada, Open File 1163, scale 1:250,000.

Rothstein, D. A., and Manning, C. E., 2003, Geothermal gradients in continental magmatic arcs: Constraints from the eastern Peninsular Ranges batholith, Baja California, Mexico: Geological Society of America Special Paper 374, p. 337-354.

Rushmer, T., 1991, Partial melting of two amphibolites: contrasting experimental results under fluid-absent conditions: Contribution to Mineralogy and Petrology, v. 107, p. 41-59.

Rusmore, M. E., Gehrels, G. E., and Woodsworth, G. J., 2001, Southern continuation of the Coast shear zone and Paleocene strain partitioning in British Columbia-southeast Alaska: Geological Society of America Bulletin, v. 113, no. 8, p. 961-95.

Rusmore, M. E., and Woodsworth, G. J., 1994, Evolution of the eastern Waddington thrust belt and its relation to the mid-Cretaceous Coast Mountains arc, western British Columbia: Tectonics, v. 13, no. 5, p. 1052-1067.

Rusmore, M. E., Woodsworth, G. J., and Gehrels, G. E., 2000, Late Cretaceous evolution of the eastern Coast Mountains, Bella Coola, British Columbia, *in* Stowell, H. H., and McClelland, W. C., eds., Tectonics of the Coast Mountains, southeastern Alaska and British Columbia: Boulder, Colorado, Geological Society of America Special Paper 343, p. 89-105.

Rusmore, M. E., Woodsworth, G. J., and Gehrels, G. E., 2005, Two-stage exhumation of midcrustal arc rocks, Coast Mountains, British Columbia: Tectonics, v. 24, doi:10.1029/2004TC001750.

Saleeby, J. B., 2000, Geochronologic investigations along the Alexander-Taku terrane boundary, southern Revillagigedo Island to Cape Fox areas, southeast Alaska, *in* Stowell, H. H., and McClelland, W. C., eds., Tectonics of the Coast Mountains in southeast Alaska and British Columbia, Geological Society of America, p. 107-143.

Schiarizza, P., Gaba, R. G., Glover, J. K., Garver, J. I., and Umhoefer, P. J., 1997, Geology and mineral occurrences of the Taseko-Bridge River area: British Columbia Ministry of Employment and Investment, Energy and Minerals Division, Geological Survey Branch.

Smith, L. M., 1998, Kinematics, age of deformation, and regional significance of the Cayoosh Creek fault, Lillooet, British Columbia [MSc thesis]: University of British Columbia, 94 p.

Struik, L. C., 1993, Intersecting intracontinental Tertiary transform fault systems in the North American Cordillera: Canadian Journal of Earth Sciences, v. 30, p. 1262-1274.

Tipper, H. W., 1969, Geology of the Anahim map area: Geological Survey of Canada Map 1202A, scale 1:250,000, 1 sheet.

Umhoefer, P. J., and Kleinspehn, K. L., 1995, Mesoscale and regional kinematics of the northwestern Yalakom fault system: Major Paleogene dextral faulting in British Columbia: Tectonics, v. 14, no. 1, p. 78-94.

Umhoefer, P. J., and Miller, R. B., 1996, Mid-Cretaceous thrusting in the southern Coast belt, British Columbia and Washington, after strike-slip reconstruction: Tectonics, v. 15, p. 545-565.

Umhoefer, P. J., Rusmore, M. E., and Woodsworth, G. J., 1994, Contrasting tectono-stratigraphy and structure in the Coast Belt near Chilko Lake, British Columbia: unrelated terranes or an arc-back-arc transect?: Canadian Journal of Earth Sciences, v. 31, p. 1700-1713.

Umhoefer, P. J., and Schiarizza, P., 1996, Latest Cretaceous to early Tertiary dextral strike-slip faulting on the southeastern Yalakom fault system, southeastern Coast Belt, British Columbia: Geological Society of America Bulletin, v. 108, no. 7, p. 768-785.

Umhoefer, P. J., Schiarizza, P., and Robinson, M., 2002, Relay Mountain Group, Tyaughton-Methow basin, southwest British Columbia: a major Middle Jurassic to Early Cretaceous terrane overlap assemblage: Canadian Journal of Earth Sciences, v. 39, p. 1143-1167.

van der Heyden, P., 1989, U-Pb and K-Ar geochronometry of the Coast Plutonic Complex, 53°to 54°N, British Columbia, and Implications for the Insular-Intermontane superterrane boundary [PhD thesis]: University of British Columbia, 392 p.

van der Heyden, P., 1990, Eastern margin of the Coast Belt in west-central British Columbia, Current Research, Part E, Geological Survey of Canada, p. 171-182.

van der Heyden, P., 1991, Preliminary U-Pb dates and field observations from the eastern Coast Belt near 52°N, British Columbia, Current Research, Part A, Geological Survey of Canada, p. 79-84.

van der Heyden, P., 1992, A Middle Jurassic to early Tertiary Andean-Sierran arc model for the Coast Belt of British Columbia: Tectonics, v. 11, p. 82-97.

van der Heyden, P., 2004, Uranium-lead and potassium-argon ages from eastern Bella Coola and adjacent parts of Anahim Lake and Mount Waddington map areas, west-central British Columbia, Current Research 2004-A2, Geological Survey of Canada, p. 14.

van der Heyden, P., Mustard, P. S., and Friedman, R. M., 1994, Northern continuation of the Eastern Waddington Thrust Belt and Tyaughton Trough, Tatla Lake-Bussel Creek map areas, west-central British Columbia, Current Research 1994-A, Geological Survey of Canada, p. 87-94.

Vanderhaeghe, O., and Teyssier, C., 2001, Crustal-scale rheological transitions during late-orogenic collapse: Tectonophysics, v. 335, p. 211-228.

Woodsworth, G. J., Anderson, R. G., and Armstrong, R. L., 1991, Plutonic Regimes, Chapter 15, *in* Gabrielse, H., and Yorath, C. J., eds., Geology of the Cordilleran Orogen in Canada, Geological Survey of Canada, p. 491-531.

Wynne, P. J., Irving, E., Maxson, J. A., and Kleinspehn, K. L., 1995, Paleomagmatism of the Upper Cretaceous strata of Mount Tatlow: Evidence for 3000 Km of northward displacement of the Eastern Coast Belt, British Columbia: Journal of Geophysical Research, v. 100, no. B4, p. 6073-6091.

CHAPTER 3

COUPLING AND DECOUPLING OF THE LOWER CRUST WITHIN THE WESTERN CANADIAN CORDILLERA: EVIDENCE FROM THE ATNARKO COMPLEX

INTRODUCTION

The interactions between crustal blocks within an active magmatic arc are recorded by deformation, metamorphism and plutonism. Establishing the temporal relationships between these processes is the key to deciphering the origins of accretionary orogens. Partitioning of strain in the crust is reflected by the overall geometry and lithologic relationships within the arc; these are transient features that vary as plate boundaries evolve. Strain partitioning is commonly synchronous with and a result of magmatism within the arc system during periods of regional deformation. Plutons are known to intrude during all phases of arc construction and the mechanisms by which melt production and intrusion of granitic material are related to deformation has been well-studied in the past decade (Brown and Solar, 1999b; Brown and Solar, 1999a; Vanderhaeghe and Teyssier, 2001a; Klepeis et al., 2003; Marchildon and Brown, 2003). In particular, orogenic collapse due to extensive melt production (Petford et al., 2000; Vanderhaeghe and Teyssier, 2001a; Klepeis et al., 2003; Marchildon and Brown, 2003). In some instances, deformation attends plutonism leading to thermal weakening and the enhancement and increase of deformation rates (Hollister and Crawford, 1986; Brown and Rushmer, 1997; Brown and Solar, 1999a). In other cases, deformation is the cause of plutonism, with compression and crustal thickening leading to the production of melt (Ducea, 2001). In both examples the presence of melt and increase in thermal regime become catalysts in orogenic collapse through weakening of the lower and middle crust, the consequence of which may be to allow the upper portions of the orogen to become decoupled from the lower crust (Dewey, 1988; Ducea, 2001; Vanderhaeghe and Teyssier, 2001b). Decoupling of crust at different levels is largely controlled by the rheology of the rocks. In magmatic arc settings rock rheology is controlled primarily by temperature and strain rate.

The thermomechanical architecture of arc crust is therefore linked to the production and emplacement of plutons and the changes in thermal regimes. The Coast plutonic complex of the western North American Cordillera is one of the largest accumulations of magmatic material in the world and records the interaction between deformation and plutonism within an arc setting that lasted for 150 million years (Woodsworth et al., 1991). The nature of the Coast plutonic complex changes dramatically in both structural style and timing of deformation at the latitude of Bella Coola, west-central British Columbia (Fig. 3.1). In the Late Cretaceous, southwest directed contraction dominated the orogen to the northwest of the Bella Coola region, while dextral strike-slip faulting characterized the area to the southeast (Umhoefer and Schiarizza, 1996; Schiarizza et al., 1997; Andronicos et al., 2003; Rusmore et al., 2005). In the northwest, compression was followed by wholesale collapse of the orogen in the Eocene time; the collapse was *perpendicular* to the orogenic axis. The style of collapse is best illustrated by exhumation of the Central Gneiss complex (Andronicos et al., 2003; Rusmore et al., 2005). Southeast of the Bella Coola region orogen collapse was local and *parallel* to the orogenic axis, and, collapse was restricted to the development of metamorphic core complexes (Friedman and Armstrong, 1988; Coleman and Parrish, 1991; Paterson et al., 2004). In contrast to the northwest, most extension was kinematically linked with dextral strike-slip faulting.

To address the possible mechanisms responsible for the significant change in along-strike crustal response to deformation within the Coast plutonic complex, the thermal and deformation histories of mid-crustal rocks exposed within the Atnarko complex are assessed. The Atnarko complex is located in the heart of the Coast plutonic complex near the Bella Coola region and through a comparison of the complex with areas along strike to the northwest and southeast a model for the response of the orogen to plate displacements through time is developed. I propose that the thermomechanical architecture of the crust prior to Eocene extension controlled the way in which the orogen responded to changing tectonic regimes. Northwest of the Atnarko complex, the upper and middle crust became decoupled from the lower crust and mantle, while the area to the southeast remained coupled to lower crust.

REGIONAL GEOLOGIC SETTING

The Atnarko complex is located near the boundary between the Insular and Intermontane superterranes (Fig. 3.1). These two large composite terranes make up the westernmost portion of the Canadian Cordillera and comprise accreted terranes that were amalgamated to the western margin of ancient North America during the Mesozoic (Coney et al., 1980; Monger et al., 1982). The more inboard Intermontane superterrane at the latitude of the study area is composed of the Stikine terrane, characterized by Early Jurassic island-arc volcanic and sedimentary rocks of the Hazelton Group and related plutonic suites (Marsden and Thorkelson, 1992; MacIntyre et al., 2001; Mahoney et al., in review). The Insular superterrane, in the region of the study area, consists of Wrangellia and the Alexander terrane. The Alexander terrane is composed of Early Paleozoic to Early Mesozoic volcanic, sedimentary and associated plutonic rocks (Woodsworth and Orchard, 1985; Gehrels and Saleeby, 1987; Gehrels and Boghossian, 2000). Wrangellia does not outcrop within the region of the study area; however, it is likely part of the material that was underplated during accretion and outcrops extensively to the south of the study area on Vancouver Island (Hollister and Andronicos, 2006). Wrangellia consists of late Paleozoic arc volcanic and sedimentary sequences overlain by Middle to Upper Triassic flood basalts and carbonates. The Alexander terrane and Wrangellia are believed to be stitched together by earliest Permian and were amalgamated to the western margin of Stikinia as one large crustal block (Gardner et al., 1988; Gehrels, 2001).

Fragments of continental margin rocks strung out from southeast Alaska to Bella Coola are located near the boundary between the two superterranes, and spatially associated with the Coast plutonic complex (Fig. 3.1). The Banks Island and Burke Channel assemblages constitute two of these fragments and are located near the study area. They have been correlated with the Yukon-Tanana terrane, an Early to Middle Paleozoic highly deformed and metamorphosed crustal block

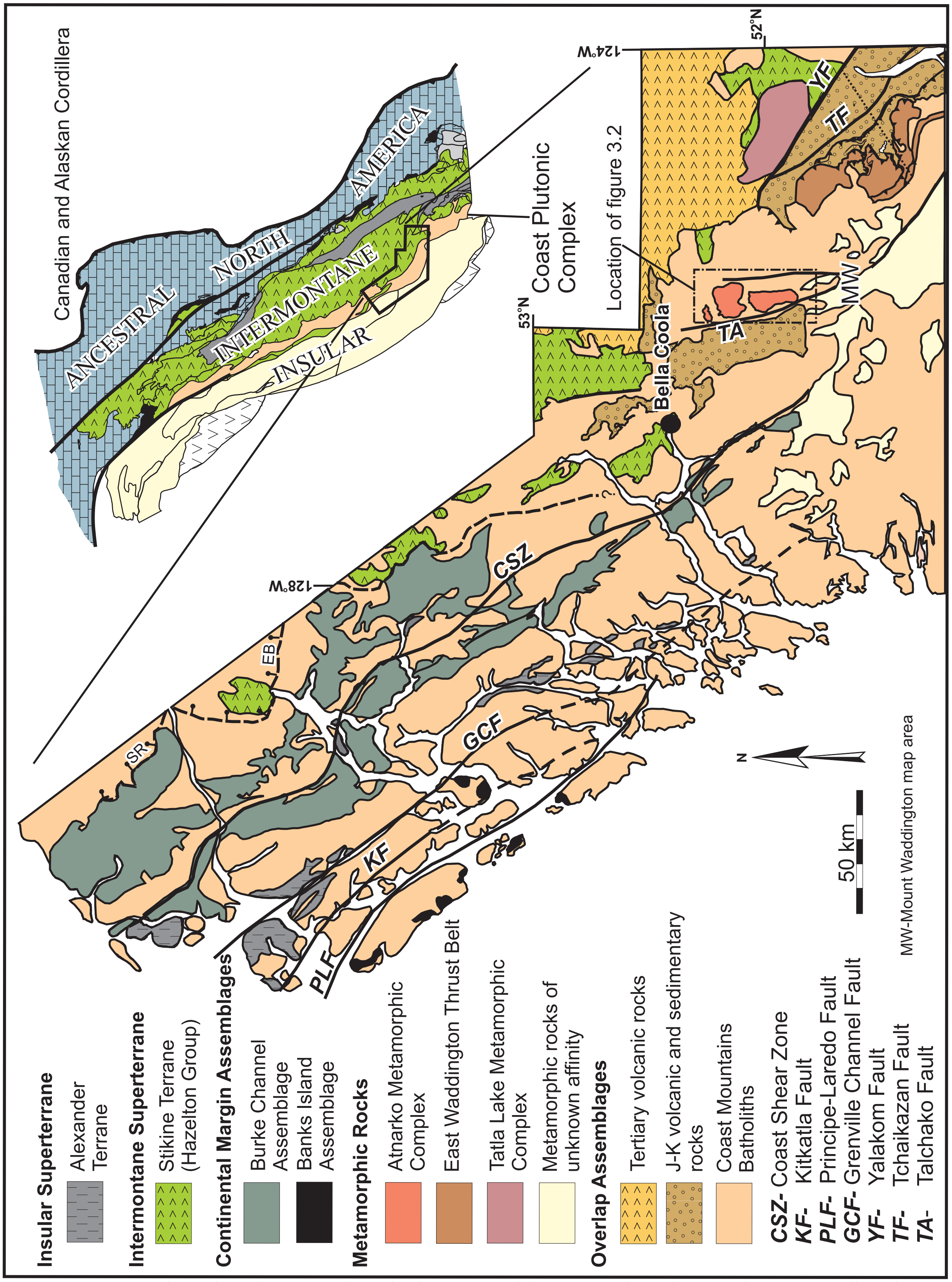

Figure 3.1. Location of study area and geologic nature of the Coast Plutonic complex surrounding the Atnarko complex. SR, EB-Shames River and Eastern Boundary detachment systems, respectively. MW-Mount Waddington Map area. Modified from Boghossian et al., [2000]; Chardon et al., [1999]; Rusmore and Woodsworth [1994]; Rusmore et al., [2005] and van der Heyden et al., [1994].

with North American affinity (Boghossian and Gehrels, 2000; Gareau and Woodsworth, 2000; Gehrels and Boghossian, 2000; Colpron et al., 2006).

Latest Jurassic to Late Cretaceous sedimentary basins and arc volcanic deposits overlie the two superterranes. Basin development was complex and characteristics of the basins change from south to north along the Cordilleran margin. In the north the basins are thought to represent pull-apart features along the margin that were created during Late Jurassic transtension (McClelland et al., 1992; van der Heyden, 1992), whereas in the south the basins appear to have been formed in a forearc setting during uplift of the arc related to accretion (Schiarizza et al., 1997; Umhoefer et al., 2002). There is some debate as to whether the volcanic stratigraphy is part of one continuous arc built across the two superterranes or two, time equivalent arcs built separately on each of the superterranes (Schiarizza et al., 1997; Rusmore et al., 2000; Umhoefer et al., 2002; Israel et al., 2006).

The earliest interaction between the Insular and Intermontane superterranes is believed to have occurred by at least Middle Jurassic and possibly as early as latest Triassic time (McClelland et al., 1992; van der Heyden, 1992; Gehrels, 2001). Initial accretion was followed by transtensional deformation forming intra-arc basins. Early to mid-Cretaceous collapse of the basins record final accretion of the Insular superterrane to the outboard margin of the Intermontane superterrane. An Early to Late Cretaceous southwest to west verging thrust system was formed along the western margin of the Coast plutonic complex. This thrust system is slightly older than, and in places is coeval with, a northeast to north verging system formed on the eastern margin (Journeay and Friedman, 1993; Rusmore and Woodsworth, 1994; Crawford et al., 2000; McClelland et al., 2000). Late Jurassic to mid-Cretaceous amalgamation was associated with sinistral strike-slip faulting that may have resulted in 800 km of left-lateral translation through the arc (Monger et al., 1994; Umhoefer et al., 2002; Israel et al., 2006). Sinistral transpression was followed by dextral transpression beginning in the Late Cretaceous (<80 Ma) and continued to the Tertiary

(Andronicos et al., 1999; McClelland et al., 2000). Extensive uplift and exhumation occurred throughout the arc beginning in the Paleocene and continuing into the Eocene (Andronicos et al., 2003; Rusmore et al., 2005).

GEOLOGY OF THE ATNARKO COMPLEX

Regional relationships

The Atnarko complex is characterized by a northwest trending belt of metavolcanic and metasedimentary rocks, gneisses and migmatites that form thrust sheets and fault panels (Fig. 3.2). Plutonic rocks of variable ages and states of deformation intrude the complex. To the west of the complex Early Cretaceous sedimentary and volcanic strata of the Monarch assemblage unconformably overlie undeformed Jurassic plutons and are juxtaposed next to the Atnarko complex across the steeply dipping Talchako fault zone. The complex is thrust to the north over variably deformed Early Cretaceous plutonic rocks. These plutonic rocks are overlain by relatively unmetamorphosed Monarch assemblage and Middle Jurassic volcanic rocks (van der Heyden, 1990; Israel and van der Heyden, 2006). The eastern boundary of the Atnarko complex is ambiguous. Batholith sized plutons characterized by extensive gneissic and mylonitic zones located at the eastern margin of the Atnarko complex may represent the eastern limit of Atnarko deformation (van der Heyden, 1991). Large pendants of metamorphic country rock similar to those found within the Atnarko complex occur within the plutons. These plutons are thrust over rocks of the Stikine terrane and comprise some of the upper plates of the East Waddington thrust belt, a northeast verging system which places rocks of the Coast plutonic complex over rocks of the Intermontane superterrane (Rusmore and Woodsworth, 1994; van der Heyden et al., 1994). To the south of the Atnarko complex metamorphosed volcanic and sedimentary rocks and gneisses and migmatites of unknown affinity are exposed throughout the Mount Waddington Map area (Roddick and Tipper, 1985). Very little is known about these rocks; however, it is likely that they share a tectonic history with the Atnarko complex.

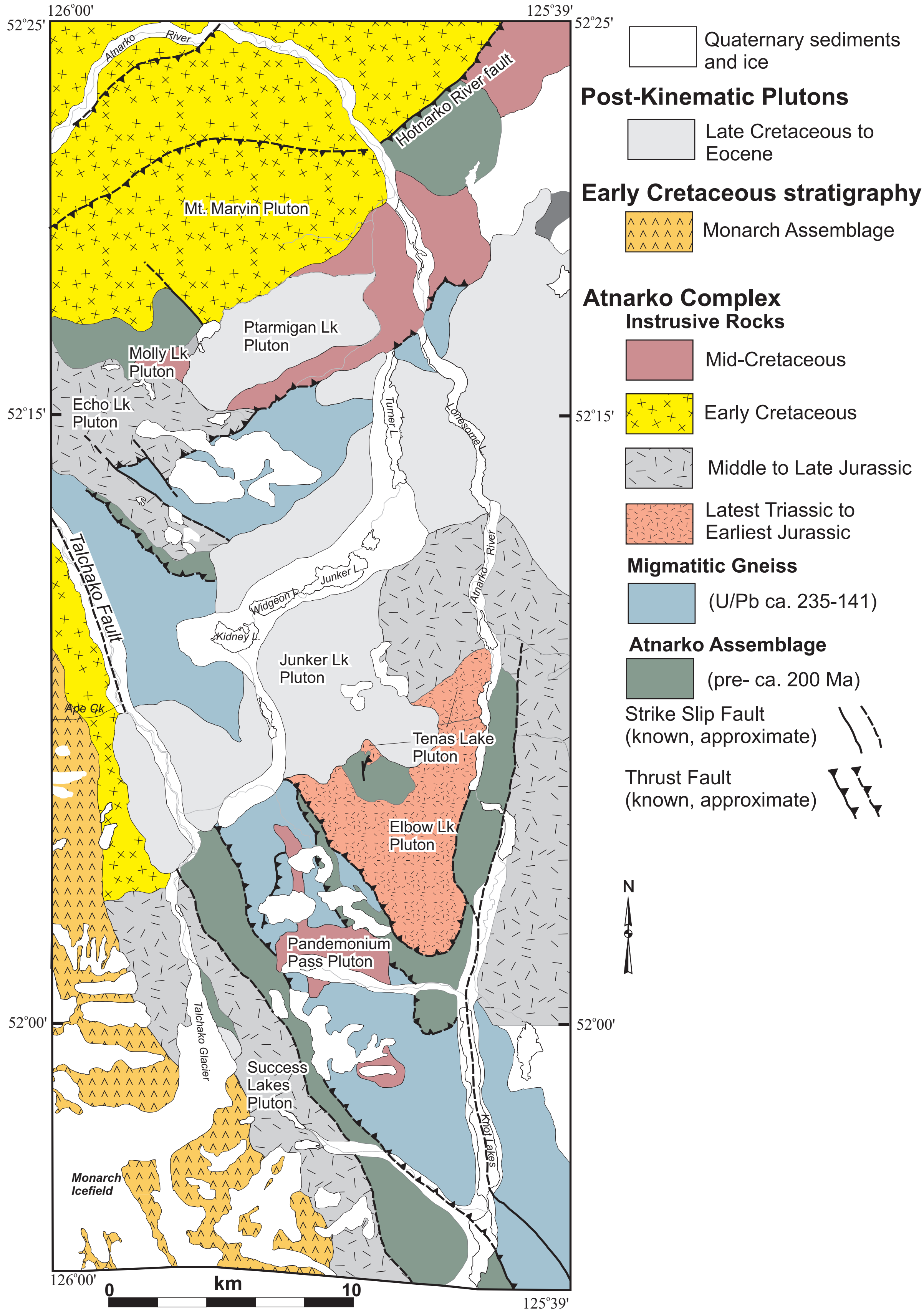

Figure 3.2. Simplified geology of the Atnarko complex. Modified from Israel and van der Heyden, 2006 and Israel et al., 2006.

Lithology

The dominant lithology in the Atnarko complex belongs to the Atnarko assemblage and comprises strongly metamorphosed and deformed mafic volcanic rocks with rare interbeds of metasedimentary rocks (Fig. 3.2). The metavolcanic rocks are basalt to basaltic andesite and occur as either massive amphibolite or thin layers of schist within metasedimentary packages (Fig. 3.3A). Lesser amounts of metasedimentary rocks are intercalated with the metavolcanic rocks and include quartz rich psammites, quartzites and rare exposures of metaconglomerate and metacarbonate (Fig. 3.3B). Little pelitic material is found within the sedimentary rocks of the Atnarko assemblage. Transposition of the Atnarko assemblage makes it difficult to ascertain whether layering between the volcanic and sedimentary portions of the Atnarko assemblage is preserved original bedding. The age of the Atnarko assemblage is not well constrained but must be older than a ca. 200 Ma quartz diorite that intrudes the assemblage in the central portion of the complex (Fig. 3.2).

Gneisses and migmatites are located within the core of the Atnarko complex where they occupy an imbricate zone in the southern portion of the complex and form hangingwall and footwall sheets in the north (Fig. 3.2). Quartz diorite to tonalite orthogneiss dominate and compositional banding is defined by bands of quartz and plagioclase separated by segregation of hornblende and biotite. Gneisses range from fine to coarse grained; coarse bands comprise large plagioclase crystals in a matrix of quartz and finer grained feldspar. Locally amphibolite layers up to several metres in thickness dominate the gneissic rocks. These layers are composed almost entirely of amphibole and plagioclase with minor quartz. Migmatites are located within the gneisses and within the Atnarko assemblage where the assemblage is structurally overlain by gneisses. The migmatitic portion of the gneisses was not mappable as a separate unit at the scale of this study. Two textural types of migmatites are recognized in the Atnarko complex and they are spatially related to one another. 1) stromatic migmatites – these are most common and are

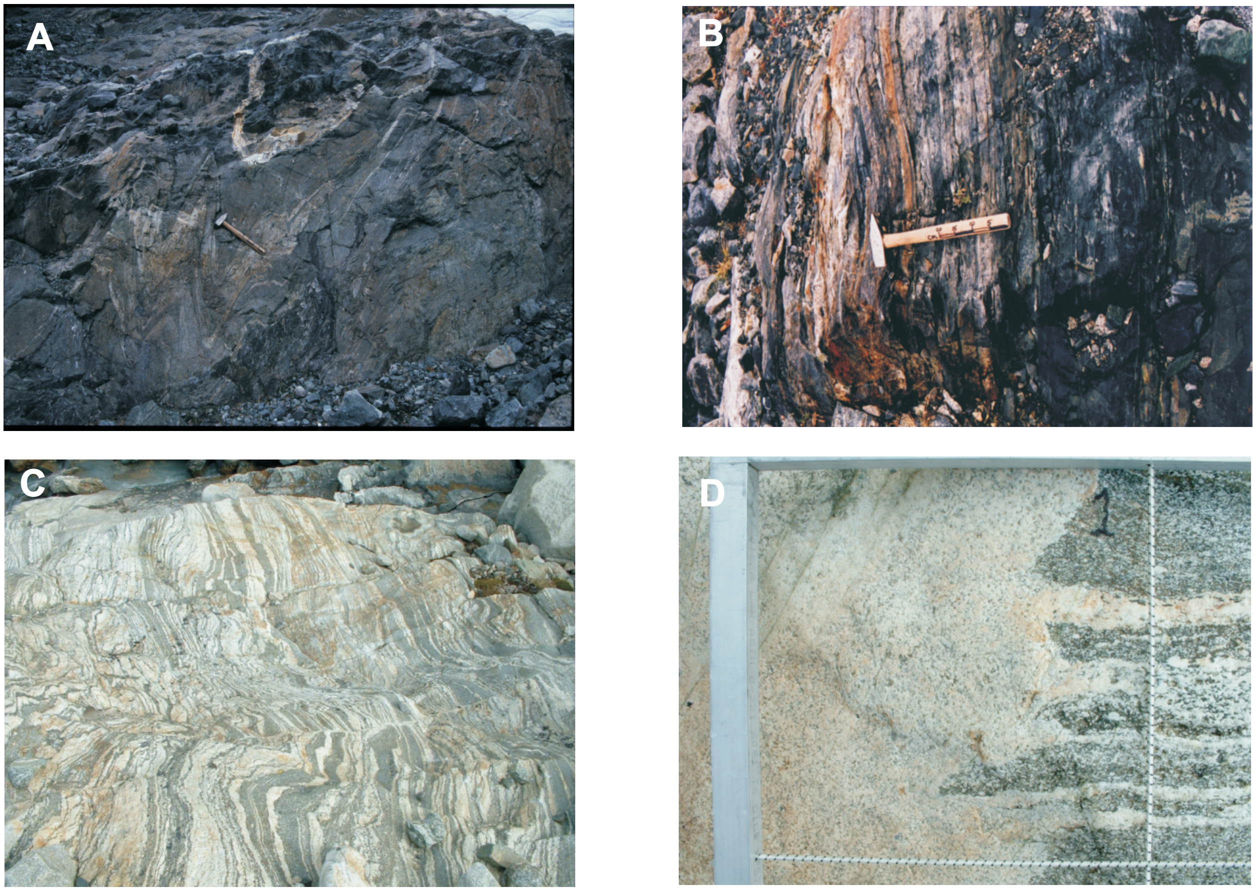

Figure 3.3. A) Folded metavolcanic rocks from the southern Atnarko complex. Folds verge towards the southwest. B) Bedded metasedimentary rocks with thin metacarbonate (light beige) within the Atnarko assemblage. C) Stromatic migmatites from the central Atnarko complex, view towards the northwest. D) Foliation parallel and cross-cutting leucosomes from the central Atnarko complex.

defined by vein/dyke-like leucosomes parallel to foliation and ranging in thickness from <1 cm to over 1 m (Fig. 3.3C). Leucosomes are composed of plagioclase, quartz, garnet, muscovite ± K-feldspar and although folded, generally show little evidence of solid state deformation displaying granitic like textures in both outcrop and thin section. 2) cross-cutting migmatite – in these occurrences the leucosomes occur at high-angles to the main foliation. The cross-cutting migmatite have the same composition and textures as the foliation parallel leucosomes (Fig. 3.3D). Network like textures and small pockets of previous in situ melt are also found locally developed within the Atnarko complex.

Structural relationships

The Atnarko complex records several major structural and tectonic events that affected the entire Coast plutonic complex. These include; 1) an enigmatic pre-Late Jurassic event, 2) Early to Late Cretaceous southwest and northeast directed contraction with associated sinistral shear, 3) Late Cretaceous high angle sinistral and dextral ductile shearing and 4) latest Cretaceous to Tertiary brittle dextral faulting (van der Heyden, 1990; van der Heyden, 1991).

Jurassic Deformation

Evidence for Jurassic deformation in the Atnarko complex includes: 1) latest Triassic to earliest Jurassic plutons with syn-magmatic deformation features intruding strongly deformed Atnarko assemblage metavolcanic and metasedimentary rocks; 2) strongly deformed quartz-diorite intruded by an amphibolitic dyke that is encompassed by a less deformed ca. 143 Ma pluton (Fig. 3.4A); 3) a 167 Ma U-Pb titanite age that records a Middle Jurassic thermal event, and, 4) zircons from two separate metarhyolite units located in the southern Atnarko, interpreted as metamorphic grains, record ages of ca. 164 Ma and 158 Ma (van der Heyden, 1991; van der Heyden, 2004).

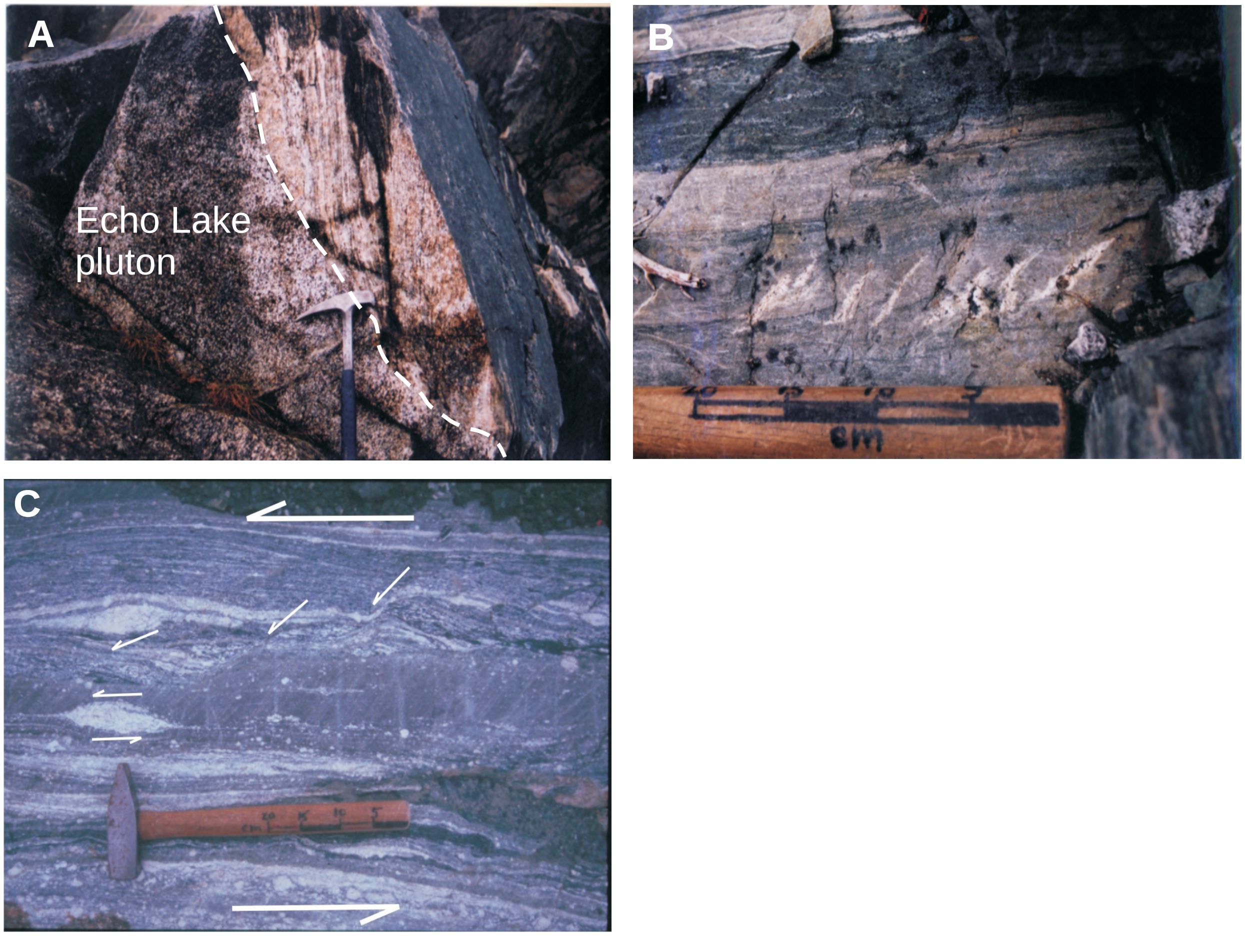

Figure 3.4. A) Outcrop showing relationship between the Echo Lake pluton and older more deformed rocks. The foliated Echo Lake pluton encloses more strongly deformed orthogneiss. B) Melt filled tension fractures within metasedimentary rocks near the late syn-tectonic Pandemonium Pass pluton. Sense of shear is sinistral. C) Portion of the main northwest striking mylonitic fabric from the southern Atnarko complex with apparent sinistral shear fabrics.

Early to Late Cretaceous Deformation

The main structural features within the Atnarko complex derive from Early to Late Cretaceous compression. Mylonite zones several hundred metres wide separate rock units and place higher metamorphic grade rocks over lower grade rocks resulting in an apparent reversal of metamorphic grade. Compression was initially southwest to west directed, began as early as ~117 Ma, and likely overlapped with younger north-northeast directed compression that lasted until ~ 80 Ma (see Chapter 2). This event, characterized by older southwest-west directed thrusting followed by north-northeast directed thrusting, is well documented throughout the Coast plutonic complex both to the northwest and southeast of the study area (Crawford et al., 1987; Journeay and Friedman, 1993; Rusmore and Woodsworth, 1994).

In the Atnarko complex compression is accompanied by sinistral translation as evidenced by: 1) oblique sinistral thrusts observed in the northern part of the complex; 2) the geometry of melt filled fractures associated with the emplacement of the Pandemonium Pass pluton, a syn-deformation pluton thrust to the north (see next section), which indicate sinistral movement in the area (Fig. 3.4B); and 3) kinematic indicators within shear zones associated with the main northwest striking foliation that suggest apparent sinistral movement (Fig. 3.4C).

Dextral and sinistral shear zones deform the main Early to Late Cretaceous foliation throughout the complex. The shear zones range in size from less than 20 cm to over several meters and occur as conjugate features. Field observations suggest that these shear zones initially developed under ductile conditions and later became brittle-ductile features. The shear zones are interpreted to be related to flattening across the complex during the waning stages of compression.

Latest Cretaceous to Tertiary Deformation

Dextral brittle faulting affects all rocks in the Atnarko complex. The event is related to large dextral strike-slip faults located east and southeast of the study area. This event affected the entire Cordillera from Alaska to southern US.

GEOCHRONOLOGY: AGE AND THERMAL HISTORY OF THE ATNARKO COMPLEX

Geochronometric analyses were determined using U-Pb TIMS and LA-ICPMS analyses of zircon, U-Pb TIMS analyses of titanites and monazites and $^{40}Ar/^{39}Ar$ analyses of hornblende, biotite and muscovite. All analyses from this study were performed at the University of British Columbia’s Pacific Centre for Isotopic and Geochemical Research. TIMS analyses were completed using conventional methods (Mortensen et al., 1995). LA-ICPMS and $^{40}Ar/^{39}Ar$ analyses employed methods described in Appendix I.

Plutonism

Magmatism within the Atnarko complex spanned approximately 150 My from latest Triassic to earliest Tertiary. The plutonic bodies vary in composition but are mainly quartz diorite to tonalitic and minor granodiorite.

Late Triassic to Early Jurassic

A package of migmatitic orthogneiss from the central part of the complex comprises the oldest dated rocks in the field area. The orthogneiss is structurally overlain by rocks of the Atnarko complex across a north-northeast dipping fault (Fig. 3.2). A sample analyzed from the orthogneiss returned complex TIMS U-Pb zircon analyses that are slightly discordant and are strung out along concordia (Fig. 3.5A; Table 3.1). A regression of seven zircon fractions results in a lower intercept of 120 ± 13 Ma and an upper intercept of 235 ± 25 Ma. The lower intercept coincides with the age of titanite growth in the same sample (see next section). LA-ICPMS analyses of zircons from the same sample returns a mean $^{206}Pb/^{238}U$ age of 194.3 ± 2.0 Ma (Fig.

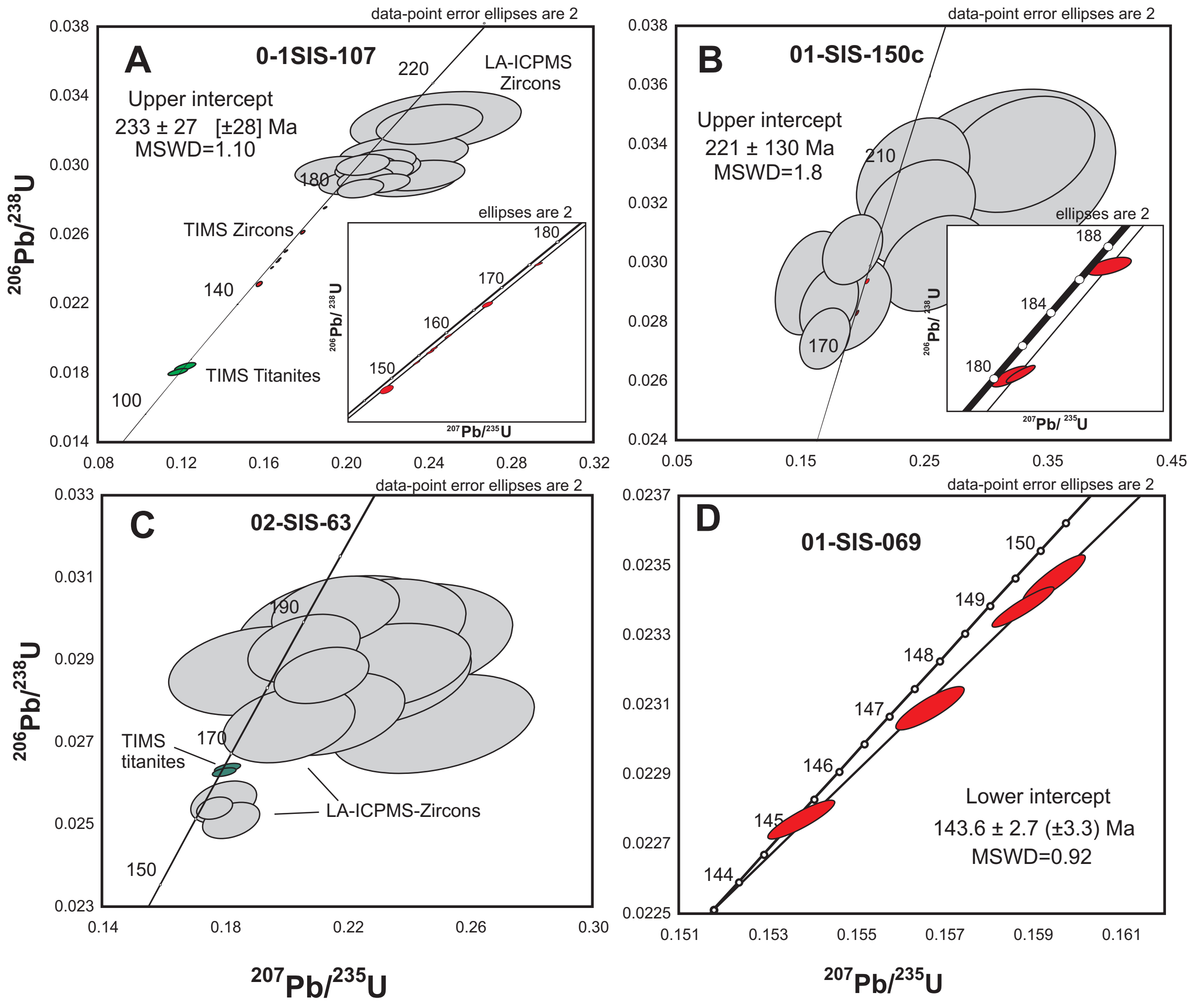

Figure 3.5. U-Pb concordia diagrams for igneous and metamorphic rocks of the Atnarko complex: A) Orthogneiss of the central Atnarko; B) Syn-tectonic, variably deformed quartz-diorite of the Tenas Lake pluton; C) Tonalitic Elbow Lake pluton; D) Variably deformed quartz-diorite of the Echo Lake pluton. Continued on next page.

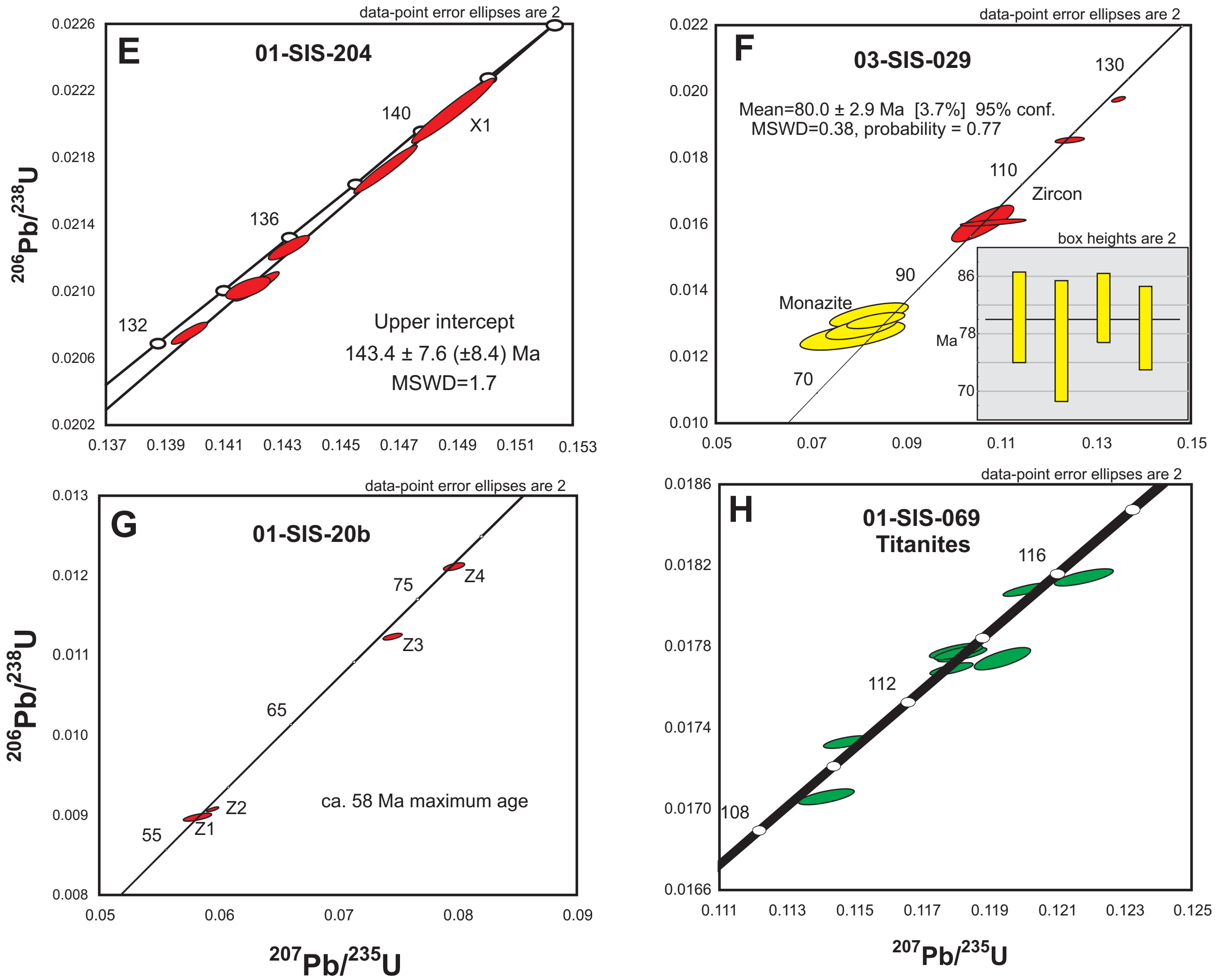

Figure 3.5. continued. F) Syn-tectonic Pandemonium Pass pluton; G) Post-tectonic Ptarmigan Lake pluton; H) Titanites from the Echo Lake pluton. Grey ellipses are LA-ICPMS zircon analyses, Red ellipses are TIMS zircon analyses except X1-exenotime, Green ellipses are TIMS titanite analyses and Yellow ellipses are TIMS monazite analyses. All error ellipses are 2σ. TIMS data presented in Table 3.1 and LA-ICPMS in Table 3.2.

Table 3.1**.** U-Pb TIMS analytical data

Fraction[1]	Wt	U^{2}	Pb^{*3}	$^{206}Pb^{4}$	Pb^{5}	Th/U[6]	Isotopic ratios (1σ,%) [7]			Apparent ages (2σ,Ma) [7]		
	(mg)	(ppm)	(ppm)	^{204}Pb	(pg)		$^{206}Pb/^{238}U$	$^{207}Pb/^{235}U$	$^{207}Pb/^{206}Pb$	$^{206}Pb/^{238}U$	$^{207}Pb/^{235}U$	$^{207}Pb/^{206}Pb$
01sis107 Orthogneiss-central Atnarko complex												
Z1 10	404	342	8.1	13466	15.7	0.16	0.02502 (0.12)	0.1711 (0.18)	0.04959 (0.09)	159.3 (0.4)	160.4 (0.5)	176.1 (4.1)
Z2 14	355	446	10.4	12055	19.7	0.16	0.02458 (0.11)	0.1681 (0.17)	0.04960 (0.09)	156.5 (0.3)	157.8 (0.5)	176.4 (4.3)
Z3 19	235	482	10.9	22144	7.5	0.14	0.02408 (0.12)	0.1644 (0.18)	0.04953 (0.08)	153.4 (0.4)	155.8 (0.4)	176.2 (0.6)
Z4 32	256	547	12.6	3564	58.9	0.16	0.02446 (0.12)	0.1673 (0.20)	0.04960 (0.11)	155.8 (0.4)	157.1 (0.6)	176.2 (5.0)
Z5 1	46	353	9.3	7575	3.6	0.20	0.02754 (0.09)	0.1900 (0.18)	0.05003 (0.11)	175.1 (0.3)	176.6 (0.6)	196.6 (5.1/5.2)
Z6 2	30	550	12.0	4916	4.8	0.14	0.02314 (0.26)	0.1582 (0.36)	0.04956 (0.30)	147.5 (0.8)	149.1 (1.0)	175 (14)
Z7 5	34	486	12.2	6569	4.0	0.20	0.02612 (0.16)	0.1793 (0.25)	0.04978 (0.18)	166.2 (0.5)	167.5 (0.8)	184.9 (8.5)
T5 9	194	112	1.9	138	198	0.12	0.01806 (0.45)	0.1191 (1.6)	0.04784 (1.4)	115.4 (1.0)	114.3 (3.5)	91 (63/66)
T6 18	157	143	2.4	121	243	0.07	0.01836 (0.52)	0.1225 (1.7)	0.0839 (1.4)	117.3 (1.2)	117.3 (3.9)	118.2 (66/69)
01sis150C Tenas Lake pluton												
Z1	175	250	7.1	1972	38.8	0.34	0.002836 (0.12)	0.1962 (0.25)	0.05017 (0.15)	180.3 (0.4)	181.9 (0.8)	202.6 (7.1/7.2)
Z3	60	215	6.1	1384	16.3	0.38	0.02834 (0.15)	0.1953 (0.32)	0.04998 (0.23)	180.1 (0.5)	181.1 (1.1)	194 (11)
Z4	27	212	6.4	2050	5.1	0.43	0.02940 (0.12)	0.2035 (0.37)	0.05020 (0.31)	186.8 (0.5)	188.1 (1.3)	204 (14)
01-SIS-63 Elbow Lake pluton												
T1	142	489	14.6	433	278	0.83	0.02637 (0.18)	0.1811 (0.95)	0.04981 (0.87)	167.8 (0.6)	169.8 (3.0)	186 (40/41)
T2	161	477	13.9	417	314	0.74	0.02627 (0.16)	0.1800 (0.88)	0.04971 (0.80)	167.1 (0.5)	168.1 (2.7)	181 (37/38)
01-SIS-69 Echo Lake pluton												
Z1 13	600	298	6.9	7358	34.8	0.32	0.02338 (0.10)	0.1588 (0.18)	0.04925 (0.09)	149.0 (0.3)	149.6 (0.5)	159.7 (4.3/4.4)
Z2 19	303	393	9.0	6934	24.3	0.34	0.02309 (0.11)	0.1567 (0.20)	0.04923 (0.11)	147.1 (0.3)	147.8 (0.5)	158.8 (5.3)
Z3 34	537	455	10.6	7218	48.6	0.33	0.02346 (0.12)	0.1595 (0.18)	0.04930 (0.09)	149.5 (0.3)	150.3 (0.5)	162.2 (4.4)
Z4 11	590	359	8.2	2594	98.2	0.35	0.02277 (0.10)	0.1538 (0.20)	0.04898 (0.12)	145.1 (0.3)	145.2 (0.5)	147.0 (5.6/5.7)
T1 8	227	501	10.6	512	265	0.98	0.01808 (0.15)	0.1201 (0.46)	0.04817 (0.36)	115.5 (0.3)	115.2 (1.0)	108 (17)
T2 11	276	624	12.2	469	432	0.73	0.01777 (0.16)	0.1181 (0.49)	0.04821 (0.38)	113.5 (0.4)	113.3 (1.1)	109 (18)
T3 13	249	528	10.5	458	338	0.79	0.01776 (0.16)	0.1182 (0.51)	0.04827 (0.40)	113.5 (0.4)	113.5 (1.1)	112 (19)
T4 9	181	477	10.5	406	257	1.13	0.01814 (0.19)	0.1218 (0.58)	0.04870 (0.46)	115.9 (0.5)	116.7 (1.3)	133 (21/22)
T5 8	226	567	11.8	488	309	0.98	0.01778 (0.17)	0.1180 (0.52)	0.04813 (0.42)	113.6 (0.4)	113.2 (1.1)	105 (20)
T6 3	120	644	12.3	491	174	0.71	0.01733 (0.15)	0.1147 (0.44)	0.04802 (0.35)	110.8 (0.3)	110.3 (0.9)	100 (16)
T7 4	143	541	11.6	469	188	1.12	0.01793 (0.15)	0.1180 (0.45)	0.04835(0.35)	113.0 (0.3)	113.2 (1.0)	117 (17)
T8 5	140	388	8.1	446	140	0.99	0.01774 (0.25)	0.1194 (0.57)	0.04801 (0.43)	113.4 (0.6)	114.5 (1.2)	139 (20)
T9 8	73	312	6.7	365	69.5	1.30	0.01706 (0.19)	0.1142 (0.59)	0.04855 (0.48)	119.0 (0.4)	109.8 (1.2)	126 (23)
01-SIS-204 Orthogneiss-southern Atnarko complex												
Z1 6	359	337	6.7	11810	13.2	0.14	0.02103 (0.17)	0.1422 (0.22)	0.04903 (0.09)	134.2 (0.5)	135.0 (0.6)	149.1 (4.3)
Z2 16	529	327	6.3	19130	11.5	0.12	0.02075 (0.13)	0.1399 (0.18)	0.04891 (0.09)	132.4 (0.3)	133.0 (0.4)	143.4 (4.3)
Z3 16	415	362	7.4	12200	16.4	0.14	0.02173 (0.27)	0.1466 (0.30)	0.04892 (0.08)	138.6 (0.8)	138.9 (0.8)	144.1 (3.9)
Z4 21	256	418	8.2	4744	29.4	0.09	0.02126 (0.14)	0.1433 (0.20)	0.04890 (0.11)	135.6 (0.4)	136.0 (0.5)	142.9 (5.1)
Z5 21	445	206	4.3	7357	16.9	0.17	0.02217 (0.10)	0.1503 (0.17)	0.04918 (0.09)	141.3 (0.3)	142.2 (0.5)	156.5 (4.4/4.5)
Z6 26	112	232	4.5	2145	15.7	0.09	0.02102 (0.13)	0.1419 (0.22)	0.04895 (0.16)	134.1 (0.4)	134.7 (0.6)	145.5 (7.7)
X1 3	88	4550	91.3	13910	38.9	0.02	0.02208 (0.36)	0.1489 (0.39)	0.04891 (0.10)	140.8 (1.0)	141.0 (1.0)	143.5 (4.8)
T2 13	99	21	0.4	29	212	0.10	0.01816 (4.1)	0.1267 (26.1)	0.05060 (24.1)	116.0 (9.4)	121 (60)	223 (846/1819)
T3 9	76	60	1.0	22	1260	0.08	0.01760 (13.5)	0.1143 (51.3)	0.04708 (43.9)	112 (30)	110 (107)	53 (1338/9999)
03sis29 Pandemonium Pass pluton												
Z1 20	18	344	5.7	339	18.9	0.46	0.01605 (0.26)	0.1083 (2.6)	0.04897 (2.4)	102.6 (0.5)	104.5 (5.2)	146 (111/119)
Z2 12	27	336	6.8	892	12.5	0.44	0.01976 (0.18)	0.1345 (0.44)	0.04937 (0.35)	126.2 (0.5)	128.2 (1.1)	165 (16)
Z3 ~60	32	337	5.3	298	37.6	0.29	0.01602 (1.4)	0.1061 (2.5)	0.04803 (1.6)	102.4 (2.9)	102.4 (5.0)	101 (75/78)
Z4 ~50	38	403	7.3	1563	11.2	0.25	0.01853 (0.19)	0.1243 (1.0)	0.04865 (0.95)	118.4 (0.5)	119.0 (2.3)	131 (44/45)
M1 9	35	676	154	24	3821	94.8	0.01328 (10.5)	0.0725 (42.6)	0.03959 (36.5)	85 (18)	71 (58)	-377 (1261/6935)
M2 17	23	621	89.4	34	784	91.8	0.01297 (3.7)	0.0783 (14.1)	0.04379 (12.0)	83.1 (6.0)	77 (21)	-122 (507/730)
M3 17	36	688	93.7	69	398	91.2	0.01327 (1.1)	0.0823 (4.1)	0.04498 (3.4)	85.0 (1.8)	80.3 (6.3)	-57 (160/177)
M4 3	20	501	85.0	58	196	93.3	0.01264 (1.4)	0.0788 (5.7)	0.04523 (4.9)	81.0 (2.2)	77.0 (8.4)	-43 (224/259)
M5 7	21	961	117	88	232	90.3	0.01310 (0.78)	0.0837 (3.0)	0.04635 (2.6)	83.9 (1.3)	81.6 (4.8)	16 (120/129)
M6 11	27	866	112	69	361	91.0	0.01287 (1.1)	0.0807 (3.8)	0.04549 (3.2)	82.4 (1.7)	78.8 (5.8)	-29 (149/164)
01sis20B Ptarmigan Lake dyke												
Z1	152	501	4.3	814	53.0	0.19	0.00907 (0.13)	0.0595 (0.36)	0.04760 (0.27)	58.2 (0.2)	58.7 (0.4)	79 (13)
Z2	56	380	3.3	343	35.9	0.26	0.00897 (0.22)	0.0583 (0.83)	0.04712 (0.70)	57.6 (0.3)	57.5 (0.9)	56 (33)
Z3	90	174	2.0	764	14.4	0.37	0.01124 (0.16)	0.0746 (0.44)	0.04812 (0.36)	72.0 (0.2)	73.0 (0.6)	105 (71)
Z4	229	95	1.2	1120	14.7	0.34	0.01211 (0.17)	0.0797 (0.44)	0.04772 (0.36)	77.6 (0.3)	77.8 (0.7)	85 (17)

[1] All zircon grains selected for analysis were air abraded prior to dissolution. Fraction ID (zircon: Z1, Z2, etc.; titanite: T1, T2, etc.; monazite: M1, M2, etc.; xenotime: X), followed by the number of grains

[2] U blank correction of 1pg ± 20%; U fractionation corrections were measured for each run with a double $^{233-235}U$ spike.

[3] Radiogenic Pb

[4] Measured ratio corrected for spike and Pb fractionation of 0.28-0.37/amu ± 20% (Daly collector) which was determined by repeated analysis of NBS Pb 981 reference material throughout the course of this study.

[5] Total common Pb in analysis based on blank isotopic composition.

[6] Model Th/U derived from radiogenic ^{208}Pb and the $^{207}Pb/^{206}Pb$ age of fraction; for monazites percent radiogenic ^{208}Pb is listed.

[7] Blank and common Pb corrected; Pb procedural blanks were ~1.5-5 pg and U <1 pg. Common Pb concentrations are based on Stacey-Kramers model Pb at the interpreted age of the rock or the $^{207}Pb/^{206}Pb$ age of the fraction (Stacey and Kramers, 1975).

3.5A; Table 3.2), but fall along the regression line defined by the TIMS analyses. Cathodoluminescence analyses of zircons used in the laser analyses indicate regular zoning patterns with no evidence of older cores or metamorphic overgrowths (Fig. 3.6A). The upper intercept age is interpreted to correspond with the crystallization age and that the orthogneiss underwent strong lead loss in Early Cretaceous time.

The Tenas Lake pluton is next oldest rock body. The Tenas Lake pluton is a variably foliated quartz-diorite to diorite, located near the eastern edge of the Atnarko complex (Fig. 3.2). The pluton intrudes rocks of the Atnarko assemblage and shows evidence for syn-kinematic intrusion such as lobate contacts with the country rocks and stretched dyklets emanating from the intrusive body (Fig. 3.7A). The spatial extent of this pluton is poorly constrained but is interpreted to include a larger body east of Tenas Lake (Fig. 3.2). The U-Pb TIMS and LA-ICPMS analyses of zircons from the Tenas Lake pluton are complicated and preclude straightforward interpretation of crystallization age. A regression line through three TIMS zircon fractions yields an upper intercept age of 221±130 Ma (Fig. 3.5B; Table 3.1). Several LA-ICPMS analyses of zircons from the same sample yield a wide range of results that likely represent significant lead loss. Imaging of the zircons reveals some evidence for sectoral zoning but no evidence for older cores or metamorphic overgrowths (Fig. 3.6B). The crystallization age is therefore interpreted as ~24 Ma, the weighted mean of the $^{207}Pb/^{206}Pb$ ages (Table 3.1).

The Elbow Lake pluton located in the central portion of the Atnarko complex is a large body of biotite ± hornblende tonalite (Fig. 3.2). It is thrust over gneisses and migmatite and metavolcanic and metasedimentary rocks of the Atnarko assemblage. Near the contact with structurally underlying rocks, the pluton is strongly deformed with well developed mylonitic fabrics several meters in thickness. The deformation within the Elbow Lake pluton decreases dramatically away from the contact and becomes relatively undeformed several hundred meters away from the lower structural contact. LA-ICPMS analyses of several zircon grains from the pluton reflect

Table 3.2. U-Pb LA-ICPMS data

Analysis #	$^{207}Pb/^{235}U$	$^{207}Pb/^{235}U$	$^{206}Pb/^{238}U$	$^{206}Pb/^{238}U$	rho	$^{207}Pb/^{206}Pb$	$^{207}Pb/^{206}Pb$	$^{207}Pb/^{235}U$	$^{207}Pb/^{235}U$	$^{206}Pb/^{238}U$	$^{206}Pb/^{238}U$	$^{207}Pb/^{206}Pb$	$^{207}Pb/^{206}Pb$
01-SIS-107 Orthogneiss-central Atnarko complex													
107S1	0.2433	0.01682	0.0325	0.00071	0.316003	0.05487	0.00357	221.1	13.74	206.2	4.44	407	139.44
107S2	0.23598	0.00875	0.0294	0.00036	0.330234	0.05793	0.00203	215.1	7.19	186.8	2.25	526.9	75.44
107S3	0.21902	0.00552	0.02961	0.00026	0.348401	0.05552	0.00132	201.1	4.59	188.1	1.62	433	51.56
107S4	0.20825	0.00527	0.03001	0.00025	0.329191	0.05119	0.00122	192.1	4.43	190.6	1.58	249.2	54.16
107S5	0.22801	0.0127	0.03063	0.00046	0.269626	0.0531	0.00282	208.6	10.5	194.5	2.9	332.8	115.89
107S6	0.21711	0.00684	0.03016	0.0003	0.315728	0.05279	0.00157	199.5	5.71	191.6	1.89	319.9	66.34
107S7	0.20956	0.00605	0.02981	0.00028	0.325349	0.05137	0.0014	193.2	5.07	189.4	1.76	257.7	61.56
107S8	0.23086	0.00933	0.02909	0.00038	0.323226	0.05688	0.00218	210.9	7.7	184.9	2.39	486.4	82.97
107S9	0.2093	0.00547	0.0292	0.00026	0.340700	0.05304	0.00131	193	4.59	185.6	1.63	330.6	54.93
107S10	0.20314	0.0066	0.02899	0.00029	0.307894	0.05174	0.0016	187.8	5.57	184.2	1.82	273.8	69.49
107S11	0.21636	0.00802	0.0298	0.00035	0.316850	0.05278	0.00187	198.9	6.69	189.3	2.2	319.5	78.53
107S12	0.24037	0.01048	0.03235	0.00047	0.333229	0.05574	0.00226	218.7	8.58	205.2	2.96	441.7	87.78
107S13b	0.19404	0.00753	0.02967	0.00034	0.295296	0.04942	0.00184	180.1	6.4	188.5	2.11	167.7	84.67
107S14	0.2192	0.00481	0.02895	0.00022	0.346314	0.05439	0.00112	201.2	4.01	184	1.39	387.3	45.36
107S15	0.20718	0.00455	0.02865	0.00022	0.349651	0.05349	0.00111	191.2	3.82	182.1	1.38	349.6	46.23
01-SIS-150c Tenas Lake pluton													
150SIS1	0.32745	0.02464	0.03368	0.0008	0.315662	0.068	0.00498	287.6	18.85	213.5	4.99	868.5	144.94
150SIS3	0.16937	0.00832	0.02748	0.00042	0.311133	0.04543	0.00222	158.9	7.23	174.8	2.6	0.1	80.74
150SIS4	0.19152	0.00992	0.03047	0.00048	0.304138	0.04579	0.00235	177.9	8.45	193.5	3.02	0.1	106.02
150SIS5	0.24552	0.0187	0.03173	0.00072	0.297926	0.05478	0.00409	222.9	15.24	201.4	4.52	403.1	159.19
150SIS6	0.24062	0.01878	0.03292	0.00081	0.315255	0.05332	0.00409	218.9	15.37	208.8	5.04	342.2	164.56
150SIS7	0.25843	0.01759	0.03001	0.00066	0.323113	0.06204	0.00417	233.4	14.19	190.6	4.11	675.3	137.44
150SIS8	0.30807	0.03941	0.03278	0.00126	0.300472	0.07016	0.00888	272.7	30.59	207.9	7.86	933.2	240.08
150SIS9	0.18914	0.01395	0.02861	0.00064	0.303299	0.04685	0.00342	175.9	11.91	181.8	3.98	41.3	166.31
150SIS10	0.17251	0.0097	0.02863	0.00052	0.323016	0.044	0.00247	161.6	8.4	182	3.24	0.1	22
150SIS11	0.15812	0.01203	0.02934	0.00071	0.318068	0.03922	0.00294	149.1	10.54	186.4	4.43	0.1	0

continuation of Table 3.2. U-Pb LA-ICPMS data

Analysis #	$^{207}Pb/^{235}U$	$^{207}Pb/^{235}U$	$^{206}Pb/^{238}U$	$^{206}Pb/^{238}U$	rho	$^{207}Pb/^{206}Pb$	$^{207}Pb/^{206}Pb$	$^{207}Pb/^{235}U$	$^{207}Pb/^{235}U$	$^{206}Pb/^{238}U$	$^{206}Pb/^{238}U$	$^{207}Pb/^{206}Pb$	$^{207}Pb/^{206}Pb$
02-SIS-63 Elbow Lake pluton													
63S1	0.21158	0.0063	0.02862	0.00028	0.328566	0.05481	0.00154	194.9	5.28	181.9	1.74	404.3	61.02
63S2	0.21472	0.0098	0.02768	0.00041	0.324537	0.05955	0.00259	197.5	8.19	176	2.56	587.3	91.79
63S3	0.24778	0.01348	0.02744	0.00049	0.328238	0.06639	0.00344	224.8	10.97	174.5	3.09	818.6	104.59
63S4	0.20108	0.00877	0.02743	0.00038	0.317634	0.05272	0.00218	186	7.41	174.5	2.4	316.8	91.47
63S5	0.21612	0.00849	0.03017	0.00035	0.295311	0.0513	0.00191	198.7	7.09	191.6	2.18	254.5	83.56
63S6	0.2312	0.01182	0.02883	0.00043	0.291739	0.05661	0.00276	211.2	9.75	183.2	2.7	475.8	104.92
63S7a	0.21757	0.01395	0.02967	0.00056	0.294371	0.05432	0.00333	199.9	11.64	188.5	3.52	384.3	131.92
63S8	0.18224	0.0038	0.0251	0.00018	0.343921	0.05378	0.00106	170	3.26	159.8	1.11	361.7	43.76
63S9	0.2284	0.01305	0.02857	0.0005	0.306299	0.05815	0.00315	208.9	10.79	181.6	3.15	534.8	115.02
63S10	0.23324	0.01654	0.02942	0.00059	0.282798	0.05612	0.00379	212.9	13.62	186.9	3.69	456.9	143.71
63S11	0.22732	0.01279	0.02974	0.0005	0.298811	0.05557	0.00298	208	10.58	188.9	3.14	434.9	115.44
63S12	0.20591	0.00745	0.02927	0.00034	0.321053	0.05185	0.00177	190.1	6.27	186	2.14	278.7	76.37
63S13	0.17985	0.00436	0.02554	0.00021	0.339174	0.05181	0.00119	167.9	3.75	162.6	1.31	277.2	51.52
63S14	0.19036	0.0116	0.02873	0.00044	0.251324	0.04921	0.00291	176.9	9.9	182.6	2.75	157.9	133.02
63S15	0.17683	0.0024	0.0254	0.00011	0.319083	0.04952	0.0006	165.3	2.07	161.7	0.71	172.4	27.9

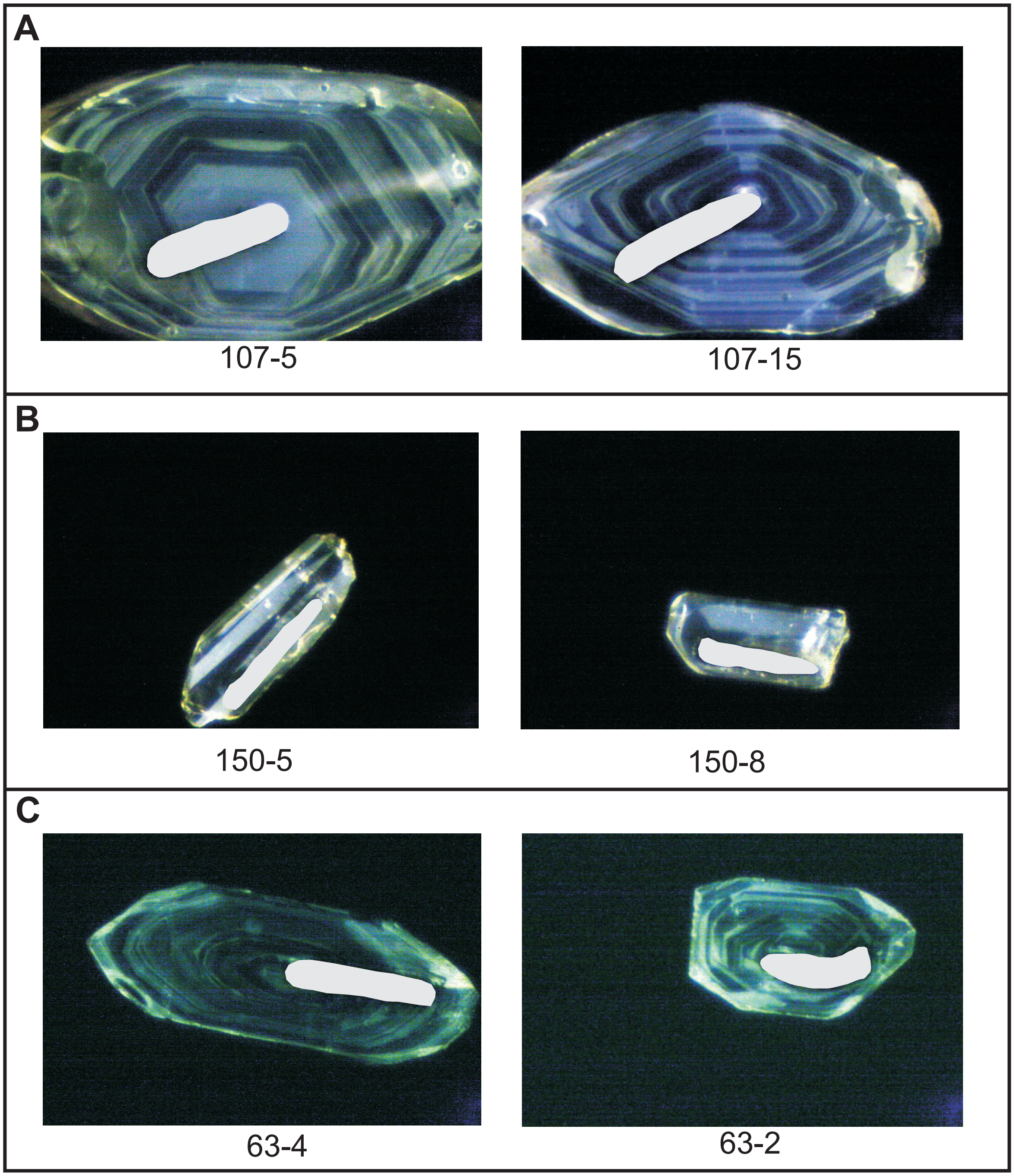

Figure 3.6. CL photomicrographs of zircons from A) Elbow Lake pluton, 02-SIS-63; B) Orthogneiss in central Atnarko complex; 01-SIS-107; C) Tenas Lake pluton 01-SIS-150C. Grey fields are laser track lines. Width of track lines A) 40 um; B) 30 um C) 25 um. Note no evidence for cores, and all track lines cross zonations in zircons.

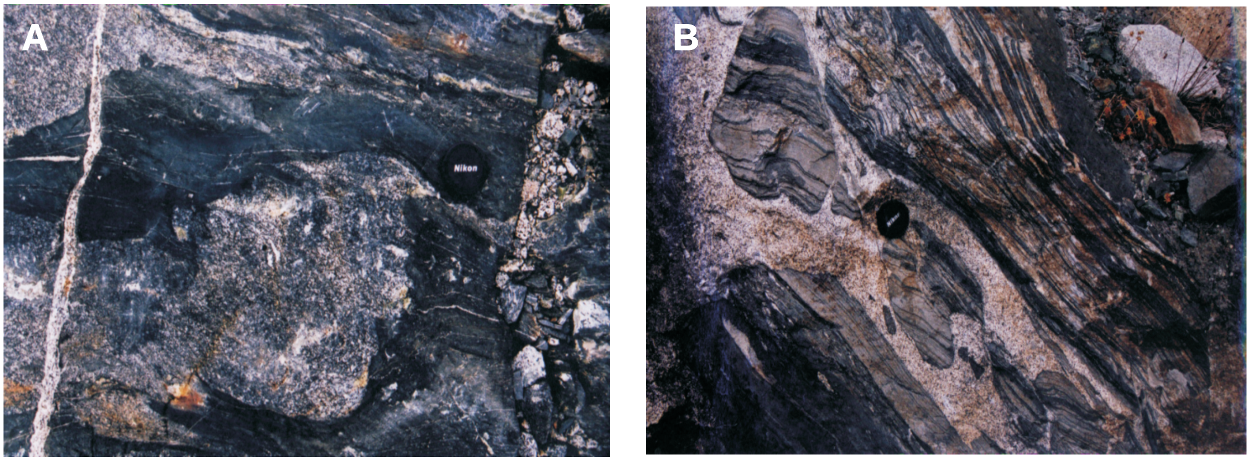

Figure 3.7. A) Looking down on outcrop of syn-tectonic features (cuspate and lobate morphology) found within the Tenas Lake pluton. Note how the intrusive rock cross-cuts and is strung-out along foliation. B) Syn-intrusion breccia near the edge of the Pandemonium Pass pluton. Magmatic material encloses fragments of wall-rock and is also folded along foliation plane.

complex systematics. A large cloud of analyses form around concordia at latest Triassic to Early Jurassic ages (Fig. 3.5C; Table 3.2). Another cluster of ages groups along concordia near 165 Ma. The Middle Jurassic ages are younger than two titanite fractions with a weighted $^{206}Pb/^{238}U$ age of 167 Ma. It is likely that the pluton underwent a lead loss event that draws the analyses down concordia from an age around latest Triassic. This is supported by Middle Jurassic titanites and cathodoluminescence images of zircons that show no evidence of older inherited cores, nor the presence of younger metamorphic overgrowth (Fig. 3.6C). The age of crystallization is interpreted as latest Triassic to earliest Jurassic.

Late Jurassic Early Cretaceous

The Echo Lake pluton is a large body of quartz diorite to diorite found in the northern portion of the study area. It structurally overlies gneisses and migmatites of the Atnarko assemblage (Fig. 3.2). The pluton is variably deformed having locally-developed, proto-mylonitic foliations, usually observed near the southern structural contact, that grades into undeformed portions of body. Screens of metavolcanic and metasedimentary rocks of the Atnarko assemblage are found within the Echo Lake pluton (Fig. 3.4A). TIMS U-Pb analyses of zircon from a sample from the Echo Lake pluton resulted in four fractions that are variably discordant (Fig. 3.5D; Table 3.1). A regression of the data indicates a lower intercept of 143.6 ± 2.7 Ma and an upper intercept of 444 ± 150 Ma. The separate fractions fall along the line becoming more discordant towards the upper intercept. LA-ICPMS analyses of the zircons from the sample return a mean $^{206}Pb/^{238}U$ age of 151.7 ± 1.8 Ma (Table 3.2). The age of the Echo Lake pluton is interpreted as corresponding to the lower intercept of the TIMS data at 143.6 ± 2.7 Ma, and the laser age and the TIMS zircon fractions the product of inheritance in the zircons.

Migmatitic orthogneiss from the southern portion of the study area represents the highest metamorphic grade core of the Atnarko complex, an imbricate zone developed during Early to Late Cretaceous thrusting (Fig. 3.2). Several zircon fractions and one xenotime fraction were analyzed using TIMS from a sample of the strongly deformed migmatitic gneiss (Fig. 3.5E; Table 3.1). Five zircon fractions define a regression line with an upper intercept at 143.4 ± 7.6 Ma. The line suggests that the zircons underwent lead loss. The single xenotime fraction analyzed is concordant with a $^{206}Pb/^{238}U$ age of 140.8 ± 1.0 Ma which is within error of the upper intercept zircon age. The crystallization age of the gneiss is interpreted as the upper intercept of the zircon fractions and the xenotime age the cooling and crystallization of xenotime soon after zircon crystallization.

In the southern portion of the study area the Success Lakes pluton, a hornblende-biotite-quartz-diorite, has a U-Pb zircon age of 157 ± 11 Ma (van der Heyden, 1991; van der Heyden, 2004). At the southeastern most margin of the Atnarko complex van der Heyden (1991) reports an earliest Cretaceous, 142.0 ± 0.5 Ma for the Wilderness Mountain pluton and considers it to be the eastern most extent of the Atnarko complex. Farther to the north, just outside the study area, the Wilderness Mountain pluton is thrust over rocks of the Intermontane superterrane across a northeast verging fault (van der Heyden et al., 1994). In the northern Atnarko complex the Mt. Marvin pluton, a strongly foliated to locally mylonitic quartz-diorite, has a reported concordant U-Pb zircon age of 129.8 ± 0.5 Ma (van der Heyden, 1991; van der Heyden, 2004). This pluton intrudes rocks of the Atnarko assemblage and is thrust towards the north-northeast over relatively undeformed granitic rocks in the north (Fig. 3.2).

Late Cretaceous

The Molly Lake pluton is a small body of strongly deformed quartz diorite found in the northern Atnarko complex (Fig. 3.2). It intrudes the Echo Lake pluton (ca. 143 Ma) as well as the Atnarko assemblage and gneisses. The Molly Lake pluton is interpreted as late-kinematic with respect to deformation in the area (van der Heyden, 1991; van der Heyden, 2004). The Molly Lake pluton is likely part of a larger body of similar composition and structural character found to the east (Fig. 3.2). A concordant U-Pb zircon age of 114.9 ± 0.3 Ma is reported for the Molly Lake pluton (van der Heyden, 1991; van der Heyden, 2004).

The Pandemonium Pass pluton is a large body of biotite ± muscovite-garnet tonalite to granodiorite located in the southern Atnarko complex (Fig. 3.2). The pluton intrudes migmatitic gneiss and rocks of the Atnarko assemblage. Dykes and apophyses off the main body both cross-cut and are folded into northeast directed shear zones and northeast verging folds and therefore the Pandemonium Pass pluton is interpreted as syn-kinematic with respect to north-northeast compression. Brecciation of the wall rock occurs locally at the margins of the pluton (Fig. 3.7B). TIMS analyses of zircon from the Pandemonium Pass pluton resulted in a scattering of four zircon fractions along concordia (Fig. 3.5F; Table 3.1). Two nearly concordant fractions, Z1 and Z3, have $^{206}Pb/^{238}U$ ages of 102.6 ± 0.5 and 102.4 ± 2.9 Ma respectively (Table 3.1). Six monazite fractions from the Pandemonium Pass pluton were analyzed and returned an 80.0 ± 2.9 Ma age for a weighted mean of the four most precise $^{207}Pb/^{238}U$ analyses (Fig. 3.5F; Table 3.1). The monazite age is interpreted as the crystallization age of the Pandemonium Pass pluton and the zircon ages reflect inheritance.

Latest Cretaceous to Tertiary

The Junker Lake pluton, located throughout the central portion of the Atnarko complex, is the largest plutonic body in the study area (Fig. 3.2). It intrudes all older rock types and cuts across all ductile deformation features. The Junker Lake pluton consists of biotite-granodiorite to tonalite with distinctive accessory titanite. van der Heyden (1991, 2004) reports a 65.2 ± 0.3 Ma TIMS zircon age for the Junker Lake pluton. A similar body of post-ductile deformation, granodiorite located near the Talchako glacier, returned a zircon age of 63.3 ± 0.3 Ma (van der Heyden, 1991; van der Heyden, 2004).

The Ptarmigan Lake pluton, located in the northern Atnarko complex, is a post-ductile deformation plutonic body (Fig. 3.2). TIMS zircon analyses of a sample of a dyke off the main Ptarmigan Lake pluton returns a maximum age of ~58 Ma (Fig. 3.5G; Table 3.1).

Thermal history

Isotopic data of titanite, hornblende, muscovite and biotite are used to determine the thermal history of the Atnarko complex. These minerals provide a record of the cooling history over the past 150 My during which the complex was deformed, metamorphosed and intruded by plutons. Estimated closure temperatures are from Hodges (2003) and presented in Table 3.3.

Titanite

Two titanite fractions were analyzed from the Elbow Lake pluton. These returned a weighted mean $^{206}Pb/^{238}U$ age of 167.5 ± 0.4 Ma (Fig. 3.7C). Two titanite analyses from orthogneiss in the northern Atnarko complex resulted in $^{206}Pb/^{238}U$ ages of 115.4 ± 1.0 and 117.3 ± 1.2 Ma. Both analyses are concordant and overlap at ca. 116 Ma (Fig. 3.5A). The lower intercept of the regression of the zircon data is within error of the titanite ages. The age for the titanites is interpreted as indicating a major thermal event that caused the lead loss for zircons in the orthogneiss.

Several titanite fractions were analyzed from the foliated quartz-dioritic Echo Lake pluton. Interestingly the fractions result in a range of $^{206}Pb/^{238}U$ ages of ca. 117 Ma and ca.115 Ma (Fig. 3.5H; Table 3.1). Titanite grains differentiated by size were analyzed separately and there is no obvious correlation between grain size and age. Lead loss in titanites can occur during ductile strain, especially in the presence of fluids (Villa, 1998). Since the titanites from the Echo Lake pluton are from samples that are strongly deformed they are interpreted as having been subjected to lead loss during deformation and the older ages (117 Ma) are thought to record the regional cooling of the Atnarko complex. This age overlaps (within error) with other titanite ages in the area and is geologically reasonable.

Table 3.3 Estimated closure temperaturs.

Mineral	**Closure Temperature (^oC)**
Monazite	987
Zircon	942
Titanite	659
Hornblende	557
Muscovite	366
Biotite	335-359

Temperatures from Hodges (2003)

Two titanite fractions from strongly deformed migmatitic gneiss returned concordant, although relatively imprecise, analyses with $^{206}Pb/^{238}U$ ages of 116.0 ± 9.4 Ma and 112 ± 30 Ma (Fig. 3.5E; Table 3.1). Although the errors are large on these analyses they overlap with the ca 116 Ma age for the other titanite analyses.

Hornblende

Hornblende cooling ages provide two clusters at Early Cretaceous and Late Cretaceous. Both ages are found in the northern and southern portions of the study area and reflect a complex cooling history. All analyses are by $^{40}Ar/^{39}Ar$ method except where indicated.

Hornblende that defines the dominant foliation within amphibolite from the Atnarko assemblage in the southern Atnarko complex returned an age of 117.5 ± 1.7 Ma. This age is interpreted to record cooling through ~560^{o}C hornblende closure temperature. A similar age, 117.7 ± 0.8 Ma, is recorded from hornblende defining the main foliation in the Mt. Marvin pluton in the northern Atnarko complex. A sample from migmatitic gneiss located in the northern Atnarko complex returned a hornblende cooling age of 106.85 ± 0.84 Ma. The hornblende from this sample defines the main foliation within the gneiss.

Two hornblende analyses from the northern and southern Atnarko complex return ages of 97.9 ± 2.2 Ma and 93.3 ± 0.8 Ma respectively (Fig. 3.8A; Table 3.4).

Muscovite

Cooling of the Atnarko complex through ~370^{o}C is recorded by muscovite taken from within the leucosomes of migmatitic gneiss of the imbricate zone in the southern Atnarko complex. The muscovite returns a $^{40}Ar/^{39}Ar$ age of 110.7 ± 1.2 Ma (Fig. 3.8B; Table 3.4). The leucosomes are stromatic and have granitic-like textures and show little evidence for solid-state deformation. The muscovite, which shows no evidence of alteration or deformation, forms interstitial grains between plagioclase, garnet and quartz. van der Heyden (1991) reports a similar muscovite K/Ar age, 113 ± 8 Ma from migmatitic amphibolitic metavolcanic rocks roughly ten kilometers along

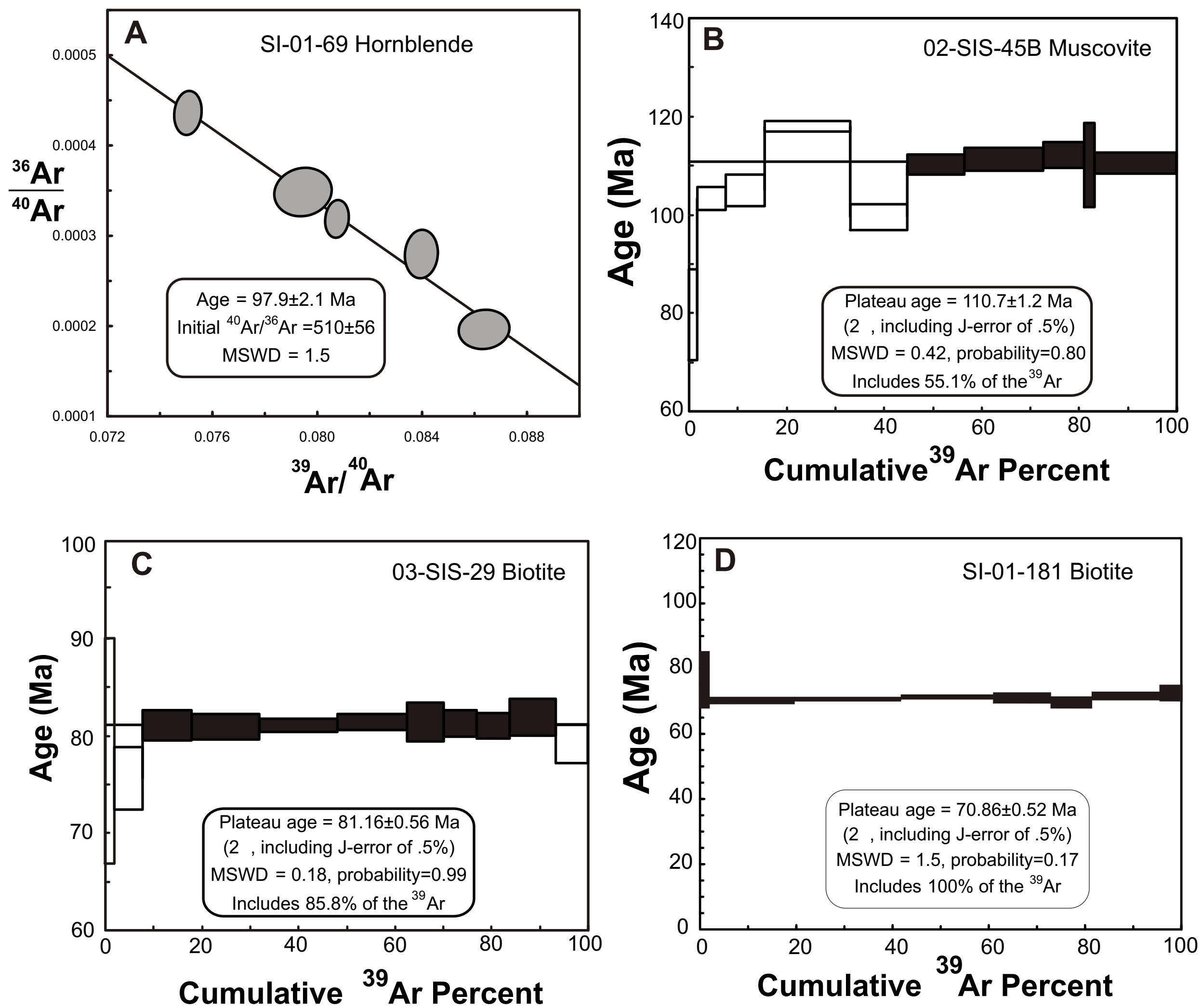

Figure 3.8. Inverse isochron and argon release spectra for step-heating analyses of biotite, muscovite and hornblende from the Atnarko complex: A) Hornblende from the Echo Lake pluton; B) Muscovite from leucosome within migmatite in southern Atnarko complex; C) Biotite from the syn-tectonic Pandemonium Pass pluton; D) Biotite from a high strain zone in the southern Atnarko. Box heights represent 2σ errors. Plateau steps are filled, rejected steps are open. Data are presented in Table 3.4.

Table 3.4 ^{40}Ar-^{39}Ar age data for hornblende, muscovite and biotite from the Atnarko complex.

Laser[1] Power (%)	Isotope Ratios ^{40}Ar/^{39}Ar	^{38}Ar/^{39}Ar	^{37}Ar/^{39}Ar	^{36}Ar/^{39}Ar	Ca/K	Cl/K	%^{40}Ar	%^{39}Ar	^{40}Ar*/^{39}Ar$_K$	Age±2σ
01-SIS-69, hornblende, J = 0.005387±0.000006; volume ^{39}ArK = 605.44 x 10^{-10} cm^3, integrated age 129.27 ± 0.49 Ma (2σ)										
2	887.553±0.030	2.568±0.045	0.461±0.073	1.266±0.036	2.079	0.682	39.01	0.09	692.519±29.238	2803.65±60.07
2.3	366.111 0.013	1.124 0.019	0.244 0.042	0.434 0.022	1.564	0.248	33.35	0.49	255.000 4.299	1559.53 17.60
2.6	88.316 0.007	0.268 0.027	0.205 0.037	0.111 0.020	1.467	0.054	33.97	1.17	58.836 0.803	496.70 5.93
2.9	22.510 0.012	0.357 0.016	0.757 0.025	0.025 0.028	6.012	0.078	27.55	4.27	16.183 0.284	150.79 2.54
3.2	13.407 0.006	0.416 0.011	0.877 0.015	0.008 0.022	6.986	0.093	12.74	12.62	11.624 0.088	109.57 0.80
3.5	12.660 0.011	0.404 0.014	0.866 0.016	0.006 0.036	6.898	0.09	10.11	15.51	11.312 0.148	106.72 1.36
3.8	12.431 0.005	0.470 0.010	0.934 0.014	0.006 0.020	7.442	0.105	9.21	26.42	11.242 0.063	106.08 0.58
4.1	11.975 0.006	0.431 0.010	0.837 0.014	0.005 0.043	6.667	0.096	8.07	19.06	10.947 0.094	103.38 0.86
4.4	11.665 0.009	0.407 0.012	0.790 0.015	0.004 0.036	6.286	0.091	5.6	13.89	10.930 0.112	103.22 1.03
4.8	12.381 0.006	0.445 0.013	0.871 0.017	0.006 0.043	6.932	0.099	6.91	6.48	11.378 0.105	107.32 0.96
02-SIS-45B, muscovite, J = 0.009737±0.000020, volume ^{39}ArK = 472.09 x 10^{-10} cm^3, intergrated age 109.26 ± 0.85 Ma (2σ)										
2	10.191±0.016	0.015±0.129	0.010±0.286	0.019±0.096	0.088	-0.001	54.61	1.72	4.634±0.545	79.62±9.16
2.2	7.358 0.008	0.013 0.080	0.004 0.260	0.005 0.100	0.041	0	18.03	5.79	6.044 0.143	103.16 2.37
2.4	7.227 0.008	0.014 0.062	0.001 0.454	0.004 0.174	0.009	0	15.1	8.01	6.148 0.199	104.89 3.29
2.6	7.586 0.005	0.013 0.039	0.001 0.262	0.002 0.078	0.009	0	8.8	17.62	6.933 0.066	117.86 1.09
2.7	6.367 0.006	0.013 0.048	0.001 0.413	0.002 0.272	0.009	0	8.72	11.74	5.823 0.157	99.50 2.61
2.9	7.089 0.007	0.013 0.107	0.001 0.258	0.002 0.171	0.011	0	9.07	11.72	6.459 0.121	110.04 2.01
3.1	7.156 0.006	0.012 0.034	0.001 0.282	0.002 0.212	0.005	0	8.98	16.09	6.527 0.145	111.16 2.39
3.3	7.126 0.007	0.014 0.080	0.002 0.239	0.002 0.264	0.014	0	7.89	8.47	6.577 0.159	111.99 2.62
3.5	8.007 0.018	0.012 0.356	0.005 0.605	0.005 0.318	0.042	-0.001	19.5	2	6.459 0.518	110.04 8.55
3.8	6.892 0.006	0.013 0.079	0.001 0.449	0.001 0.283	0.007	0	6.18	16.83	6.479 0.128	110.37 2.12
03-SIS-29,biotite, J = 0.009729±0.000016, volume ^{39}ArK = 866.79 x 10^{-10} cm^3, intergrated age 180.68 ± 0.54 Ma (2σ)										
2	22.889±0.012	0.024±0.146	0.018±0.114	0.063±0.038	0.162	-0.001	80.08	1.82	4.567±0.689	78.42±11.58
2.2	8.504 0.006	0.016 0.048	0.009 0.095	0.014 0.045	0.079	0	48.39	5.86	4.396 0.192	75.56 3.23
2.4	6.181 0.005	0.014 0.053	0.005 0.091	0.005 0.059	0.045	0	23.77	10.15	4.720 0.091	81.01 1.53
2.6	5.427 0.005	0.013 0.030	0.006 0.048	0.002 0.102	0.05	0	13.29	14.07	4.715 0.079	80.91 1.32
2.8	5.155 0.005	0.013 0.019	0.004 0.059	0.002 0.070	0.033	0	8.58	16.15	4.721 0.040	81.02 0.66
3	5.182 0.005	0.013 0.039	0.004 0.063	0.002 0.092	0.033	0	8.64	14.5	4.743 0.048	81.39 0.81
3.2	5.366 0.007	0.013 0.069	0.007 0.072	0.002 0.172	0.059	0	11.81	7.74	4.741 0.116	81.36 1.95
3.4	5.469 0.007	0.013 0.082	0.008 0.070	0.003 0.096	0.072	0	13.61	6.65	4.733 0.081	81.21 1.36
3.6	5.544 0.005	0.014 0.076	0.014 0.064	0.003 0.085	0.12	0	15.04	6.93	4.719 0.077	80.98 1.29
3.9	5.423 0.006	0.013 0.047	0.014 0.065	0.002 0.161	0.126	0	12.22	9.65	4.769 0.113	81.82 1.90
4.2	5.209 0.006	0.013 0.060	0.025 0.041	0.002 0.183	0.22	0	11.73	6.48	4.606 0.118	79.09 1.99
01-SIS-181, biotite, J = 0.005386±0.000006, volume ^{39}ArK = 173.71 x 10^{-10} cm^3, intergrated age 70.95±0.47 Ma (2σ)										
2	17.295±0.011	0.054±0.117	0.058±0.099	0.045±0.068	0.094	0.006	49.38	2.14	8.048±0.947	76.55±8.82
2.3	8.646 0.005	0.054 0.028	0.016 0.075	0.006 0.061	0.081	0.009	12.3	17.61	7.365 0.116	70.18 1.08
2.6	8.171 0.005	0.074 0.022	0.018 0.062	0.004 0.051	0.106	0.014	7	21.98	7.406 0.070	70.56 0.65
2.9	7.905 0.005	0.026 0.038	0.016 0.063	0.003 0.073	0.084	0.003	2.49	19.11	7.481 0.075	71.27 0.70
3.2	7.868 0.006	0.026 0.040	0.019 0.066	0.004 0.144	0.086	0.002	0.92	11.91	7.451 0.174	70.99 1.63
3.5	7.872 0.006	0.028 0.051	0.024 0.079	0.005 0.114	0.101	0.003	1.37	8.56	7.303 0.191	69.60 1.79
4	8.071 0.006	0.026 0.048	0.018 0.076	0.004 0.104	0.087	0.002	3.32	14.03	7.512 0.132	71.56 1.24
4.5	8.623 0.007	0.028 0.115	0.035 0.106	0.010 0.087	0.108	0.002	2.58	4.66	7.607 0.268	72.44 2.50

[1] "<" indicates step used in plateau age calculations, ">'" indicates step used in inverse correlation calculations.

Neutron flux monitors: 24.36 Ma MAC-83 biotite (Sandeman et al. 1999); 28.02 Ma FCs (Renne et al., 1998)

Isotope production ratios: (^{40}Ar/^{39}Ar)$_K$=0.0302, (^{37}Ar/^{39}Ar)$_{Ca}$=1416.4306, (^{36}Ar/^{39}Ar)$_{Ca}$=0.3952, Ca/K=1.83(^{37}Ar$_{Ca}$/^{39}Ar$_K$).

strike to the south of this area. The K/Ar age is not as precise as the $^{40}Ar/^{39}Ar$ age; however, it is within error and reflects the same time of cooling of the Atnarko complex.

Biotite

Biotite ages from the Atnarko complex reflect a complex cooling through ~ 360^{o}C. Biotite from the Pandemonium Pass pluton in the southern Atnarko complex returns a $^{40}Ar/^{39}Ar$ age of 81.2 ± 0.6 Ma (Fig. 3.8C; Table 3.4). The biotite is fresh within an igneous textured matrix. A biotite cooling age of 77.45 ± 0.43 Ma was obtained from migmatitic gneiss in the southern portion of the complex, where the biotite is found along the main foliation and shows some evidence for replacement by chlorite. Biotite found within migmatitic gneiss in the northern portion of the complex returned an age of 70.5 ± 0.5 Ma. This biotite is also found along the main gneissic foliation and shows some evidence of replacement by chlorite. A mylonitic shear zone in the southern portion of the Atnarko complex with biotite along the foliation plane returned an age of 70.9 ± 0.5 Ma (Fig. 3.8D; Table 3.3).

T-t paths for the Atnarko complex

Geochronologic and thermochronologic data are used to examine the thermal history of the Atnarko complex. Temperature-time (T-t) plots are constructed using the isotopic ages and closure temperatures of each of the different mineral isotope systems (e.g., U-Pb zircon and titanite; $^{40}Ar/^{39}Ar$ hornblende, muscovite and biotite) in order to map the thermal history of the Atnarko complex and to decipher the relationships between deformation and plutonism (Fig. 3.9). Thermochronologic data is presented from three areas within the Atnarko complex, and discussed from south to north.

Southern Atnarko complex

The cooling history is deduced from $^{40}Ar/^{39}Ar$ ages collected from migmatitic gneiss located within the imbricate zone in the southern Atnarko complex. The crystallization age of the gneiss is interpreted to 143 Ma. Titanite ages of ~116 Ma from the gneiss reflect a substantial heating

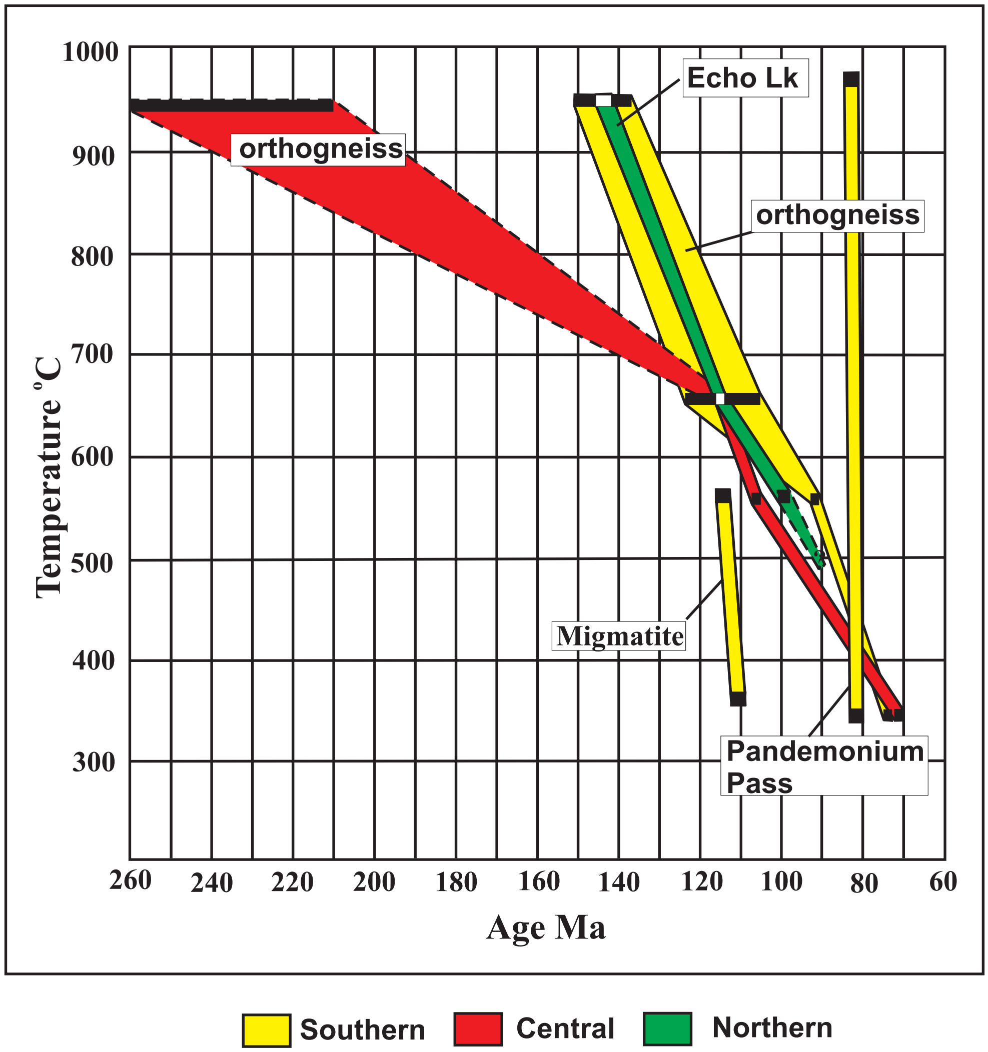

Figure 3.9. Temperature-time paths for samples collected from the southern, northern and central Atnarko complex (see text for details). Black boxes approximate errors on ages. Coloured areas indicate estimated cooling paths and slope of the areas define the cooling rate. Closure temperatures for zircon, titanite, hornblende, muscovite and biotite taken from Hodges (*2003)*.

event that initiated the growth of titanite. This heating event is interpreted to be a result of migmatization in the southern Atnarko complex (see below). Following titanite growth, hornblende cooling age of ca. 93 Ma is interpreted as indicating the cooling of the southern Atnarko complex through uplift during contraction. Final cooling of the southern portion of the complex coincides with biotite ages of ~77 Ma.

The southern Atnarko complex underwent three separate cooling stages indicated by slope changes on Figure 3.9. The first stage between crystallization and the titanite age suggests a cooling rate of 10^{o}C/My. However, caution must be used for this first segment of cooling as the zircon age is interpreted as an igneous crystallization age and not a metamorphic age. The regular cooling of a pluton to the ambient temperatures at the depth at which it has been emplaced usually lasts only tens to hundreds of thousands of years rather than tens of millions of years (Coulson et al., 2002; Rothstein and Manning, 2003). Because of this it is unlikely that the cooling rate shown on Figure 3.9 represents a true cooling rate of the southern part of the complex through that time period. Rather, the titanite age records the timing of peak metamorphic conditions and a disturbance in the normal cooling trend of the complex.

Following titanite formation the southern Atnarko cooled from 650^{o}C to 560^{o}C by ca. 93 Ma implying a steady state cooling rate of 4.6^{o}C/My (Fig. 3.9). The final stage reflects cooling from 560^{o}C to 360^{o}C, through the biotite closure temperature, and corresponds to rates of 12.5^{o}C/My. This final stage of the thermal history is interpreted to reflect final uplift and cooling of the southern Atnarko complex.

The cooling history of the southern Atnarko, however, was not uniform. Hornblende ages from amphibolite near the base of the imbricate zone record cooling ages of 117 Ma and cooling of muscovite from leucosomes within the amphibolite at 110 Ma. Cooling rates here are on the order of $\sim 30^{o}$C/My, much faster than noted in most other locations in the complex (Fig. 3.9). Similarly, the Pandemonium Pass pluton reflects extremely rapid cooling. Emplacement age is synchronous with monazite ages with an upper age of 83 Ma. Biotite from the pluton records cooling through 360^{o}C by ca. 80 Ma, indicating cooling rates of at least 206^{o}C/My (Fig. 3.9).

Central Atnarko complex

The crystallization age of a migmatitic orthogneiss is interpreted to be 235 ± 25 Ma (sample 01-SIS-107). Titanite analyzed from the gneiss produced ages of ~116 Ma, the same age as titanite in the southern portion of the complex. Hornblende cooling ages, ~106 Ma in the central portion of the complex, are 13 My older than those from gneiss in the south. A 70 Ma biotite age from the central Atnarko is slightly younger than that of biotite in the southern Atnarko and indicates that final cooling of the central portion of the complex lagged behind the south by ca. 7 My.

The rate of cooling, calculated from the closure of titanite to the cooling of hornblende in the central Atnarko is 11.4^{o}C/My. This rate is faster than the recorded rate of just 4.6^{o}C/My in the south. A cooling rate of 5.4^{o}C/My is calculated for the central Atnarko from hornblende to biotite closure temperatures and reflects slow cooling between 106 and 70 Ma. This rate is lower than that recorded for the southern Atnarko.

Northern Atnarko complex

Samples from the variably deformed Echo Lake pluton are used to constrain the cooling history of the northern Atnarko complex. The Echo Lake pluton is thrust over gneisses and migmatites and is strongly deformed at its margins and less deformed to relatively undeformed away from major shear zones. A U-Pb zircon crystallization age of ca. 143 Ma for the pluton coincides with that of the migmatitic gneiss in the southern Atnarko complex. Titanite cooling ages of ~116 Ma overlap with titanite ages from the south and central portions of the Atnarko complex. Hornblende ages reflect cooling below ~560^{o}C by 98 Ma. Cooling through the biotite closure temperature, related to uplift, was not recorded in the north because intrusion of latest Cretaceous to Paleogene plutons reset all biotites analyzed.

Cooling rates for the northern part of the Atnarko complex from ~115-98 Ma are on the order of 5.9^{o}C/My. This rate is slower than that of the central Atnarko but equivalent to the cooling rate calculated for the southern Atnarko complex (Fig. 3.9).

DISCUSSION

Deformation and plutonism

Magmatic events within the Coast plutonic complex appear to be episodic with periods of little to no activity separated by intrusion of voluminous igneous material (Armstrong, 1988; Friedman and Armstrong, 1995). In some areas plutonic episodes appear to follow periods of crustal thickening that overlap temporally with magmatic lulls (Hollister and Crawford, 1986; Crawford et al., 1987). A proposed set of tectonic steps may occur in convergent margins that include: 1) initial stages of crustal thickening associated with a magmatic lull; 2) crustal anatexis in the lower and middle crust leading to pluton emplacement; and, 3) final collapse of the orogen (Dewey, 1988; Hollister, 1993; Vanderhaeghe and Teyssier, 2001a; Vanderhaeghe and Teyssier, 2001b; Mair et al., 2006). This tectonic sequence has been proposed for the Californian arc, the Coast plutonic complex and areas of the northern Canadian and Alaskan Cordillera (Ducea, 2001; Mair et al., 2006; Mahoney et al., in review). The presence of magmatic material prior to and during deformation affects how an orogen will react to changing tectonic regimes (Hollister, 1993). The style of deformation is also important as shear zones create pathways for melt to migrate, either slowly or rapidly to upper crustal levels (Andronicos et al., 2003; Klepeis et al., 2003).

Ages of deformation and plutonic activity from the Atnarko complex suggest that deformation and plutonism were linked. Figure 3.10 summarizes the relationship between deformation and plutonic activity within the Atnarko complex. Three phases of syn-tectonic plutonism are observed in the Atnarko complex; an Early Jurassic, an Early Cretaceous and a Late Cretaceous event. The Early Jurassic event is not important in the context of this paper and is not discussed.

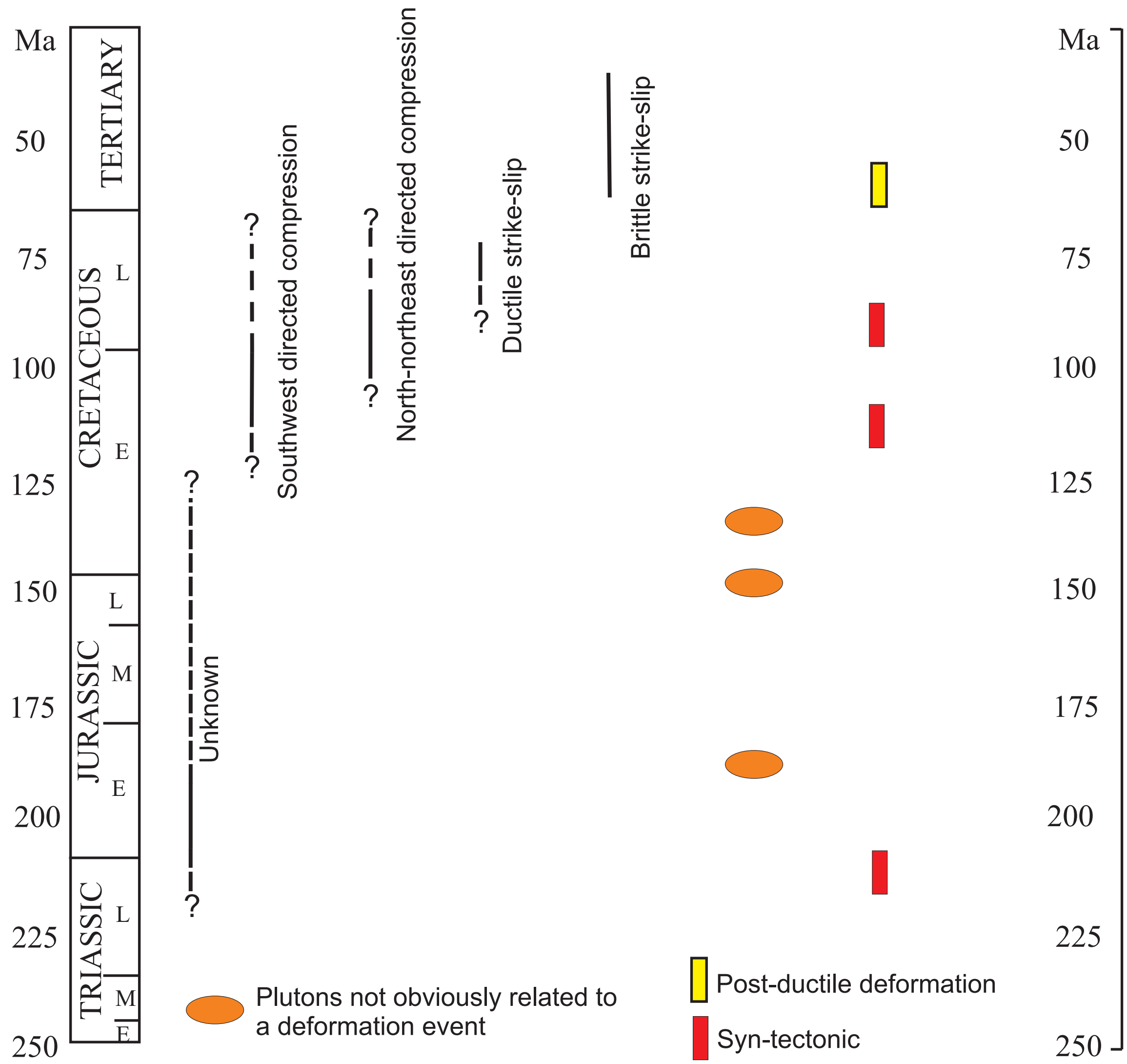

Figure 3.10. Summary diagram illustrating the relationships between plutonism and deformation from the Atnarko complex.

The Early Cretaceous event is documented by the syn-tectonic Molly Lake pluton, complex-wide ~116 Ma titanite ages and hornblende cooling ages related to the leucosomes within the southern portion of the complex. The data suggests that melt migrating from the lower crust to the middle crust caused a regional thermal event that affected the entire Atnarko complex. The fabrics and observed within the Molly Lake pluton are interpreted to indicate that the pluton intruded during compressional deformation. Hornblende with cooling ages of ~117 Ma from the nearby Mt. Marvin pluton also records this thermal event.

In the Late Cretaceous the latest stages of compressional deformation in the Atnarko complex increased crustal thickness and moved lower crustal rocks into higher crustal levels. Steepening of fabrics and the development of near vertical dextral and sinistral shear zones occurred at the waning stages of compression. The shear zones and steep fabrics provided conduits for melt from lower in the crust to move rapidly to upper crustal levels. This is indicated by the extremely fast cooling rate experienced by the Pandemonium Pass pluton. This pluton is syn-kinematic with respect to the waning stages of ductile deformation and unlike older plutonic bodies, was intruded into higher crustal levels where ambient temperatures were well below ~360^{o}C (Fig. 3.11B).

Crustal architecture and tectonic implications

Crustal architecture of the Atnarko complex

Figure 3.11 depicts the crustal architecture of the Atnarko complex just prior to and after Early to Late Cretaceous thrusting. A crustal section with partial melt present at ~25 km depth is proposed. This depth is based on temperature of formation of melt in amphibolites, ~800^{o}C (Rushmer, 1991) and an average crustal geotherm for an active arc environment of ~30^{o}C/km (Rothstein and Manning, 2003). During Jurassic and earliest Cretaceous deformation the lower-middle crust beneath the Atnarko complex in the Early Cretaceous was buried deep enough for the rocks to attain amphibolite grade metamorphism. A period of partial melting of the lower-

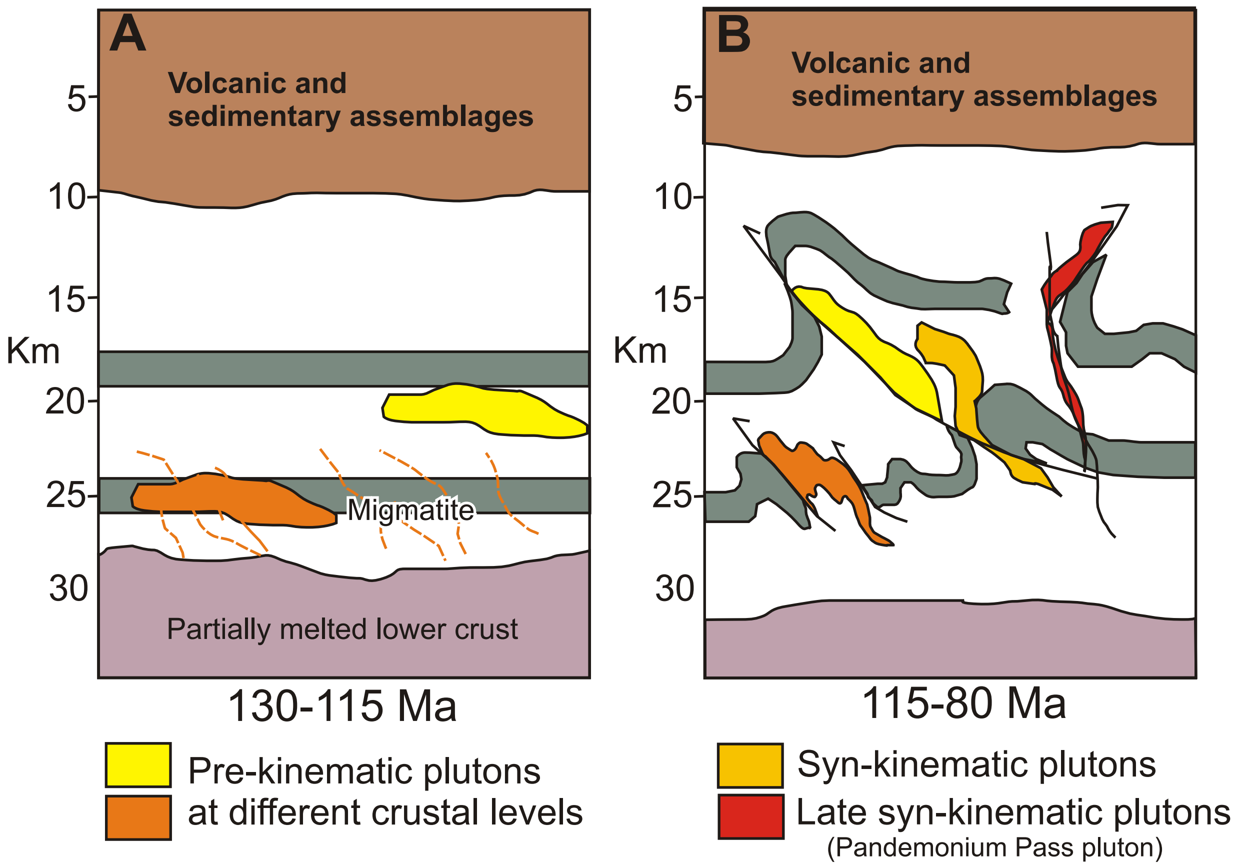

Figure 3.11. A) Schematic crustal section through the Atnarko complex ca. 130-115 Ma. Pr-kinematic intrusion of Latest Jurassic and Earliest Cretaceous plutons was followed by melt migration along forming D1 fabrics. B) Melt migration led to the intrusion of syn-D1 plutons (e.g. Molly Lake pluton) along D1 thrusts. Near the waning stages of compression, fabrics steepened and near vertical shear zones were developed allowing late syn-kinematic plutons to rise rapidly into the upper crust.

middle crust distributed melt along syn-tectonic fabrics and structures (Fig. 3.11A). Increased melt generation and thermal perturbation caused thermally enhanced weakening of the rocks causing the rate of deformation to increase and creating multiple pathways for melt to migrate to higher levels in the crust (Hollister, 1993; Brown and Solar, 1999b; Vanderhaeghe and Teyssier, 2001a; Brown, 2004). An increase in deformation rate increased the flow of melt such that after emplacement of the ca. 114 Ma Molly Lake pluton, the melt source was tapped dry. *Ducea* (2001) proposes this kind of mechanism for the shutting down of the California arc.

In the Atnarko complex, after the intrusion of the Molly Lake pluton, magmatic activity ceased until the intrusion of the Pandemonium Pass pluton at ca. 80 Ma. Crustal thickening continued during the lull in magmatism recorded in Atnarko complex and within much of the Coast plutonic complex (Journeay and Friedman, 1993; Rusmore and Woodsworth, 1994; van der Heyden et al., 1994). Whether or not the Pandemonium Pass pluton is the result of melting of lower crust is difficult to ascertain as the melt pathways are not exposed in the Atnarko complex. The Pandemonium Pass pluton clearly cuts across leucosomes related to the Early Cretaceous melt migration and cooled to below biotite closure temperatures almost immediately after intrusion. This indicates that the Atnarko complex was already uplifted substantially by this time.

Intrusion of latest Cretaceous to earliest Tertiary plutons in the Atnarko complex is not related to any identifiable ductile deformation event. However, these plutons are very large and required large volumes of melt for their formation. The east-west linearity of the Junker Lake pluton may suggest that it was intruded into a preexisting steeply dipping structure. This and similar structures may have allowed melt from the lower crust to migrate rapidly to upper crustal levels. Thus the crust in this area became stabilized by distributing heat throughout the whole crust rather than at depth where it could localize forming a thermally weak layer.

Coupling and decoupling in the Coast plutonic complex

Construction of orogens is caused mainly by crustal thickening as a result of compressional tectonics and the addition of plutonic material at deeper levels. How orogens finally collapse is not as straight forward.

There are two main mechanisms responsible for orogenic collapse; 1) gravity driven collapse where overthickened crust becomes unstable and the orogen collapses under its own weight along weak zones lubricated by the presence of melt (Rey et al., 2001; Vanderhaeghe and Teyssier, 2001b), and 2) collapse due to oblique collision or transtension that pulls apart the orogen (Friedman and Armstrong, 1988; Andronicos et al., 2003; Paterson et al., 2004; Rusmore et al., 2005). Gravitational collapse of an orogen requires a decoupling within the orogenic system at some crustal level, generally a decoupling between upper and lower crust or lower crust and mantle. A link, or coupling, between the subducting plate and the overriding plate must occur where the orogen reacts to plate motions.

Whitney et al., (2004) describe a change in the mechanical behavior of the western Cordillera from Baja to British Columbia and suggest that the upper plate in the northern portion of the orogen (Cascades northward into British Columbia) is geodynamically coupled to the subducting plate and that the southern Cordillera shows no evidence for coupling after the Late Cretaceous. This implies variable states of coupling and decoupling can occur along the same convergent margin. The same can be said for the Coast plutonic complex.

Northwest of the Atnarko complex massive orogen-perpendicular Eocene exhumation and uplift excised 10-6 km of upper crust overlying the Central Gneiss complex between 54-50 Ma along east dipping mylonitic shear zones (Andronicos et al., 2003; Rusmore et al., 2005). Hollister and Andronicos (2006) and Andronicos et al. (2003) suggest that flow of melt during extension passed upwards from lower and middle crustal levels in response to the large exhumation. Channels of return flow were formed as a response to the rising melt (Andronicos et al., 2003). They also suggest that the presence of abnormally thin crust within the Coast plutonic complex supports evidence for lower crustal flow (Andronicos et al., 2003). Lower crustal flow enabled detachment of the middle and upper crust from the lower crust with the result being orogenic collapse under gravitational forces with extension perpendicular to the orogen along shallowly dipping extensional shear zones exposing lower crustal rocks in what in now the Central Gneiss Complex (Fig. 3.12A).

The area east and southeast of the Atnarko complex is dominated by latest Cretaceous to Eocene dextral strike-slip and associated steeply dipping faults (Umhoefer and Schiarizza, 1996). Transtensional deformation followed transpressive deformation as relative plate motion changed along the margin (Engebretson et al., 1985). Extension is limited to localized metamorphic core complexes that are kinematically linked to the largest of the dextral strike-slip faults (Friedman and Armstrong, 1988; Coleman and Parrish, 1991; Smith, 1998; Paterson et al., 2004). Eocene plutons are found everywhere that middle to lower crustal rocks are exposed at surface. Ages and textures suggest that many of these plutons are pre- to syn-tectonic (Friedman and Armstrong, 1988; Coleman and Parrish, 1991; Smith, 1998). Syn-tectonic plutons can provide a thermally and mechanically weak layer where deformation was focused. The localization of the shear zones that exhumed the metamorphic core complexes was dependant on the weak layers and the extension was kinematically linked to the main deformation which was dextral strike-slip faulting (Fig. 3.12B; Friedman and Armstrong, 1988; Coleman and Parrish, 1991; Paterson et al., 2004).

Late Cretaceous and Early Tertiary plutons in the Atnarko complex and adjacent areas were all intruded at high crustal levels (above brittle-ductile transition). East and southeast of the Atnarko complex the plutonic record suggests that melts from the lower and middle crust intruded upper crustal levels and cooled rapidly to stabilize the Late Cretaceous and Early Tertiary crust. This is supported by the numerous plutons of this age that intrude into relatively undeformed and

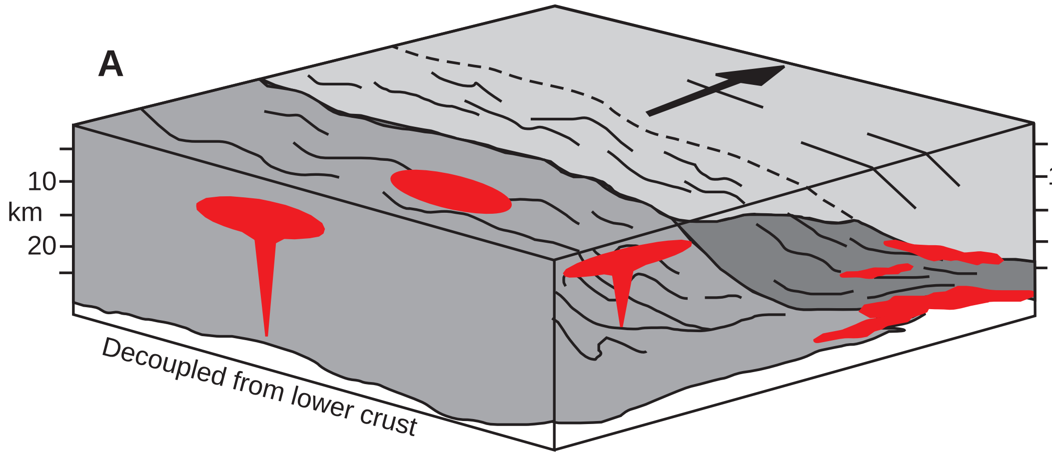

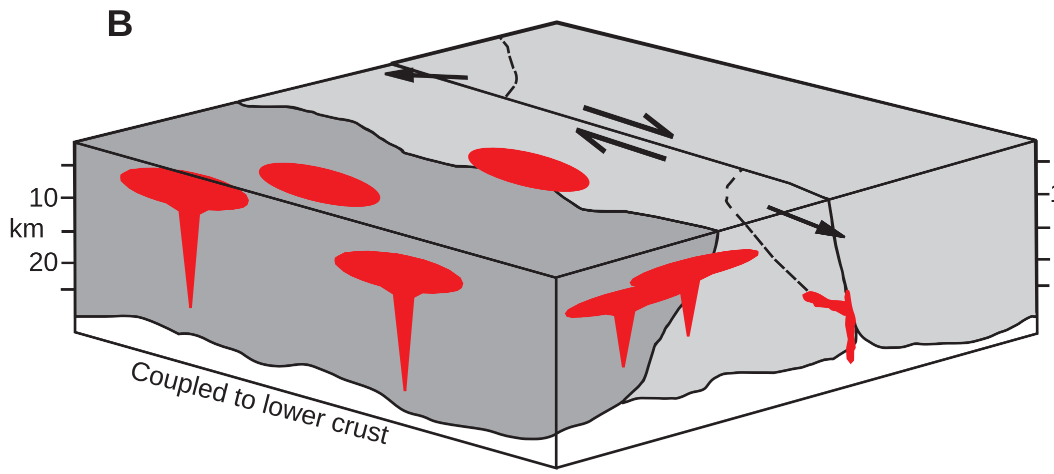

Figure 3.12. Block diagrams representing the western Canadian Cordillera just prior to Eocene extension. Area of extension depicted by dashed line. Arrows indicate direction of extension. A) The region northwest of the study area is dominated by early crustal thickening and subsequent collapse along thermally weakened layers at depth. These layers allow the orogen to become decoupled from the lower crust and result in perpendicular extension and large-scale exhumation of the Central Gneiss complex. B) The Atnarko complex and areas southeast are dominated by strike-slip deformation and localization of orogen parallel extension. Plutons generated at depth move quickly to the upper crust which dissipates heat from the lower crust and stabilizes the upper and lower crust. The heat transfer allows the orogen to remain coupled with the lower crust and transtensional relative plate motions.

unmetamorphosed upper crustal rocks and by the similarity between zircon crystallization ages and biotite cooling ages for the plutons (van der Heyden, 2004). The rapid rise of magmatic material to the upper crust was likely facilitated by numerous steeply dipping strike-slip faults. Heat that was present in the lower and middle crust was dissipated and no thermally weak zones were developed after this time or thermally weak zones that were developed were steeply dipping shear zones that facilitated strike-slip faulting. Northwest of the Atnarko complex plutons of this age intruded into the lower and middle crust (Andronicos et al., 2003; Rusmore et al., 2005; Hollister and Andronicos, 2006). The plutons in the northwest intruded along shallowly dipping shear zones, slowing their rise to upper crustal levels resulting in slow isothermal decompression during continued crustal thickening (Andronicos et al., 1999; Andronicos et al., 2003; Rusmore et al., 2005).

In the northwest, the middle and lower crust were decoupled. At lower crustal levels the heat introduced by Late Cretaceous and Eocene intrusions maintained high thermal regimes along shallowly dipping shear zones. The shear zones acted as weakened layers along which detachment zones were formed (i.e., Shames River shear zone and Eastern Boundary detachment). Continued transtension along the tectonic margin allowed the shear zones to migrate upwards into the middle and upper crust facilitating perpendicular collapse of the orogen. In contrast crustal heat in areas to the east and southeast of the Atnarko complex was dissipated throughout the entire crustal section. This resulted in a relatively strong crustal section that was coupled to the lower crust. In response to a transtensional tectonic regime, orogen parallel translation was accommodated along mostly dextral strike-slip faulting.

CONCLUSIONS

A change in the thermal mechanical properties of the crust within the Coast plutonic complex led to coupling between the lower and middle crust from the Atnarko complex southeast. In contrast, the middle crust within the Coast plutonic complex was decoupled from the lower crust to the northwest of the Atnarko complex. Melt channels are interpreted to have been developed in the northwest along shallowly dipping shear zones that allowed the orogen to collapse under gravitational forces. In the Atnarko complex and areas to the east and southeast the crust was thermomechanically stronger and cooler in the Late Cretaceous to Eocene because melt was able to travel rapidly to upper crustal levels, likely along steeply dipping shear zones. In effect the upper, middle and lower crusts were coupled. Localized areas of thermally weakened crust developed into extensional zones that were kinematically linked to large-strike slip faults resulting in the exhumation of small metamorphic core complexes.

REFERENCES

Andronicos, C. L., Chardon, D. H., and Hollister, L. S., 2003, Strain partitioning in an obliquely convergent orogen, plutonism, and synorogenic collapse: Coast Mountains Batholiths, British Columbia, Canada: Tectonics, v. 22, no. 2.

Andronicos, C. L., Hollister, L. S., Davidson, C., and Chardon, D., 1999, Kinematics and tectonic significance of transpressive structures within the Coast Plutonic Complex, British Columbia: Journal of Structural Geology, v. 21, p. 229-243.

Armstrong, R. L., 1988, Mesozoic and early Cenozoic magmatic evolution of the Canadian Cordillera, *in* Clark, S. P., Jr., Burchfield, B. C., and Suppe, J., eds., Processes in continental lithospheric deformation, Geological Society of America, p. 55-91.

Boghossian, N. D., and Gehrels, G. E., 2000, Nd isotopic signature of metasedimentary pendants in the Coast Mountains between Prince Rupert and Bella Coola, British Columbia, *in* Stowell, H. H., and McClelland, W. C., eds., Tectonics of the Coast Mountains, southeastern Alaska and British Columbia: Boulder, Colorado, Geological Society of America Special Paper 343, p. 77-87.

Brown, M., 2004, The mechanism of melt extraction from lower continental crust of orogens: Transactions of the Royal Society of Edinburgh: Earth Sciences, v. 95, p. 35-48.

Brown, M., and Rushmer, T., 1997, The role of deformation in the movement of granitic melt: views from the laboratory and the field, *in* Holness, M., ed., Deformation-enhanced melt segregation and metamorphic fluid transport: London, Chapman & Hall, p. 111-144.

Brown, M., and Solar, G. S., 1999a, Granite ascent and emplacement during contractional deformation in convergent orogens: Journal of Structural Geology, v. 20, p. 1365-1393.

Brown, M., and Solar, G. S., 1999b, Shear zone systems and melts: feedback relations and self-organization in orogenic belts: Journal of Structural Geology, v. 20, p. 211-227.

Coleman, M. E., and Parrish, R. R., 1991, Eocene dextral strike-slip and extensional faulting in the Bridge River terrane, southwest British Columbia: Tectonics, v. 10, p. 1222-1238.

Colpron, M., Nelson, J. L., Roots, C. F., Gehrels, G. E., and others, 2006, A tectonostratigraphic framework for the pericratonic terranes of the northern Cordillera, *in* Colpron, M., Nelson, J. L., and Thompson, R. I., eds., Paleozoic evolution and metallogeny of pericratonic terranes at the ancient Pacific margin of North America, Canadian and Alaskan Cordillera, Geological Association of Canada.

Coney, P. J., Jones, D. L., and Monger, J. W. H., 1980, Cordilleran suspect terranes: Nature, v. 288, no. 27 November 1980, p. 329-333.

Coulson, I. M., Villeneuve, M. E., Dipple, G. M., Duncan, R. A., Russell, J. K., and Mortensen, J. K., 2002, Time-scales of assembly and thermal history of a composite felsic pluton: constraints from the Emerald Lake area, northern Canadian Cordillera, Yukon: Journal of Volcanology and Geothermal Research, v. 114, p. 331-356.

Crawford, M. L., Crawford, W. A., and Gehrels, G. E., 2000, Terrane assembly and structural relationships in the eastern Prince Rupert quadrangle, British Columbia, *in* Stowell, H. H., and McClelland, W. C., eds., Tectonics of the Coast Mountains, southeastern Alaska and British Columbia: Boulder, Colorado, Geological Society of America Special Paper 343, p. 1-21.

Crawford, M. L., Hollister, L. S., and Woodsworth, G. J., 1987, Crustal deformation and regional metamorphism across a terrane boundary, Coast Plutonic Complex, British Columbia: Tectonics, v. 6, no. 3, p. 343-361.

Dewey, J. F., 1988, Extensional collapse of orogens: Tectonics, v. 7, p. 1123-1139.

Ducea, M., 2001, The California arc: thick granitic batholiths, ecologitic residues, lithospheric-scale thrusting, and magmatic flare-ups: GSA Today, v. 11, no. 11, p. 4-10.

Engebretson, D. C., Cox, A., and Gordon, R. G., 1985, Relative motions between oceanic and continental plates in the Pacific basin: Geological Society of America Special Paper 206, p. 58.
Friedman, R. M., and Armstrong, R. L., 1988, Tatla Lake metamorphic complex: An Eocene metamorphic core complex on the southwestern edge of the Intermontane Belt of British Columbia: Tectonics, v. 7, no. 6, p. 1141-1166.
Friedman, R. M., and Armstrong, R. L., 1995, Jurassic and Cretaceous geochronology of the southern Coast Belt, British Columbia, 49^{o} to 51^{o}N, *in* Miller, D. M., and Busby, C., eds., Jurassic magmatism and tectonics of the North American Cordillera, Geological Society of America Special Paper 299, pp. 95-139.
Gardner, M. C., Bergman, S. C., Cushing, G. W., MacKevett, E. M., Plafker, G., Campbell, R. B., Dodds, C. J., McClelland, W. C., and Mueller, P. A., 1988, Pennsylvanian pluton stitching of Wrangellia and the Alexander Terrane, Wrangell Mountains, Alaska: Geology, v. 16, no. 11, p. 967-971.
Gareau, S. A., and Woodsworth, G. J., 2000, Yukon-Tanana terrane in the Scotia-Quaal belt, Coast Plutonic Complex, central-Western British Columbia, *in* Stowell, H. H., and McClelland, W. C., eds., Tectonics of the Coast Mountains in SE Alaska and Coastal British Columbia: Boulder, Colorado, Geological Society of America Special Paper 343, p. 23-43.
Gehrels, G. E., 2001, Geology of the Chatham Sound region, southeast Alaska and coastal British Columbia: Canadian Journal of Earth Sciences, v. 38, p. 1579-1599.
Gehrels, G. E., and Boghossian, N. D., 2000, Reconnaissance geology and U-Pb geochronology of the west flank of the Coast Mountains between Bella Coola and Prince Rupert, coastal British Columbia, *in* Stowell, H. H., and McClelland, W. C., eds., Tectonics of the Coast Mountains, SE Alaska and Coastal British Columbia, Geological Society of America, p. 61-76.
Gehrels, G. E., and Saleeby, J. B., 1987, Geology of southern Prince of Wales Island, southeastern Alaska: Geological Society of America Bulletin, v. 98, no. 2, p. 123-137.
Hodges, K. V., 2003, Geochronology and thermochronology in orogenic systems, *in* Holland, H. D., and Turekian, K. K., eds., The Crust (ed. R.L. Rudnick) Vol. 3 Treatise on Geochemistry: Oxford, Elsevier-Pergamon, p. 263-292.
Hollister, L. S., 1993, The role of melt in the uplift and exhumation of orogenic belts: Chemical Geology, v. 108, p. 31-48.
Hollister, L. S., and Andronicos, C. L., 2006, Formation of new continental crust in Western British Columbia during transpression and transtension: Earth and Planetary Science Letters, v. 249, p. 29-38.
Hollister, L. S., and Crawford, M. L., 1986, Melt-enhanced deformation: A major tectonic process: Geology, v. 14, no. 6, p. 558-561.
Israel, S., Schiarizza, P., Kennedy, L. A., Friedman, R. M., and Villeneuve, M. E., 2006, Evidence for Early to Late Cretaceous, sinistral deformation in the Tchaikazan River area, southwestern British Columbia: Implications for the tectonic evolution of the southern Coast Belt, *in* Haggart, J., Enkin, R., and Monger, J. W. H., eds., Paleogeography of the western North American Cordillera, Geological Association of Canada, Special Paper 46, p. 331-350.
Israel, S., and van der Heyden, P., 2006, Geology, Atnarko (93C/05), British Columbia: Geological Survey of Canada, scale 1:50,000.
Journeay, J. M., and Friedman, R. M., 1993, The Coast Belt thrust system: evidence of late Cretaceous shortening in southwest British Columbia: Tectonics, v. 12, no. June 1993, p. 756-775.

Klepeis, K. A., Clarke, G. L., and Rushmer, T., 2003, Magma transport and coupling between deformation and magmatism in the continental lithosphere: GSA Today, v. 13, p. 4-11.

MacIntyre, D. G., Villeneuve, M. E., and Schiarizza, P., 2001, Timing and tectonic setting of the Stikine Terrane magmatism, Babine-Takla lakes area, central British Columbia: Canadian Journal of Earth Sciences, v. 38, p. 579-601.

Mahoney, J. B., Gordee, S. M., Haggart, J. W., Friedman, R. M., Diakow, L. J., and Woodsworth, G. J., in review, Magmatic evolution of the Eastern Coast Plutonic complex, Bella Coola region, west-central British Columbia.

Mair, J. L., Hart, C. J. R., and Stephens, J. R., 2006, Deformation history of the northwestern Selwyn Basin, Yukon, Canada: Implications for orogen evolution and mid-Cretaceous magmatism: Geological Society of America Bulletin, v. 118, no. 3/4, p. 304-323.

Marchildon, N., and Brown, M., 2003, Spatial distribution of melt-bearing structures in anatectic rocks from southern Brittany, France: Implications for melt transfer at grain- to orogen-scale: Tectonophysics, v. 364, p. 215-235.

Marsden, H., and Thorkelson, D., 1992, Geology of the Hazelton volcanic belt in British Columbia: Implications for the Early to Middle Jurassic evolution of Stikinia: Tectonics, v. 11, no. 6, p. 1266-1287.

McClelland, W. C., Gehrels, G. E., and Saleeby, J. B., 1992, Upper Jurassic-Lower Cretaceous basinal strata along Cordilleran margin: Implications for the accretionary history of the Alexander-Wrangellia-Peninsular terrane: Tectonics, v. 11, p. 823-835.

McClelland, W. C., Tikoff, B., and Manduca, C. A., 2000, Two-phase evolution of accretionary margins: examples from the North American Cordillera: Tectonophysics, v. 326, p. 37-55.

Monger, J. W. H., Price, R. A., and Templeman-Kluit, D. J., 1982, Tectonic accretion and the origin of two metamorphic and plutonic welts in the Canadian Cordillera: Geology, v. 10, p. 70-75.

Monger, J. W. H., van der Heyden, P., Journeay, J. M., Evenchick, C. A., and Mahoney, J. B., 1994, Jurassic-Cretaceous basins along the Canadian Coast belt: Their bearing on pre-mid-Cretaceous sinistral displacements: Geology, v. 22, p. 175-178.

Mortensen, J. K., Ghosh, D., and Ferri, F., 1995, U-Pb age constraints of intrusive rocks associated with copper-gold porphyry deposits in the Canadian Cordillera, *in* Shroeter, T. G., ed., Porphyry deposits of the northwestern Cordillera of North America, Canadian Institute of Mining and Metallurgy, p. 142-158.

Paterson, S., R, Miller, R. B., Alsleben, H., Whitney, D. L., Valley, P. M., and Hurlow, H., 2004, Driving mechanism for >40 km of exhumation during contraction and extension in a continental arc, Cascades core, Washington: Tectonics, v. 23.

Petford, N., Cruden, A. R., McCaffrey, K. J. W., and Vigneresse, J.-L., 2000, Granite magma formation, transport and emplacement in the Earth's crust: Nature, v. 408, p. 669-673.

Rey, P., Vanderhaeghe, O., and Teyssier, C., 2001, Gravitational collapse of the continental crust: definitions, regimes, mechanisms and modes: Tectonophysics, v. 342, p. 435-449.

Roddick, J. A., and Tipper, H. W., 1985, Geology, Mount Waddington (92N) map area: Geological Survey of Canada, scale 1:250,000.

Rothstein, D. A., and Manning, C. E., 2003, Geothermal gradients in continental magmatic arcs: Constraints from the eastern Peninsular Ranges batholith, Baja California, Mexico: Geological Society of America Special Paper 374, p. 337-354.

Rushmer, T., 1991, Partial melting of two amphibolites: contrasting experimental results under fluid-absent conditions: Contribution to Mineralogy and Petrology, v. 107, p. 41-59.

Rusmore, M. E., and Woodsworth, G. J., 1994, Evolution of the eastern Waddington thrust belt and its relation to the mid-Cretaceous Coast Mountains arc, western British Columbia: Tectonics, v. 13, no. 5, p. 1052-1067.

Rusmore, M. E., Woodsworth, G. J., and Gehrels, G. E., 2000, Late Cretaceous evolution of the eastern Coast Mountains, Bella Coola, British Columbia, *in* Stowell, H. H., and McClelland, W. C., eds., Tectonics of the Coast Mountains, southeastern Alaska and British Columbia: Boulder, Colorado, Geological Society of America Special Paper 343, p. 89-105.

Rusmore, M. E., Woodsworth, G. J., and Gehrels, G. E., 2005, Two-stage exhumation of midcrustal arc rocks, Coast Mountains, British Columbia: Tectonics, v. 24.

Schiarizza, P., Gaba, R. G., Glover, J. K., Garver, J. I., and Umhoefer, P. J., 1997, Geology and mineral occurrences of the Taseko-Bridge River area: British Columbia Ministry of Employment and Investment, Energy and Minerals Division, Geological Survey Branch.

Smith, L. M., 1998, Kinematics, age of deformation, and regional significance of the Cayoosh Creek fault, Lillooet, British Columbia [MSc thesis]: University of British Columbia, 94 p.

Umhoefer, P. J., and Schiarizza, P., 1996, Latest Cretaceous to early Tertiary dextral strike-slip faulting on the southeastern Yalakom fault system, southeastern Coast Belt, British Columbia: Geological Society of America Bulletin, v. 108, no. 7, p. 768-785.

Umhoefer, P. J., Schiarizza, P., and Robinson, M., 2002, Relay Mountain Group, Tyaughton-Methow basin, southwest British Columbia: a major Middle Jurassic to Early Cretaceous terrane overlap assemblage: Canadian Journal of Earth Sciences, v. 39, p. 1143-1167.

van der Heyden, P., 1990, Eastern margin of the Coast Belt in west-central British Columbia, Current Research, Part E, Geological Survey of Canada, p. 171-182.

van der Heyden, P., 1991, Preliminary U-Pb dates and field observations from the eastern Coast Belt near 52^{o}N, British Columbia, Current Research, Part A, Geological Survey of Canada, p. 79-84.

van der Heyden, P., 1992, A Middle Jurassic to early Tertiary Andean-Sierran arc model for the Coast Belt of British Columbia: Tectonics, v. 11, p. 82-97.

van der Heyden, P., 2004, Uranium-lead and potassium-argon ages from eastern Bella Coola and adjacent parts of Anahim Lake and Mount Waddington map areas, west-central British Columbia, Current Research 2004-A2, Geological Survey of Canada, p. 14.

van der Heyden, P., Mustard, P. S., and Friedman, R. M., 1994, Northern continuation of the Eastern Waddington Thrust Belt and Tyaughton Trough, Tatla Lake-Bussel Creek map areas, west-central British Columbia, Current Research 1994-A, Geological Survey of Canada, p. 87-94.

Vanderhaeghe, O., and Teyssier, C., 2001a, Crustal-scale rheological transitions during late-orogenic collapse: Tectonophysics, v. 335, p. 211-228.

Vanderhaeghe, O., and Teyssier, C., 2001b, Partial melting and flow of orogens: Tectonophysics, v. 342, p. 451-472.

Villa, I. M., 1998, Isotopic closure: Terra Nova, v. 10, p. 42-47.

Whitney, D. L., Paterson, S., R, Schmidt, K. L., Glazner, A. F., and Kopf, C. F., 2004, Growth and demis of continental arcs and orogenic plateaux in the North American Cordillera: Baja to British Columbia, *in* Grocott, J., McCaffrey, K. J. W., Taylor, G., and Tikoff, B., eds., Vertical coupling and decoupling in the lithosphere: London, Geological Society, London, Special Publications 227, p. 167-175.

Woodsworth, G. J., Anderson, R. G., and Armstrong, R. L., 1991, Plutonic Regimes, Chapter 15, *in* Gabrielse, H., and Yorath, C. J., eds., Geology of the Cordilleran Orogen in Canada, Geological Survey of Canada, p. 491-531.

Woodsworth, G. J., and Orchard, M. J., 1985, Upper Paleozoic to lower Mesozoic strata and their conodonts, western Coast Plutonic Complex, British Columbia: Canadian Journal of Earth Sciences, v. 22, p. 1329-1344.

CHAPTER 4

THE NATURE OF SUPERTERRANE BOUNDARIES FROM ALASKA TO SOUTHWESTERN BRITISH COLUMBIA

INTRODUCTION

The western Canadian Cordillera is composed of the Insular and Intermontane superterranes separated by the Coast belt (Fig. 4.1). The Coast belt includes plutonic and metamorphic assemblages of the Coast plutonic complex and fringing overlap sequences that stretch from Alaska through British Columbia. Much of the plutonism and metamorphism found within the Coast plutonic complex are believed to reflect the interaction between the Intermontane and Insular superterranes. Links between the complex and the two superterranes are provided by Mesozoic overlap assemblages (Monger et al., 1982; McClelland et al., 1992; van der Heyden, 1992; Monger et al., 1994).

There is still debate over the nature and timing of the accretion of the Insular superterrane to the western margin of the Intermontane superterrane with some workers suggesting mid-Cretaceous terrane linkages while others invoke Middle Jurassic or possibly Late Triassic interactions (McClelland et al., 1992; van der Heyden, 1992; Monger et al., 1994; Gehrels, 2001; Price and Monger, 2003; Dickinson, 2004; Saleeby, 2004).

In the central Coast belt, metamorphic and plutonic rocks from the Atnarko complex are found at the eastern margin of the Coast plutonic complex near the boundary with the Intermontane superterrane (Fig. 4.2). The Atnarko complex records structural and plutonic histories that span 150 My from latest Triassic to the Tertiary and provides detailed information about the Coast plutonic complex within the central Coast belt.

The purpose of this paper is to: 1) compare the characteristics of supracrustal and metaigneous rocks from the Atnarko complex to established stratigraphic and tectonic elements of the western Canadian and southeastern Alaskan Cordillera; 2) place the Atnarko complex within a regional tectonic framework; and, 3) develop a tectonic model that explains the tectonostratigraphic relationships along the Intermontane-Coast belt-Insular boundaries.

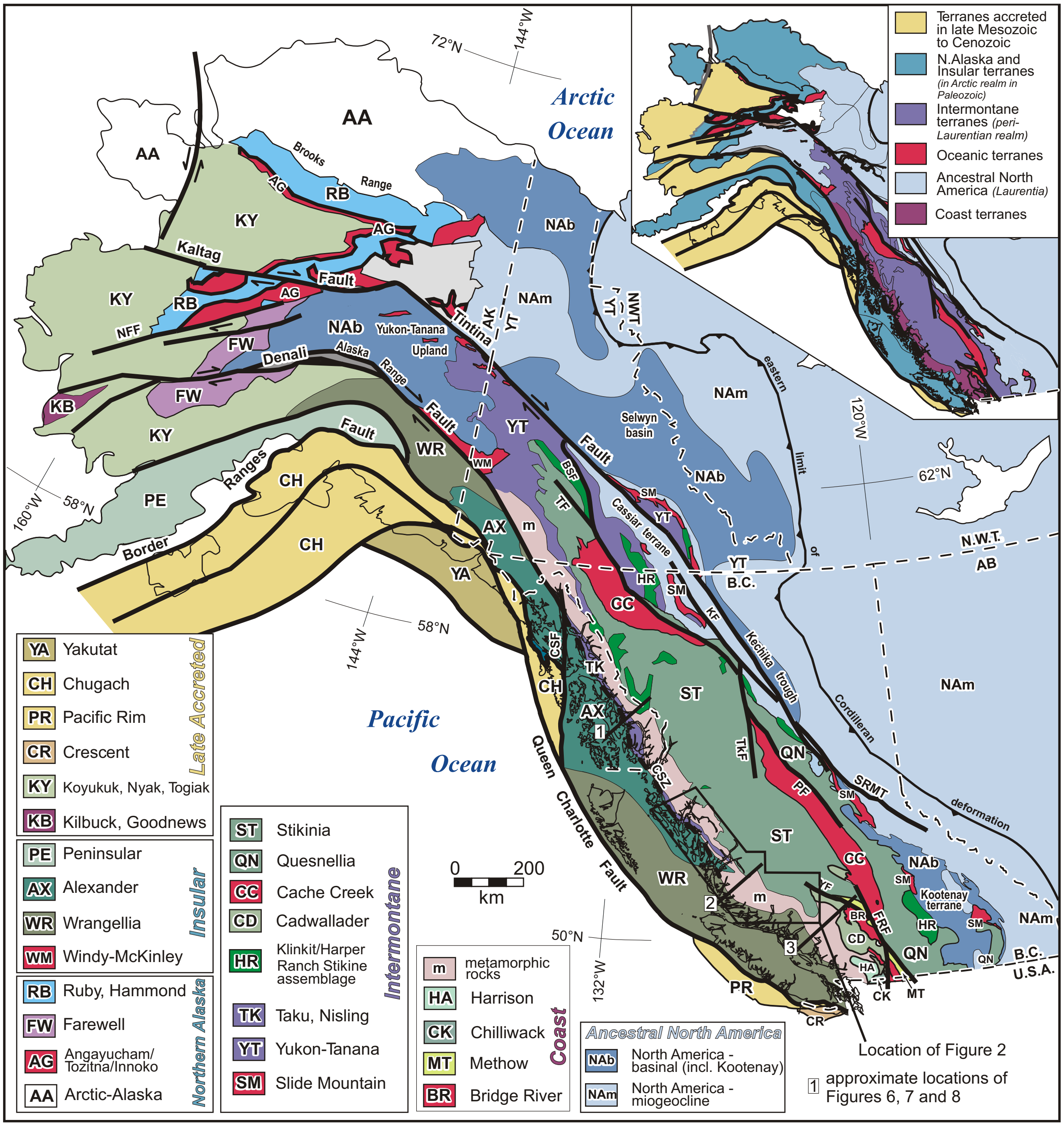

Figure 4.1. Terranes of the Alaska-Canadian Cordillera. Inset showing the tectonic realms as defined by Colpron et al., (2007). Location of Figure 2 indicated by outline. Numbers illustrate the approximate location of Figures 6, 7 and 8. Faults: BSF-Big Salmon fault; CSF-Chatham Strait fault; CSZ-Coast shear zone; FRF-Fraser River fault; KF-Kechika fault; NFF-Nixon Fork-Iditarod fault; PF-Pinchi fault; SMRT-southern Rocky Mountain trench; TkF-Takla-Finlay-Ingenika fault system; YK-Yalakom fault. Modified from Colpron et al., (2007).

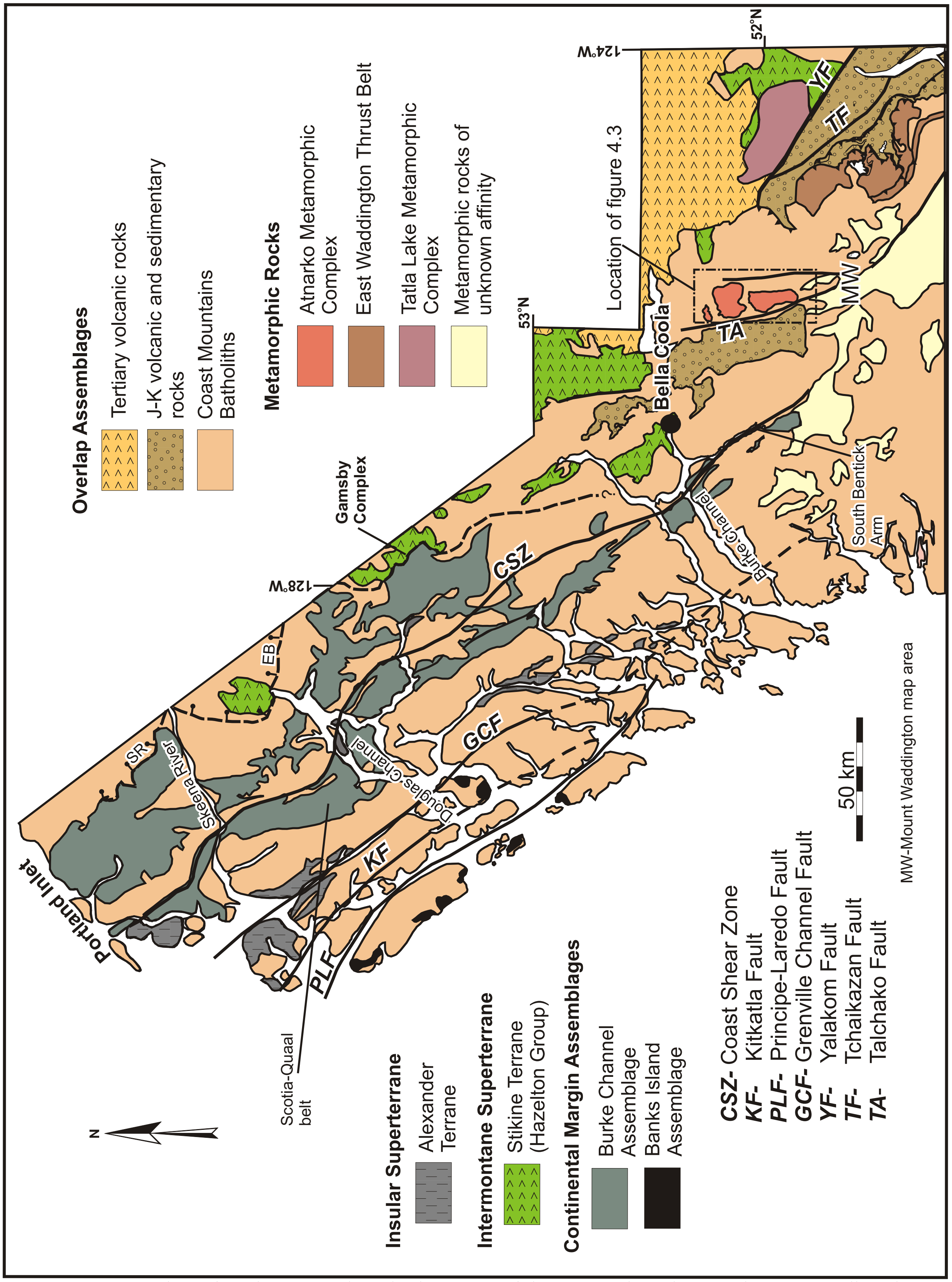

Figure 4.2. Location of study area and geologic nature of the Coast Plutonic complex surrounding the Atnarko complex. SR, EB-Shames River and Eastern Boundary detachment systems, respectively. MW-Mount Waddington Map area. Modified from Boghossian et al., [2000]; Chardon et al., [1999]; Rusmore and Woodsworth [1994]; Rusmore et al., [2005] and van der Heyden et al., [1994].

REGIONAL GEOLOGIC SETTING

Insular superterrane

Located west-southwest of the Atnarko complex, the Insular superterrane is characterized by rocks of the Alexander terrane found as pendants within Jurassic to Cretaceous batholiths (Figs. 4.1, 4.2; Baer, 1973; Gehrels and Boghossian, 2000). The Alexander terrane consists of variably deformed, low to medium grade, Late Proterozoic to Triassic metavolcanic, metasedimentary and metaigneous rocks (Woodsworth and Orchard, 1985; Gehrels and Saleeby, 1987; Gehrels and Boghossian, 2000). West of the Alexander terrane quartzite, quartzofeldspathic schist, marble and minor amounts of metapelite and metabasalt of uncertain ages and affinity are assigned to the Banks Island assemblage (Boghossian and Gehrels, 2000; Gehrels and Boghossian, 2000). Based on detrital zircons and isotope analyses, the Banks Island assemblage may have some relationship to continental margin assemblages found within the Coast plutonic complex, along the length of the Cordillera from Bella Coola into southeast Alaska (Boghossian and Gehrels, 2000; Gehrels and Boghossian, 2000).

Coast Belt

The Coast belt is a morphogeological belt that includes topographically high terrain composed of rocks from the Coast plutonic complex, the Insular and Intermontane superterranes and late Mesozoic and Cenozoic overlap assemblages.

The Coast plutonic complex is characterized by pendants of gneiss, metavolcanic and metasedimentary rocks within Jurassic to Tertiary plutons (Fig. 4.2). To the northwest of the Atnarko complex metamorphosed supracrustal rocks of the Coast plutonic complex crop out over a vast area that was unroofed during Eocene extension (Hollister and Andronicos, 2000). These rocks are strongly deformed metavolcanic, metasedimentary and metaigneous rocks of uncertain age and affinity that have been assigned to the Burke Channel assemblage, a package of rocks with ties to the North American continental margin (Gehrels and Boghossian, 2000; Gehrels, 2001). To the southeast of the Atnarko complex metamorphic and metasedimentary rocks and gneisses belonging to the Coast plutonic complex crop out within the Waddington fold and thrust belt, forming the hanging walls of the upper most thrust sheets (Rusmore and Woodsworth, 1994). These rocks mark the eastern boundary of the Coast belt and can be traced westward into the Mount Waddington map sheet where their age and affinity to other metamorphic rocks in the Coast plutonic complex is uncertain (Tipper, 1968).

Intermontane superterrane

Located to the east of the Coast plutonic complex are relatively unmetamorphosed rocks of the Intermontane superterrane that have been intruded by Early Jurassic to Eocene plutons (Fig. 4.2). To the northwest of the Atnarko complex, the boundary between the Coast plutonic complex and the Intermontane superterrane is marked by a low angle, east dipping detachment fault with volcanic and sedimentary rocks of the Stikine terrane in the hangingwall (Andronicos et al., 2003; Rusmore et al., 2005). To the southeast, the boundary coincides with the leading edge of the northeast-north verging Waddington thrust belt that places rocks of the Coast plutonic complex over rocks of the Stikine terrane and sedimentary overlap assemblages that were partially coeval with thrusting (Rusmore and Woodsworth, 1994; Umhoefer et al., 1994). The Intermontane superterrane near the Atnarko complex consists of Early to Middle Jurassic volcanic and associated sedimentary rocks of the Stikine terrane overlain by Early to mid-Cretaceous volcanic and sedimentary rocks of the Monarch assemblage (Haggart et al., 2003; Haggart et al., 2006).

THE ATNARKO COMPLEX

The Atnarko complex is a metamorphic and structural culmination that is located within the Coast plutonic complex near the boundary with the Intermontane superterrane. The complex is bound to the west by the steeply dipping Talchako fault that separates it from relatively unmetamorphosed volcanic and sedimentary rocks of the Stikine terrane and Cretaceous overlap assemblages (Figs. 4.2, 4.3). To the north gneissic plutonic rocks of the Atnarko complex are thrust northward over relatively undeformed plutons (Fig. 4.3). The southern boundary of the Atnarko complex is not well established; however, it is suspected that the complex continues along strike into the Mount Waddington area where similar metamorphic rocks of unknown affinity crop out extensively (Roddick and Tipper, 1985). The eastern boundary of the complex is also not well constrained, mainly due to the vast amounts of Neogene volcanic and sedimentary cover; however, van der Heyden and Mustard (1994) identify a gneissic Jurassic pluton, that may be part of the Atnarko complex, thrust to the northeast over rocks of the Intermontane superterrane (Fig. 4.2).

Below, the lithologic and structural characteristics of the Atnarko complex are described in order to later compare with other tectonostratigraphic elements along the Insular superterrane-Coast belt-Intermontane superterrane boundaries.

Lithology

Atnarko assemblage

The Atnarko assemblage is a package of metavolcanic and metasedimentary rocks that outcrop extensively within the Atnarko complex (Fig. 4.3). The assemblage occurs as sheets within a thrust package that includes gneisses and migmatites. Deformation throughout the assemblage varies considerably from very strongly deformed to moderately deformed. Metamorphic grade of the assemblage is from upper greenschist to mid- to upper amphibolite facies. Metavolcanic and metasedimentary rocks are transposed by deformation which precludes detailed stratigraphic study.

The Atnarko assemblage is dominated by metavolcanic rocks of mafic to intermediate compositions. The metavolcanic rocks are layered to massive with little to no original volcanic textures preserved. Locally layering, characterized by alternating bands of quartz-feldspar layers and hornblende-biotite layers, within the metavolcanics appear to define original deposition

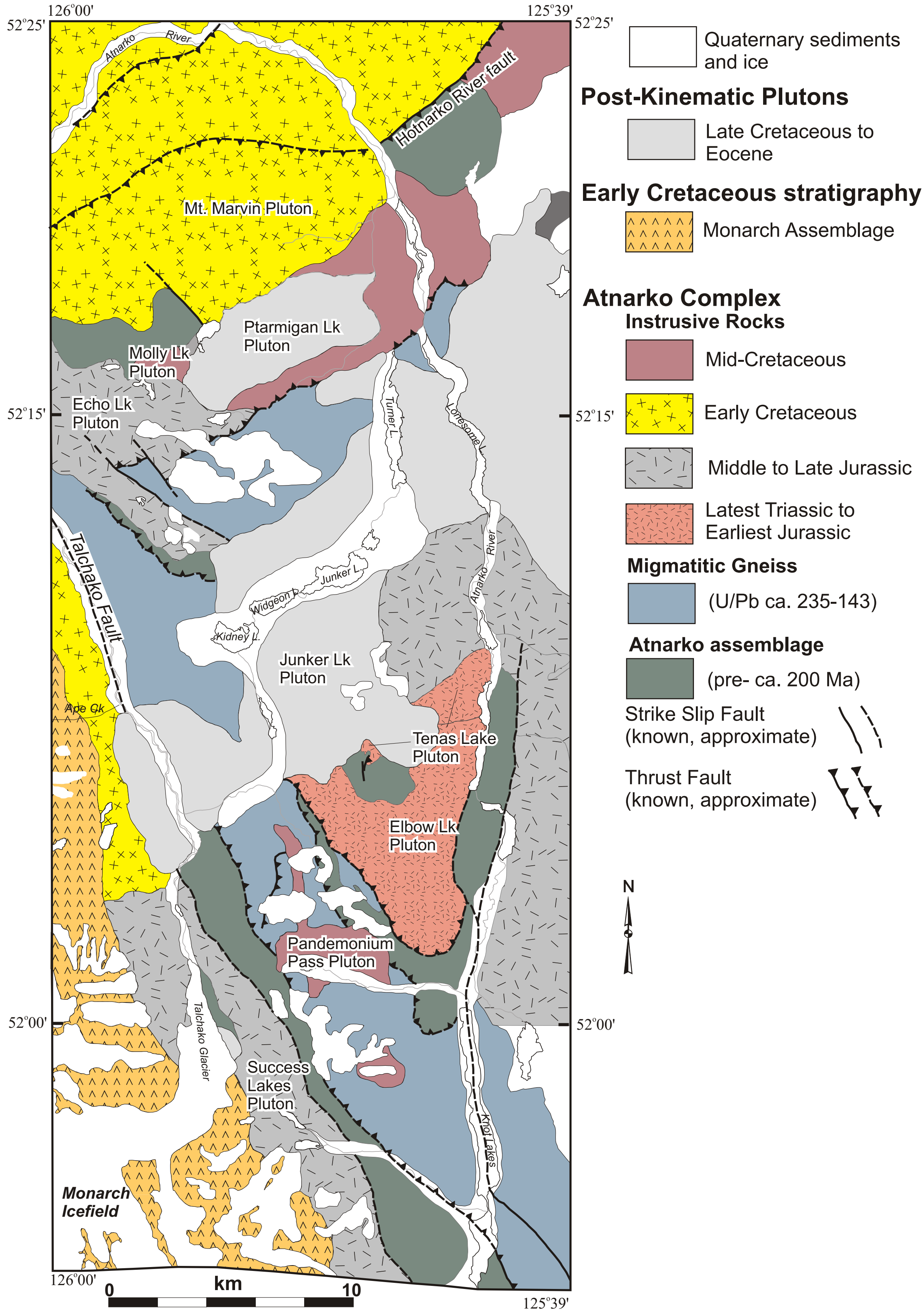

Figure 4.3. Generalized geology map of the Atnarko complex and surrounding area. Adapted from Israel and van der Heyden (2006) and Israel et al., (2006b).

however it is difficult to discern whether it might be related to bedding within volcaniclastics or between separate flows (Fig. 4.4A). Epidote and chlorite alteration highlights the layering and compositional variations within the unit (Fig. 4.4B). Rare felsic metavolcanic rocks crop out sporadically and occur as thin layers no more than two metres in thickness within more mafic packages (Fig. 4.4C). Geochemical analyses of the least deformed and altered mafic metavolcanics from the Atnarko assemblage indicate the rocks are calc-alkaline and have the typical 'arc-type' signature with distinct negative Nb and more subtle negative Ti with respect to Th and La (Fig. 4.5A, B).

Metasedimentary rocks of the Atnarko assemblage are more abundant in the central and southern portions of the complex where they occur as thick packages or as thin beds intercalated with the metavolcanics. Original bedding was observed at some outcrops; however transposition during deformation makes it difficult to define depositional characteristics. Metasedimentary rocks are quartz-rich with little pelitic material and range from very fine-grained to medium grained. Light grey quartzites are common and are typically interlayered with dark grey psammites (Fig. 4.4D). Rare metacarbonate occurs as thin, fine-grained, beige to light-brown layers typically within or in very close proximity to metavolcanic rocks (Fig. 4.4E). In the southernmost portion of the Atnarko complex, strained pebble to cobble conglomerate outcrops in faulted contact with mafic metavolcanics. Clasts are mainly quartzite and are found within a quartz rich matrix. The clasts are considerably stretched and flattened (Fig. 4.4F).

The age of the Atnarko assemblage is not well constrained. It is intruded by a quartz-diorite pluton that has a U-Pb zircon age of ca. 200 Ma making the assemblage at least latest Triassic to earliest Jurassic in age.

Gneisses

Structurally interleaved with the Atnarko assemblage are several packages of orthogneiss with quartz-diorite to tonalite compositions (Fig. 4.3). Layering in the gneiss is defined by hornblende

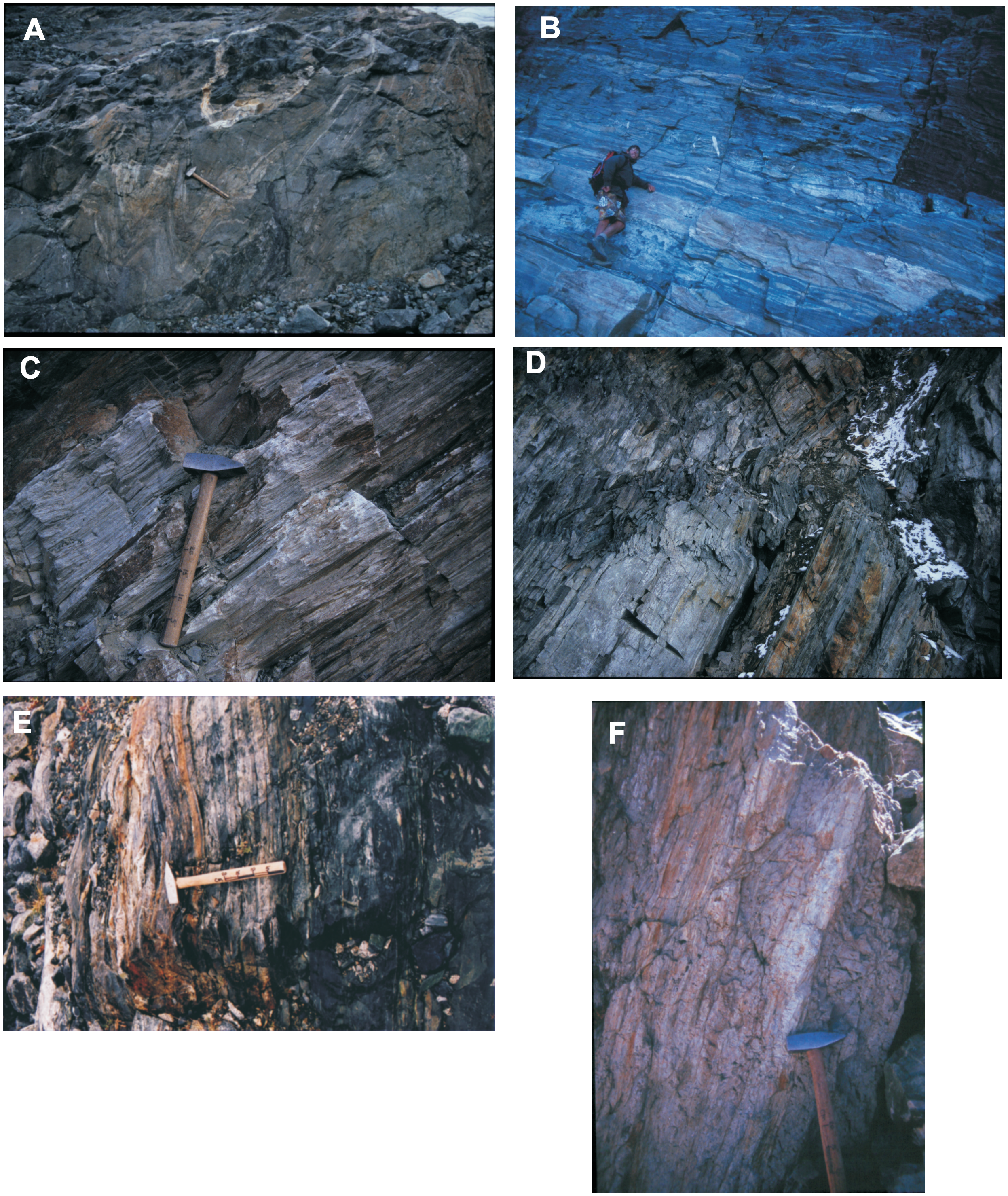

Figure 4.4. A) Lighter coloured layers within metavolcanic rocks of the Atnarko assemblage. B) Epidote and chlorite alteration within metavolcanic rocks highlights different compositions of layers. C) Rare felsic metavolcanic rocks within the Atnarko assemblage. D) Light grey quartzite interbedded with darker grey psammitic metasedimentary rocks within the Atnarko assemblage. E) Intercalated carbonate (light grey-beige) and mafic metavolcanic rocks of the Atnarko assemblage. F) Strongly deformed quartzite cobble conglomerate from the southern Atnarko complex.

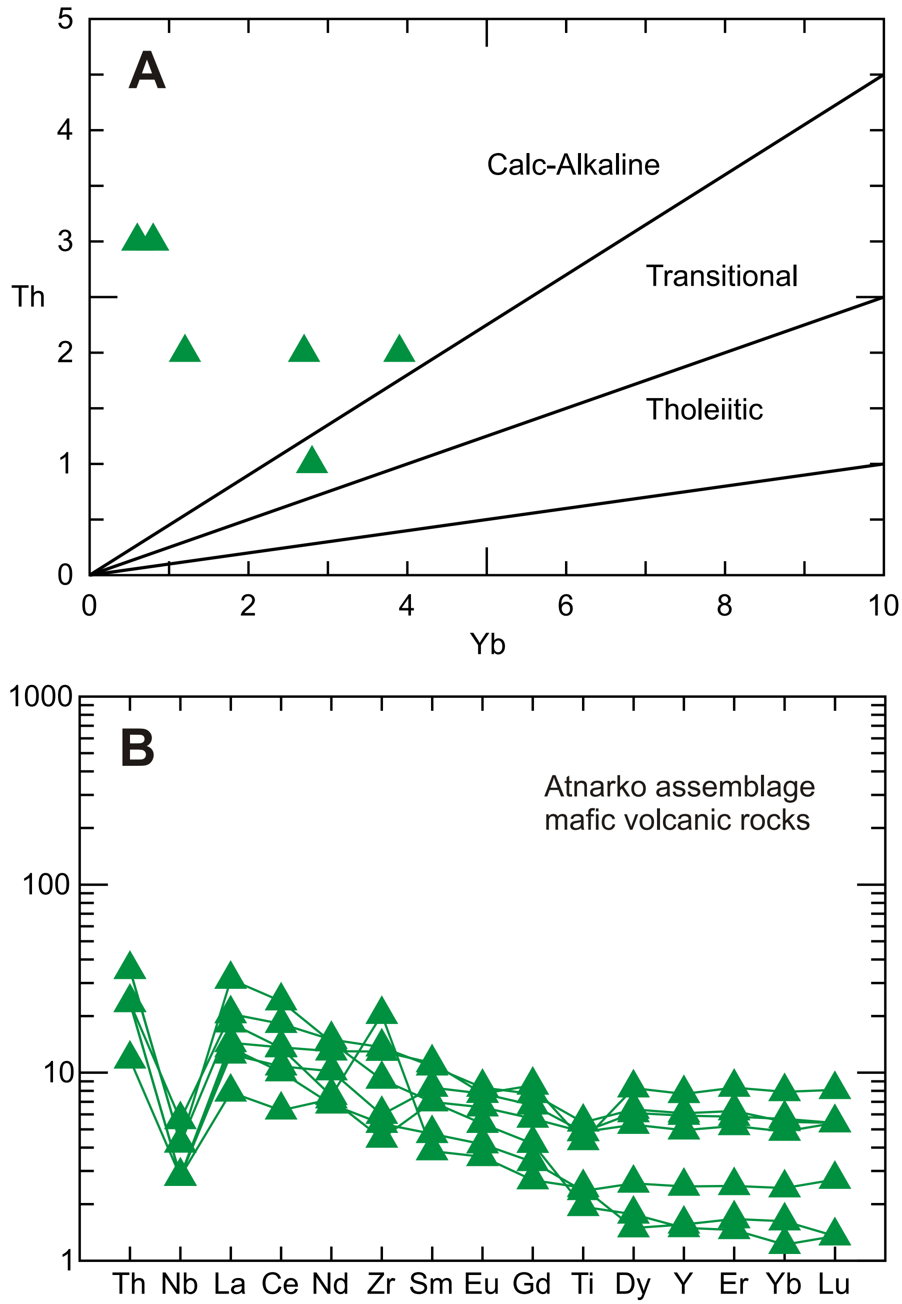

Figure 4.5. A) Th-Yb discrimination diagram for Atnarko complex mafic metavolcanic rocks. B) Primitive mantle normalized plot for Atnarko complex mafic metavolcanic rocks.

and biotite separated by plagioclase-quartz ± K-feldspar layers. Migmatite is common and leucosomes are composed of plagioclase, quartz and muscovite ± garnet ± K-feldspar. The majority of the migmatite is stromatic in form with leucosome developed along and helping to define the main gneissic foliation. Locally, leucosomes cross-cut the main foliation yet appear to have optical and mineralogical continuity with the foliation parallel material. The age of gneisses range from Middle Triassic to Late Jurassic-Early Cretaceous.

Plutonism

Plutons of several ages are found within the Atnarko complex and range in composition from quartz-diorite to granodiorite. Many of the plutons are syn-tectonic and include Early Jurassic and mid-Cretaceous plutons associated with Jurassic deformation and mid-Cretaceous thrusting (van der Heyden, 1991, 2004). Several other plutons intrude in between deformation events or are post-kinematic.

Structural geology

An enigmatic Early Jurassic event is suspected to have affected the older rocks located within the Atnarko complex. Little is known about this event other than that it accompanied intrusion of quartz-dioritic plutons (see previous chapter). Scattered evidence, such as deformed xenoliths within Late Jurassic plutons and apparent syn-tectonic fabrics within a Late Triassic to Early Jurassic pluton, is preserved yet all kinematics and defining characteristics of the event have been obscured by younger deformation.

The main structural grain of the Atnarko complex is the result of mid-Cretaceous (~117-80 Ma) southwest to west directed thrusting that imbricated rocks of the Atnarko assemblage with migmatitic gneisses and plutons (Fig. 4.3). An inverted metamorphic grade was developed during compression with lowest grade rocks found in the southwestern most portion of the complex. Early Late Cretaceous (~80 Ma) north-northeast compression overlaps with, and overprints, earlier thrusting. Steepening of fabrics during the latter stages of thrusting led to flattening across the complex and the development of dextral and sinistral, steeply dipping near conjugate shear zones. Brittle faults related to latest Cretaceous to Eocene dextral strike-slip systems cut through all older fabrics and plutonic rocks within the Atnarko complex.

CORRELATION OF UNITS

There are three different tectonostratigraphic packages that may correlate with the Atnarko assemblage and associated gneisses: 1) the Stikine terrane of the Intermontane superterrane; 2) the Alexander terrane of the Insular superterrane; and, 3) the Burke Channel assemblage. Below lithologic characteristics from each of the possible three units are described and the merits of correlating each with the Atnarko assemblage is discussed.

Stikine terrane

To the north and east of the Atnarko complex the Stikine terrane is mainly composed of Devonian through to Jurassic volcanic and sedimentary rocks. Paleozoic strata include Devonian mafic volcanic rocks interbedded with carbonates, overlain by Carboniferous volcaniclastics, carbonates and thick packages of Permian limestone that all belong to the Stikine assemblage (Gunning et al., 2006). The Stikine assemblage is overlain by mafic volcanic, volcaniclastic and sedimentary rocks of the Late Triassic Stuhini Group (Evenchick and Thorkelson, 2005). An Early to Middle Jurassic bimodal volcanic succession intercalated with clastic sedimentary and volcaniclastic deposits define the Hazelton Group which is part of a Jurassic arc built on Stikinia (Evenchick and Thorkelson, 2005) that overlies the Stuhini Group and forms the most aerially extensive Stikine terrane rocks near the Bella Coola region (Gordee, 2005; Haggart et al., 2006).

The Gamsby complex, located at the Coast plutonic complex-Intermontane superterrane boundary north of the study area (Fig. 4.2), is characterized by metavolcanic and metaplutonic rocks with latest Triassic to Late Cretaceous ages (van der Heyden, 1989; Mahoney et al., 2007). Portions of the metavolcanic rocks within the Gamsby complex in turn have been correlated with the Early to Middle Jurassic Hazelton Group (van der Heyden, 1989). The Gamsby complex and adjacent Hazelton Group rocks are deformed by east verging thrusts (Mahoney et al., 2007). These thrusts and related folds are interpreted as early Late Jurassic to Early Cretaceous in age that were overprinted by mid-Cretaceous brittle structures (van der Heyden, 1989).

van der Heyden (1991) proposed a correlation of the Atnarko complex with the Gamsby complex; however, at least a portion of the Atnarko assemblage is older than the ca. 197 Ma ages reported for metarhyolite from the Gamsby complex (van der Heyden, 1989). In addition, the presence of quartz-rich sedimentary rocks within the Atnarko complex differs from carbonaceous pelite found in the Gamsby complex (Mahoney et al., 2007). Abundant felsic metavolcanic rocks within the Gamsby complex are not found within the Atnarko complex. Deformation styles in the two complexes differ greatly, with the Gamsby reflecting Late Jurassic to Early Cretaceous east directed thrusting while the Atnarko is dominated by southwest to west directed compression of Early to mid-Cretaceous age.

Correlation of the Atnarko assemblage with older units within the Stikine terrane is also difficult to justify as both the Stikine assemblage and the Stuhini Group includes large amounts of carbonates and pelitic sediments that are not found within the Atnarko complex (Evenchick and Thorkelson, 2005).

The Stikine terrane is therefore not considered a good correlative for the Atnarko assemblage.

Alexander terrane

The Alexander terrane at the latitude of the Atnarko complex consists of mafic volcanic and volcaniclastic rocks, argillites, carbonates and sandstones (Saleeby, 2000). Late Proterozoic (?) to Early Devonian mafic, arc volcanic rocks are intruded by Ordovician to Silurian plutons (Gehrels and Saleeby, 1987). Middle Devonian through Permian shallow marine carbonates are typical of the Alexander terrane in this area. Late Triassic rift related sedimentary and volcanic rocks overlie all other rocks and define the top of the terrane (Gehrels and Saleeby, 1987).

Correlation between the Atnarko assemblage and the Alexander terrane is difficult to justify based on a number of factors. Firstly, the position of the Alexander terrane west of the Coast plutonic complex is quite different than the position of the Atnarko assemblage at the eastern edge of the Coast plutonic complex. Secondly, the large quantity of carbonate and clastic sedimentary rocks, many of them argillaceous that have a deep basinal origin, are quite different from the quartz-rich and psammitic compositions for the sedimentary rocks in the Atnarko assemblage. Finally, Triassic volcanic rocks of the Alexander terrane are strongly bimodal and the Atnarko assemblage is dominantly mafic with rare felsic units. Therefore no correlation between the Atnarko assemblage and the Alexander terrane is proposed.

Burke Channel assemblage

The Burke Channel assemblage occurs as large pendants within the Coast plutonic complex from the southern end of South Bentick Arm, north to Douglas Channel (Fig. 4.2). The assemblage is characterized by mafic to felsic metavolcanic rocks and interlayered quartzite, marble and metapelite (Gehrels and Boghossian, 2000). Lesser amounts of layered marble, layered quartzite and quartz cobble conglomerate are locally present (Gehrels and Boghossian, 2000). The proportion of metavolcanic rocks increases to the south in the pendants (Gehrels and Boghossian, 2000). Rusmore et al., (2000) indicate a dominance of amphibolite within the pendants of the Burke Channel assemblage along Burke Channel and South Bentick Arm (Fig. 4.2). The amphibolite is interspersed with psammitic schist and pelite with lesser amounts of quartzite and marble (Rusmore et al., 2000).

Structures within the Burke Channel assemblage are complex and show evidence for pre-mid-Cretaceous deformation and folds and thrusts related to mid-Cretaceous compression (Gareau, 1991; Crawford et al., 2000; Gehrels, 2000). Mid-Cretaceous compression is related to west to southwest verging thrust systems developed along the western margin of the Coast plutonic complex (Crawford et al., 1987; Crawford et al., 2000; Andronicos et al., 2003). Amphibolites are isoclinally folded and locally refolded with Type III interference patterns exposed near Bella Coola (Rusmore et al., 2000). These folds are overprinted by northeast and southwest plunging folds with axial planes that dip towards the northeast (Rusmore et al., 2000).

The age of the Burke Channel assemblage is not well constrained. Gehrels and Boghossian (2000) correlate the assemblage with the Scotia-Quaal belt. The correlation is on the basis of similar lithologies, similar ages of detrital zircons and similar isotopic compositions for the corresponding metasediments and metavolcanic rocks. The Scotia-Quaal belt is a package of gneissic metaplutonic, metavolcanic and metasedimentary rocks located between Douglas Channel and the Skeena River that includes Devonian orthogneiss (Fig. 4.2; Gareau and Woodsworth, 2000). The upper age of the belt is not known (Gareau and Woodsworth, 2000). The only constraint on the upper age is pre-Early Jurassic as much of the belt is cut by plutons of this age (Gareau, 1991; Gareau and Woodsworth, 2000).

The Burke Channel assemblage is the most likely candidate for correlation with the Atnarko assemblage. This correlation is supported by the following observations: 1) the character of the Burke Channel assemblage becomes more mafic volcanic-rich to the southeast, a trend that continues into the Atnarko assemblage, 2) similar amounts of quartzite and psammite are found in both the Atnarko assemblage and the Burke Channel assemblage, 3) the ages of the two assemblages may overlap as the upper age of the Burke Channel is constrained to pre-Early Jurassic and the Atnarko assemblage is older than Early Jurassic, 4) both assemblages contain minor amounts of quartzite, carbonate and quartz pebble conglomerate, 5) Early to mid-Cretaceous compressional structures are shared by the Burke Channel and the Atnarko assemblages, and, 6) as much as 40 km of sinistral translation along the Talchako fault occurred in the Late Cretaceous and restoration of this displacement places rocks of the Atnarko assemblage along strike of the Burke Channel assemblage (see Chapter 2).

TECTONOSTRATIGRAPHIC RELATIONSHIPS

In the following discussion the known tectonostratigraphic and structural relationships from three areas along the Insular superterrane-Coast belt-Intermontane superterrane boundaries are presented. The different terranes and assemblages discussed below are depicted in figures 4.6, 4.7 and 4.8. The Coast belt is used, rather than the Coast plutonic complex, in order to address the relationships and tectonic roles of the overlap assemblages that characterize the belt.

Southeast Alaska

The geological relationships across the western Cordilleran margin in southeast Alaska have been examined in detail (e.g., McClelland et al., 1992; Crawford et al., 2000; Saleeby, 2000; Gehrels, 2001). Figure 4.6 illustrates the stratigraphic relationships within southeast Alaska.

Insular superterrane

In southeast Alaska the main components of the Insular superterrane are the Alexander terrane and Wrangellia, Paleozoic arc volcanic and sedimentary rocks and Triassic flood basalts and carbonates. Wrangellia and Alexander are both intruded by a Pennsylvanian stitching pluton (Gardner et al., 1988) and were part of a continuous tectonic block (the Insular superterrane) from at least the Pennsylvanian. Both the Alexander terrane and Wrangellia are overlain by Middle Jurassic volcanic rocks and Upper Jurassic to Early Cretaceous sedimentary, volcanic and volcaniclastic rocks of the Gravina belt (Fig. 4.6; Rubin and Saleeby, 1991; McClelland et al., 1992). Detrital zircons from the Gravina belt indicate a link to both Yukon-Tanana and Stikine terranes and either a depositional tie between the Insular and Intermontane superterranes or at the very least close proximity of the two superterranes (McClelland et al., 1992; Gehrels, 2001).

Coast Belt

Paleozoic rocks within the Coast belt are correlated with the Yukon-Tanana terrane and are part of a string of continental margin assemblages found along the length of the belt (Gehrels,

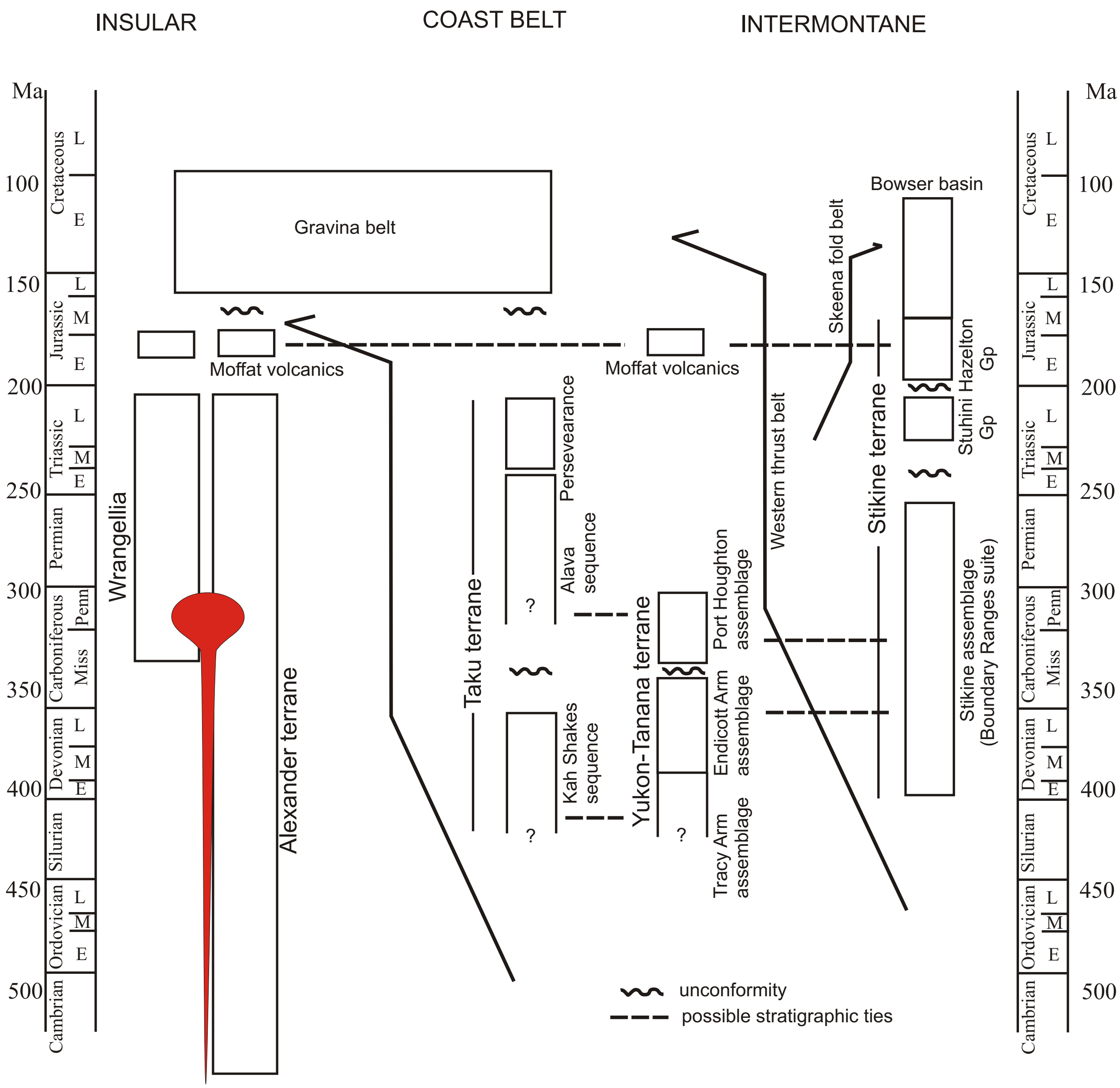

Figure 4.6. Schematic stratigraphic sections for the Insular superterrane, the Coast Belt and the Intermontane superterrane for southeastern Alaska. Pre-Late Jurassic and mid-Cretaceous thrust belts indicate general movement. Data from Colpron et al., (2006), Currie and Parrish (1997), Gardner et al., (1988), Gehrels (2001), Gunning et al., (2006), Saleeby (2000).

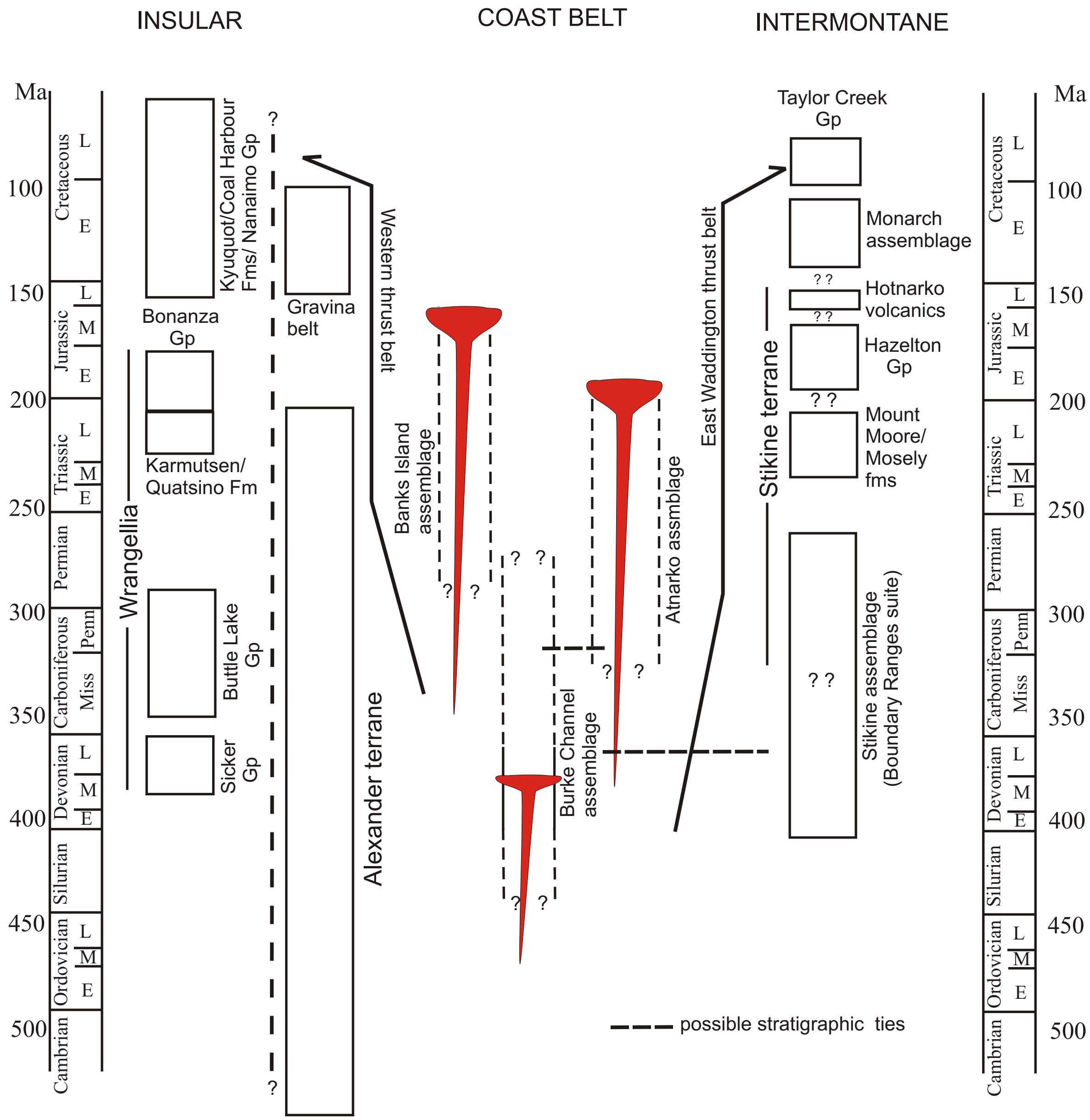

Figure 4.7. Schematic stratigraphic sections for the Insular superterrane, the Coast Belt and the Intermontane superterrane for west-central British Columbia. Data from Boghossian and Gehrels (2000), Gehrels and Boghossian (2000), Haggart et al., (2006), Rusmore and Woodsworth (1994), van der Heyden, (1991; 2004), Wheeler and McFeely (1991), (*this study*)

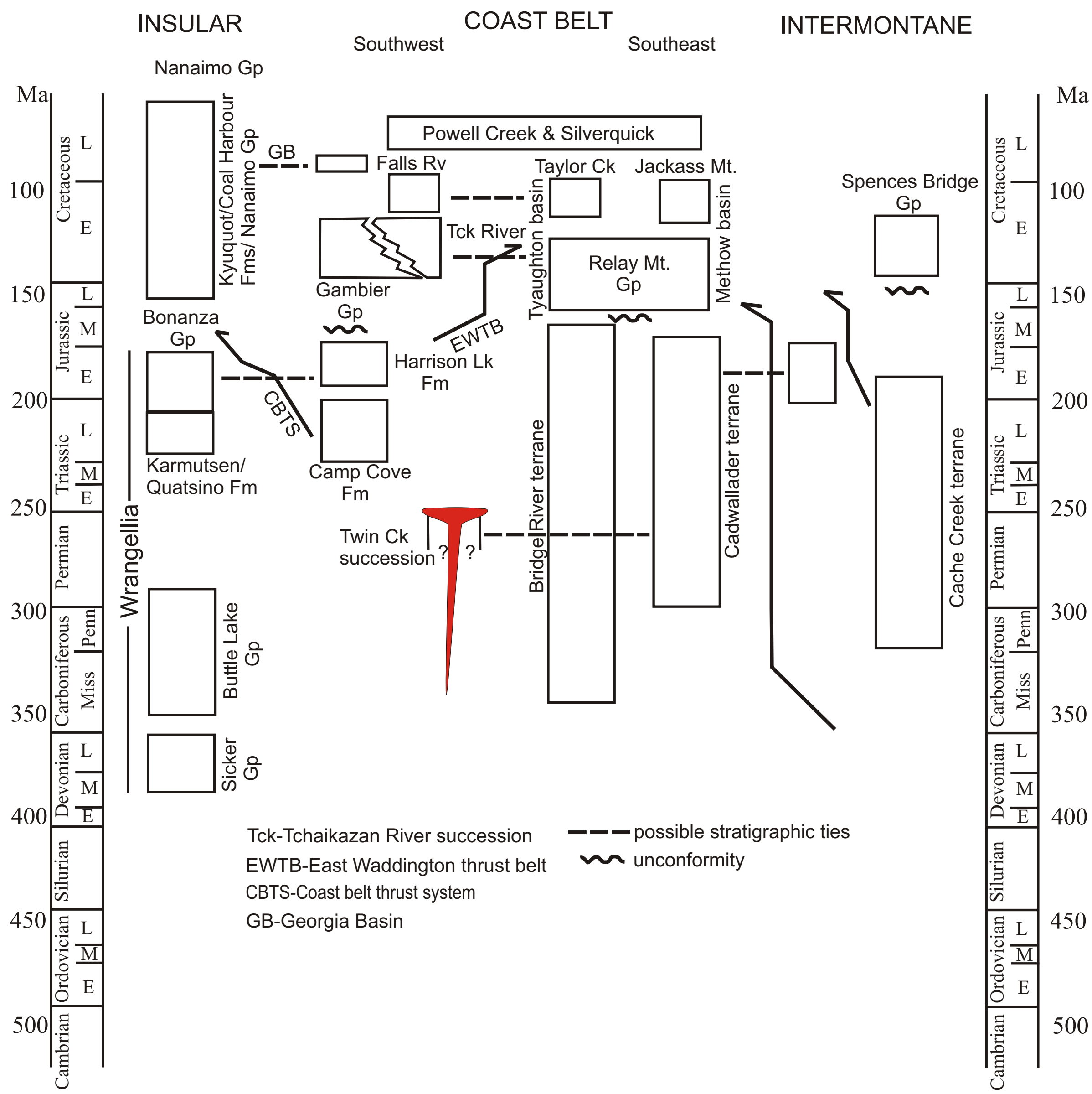

Figure 4 8. Schematic stratigraphic sections for the Insular superterrane, the Coast Belt and the Intermontane superterrane for southwestern British Columbia. Data from Israel et al., (2006), Price and Monger (2003), Schiarizza et al., (1997), Umhoefer et al., (1994), Umhoefer et al., (2002), Wheeler and McFeely (1991).

2000, 2001; Colpron et al., 2006). The lowest member of the Yukon-Tanana terrane, the Tracy Arm assemblage resembles and may be related to the Silurian (?) to Devonian Kah Shakes sequence of the Taku terrane. The Kah Shakes sequence is composed of Silurian (possibly older) metasedimentary and metavolcanic rocks, unconformably overlain by meta-arc basinal deposits that get as young as upper Triassic (Fig. 4.6; Gehrels et al., 1992; Saleeby, 2000). These relationships suggest a tie between the Intermontane and continental margin assemblage rocks of the Coast belt by the Paleozoic.

Middle Jurassic Moffat volcanic rocks overlie the Yukon-Tanana and the Alexander terranes, tying these terranes together by at least the Middle Jurassic (Gehrels, 2001).

Intermontane superterrane

The Intermontane superterrane in southeast Alaska consists of Paleozoic to Middle Jurassic rocks of Stikinia overlain by sedimentary rocks of the Bowser basin (Fig. 4.6). The Paleozoic section of Stikinia is the Stikine assemblage that is partially correlated to the Boundary Ranges suite, a package of metavolcanic and metasedimentary rocks of Paleozoic age (Currie and Parrish, 1997). Unconformably overlying the Stikine assemblage is the Stuhini Group which in turn is unconformably overlain by the Hazelton Group (Fig. 4.6). Middle Jurassic to Early Cretaceous sedimentary rocks of the Bowser Basin are deposited on top of the Hazelton Group and were in part deposited during Cretaceous thrusting (Evenchick, 1992).

Currie and Parrish (1997) propose a possible correlation between continental margin assemblages within the Coast belt with the Stikine assemblage and consequently a link between the Alava sequence of the Taku terrane and the Port Houghton assemblage of the Yukon-Tanana terrane (Fig. 4.6). The correlation between the Stikine assemblage, the Taku terrane and the Yukon-Tanana terrane suggests a stratigraphic link between the Yukon-Tanana terrane and Stikinia by Paleozoic time (2001). Therefore, during the Paleozoic the Intermontane and Insular superterranes were amalgamated by this time. Gehrels (2001) identified a package of Middle

Jurassic volcanic rocks (the Moffat volcanics) that unconformably overlies both the Yukon-Tanana and the Alexander terranes indicating that the two terranes were linked by this time. These Middle Jurassic volcanic rocks have also been related to the Hazelton Group as a large Jurassic overlap assemblage (van der Heyden, 1992; Monger and Nokelberg, 1996). Similarly, Saleeby (2000) demonstrates a pre-Late Jurassic structural tie between the Taku and the Alexander terranes. These relationships indicate that initial docking of the Insular superterrane and the Intermontane superterrane (including Yukon-Tanana terrane) occurred by the Middle Jurassic and possibly earlier (*cf.* (McClelland et al., 1992; van der Heyden, 1992; Monger et al., 1994; Saleeby, 2000; Gehrels, 2001).

West-central British Columbia

Insular superterrane

The Insular superterrane in west-central British Columbia is characterized exclusively by Wrangellia. There is no evidence for Alexander terrane rocks south of about 51^{o}N latitude (Fig. 4.1). However just to the north of the study area Alexander terrane rocks crop out and it is likely that some of the metamorphic rocks included within the Coast plutonic complex at this latitude belong to the Alexander terrane (Fig. 4.7; Wheeler and McFeely, 1991). Paleozoic rocks of Wrangellia are characterized by Devonian arc rocks of the Sicker Group overlain by deep marine sediments and carbonate rocks of the Buttle Lake Group (Price and Monger, 2003). Middle to Late Triassic rocks include flood basalts of the Karmutsen Formation and limestones of the Quatsino Formation that are conformably overlain by a package of Latest Triassic to Middle Jurassic sedimentary and volcanic rocks of the Bonanza Group (Nixon and Orr, 2006).

Coast Belt

The Coast belt in west-central British Columbia is characterized mainly by the Coast plutonic complex. The complex at this latitude comprises strongly deformed and metamorphosed pendants and packages of rock within Early Jurassic to Tertiary plutons. Supracrustal rocks within the complex include the Banks Island, Burke Channel and Atnarko assemblages (Gehrels and Boghossian, 2000; Rusmore et al., 2000). The Banks Island assemblage is composed of quartzite, marble and metapelite and minor amounts of mafic volcaniclastics (Gehrels and Boghossian, 2000). Nd-Sr isotopic signatures of quartzite within the assemblage point to a cratonal source (Boghossian and Gehrels, 2000); however, the relationship with other continental margin rocks within the Coast plutonic complex is not known (Gehrels and Boghossian, 2000). The age of the Banks Island assemblage is constrained only as pre-Late Jurassic based upon Late Jurassic plutons that intrude the assemblage (van der Heyden, 1989). The Burke Channel assemblage has been related to the Scotia Quaal belt that has a Middle Devonian (ca. 385 Ma) age for lower units and no upper age limit (Fig. 4.2; Gareau, 1991; Gareau and Woodsworth, 2000; Gehrels and Boghossian, 2000). The Atnarko assemblage is correlated with the Burke Channel assemblage.

Intermontane superterrane

The Intermontane superterrane consists of Triassic to Cretaceous volcanic and sedimentary rocks of the Stikine terrane (Fig. 4.7). A package of orthogneiss and migmatitic gneisses found near Bella Coola, an area mainly composed of Stikine terrane rocks (Haggart et al., 2006), may represent a portion of the Stikine assemblage or Boundary Ranges suite described earlier. The Mount Moore and Mosely formations are Late Triassic volcanic and sedimentary rocks found within the Waddington thrust belt (Fig. 4.2 and 4.7) and are correlated with the Stikine terrane (Rusmore and Woodsworth, 1991; Umhoefer et al., 1994). Early to Middle Jurassic Hazelton Group outcrops extensively in and around the Bella Coola region and are the most areally extensive unit of the Stikine terrane units (Haggart et al., 2006). A small package of Late Jurassic volcanic and sedimentary rock found just north of the Atnarko complex, referred to as the Hotnarko volcanics, likely represent the youngest part of the Hazelton Group (van der Heyden, 1991). Early Cretaceous sedimentary and volcanic rocks of the Monarch assemblage unconformably overly rocks of the Hazelton Group in the Bella Coola area and have an uncertain relationship with the Hotnarko volcanics. Similar Early Cretaceous rocks include the Ottarasko and Cloud Drifter formations found in the Waddington thrust belt (Mustard and van der Heyden, 1994; Umhoefer et al., 1994). Mid-Cretaceous sedimentary deposits of the Taylor Creek Group outcrop sporadically within the Bella Coola area and more extensively in the Waddington thrust belt. This is a syn-thrusting package of rocks that are found mainly farther south in southwestern British Columbia (see next section). They form the upper portion of the Tyaughton basin and are the product of eroding thrust sheets of late Early to Late Cretaceous age (Garver, 1992; Schiarizza et al., 1997).

Known stratigraphic links across the boundaries in west-central British Columbia are scarce (Fig. 4.7). The Burke Channel assemblage has been correlated to the Scotia Quaal belt (Gehrels and Boghossian, 2000) which in turn has been correlated to the Yukon-Tanana terrane (Gareau and Woodsworth, 2000). Therefore continental margin assemblages are present at least as far south as Bella Coola (Fig. 4.2). Alternatively, Currie and Parrish (1997) correlate the Scotia Quaal belt with the Stikine assemblage and if this is correct, then the Burke Channel and consequently the Atnarko assemblage could be related to the Stikine terrane instead of the Yukon-Tanana terrane. However, rocks of the Burke Channel assemblage are thrust to the west over Alexander terrane rocks (Boghossian and Gehrels, 2000) and the Atnarko assemblage is also involved in west verging thrusts. Nowhere along the margin are rocks of the Stikine terrane observed thrust over rocks of the Alexander terrane and I propose that the correlation of the Scotia Quaal belt with the Yukon-Tanana terrane is more appropriate. Although there is some evidence for Jurassic deformation within the rocks of the Coast plutonic complex of west-central British Columbia, it has been extensively overprinted by Cretaceous and younger deformation.

Southwestern British Columbia

The Insular superterrane-Coast belt-Intermontane superterrane relationships within southwestern British Columbia are quite significantly different than those observed along strike to the northwest. The major difference is the division of the Coast belt into southwest and southeast portions and the presence of bona fide oceanic basement rocks (Fig. 4.8; Monger and Journeay, 1994; Schiarizza et al., 1997). The character of the Intermontane superterrane also changes in the south with the absence of Jurassic arc rocks.

Insular superterrane

The Insular superterrane in southwest British Columbia is characterized mainly by Wrangellia, with no evidence for Alexander terrane (Wheeler and McFeely, 1991).

Coast Belt

The Coast belt in southwestern British Columbia is divided into southwest and southeast Coast belts based on the character of supracrustal rocks and ages and amount of plutonic rocks (Fig. 4.8; Monger and Journeay, 1994).

The southwest Coast belt is characterized by up to 80% plutonic rocks that intrude Triassic to Jurassic sedimentary and volcanic rocks of the Camp Cove and Harrison Lake formations (Fig. 4.8). Unconformably overlying these formations and older plutons are volcanic and sedimentary rocks of the Gambier Group, part of an Early Cretaceous arc deposited on the southwestern Coast belt (Monger and Journeay, 1994; Price and Monger, 2003). Permo-Triassic sedimentary rocks found within the southwest belt, the Twin Creek succession, have uncertain relationships with other rocks within the southwestern Coast belt, but are probably unconformably overlain by Early Cretaceous Gambier equivalent rocks (Israel et al., 2006).

The early history of the southeastern Coast belt is quite different than the southwestern Coast belt (Fig. 4.8). A Mississippian to Jurassic oceanic terrane, the Bridge River terrane, underlies younger sedimentary deposits. A portion of the Bridge River terrane, the Bridge River complex, is a Middle Triassic to Middle Jurassic accretion-subduction complex that records Middle Triassic blueschist facies metamorphism (Schiarizza et al., 1997). Inboard to the east of the Bridge River terrane, volcanic and sedimentary rocks of the Late Paleozoic to Middle Jurassic Cadwallader terrane characterize the eastern margin of the southeastern Coast belt. Unconformably overlying both the Bridge River and Cadwallader terranes is the Middle Jurassic to mid-Cretaceous Tyaughton and Methow basins (Fig. 4.8). The lower portions of the basins are characterized by the Late Jurassic to Early Cretaceous Relay Mountain Group and were connected as one basin until Early to mid-Cretaceous compression across the belt separated the two basins into the Tyaughton and Methow basins (Garver, 1992; Schiarizza et al., 1997).

Overlying both the southeast and southwest Coast belts are the Powell Creek and Silverquick formations (Fig. 4.8). The Powell Creek formation is a thick sequence of Late Cretaceous dominantly non-marine volcanic and volcaniclastic rocks that lie gradationally over non-marine conglomeratic rocks of the Silverquick formation (Schiarizza et al., 1997).

Intermontane superterrane

The Intermontane superterrane, unlike the orogen along strike to the northwest, is characterized by the Cache Creek terrane and not by the Stikine terrane (Fig. 4.8). The Cache Creek is an oceanic terrane that is characterized by radiolarian chert, mafic volcanics, ultramafics and carbonate that ranges in age from Pennsylvanian to Early Jurassic. It mainly occurs between Stikinia and Quesnellia in the southern part of British Columbia (Fig. 4.1). The Cache Creek terrane is thrust to the west over a package of undifferentiated Jurassic sedimentary rocks (Rusmore and Woodsworth, 1991). Overlying most of the area within the western Intermontane is the Early Cretaceous Spences Bridge Group, a dominantly volcanic package of rocks deposited on the western edge of Quesnellia (Wheeler and McFeely, 1991).

Southwestern British Columbia amalgamation

Possible ties across the different belts in southwestern British Columbia are illustrated in Figure 4.8. Few links can be made across the Insular and the Coast belt before mid-Cretaceous. However, Mahoney and Debari (1995) suggest a possible link between the Bonanza Group of the Insular superterrane and the Harrison Lake Formation of the southwest Coast belt. If correct this would indicate a link between the Insular superterrane and the southwest Coast belt by the Middle Jurassic and that much of the southwest Coast belt is underlain by the Insular superterrane. By Late Cretaceous time, rocks within the Georgia basin, including the Nanaimo Group (Figure 4.8), overly units from within the Insular and southwestern Coast belt.

Ties between the southeast and southwest Coast belts can be made by the Early to mid-Cretaceous and possibly as early as the Permo-Triassic. Permian rocks of the Twin Creek succession correlated with rocks of the Cadwallader terrane provide a tentative link between the two belts by the Permo-Triassic (Israel et al., 2006). By the Early Cretaceous, volcanic and volcaniclastic rocks of the Tchaikazan River succession (and other equivalent volcanic packages) are believed to have provided source material for a mid-Cretaceous overlap sequences found on both belts (Umhoefer et al., 2002; Israel et al., 2006).

A connection between the Cadwallader terrane and the Stikine terrane suggests the possibility that the Cadwallader terrane is the southern extension of the Stikine terrane and was faulted off and overlain by rocks of the southeastern Coast belt (Friedman and Schiarizza, 1999; Friedman et al., 2001; Israel et al., 2006). Rusmore and Woodsworth (1991) suggest a link between the Cadwallader terrane and undifferentiated rocks within the Intermontane superterrane indicating a tie between the Coast belt and the Intermontane superterrane by Earliest Jurassic (Fig. 4.8).

Mid-Cretaceous compressional structures dominate the structural relationships between the terranes. These structures are typically overprinted by younger strike-slip faults, yet the structural stacking between the terranes is preserved. Some evidence for pre-Cretaceous deformation exists in both the southeast and southwest Coast belts. In the southeast Coast belt the initiation of volcanic dominated detritus being shed into the Relay Mountain Group basin from the west has been sited as an indication of a change in environment brought on by the southern movement of the outboard southwest Coast belt and related terranes (the Insular superterrane) (Schiarizza et al., 1997; Umhoefer et al., 2002; Umhoefer, 2003). The arrival of the Insular superterrane is related to Jurassic to mid-Cretaceous sinistral faulting that occurred between the Insular and Intermontane (Monger et al., 1994; Schiarizza et al., 1997; Umhoefer et al., 2002; Israel et al., 2006).

TECTONIC IMPLICATIONS

The Insular superterrane, the Coast belt and the Intermontane superterrane from southeast Alaska to southwestern British Columbia were tied together by Middle Jurassic and possibly much earlier. In west-central British Columbia, around the Atnarko complex, younger, overprinting deformation makes it difficult to make ties across the boundaries, which are now purely structural in nature. In southeast Alaska the ties between the Yukon-Tanana terrane and the Stikine assemblage point towards the possibility that the Intermontane is underlain by the continental margin assemblages. For example, Colpron et al., (2007) suggest that the Yukon-Tanana terrane is the underpinning of the Intermontane superterrane with Mesozoic arcs built on top. Gehrels (2001) presents similar ideas and has included the Taku terrane with the Yukon-Tanana terrane, and Stikinia.

Evidence for the Yukon-Tanana terrane-Intermontane superterrane connection is difficult to illustrate in west-central British Columbia; however, the potential correlation between the Scotia Quaal belt and the Stikine assemblage (Currie and Parrish, 1997) represents a connection between the Yukon-Tanana terrane and the Intermontane superterrane. A correlation between the Scotia Quaal belt and the Yukon-Tanana terrane (Gareau and Woodsworth, 2000) implies that the Scotia Quaal belt and the Yukon-Tanana terrane is related to the Intermontane superterrane because of the ties between the Yukon-Tanana terrane and the Stikine assemblage proposed in southeast Alaska (Currie and Parrish, 1997; Gehrels, 2001). A package of Late Jurassic volcanic rocks deposited on the western edge of Stikinia has zircons that have a distinct late Proterozoic inheritance indicating an older, possibly continentally associated basement beneath western Stikinia (van der Heyden, 1991, 2004). This basement is the Stikine assemblage equivalent or Yukon-Tanana terrane equivalent. The presence of rocks correlated with the Yukon-Tanana terrane, the Atnarko assemblage of this study and the Burke Channel assemblage of Gehrels and Boghossian (2000), supports the possibility that continental margin assemblage rocks correlated with the Yukon-Tanana terrane underlie western Stikinia in west-central British Columbia.

The character of the basement rocks and the overlapping assemblages in southwestern British Columbia changes dramatically. In southwestern British Columbia an oceanic terrane, the Bridge River terrane, occurs between the outboard Insular and southwest Coast belt terranes and the Intermontane terranes (Fig. 4.1). The Bridge River ocean basin was open to the west until at least Late Jurassic time when the arrival of a volcanic rich source (i.e. the southwestern Coast belt) provided material for the Late Jurassic to Early Cretaceous portions of the Tyaughton basin (Fig. 4.9; Schiarizza et al., 1997; Umhoefer et al., 2002; Israel et al., 2006). Rocks of the southwest Coast belt began forming on Wrangellia and possibly across the Intermontane terranes (Fig. 4.9). Sedimentary rocks of the southeast Coast belt were forming on the Bridge River terrane as a forearc basin (Fig. 4.9). During the early Late Jurassic to Early Cretaceous, sinistral translation brought the Insular superterranes south, cutting off the Bridge River ocean basin and providing material to be deposited in the intervening Tyaughton-Methow basin. Final accretion occurred during mid-Cretaceous compression, closing the basins and structurally interleaving the terranes in southeast Alaska, west-central and southwest British Columbia (Monger et al., 1994; Umhoefer et al., 2002; Israel et al., 2006).

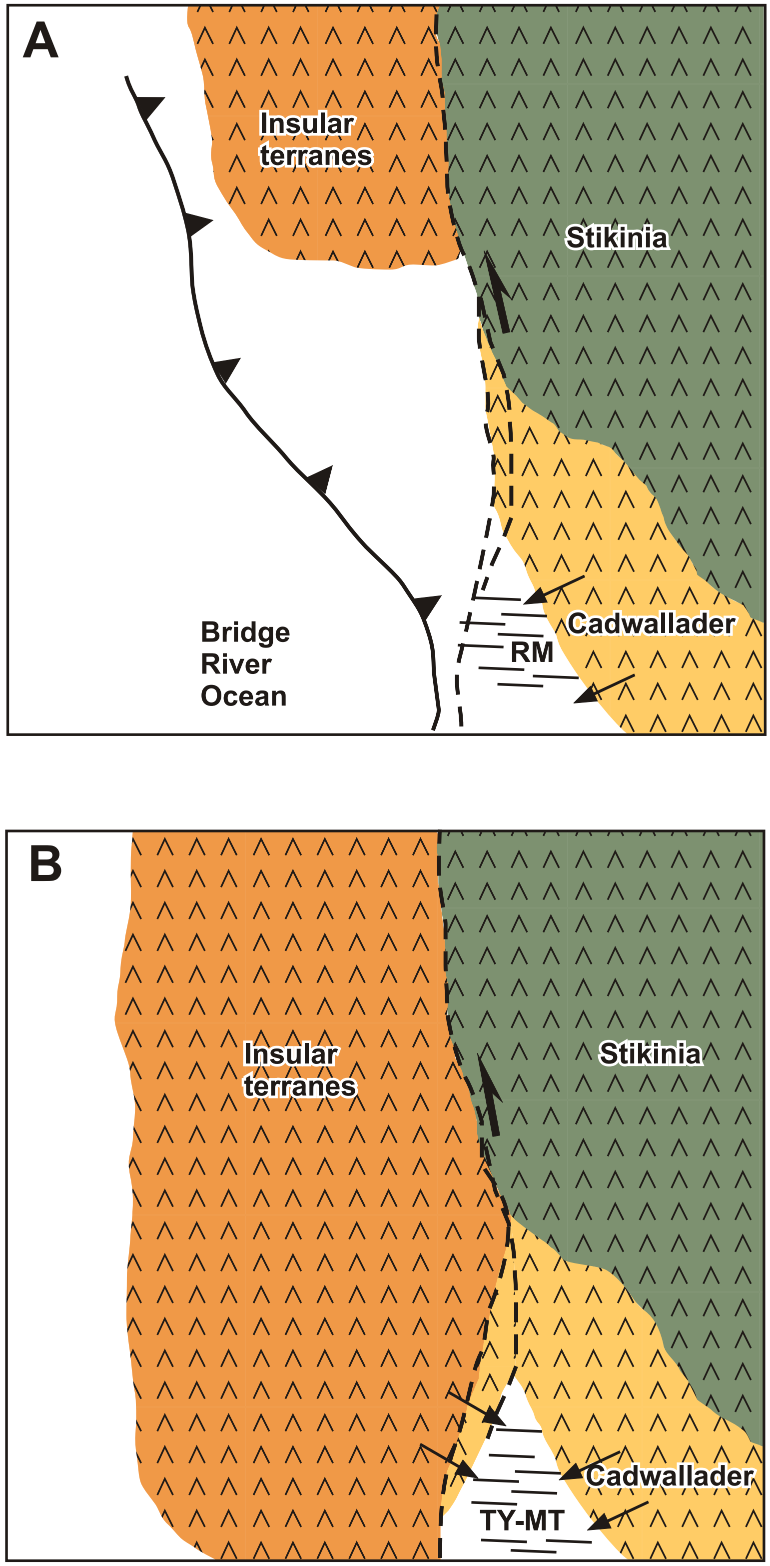

Figure 4.9. Schematic tectonic relationships for southeastern Alaska to southwest British Columbia for A) Middle Jurassic and B) Late Jurassic to mid-Cretaceous. RM-Relay Mountain Group, TY-Tyaughton Basin, MT-Methow Basin.

The above description does not address the presence of continental margin assemblage rocks within the Coast belt and what role they have on the overall tectonic evolution. Two possible tectonic models for the occurrence of these rocks that do not necessarily affect the Middle Jurassic to Cretaceous history described above are presented in Figure 4.10. These models help to examine the present day distribution of the continental margin assemblages in the context of the relationships described above.

Model 1

In this model it is assumed that the Intermontane arc assemblages were built upon the Yukon-Tanana terrane after it was rifted away from the Laurentian margin in Devonian to Early Mississippian time (Nelson et al., 2006; Colpron et al., 2007). Figure 4.10A illustrates the initial geographical position of the terranes. The Cadwallader terrane is located at the northern tip of the Stikine terrane and the Bridge River ocean basin opens towards the north. Cordey and Schiarizza (1993) noted similar ages and lithologies of the Bridge River terrane and the oceanic terranes of Angayucham and Innoko in Alaska (Fig. 4.1). The age and lithologic similarities suggest that they were once part of the same northern ocean basin. Interaction between the Insular and Intermontane superterranes began by Middle Jurassic. Wrangellia and the Alexander terrane were together by the Pennsylvanian. A northern latitudinal position for the two terranes is proposed by the presence of northern latitude faunal assemblages in Jurassic stratigraphy within both (Pedder, 2006; Schroder-Adams and Haggart, 2006). The Insular superterrane attained its present day configuration by movement on a system of dextral faults, some of which may be preserved in southeast Alaska (Gehrels, 2001). The arrangement of terranes in Figure 4.10B is dependant on the validity of the oroclinal model proposed by Mihalynuk et al. (1994). This model proposes a tectonic scale folding of the Intermontane superterrane such that Stikinia, originally formed north of Quesnellia, is found outboard of Quesnellia with oceanic rocks trapped between (Fig. 4.10 A, B). The dextral fault system observed by Gehrels (2001) could be

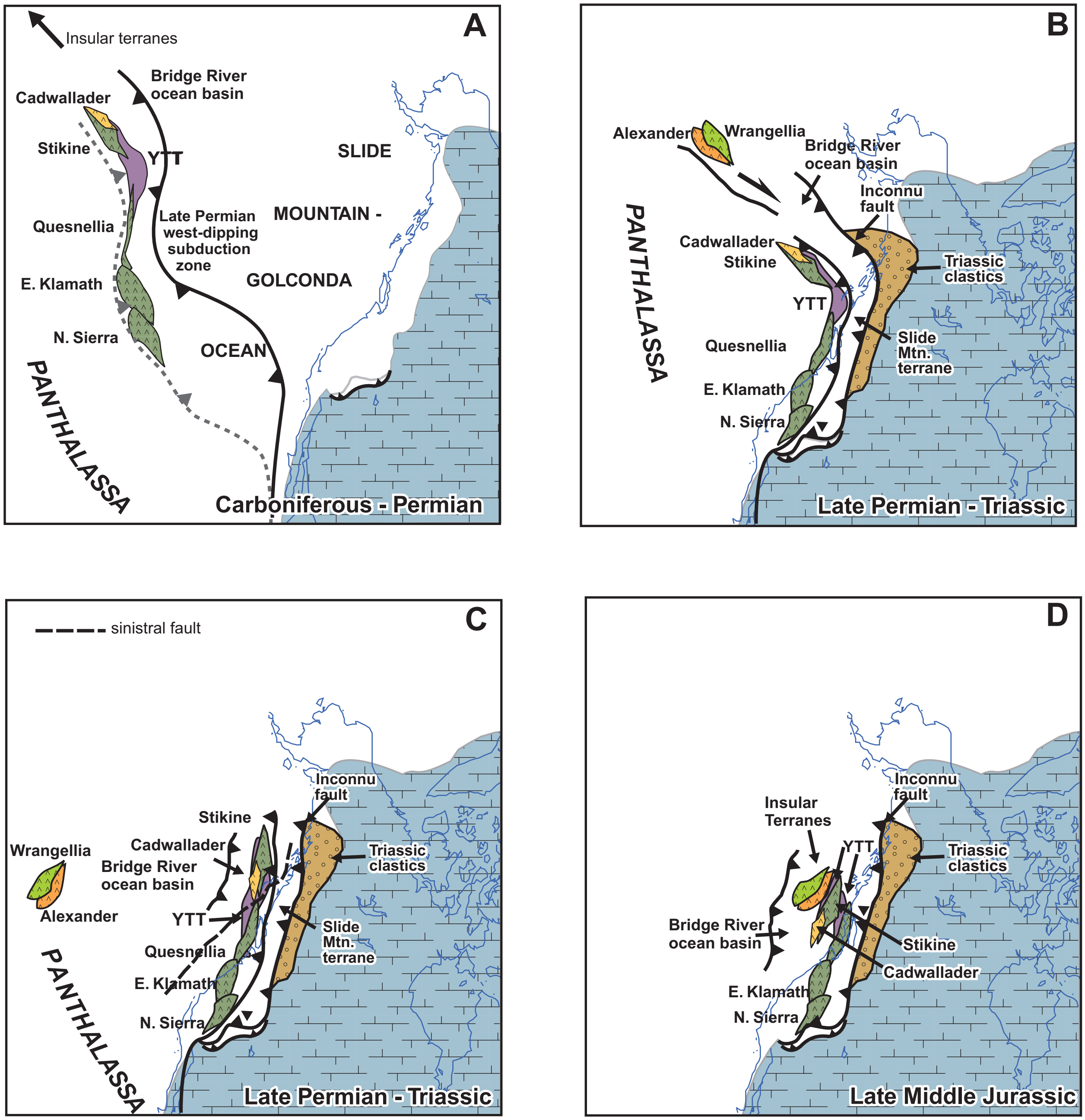

Figure 4.10. Possible tectonic scenarios for the amalgamation of terranes of the western Canadian Cordillera. A and B depict the oroclinal bending model of Mihalynuk et al., (1994) with the Cadwallader terrane formed on the northern edge of Stikinia and a northern position for the Bridge River ocean. C and D depict the strike slip model, with Cadwallader occupying a the southern portion of Stikinia and a more southerly position for the Bridge River ocean outboard. Modified from Colpron et al., (2007).

the shear faults on the western limb of the orocline analogous to shearing along bedding planes in a fold (Fig. 4.10B). Following the final closure of the orocline, plate vectors changed and Late Jurassic to Cretaceous sinistral faulting began as described above.

Model 2

Although the proposed ties between Stikinia and the Yukon-Tanana terrane by pre-Mesozoic times (Colpron et al., 2007) and reference therein) are gaining acceptance, the orocline model is not universally accepted. A second scenario to explain the general terrane framework involves a series of sinistral faults that dissect the margin and place Stikinia west of the Cache Creek terrane and Quesnellia (Fig. 4.10C). To explain the relationships observed along the Insular superterrane-Coast belt-Intermontane superterrane boundaries the Mesozoic portion of Stikinia is assumed to have been built upon the continental margin assemblages that were part of the Stikinian basement. The basement rocks were exposed within the Coast belt during exhumation of the middle and lower crust during the accretion of the Insular terranes. The structural interleaving of the Cache Creek and Stikinia by Early Jurassic (Monger and Nokelberg, 1996) forces the timing for sinistral faulting to pre-Jurassic (Fig. 4.10D).

CONCLUSIONS

The Atnarko assemblage is correlated with the Burke Channel assemblage and associated continental margin assemblages found within the Coast plutonic complex of the western Canadian and southeastern Alaskan Cordillera. This correlation is based upon lithologic resemblance and similarities in structural histories. If this correlation is correct, continental margin assemblages are extended farther south than previously proposed. The presence of continental margin assemblages suggest that much of Stikinia and Mesozoic strata of the Insular superterrane were built upon older continentally derived strata, tying together the Insular and Intermontane superterranes by the Mesozoic.

REFERENCES

Andronicos, C. L., Chardon, D. H., and Hollister, L. S., 2003, Strain partitioning in an obliquely convergent orogen, plutonism, and synorogenic collapse: Coast Mountains Batholiths, British Columbia, Canada: Tectonics, v. 22, no. 2, doi:10.1029/2001TC001312.

Baer, A. J., 1973, Bella Coola-Laredo Sound map areas: British Columbia, Geological Survey of Canada Memoir 372, 122 p.

Boghossian, N. D., and Gehrels, G. E., 2000, Nd isotopic signature of metasedimentary pendants in the Coast Mountains between Prince Rupert and Bella Coola, British Columbia, *in* Stowell, H. H., and McClelland, W. C., eds., Tectonics of the Coast Mountains, southeastern Alaska and British Columbia: Boulder, Colorado, Geological Society of America Special Paper 343, p. 77-87.

Colpron, M., Nelson, J. L., and Murphy, D. C., 2007, Northern Cordilleran terranes and their interactions through time: GSA Today, v. 17, no. 4/5, p. 1-10.

Colpron, M., Nelson, J. L., Roots, C. F., Gehrels, G. E., and others, 2006, A tectonostratigraphic framework for the pericratonic terranes of the northern Cordillera, *in* Colpron, M., Nelson, J. L., and Thompson, R. I., eds., Paleozoic evolution and metallogeny of pericratonic terranes at the ancient Pacific margin of North America, Canadian and Alaskan Cordillera, Geological Association of Canada.

Crawford, M. L., Crawford, W. A., and Gehrels, G. E., 2000, Terrane assembly and structural relationships in the eastern Prince Rupert quadrangle, British Columbia, *in* Stowell, H. H., and McClelland, W. C., eds., Tectonics of the Coast Mountains, southeastern Alaska and British Columbia: Boulder, Colorado, Geological Society of America Special Paper 343, p. 1-21.

Crawford, M. L., Hollister, L. S., and Woodsworth, G. J., 1987, Crustal deformation and regional metamorphism across a terrane boundary, Coast Plutonic Complex, British Columbia: Tectonics, v. 6, no. 3, p. 343-361.

Currie, L. D., and Parrish, R. R., 1997, Paleozoic and Mesozoic rocks of Stikinia exposed in northwestern British Columbia: Implications for correlations in the northern Cordillera: Geological Society of America Bulletin, v. 109, no. 11, p. 1402-1420.

Dickinson, W. R., 2004, Evolution of the North American Cordillera: Annual Reviews of Earth and Planetary Science, v. 32, p. 13-45.

Evenchick, C. A., 1992, The Skeena fold belt: a link between the Coast Plutonic Complex, the Omineca belt and the Rocky Mountain fold and thrust belt, *in* McClay, K. R., ed., Thrust Tectonics: London, Chapman & Hall, p. 365-375.

Evenchick, C. A., and Thorkelson, D., 2005, Geology of the Spatsizi River map area, north-central British Columbia, Geological Survey of Canada Bulletin 577, p. 276.

Friedman, R. M., and Schiarizza, P., 1999, Permian and Triassic intrusions and volcanics in southwestern British Columbia: Implications for tectonic setting and terrane correlations: Geological Society of America, Cordilleran section, Abstracts with Programs, v. 31, no. 6.

Friedman, R. M., Schiarizza, P., and Israel, S., 2001, U-Pb geochronology and geochemistry of Permian and Triassic intrusions and volcanics in southwestern British Columbia: Implications for tectonic setting and terrane correlations, *in* Slave-Northern Cordillera Lithospheric Evolution (SNORCLE) Transect and Cordilleran Tectonics Workshop meeting, Pacific Geoscience Centre, p. 247.

Gardner, M. C., Bergman, S. C., Cushing, G. W., MacKevett, E. M., Plafker, G., Campbell, R. B., Dodds, C. J., McClelland, W. C., and Mueller, P. A., 1988, Pennsylvanian pluton

stitching of Wrangellia and the Alexander Terrane, Wrangell Mountains, Alaska: Geology, v. 16, no. 11, p. 967-971.
Gareau, S. A., 1991, The Scotia-Quaal metamorphic belt: a distinct assemblage with pre-early Late Cretaceous deformational and metamorphic history, Coast Plutonic Complex: Canadian Journal of Earth Sciences, v. 28, p. 870-880.
Gareau, S. A., and Woodsworth, G. J., 2000, Yukon-Tanana terrane in the Scotia-Quaal belt, Coast Plutonic Complex, central-Western British Columbia, *in* Stowell, H. H., and McClelland, W. C., eds., Tectonics of the Coast Mountains in SE Alaska and Coastal British Columbia: Boulder, Colorado, Geological Society of America Special Paper 343, p. 23-43.
Garver, J. I., 1992, Provenance of Albian-Cenomanian rocks of the Methow and Tyaughton basins, southern British Columbia: a mid-Cretaceous link between North America and the Insular terrane: Canadian Journal of Earth Sciences, v. 29, p. 1274-1295.
Gehrels, G. E., 2000, Reconnaissance geology and U-Pb geochronology of the western flank of the Coast Mountains between Juneau and Skagway, southeastern Alaska, *in* Stowell, H. H., and McClelland, W. C., eds., Tectonics of the Coast Mountains in SE Alaska and Coastal British Columbia, Geological Society of America, p. 213-234.
Gehrels, G. E., 2001, Geology of the Chatham Sound region, southeast Alaska and coastal British Columbia: Canadian Journal of Earth Sciences, v. 38, p. 1579-1599.
Gehrels, G. E., and Boghossian, N. D., 2000, Reconnaissance geology and U-Pb geochronology of the west flank of the Coast Mountains between Bella Coola and Prince Rupert, coastal British Columbia, *in* Stowell, H. H., and McClelland, W. C., eds., Tectonics of the Coast Mountains, SE Alaska and Coastal British Columbia, Geological Society of America, p. 61-76.
Gehrels, G. E., McClelland, W. C., Samson, S. D., Patchett, P. J., and Orchard, M. J., 1992, Geology of the western flank of the Coast Mountains between Cape Fanshaw and Taku Inlet, southeastern Alaska: Tectonics, v. 11, p. 567-585.
Gehrels, G. E., and Saleeby, J. B., 1987, Geology of southern Prince of Wales Island, southeastern Alaska: Geological Society of America Bulletin, v. 98, no. 2, p. 123-137.
Gordee, S. M., 2005, Volcanostratigraphy, age and geologic setting of the Lower-Middle Jurassic upper Hazelton Group, west-central British Columbia [MSc thesis]: University of British Columbia, 173 p.
Gunning, M. H., Hodder, R. W. H., and Nelson, J. L., 2006, Contrasting volcanic styles and their tectonic implications for the Paleozoic Stikine Assemblage, western Stikine terrane, northwestern British Columbia, *in* Colpron, M., Nelson, J. L., and Thompson, R. I., eds., Paleozoic evolution and metallogeny of pericratonic terranes at the Ancient Pacific Margin of North America, Canadian and Alaskan Cordillera, Geological Association of Canada Special Paper 45, p. 201-227.
Haggart, J. W., Diakow, L. J., Mahoney, J. B., Woodsworth, G. J., Struik, L. C., Gordee, S. M., and Rusmore, M. E., 2006, Geology, Bella Coola region (93D/01,/07,/08,/10,/15 and parts of 93D/02,/03,/06,/09,/11,/14,/16 and 92M/15 and /16), British Columbia: Geological Survey of Canada, Open File 5385, scale 1:100 000.,Geological Survey of Canada, Open File 5385, scale.
Haggart, J. W., Mahoney, J. B., Daikow, L. J., Woodsworth, G. J., Gordee, S. M., Snyder, L. D., Poulton, T. P., Friedman, R. M., and Villeneuve, M. E., 2003, Geological setting of the eastern Bella Coola map area, west-central British Columbia, Current Research 2003-A4, Geological Survey of Canada, p. 9.
Hollister, L. S., and Andronicos, C. L., 2000, The Central Gneiss Complex, Coast Mountains, British Columbia, *in* Stowell, H. H., and McClelland, W. C., eds., Tectonics of the Coast

Mountains, southeastern Alaska and British Columbia: Boulder, Colorado, Geological Society of America Special Paper 343, p. 45-59.

Israel, S., Schiarizza, P., Kennedy, L. A., Friedman, R. M., and Villeneuve, M. E., 2006, Evidence for Early to Late Cretaceous, sinistral deformation in the Tchaikazan River area, southwestern British Columbia: Implications for the tectonic evolution of the southern Coast Belt, *in* Haggart, J., Enkin, R., and Monger, J. W. H., eds., Paleogeography of the western North American Cordillera, Geological Association of Canada, Special Paper 46, p. 331-350.

Mahoney, J. B., and DeBari, S. M., 1995, Geochemical and isotopic characteristics of Early to Middle Jurassic volcanism in southern British Columbia: relationship of the Bonanza and Harrison arc systems: Geological Association of Canada Abstracts with Program, v. 20, p. A-65.

Mahoney, J. B., Haggart, J., Hooper, R. L., Snyder, L. D., Woodsworth, G. J., and Friedman, R. M., 2007, New geologic mapping and implications for mineralization in southern and western Whitesail Lake map area (NTS 93E), Geological Fieldwork 2006, B*ritish Columbia Ministry of Energy, Mines and Petroleum Resources*, Paper 2007-1 and *Geoscience BC,* Report 2007-1, p. 341-354.

McClelland, W. C., Gehrels, G. E., and Saleeby, J. B., 1992, Upper Jurassic-Lower Cretaceous basinal strata along Cordilleran margin: Implications for the accretionary history of the Alexander-Wrangellia-Peninsular terrane: Tectonics, v. 11, p. 823-835.

Mihalynuk, M. G., Nelson, J., and Diakow, L. J., 1994, Cache Creek terrane entrapment: Oroclinal paradox within the Canadian Cordillera: Tectonics, v. 13, p. 575-595.

Monger, J. W. H., and Journeay, J. M., 1994, Guide to the geology and tectonic evolution of the southern Coast Mountains: Geological Survey of Canada Open File 2490.

Monger, J. W. H., and Nokelberg, W. J., 1996, Evolution of the North America Cordillera: generation, fragmentation, displacement and accretion of successive North American plate-margin arcs, *in* Coyner, A. R., and Fahey, P. L., eds., Geology and ore deposits of the North American Cordillera: Symposium Proceedings: Reno-Sparks, Nevada, Geological Society of Nevada, p. 1133-1152.

Monger, J. W. H., Price, R. A., and Templeman-Kluit, D. J., 1982, Tectonic accretion and the origin of two metamorphic and plutonic welts in the Canadian Cordillera: Geology, v. 10, p. 70-75.

Monger, J. W. H., van der Heyden, P., Journeay, J. M., Evenchick, C. A., and Mahoney, J. B., 1994, Jurassic-Cretaceous basins along the Canadian Coast belt: Their bearing on pre-mid-Cretaceous sinistral displacements: Geology, v. 22, p. 175-178.

Mustard, P. S., and van der Heyden, P., 1994, Stratigraphy and sedimentology of the Tatla Lake-Bussel Creek map areas, west-central British Columbia, Current Research, 1994-A, Geological Survey of Canada, p. 95-104.

Nelson, J. L., Colpron, M., Piercey, S. J., Dusel-Bacon, C., Murphy, D. C., and Roots, C. F., 2006, Paleozoic tectonic and metallogenic evolution of the pericratonic terranes in Yukon, northern British Columbia and eastern Alaska, *in* Colpron, M., Nelson, J. L., and Thompson, R. I., eds., Paleozoic evolution and metallogeny of pericratonic terranes at the ancient Pacific margin of North America, Canadian and Alaskan Cordillera, Geological Association of Canada, Special Paper 45, p. 323-360.

Nixon, G. T., and Orr, A. J., 2006, Recent revisions to the Early Mesozoic stratigraphy of northern Vancouver Island (NTS 102I; 092L) and metallogenic implications, British Columbia, *in* Geologic Fieldwork 2006, *British Columbia Ministry of Energy, Mines and Petroleum Resources,* Paper 2007-1 and *Geoscience BC,* Report 2007-1, p. 163-178.

Pedder, A. E. H., 2006, Zoogeographic data from studies of Paleozoic corals of the Alexander terrane, southeastern Alaska and British Columbia, *in* Haggart, J. W., Enkin, R., and Monger, J. W. H., eds., Paleogeography of the North American Cordillera: Evidence for and against large-scale displacements, Geological Association of Canada Special Paper 46, p. 29-57.
Price, R. A., and Monger, J. W. H., 2003, A transect of the southern Canadian Cordillera from Calgary to Vancouver: Vancouver, B.C., Geological Association of Canada, Cordilleran Section, 164 p.
Roddick, J. A., and Tipper, H. W., 1985, Geology, Mount Waddington (92N) map area: Geological Survey of Canada, Open File 1163, scale 1:250,000.
Rubin, C. M., and Saleeby, J. B., 1991, Tectonic framework of the upper Paleozoic and lower Mesozoic Alava sequence: a revised view of the polygenetic Taku terrane in southern southeastern Alaska: Canadian Journal of Earth Sciences, v. 28, p. 881-893.
Rusmore, M. E., and Woodsworth, G. J., 1991, Distribution and tectonic significance of Upper Triassic terranes in the eastern Coast Mountains and adjacent Intermontane Belt, British Columbia: Canadian Journal of Earth Sciences, v. 28, p. 532-541.
Rusmore, M. E., and Woodsworth, G. J., 1994, Evolution of the eastern Waddington thrust belt and its relation to the mid-Cretaceous Coast Mountains arc, western British Columbia: Tectonics, v. 13, no. 5, p. 1052-1067.
Rusmore, M. E., Woodsworth, G. J., and Gehrels, G. E., 2000, Late Cretaceous evolution of the eastern Coast Mountains, Bella Coola, British Columbia, *in* Stowell, H. H., and McClelland, W. C., eds., Tectonics of the Coast Mountains, southeastern Alaska and British Columbia: Boulder, Colorado, Geological Society of America Special Paper 343, p. 89-105.
Rusmore, M. E., Woodsworth, G. J., and Gehrels, G. E., 2005, Two-stage exhumation of midcrustal arc rocks, Coast Mountains, British Columbia: Tectonics, v. 24, doi:10.1029/2004TC001750.
Saleeby, J. B., 2000, Geochronologic investigations along the Alexander-Taku terrane boundary, southern Revillagigedo Island to Cape Fox areas, southeast Alaska, *in* Stowell, H. H., and McClelland, W. C., eds., Tectonics of the Coast Mountains in southeast Alaska and British Columbia, Geological Society of America, p. 107-143.
Saleeby, J. B., 2004, The Alexander terrane boundary with North American margin terranes lies west of the Coast batholith in southern southeast Alaska: Geological Society of America *Abstracts with Programs*, v. 36, no. 5, p. 344.
Schiarizza, P., Gaba, R. G., Glover, J. K., Garver, J. I., and Umhoefer, P. J., 1997, Geology and mineral occurrences of the Taseko-Bridge River area: British Columbia Ministry of Employment and Investment, Energy and Minerals Division, Geological Survey Branch.
Schroder-Adams, C., and Haggart, J. W., 2006, Biogeography of Foraminifera in tectonic reconstructions: Limitations and constraints on the paleogeographic position of Wrangellia, *in* Haggart, J. W., Enkin, R., and Monger, J. W. H., eds., Paleogeography of the North American Cordillera: Evidence for and against large-scale displacements, Geological Association of Canada, Special Paper 46, p. 95-108.
Tipper, H. W., 1968, Geology, Mount Waddington: Geological Survey of Canada, Preliminary Map, 5-1968.
Umhoefer, P. J., 2003, A model for the North America Cordillera in the Early Cretaceous: Tectonic escape related to arc collision of the Guerrero terrane and a change in North America plate motion, *in* Johnson, S. E., Paterson, S., R, Fletcher, J. M., Girty, G. H., Kimbrough, D., and Martin-Barajas, A., eds., Tectonic evolution of northwestern Mexico

and the southwestern USA, Geological Society of America Special Paper 374, p. 117-134.
Umhoefer, P. J., Rusmore, M. E., and Woodsworth, G. J., 1994, Contrasting tectono-stratigraphy and structure in the Coast Belt near Chilko Lake, British Columbia: unrelated terranes or an arc-back-arc transect?: Canadian Journal of Earth Sciences, v. 31, p. 1700-1713.
Umhoefer, P. J., Schiarizza, P., and Robinson, M., 2002, Relay Mountain Group, Tyaughton-Methow basin, southwest British Columbia: a major Middle Jurassic to Early Cretaceous terrane overlap assemblage: Canadian Journal of Earth Sciences, v. 39, p. 1143-1167.
van der Heyden, P., 1989, U-Pb and K-Ar geochronometry of the Coast Plutonic Complex, 53^{o} to 54^{o}N, British Columbia, and Implications for the Insular-Intermontane superterrane boundary [PhD thesis]: University of British Columbia, 392 p.
van der Heyden, P., 1991, Preliminary U-Pb dates and field observations from the eastern Coast Belt near 52^{o}N, British Columbia, Current Research, Part A, Geological Survey of Canada, p. 79-84.
van der Heyden, P., 1992, A Middle Jurassic to early Tertiary Andean-Sierran arc model for the Coast Belt of British Columbia: Tectonics, v. 11, p. 82-97.
van der Heyden, P., 2004, Uranium-lead and potassium-argon ages from eastern Bella Coola and adjacent parts of Anahim Lake and Mount Waddington map areas, west-central British Columbia, Current Research 2004-A2, Geological Survey of Canada, p. 14.
van der Heyden, P., Mustard, P. S., and Friedman, R. M., 1994, Northern continuation of the Eastern Waddington Thrust Belt and Tyaughton Trough, Tatla Lake-Bussel Creek map areas, west-central British Columbia, Current Research 1994-A, Geological Survey of Canada, p. 87-94.
Wheeler, J. O., and McFeely, P., 1991, Tectonic assemblage map of the Canadian Cordillera and adjacent parts of the United States of America: Geological Survey of Canada1:2,000,000.
Woodsworth, G. J., and Orchard, M. J., 1985, Upper Paleozoic to lower Mesozoic strata and their conodonts, western Coast plutonic complex, British Columbia: Canadian Journal of Earth Sciences, v. 22, p. 1329-1344.

CHAPTER FIVE

CONCLUSION

Each of the previous chapters had specific conclusions from my work in the Atnarko complex. Here, I summarize the conclusions to parallel the stated objectives of the thesis (Chapter 1). In addition a set of recommendations are given for future work in the area.

Geology of the Atnarko complex

The Atnarko complex records more than 150 My of plutonism, deformation and metamorphism. Variably deformed latest Triassic to Paleocene plutonic rocks, mainly of quartz diorite to tonalite compositions intrude metavolcanic and metasedimentary rocks of the Atnarko assemblage. The age of the Atnarko assemblage is constrained only to pre-Early Jurassic and could be older. It is tentatively correlated with the Burke Channel assemblage, which is a continental margin assemblage associated with the Yukon-Tanana terrane.

Several phases of deformation are identified in the Atnarko complex, including: Jurassic, Early to mid-Cretaceous and Late Cretaceous. Evidence for Jurassic deformation includes: 1) a syn-tectonic earliest Jurassic quartz diorite that intrudes strongly deformed Atnarko assemblage; 2) gneissic to strongly deformed xenoliths found within an Early Cretaceous pluton; and 3) Middle Jurassic titanite ages within a latest Triassic to earliest Jurassic pluton, indicate thermal reheating of the pluton. The nature and extent of the Jurassic event is not well constrained because of overprinting by younger deformation events.

The main structural grain of the Atnarko complex is the result of Early to mid-Cretaceous southwest-west directed compression. Data from the Atnarko complex suggest sinistral translation accompanied compression. Peak metamorphic conditions and migmatite generation coincide with the beginning of thrusting. North-northeast directed contraction slightly overlaps with, and overprints, earlier contraction. North to northeast contraction began by at least 80 Ma and may have lasted until ~70 Ma.

Late Cretaceous (~75-65 Ma) steeply dipping ductile to brittle strike slip faulting overlap with the waning stages of contraction and represent flattening across the complex. All ductile deformation ended by 65 Ma. A period of dextral brittle faulting, likely latest Cretaceous to Eocene in age, affects the entire complex and is part of the western Cordilleran-wide dextral strike-slip event.

Orogenic evolution

The evolution of the western Canadian and southeast Alaskan Cordillera began by at least Middle Jurassic and possibly earlier. Investigation into the geologic history of the Atnarko complex and its comparison to rocks along strike reveals the similarities and the differences in structural styles through the length of the orogen. Compressional deformation dominated the margin from Early to mid-Cretaceous, with southwest-west directed compression along the western margin of the Coast plutonic complex and northeast-north directed compression on the eastern margin. Following compression the orogen accommodates strain differently along strike of the Atnarko complex. Northwest of the Atnarko complex southwest compression related to transpression continued to the Latest Cretaceous to Tertiary. In contrast, the Atnarko complex and regions to the east and southeast of the complex were dominated by dextral strike slip faulting.

Differences in deformation kinematics are the result of strain partitioning in a dextral transpressional regime. Partitioning of strain sets the stage for the development of different thermomechanical characteristics of the lower to upper crust along strike of the orogen. Crustal thickening northwest of the Atnarko complex resulted in thermal weakening of the lower and middle crustal rocks. This weakening was caused by partial melting and contemporaneous intrusive activity. Within the Atnarko complex and areas to the east and southeast, contraction had ended by ~70 Ma. Plutons of this age were intruded into higher, cooler levels in the crust, dissipating heat from the lower crust and in effect strengthening the lower and middle crust. A change in plate dynamics to transtension brought on full-scale orogenic collapse along the weakened layers in the crust northwest of the complex. This provided a mechanism by which the middle and upper crust became decoupled from the lower crust allowing the orogen to freely extend perpendicular to its strike. Within the Atnarko complex and to the area east and southeast, smaller metamorphic core complexes developed where localized thermal weakening of the lower crust caused orogen parallel extension that was kinematically linked to large right lateral strike-slip faults. The majority of the crust in this area of the orogen is interpreted to have remained coupled during this time.

Tectonostratigraphic relationships

The Atnarko assemblage is correlated with rocks of the Burke Channel assemblage. This correlation extends the presence of continental margin assemblages farther south within the Coast plutonic complex. Many of the metamorphic rocks of the Coast plutonic complex that have no known affinity may be related to the continental margin assemblages found to the north. This supports the hypotheses that Stikinia is built upon, or at least has some ties, to the Yukon-Tanana terrane (Nelson et al., 2006; Colpron et al., 2007).

Ties between terranes indicate that a coherent tectonic block (Intermontane superterrane) composed of Stikinia, the Yukon-Tanana terrane and the Taku terrane was together by at least Early Jurassic and it is likely that the terranes were united in the Paleozoic. The Insular superterrane, mainly Wrangellia and the Alexander terrane were together as one entity by Pennsylvanian time. Based on structural overlapping of the Taku and Alexander terranes and stratigraphic ties, interaction between the two superterranes began as early as Middle Jurassic.

Recommendations for future work

In spite of this new understanding regarding the structural and metamorphic history of the Atnarko complex there remain outstanding questions. The following recommendations are for further research within the Atnarko complex and surrounding areas that will increase the geologic knowledge and better constrain the relationships deduced in this study.

Constraints on the Atnarko assemblage

The correlation of the Atnarko assemblage with the Burke Channel assemblage is tentative and is based purely on lithologic and deformation similarities. To better constrain the correlation several techniques that were not utilized in this study can be used. Firstly, a detrital zircon study of several of the metasedimentary packages. It is likely that there are separate units within the Atnarko assemblage that may differ drastically in age. In particular the least deformed and metamorphosed packages in the southern Atnarko might be substantially different in age and depositional environment than the rest of the assemblage. Detrital ages could be compared to existing studies from the continental assemblages, Stikinia and the Alexander terrane. Secondly, isotopic studies on the metasediments from the Atnarko assemblage (e.g., Nd and Sr) would indicate whether the assemblage has a crustal component or whether it was derived from a juvenile source. Again this data could be compared to existing studies for the surrounding terranes.

Constraints on metamorphic conditions

During the course of this study several techniques were employed to gain a better understanding of the metamorphic conditions that affected the Atnarko complex. These include aluminum in hornblende geobarometry of plutonic rocks, P-T pseudosections of various rocks collected from the complex and traditional geothermometry and barometry. None of these provided useful information. However, I believe that with more selective sampling focusing on the metasedimentary rocks, it may be possible to obtain rocks with compositions that will provide insight into the metamorphic conditions. In addition a more detailed study of the migmatites may reveal better constraints on metamorphism by looking at leucosome rich areas. Specifically detailed geochronological studies of zircons from within leucosomes using either LA-ICPMS or SHRIMP technology coupled with detailed SEM images of the zircons may provide information on metamorphic zircon growth.

Constraints on structures

The Jurassic event is poorly constrained and because of the complex overprinting of younger structures and plutonic events it is difficult to place better timing constraints on this event. A detailed study of the syn-tectonic Elbow Lake pluton that intrudes the Atnarko assemblage would provide better timing constraints. Sorting out the characteristics of this event would be invaluable in determining the earliest time of accretion between the Insular and Intermontane superterranes.

Contributions of research

This dissertation provides a geological foundation for the Atnarko complex and surrounding region. The data presented here, along with the two 1:50 000- scale maps are the building blocks for the next generation of geological investigations and provide background and baseline data that can be utilized by researchers from a variety of disciplines.

My research documents that the Canadian Cordillera responded differently along strike to changing relative plate motions. The partitioning of strain throughout the crust is shown to occur at all scales. Convergent margins are complex systems that do not inclusively involve thickening of crust and the development of compression related structures. This research indicates that the response of orogens to changing relative plate motions can be significantly different and that this difference is directly attributed to the evolution of the orogen through time. This underscores the importance of evaluating the orogen at different scales. Results from this study can be applied to other convergent margins throughout the world.

REFERENCES

Colpron, M., Nelson, J. L., and Murphy, D. C., 2007, Northern Cordilleran terranes and their interactions through time: GSA Today, v. 17, no. 4/5, p. 1-10.

Nelson, J. L., Colpron, M., Piercey, S. J., Dusel-Bacon, C., Murphy, D. C., and Roots, C. F., 2006, Paleozoic tectonic and metallogenic evolution of the pericratonic terranes in Yukon, northern British Columbia and eastern Alaska, *in* Colpron, M., Nelson, J. L., and Thompson, R. I., eds., Paleozoic evolution and metallogeny of pericratonic terranes at the ancient Pacific margin of North America, Canadian and Alaskan Cordillera, Geological Association of Canada, Special Paper 45, p. 323-360.

APPENDIX I

GEOCHRONOLOGY DATA

Geochron sample locations displayed in Table AIa. Methodology for each technique used presented below.

U-Pb TIMS methodology

U-Pb TIMS data presented in Table AIb. TIMS U-Pb samples were processed at the University of British Columbia, Pacific Centre for Isotopic and Geochemical Research using standard geochron sample preparation. All sample preparation, geochemical separations and mass spectrometry were done at the Pacific Centre for Isotopic and Geochemical Research in the Department of Earth and Ocean Sciences, University of British Columbia. Zircon and titanite were separated from samples using conventional crushing, grinding, and Wilfley table techniques, followed by final concentration using heavy liquids and magnetic separations. Mineral fractions for analysis were selected on the basis of grain quality, size, magnetic susceptibility and morphology. All zircon fractions were air abraded prior to dissolution to minimize the effects of post-crystallization Pb-loss, using the technique of Krogh (1982). Zircons were dissolved in sub-boiled 48% HF and 16 M HNO3 (ratio of ~10:1, respectively) in the presence of a mixed $^{233\text{-}235}$U-^{205}Pb tracer; zircons for 40 hours at 240°C in 300 µL PTFE and PFA microcapsules contained in high pressure vessels (Parr™ acid digestion vessels with 125 mL PTFE liners), and titanites and monazites on a hotplate in 7 mL screwtop PFA beakers for at least 48 hours at ~130°C. Titanites were dissolved in sub-boiled HF/nitric and monazites in sub-boiled 6.2 N HCl. Sample solutions were then dried to salts at ~130°C. Zircon residues were redissolved in ~200 µL of sub-boiled 3.1 M HCl for 12 hours at 210°C in high pressure vessels and titanite residues on a hotplate in 1 mL of sub-boiled 6.2 M HCl in 7 mL screwtop PFA

Table AIa. Locations of samples used for geochronology.

Sample	UTM East	UTM North	Rock Type	Minerals	Method
01-SIS-20B	302087	5797958	Gneissic hble, biot, quartz-diorite	z	T
01-SIS-20C	302087	5797958	Gneissic hble, biot, quartz-diorite	h	A
01-SIS-34	300729	5796148	Gneissic hble, biot, quartz-diorite	h	A
01-SIS-69	302288	5791461	Gneissic hble, biot, quartz-diorite	z, t, h, b	T, L, A
01-SIS-107	299354	5786417	Migmatitic orthogneiss	z, t, h, b	T, L, A
01-SIS-150C	308851	5777359	Foliated quartz-diorite	z	T, L
01-SIS-181	304249	5768712	Mylonitic metavolcanic	b	A
01-SIS-204	304962	5769511	Migmatitic orthogneiss	z, t, h, b	T, L, A
02-SIS-45B	303494	5769428	Migmatite leucosome	m	A
02-SIS-45D	303494	5769428	Migmatitic amphibolite	h	A
02-SIS-46	303636	5769357	Mylonitic amphibolite	h	A
02-SIS-63	309512	5769798	Variably foliated tonalite-quartz diorite	z, t	T, L
02-SIS-110B	306224	5772534	Mylonitic metarhyolite	z	L
03-SIS-16	704064	5789195	Mylonitic quartz-diorite	h	A
03-SIS-29	306079	5766316	Biotite, tonalite to quartz diorite	z, m, b	T, A

All coordinates NAD 83, UTM Zone 10, except 03-SIS-16, NAD 83 UTM Zone 9
z-zircon, t-titanite, m, monazite, h-hornblende, m-muscovite, b-biotite
T-U-Pb TIMS; L-U-Pb LA-ICPMS; A-Argon-Argon

Table AIb. U-Pb TIMS analyses

Sample Fraction[1]	Wt (mg)	U^{2} (ppm)	Pb^{*3} (ppm)	$^{206}Pb^{4}/^{204}Pb$	Pb^{5} (pg)	Th/U^{6}	Isotopic ratios (1σ,%) [7] $^{206}Pb/^{238}U$	$^{207}Pb/^{235}U$	$^{207}Pb/^{206}Pb$	Apparent ages (2σ,Ma) [7] $^{206}Pb/^{238}U$	$^{207}Pb/^{235}U$	$^{207}Pb/^{206}Pb$
01-SIS-63												
T1	142	489	14.6	433	278	0.83	0.02637 (0.18)	0.1811 (0.95)	0.04981 (0.87)	167.8 (0.6)	169.8 (3.0)	186 (40/41)
T2	161	477	13.9	417	314	0.74	0.02627 (0.16)	0.1800 (0.88)	0.04971 (0.80)	167.1 (0.5)	168.1 (2.7)	181 (37/38)
01-SIS-69												
Z1 13	600	298	6.9	7358	34.8	0.32	0.02338 (0.10)	0.1588 (0.18)	0.04925 (0.09)	149.0 (0.3)	149.6 (0.5)	159.7 (4.3/4.4)
Z2 19	303	393	9.0	6934	24.3	0.34	0.02309 (0.11)	0.1567 (0.20)	0.04923 (0.11)	147.1 (0.3)	147.8 (0.5)	158.8 (5.3)
Z3 34	537	455	10.6	7218	48.6	0.33	0.02346 (0.12)	0.1595 (0.18)	0.04930 (0.09)	149.5 (0.3)	150.3 (0.5)	162.2 (4.4)
Z4 11	590	359	8.2	2594	98.2	0.35	0.02277 (0.10)	0.1538 (0.20)	0.04898 (0.12)	145.1 (0.3)	145.2 (0.5)	147.0 (5.6/5.7)
T1 8	227	501	10.6	512	265	0.98	0.01808 (0.15)	0.1201 (0.46)	0.04817 (0.36)	115.5 (0.3)	115.2 (1.0)	108 (17)
T2 11	276	624	12.2	469	432	0.73	0.01777 (0.16)	0.1181 (0.49)	0.04821 (0.38)	113.5 (0.4)	113.3 (1.1)	109 (18)
T3 13	249	528	10.5	458	338	0.79	0.01776 (0.16)	0.1182 (0.51)	0.04827 (0.40)	113.5 (0.4)	113.5 (1.1)	112 (19)
T4 9	181	477	10.5	406	257	1.13	0.01814 (0.19)	0.1218 (0.58)	0.04870 (0.46)	115.9 (0.5)	116.7 (1.3)	133 (21/22)
T5 8	226	567	11.8	488	309	0.98	0.01778 (0.17)	0.1180 (0.52)	0.04813 (0.42)	113.6 (0.4)	113.2 (1.1)	105 (20)
T6 3	120	644	12.3	491	174	0.71	0.01733 (0.15)	0.1147 (0.44)	0.04802 (0.35)	110.8 (0.3)	110.3 (0.9)	100 (16)
T7 4	143	541	11.6	469	188	1.12	0.01793 (0.15)	0.1180 (0.45)	0.04835(0.35)	113.0 (0.3)	113.2 (1.0)	117 (17)
T8 5	140	388	8.1	446	140	0.99	0.01774 (0.25)	0.1194 (0.57)	0.04801 (0.43)	113.4 (0.6)	114.5 (1.2)	139 (20)
T9 8	73	312	6.7	365	69.5	1.30	0.01706 (0.19)	0.1142 (0.59)	0.04855 (0.48)	119.0 (0.4)	109.8 (1.2)	126 (23)
01-SIS-204												
Z1 6	359	337	6.7	11810	13.2	0.14	0.02103 (0.17)	0.1422 (0.22)	0.04903 (0.09)	134.2 (0.5)	135.0 (0.6)	149.1 (4.3)
Z2 16	529	327	6.3	19130	11.5	0.12	0.02075 (0.13)	0.1399 (0.18)	0.04891 (0.09)	132.4 (0.3)	133.0 (0.4)	143.4 (4.3)
Z3 16	415	362	7.4	12200	16.4	0.14	0.02173 (0.27)	0.1466 (0.30)	0.04892 (0.08)	138.6 (0.8)	138.9 (0.8)	144.1 (3.9)
Z4 21	256	418	8.2	4744	29.4	0.09	0.02126 (0.14)	0.1433 (0.20)	0.04890 (0.11)	135.6 (0.4)	136.0 (0.5)	142.9 (5.1)
Z5 21	445	206	4.3	7357	16.9	0.17	0.02217 (0.10)	0.1503 (0.17)	0.04918 (0.09)	141.3 (0.3)	142.2 (0.5)	156.5 (4.4/4.5)
Z6 26	112	232	4.5	2145	15.7	0.09	0.02102 (0.13)	0.1419 (0.22)	0.04895 (0.16)	134.1 (0.4)	134.7 (0.6)	145.5 (7.7)
X1 3	88	4550	91.3	13910	38.9	0.02	0.02208 (0.36)	0.1489 (0.39)	0.04891 (0.10)	140.8 (1.0)	141.0 (1.0)	143.5 (4.8)
T2 13	99	21	0.4	29	212	0.10	0.01816 (4.1)	0.1267 (26.1)	0.05060 (24.1)	116.0 (9.4)	121 (60)	223 (846/1819)
T3 9	76	60	1.0	22	1260	0.08	0.01760 (13.5)	0.1143 (51.3)	0.04708 (43.9)	112 (30)	110 (107)	53 (1338/9999)
01sis107												
Z1 10	404	342	8.1	13466	15.7	0.16	0.02502 (0.12)	0.1711 (0.18)	0.04959 (0.09)	159.3 (0.4)	160.4 (0.5)	176.1 (4.1)
Z2 14	355	446	10.4	12055	19.7	0.16	0.02458 (0.11)	0.1681 (0.17)	0.04960 (0.09)	156.5 (0.3)	157.8 (0.5)	176.4 (4.3)
Z3 19	235	482	10.9	22144	7.5	0.14	0.02408 (0.12)	0.1644 (0.18)	0.04953 (0.08)	153.4 (0.4)	155.8 (0.4)	176.2 (0.6)
Z4 32	256	547	12.6	3564	58.9	0.16	0.02446 (0.12)	0.1673 (0.20)	0.04960 (0.11)	155.8 (0.4)	157.1 (0.6)	176.2 (5.0)
Z5 1	46	353	9.3	7575	3.6	0.20	0.02754 (0.09)	0.1900 (0.18)	0.05003 (0.11)	175.1 (0.3)	176.6 (0.6)	196.6 (5.1/5.2)
Z6 2	30	550	12.0	4916	4.8	0.14	0.02314 (0.26)	0.1582 (0.36)	0.04956 (0.30)	147.5 (0.8)	149.1 (1.0)	175 (14)
Z7 5	34	486	12.2	6569	4.0	0.20	0.02612 (0.16)	0.1793 (0.25)	0.04978 (0.18)	166.2 (0.5)	167.5 (0.8)	184.9 (8.5)
T5 9	194	112	1.9	138	198	0.12	0.01806 (0.45)	0.1191 (1.6)	0.04784 (1.4)	115.4 (1.0)	114.3 (3.5)	91 (63/66)
T6 18	157	143	2.4	121	243	0.07	0.01836 (0.52)	0.1225 (1.7)	0.0839 (1.4)	117.3 (1.2)	117.3 (3.9)	118.2 (66/69)
03sis29												
Z1 20	18	344	5.7	339	18.9	0.46	0.01605 (0.26)	0.1083 (2.6)	0.04897 (2.4)	102.6 (0.5)	104.5 (5.2)	146 (111/119)
Z2 12	27	336	6.8	892	12.5	0.44	0.01976 (0.18)	0.1345 (0.44)	0.04937 (0.35)	126.2 (0.5)	128.2 (1.1)	165 (16)
Z3 ~60	32	337	5.3	298	37.6	0.29	0.01602 (1.4)	0.1061 (2.5)	0.04803 (1.6)	102.4 (2.9)	102.4 (5.0)	101 (75/78)
Z4 ~50	38	403	7.3	1563	11.2	0.25	0.01853 (0.19)	0.1243 (1.0)	0.04865 (0.95)	118.4 (0.5)	119.0 (2.3)	131 (44/45)
M1 9	35	676	154	24	3821	94.8	0.01328 (10.5)	0.0725 (42.6)	0.03959 (36.5)	85 (18)	71 (58)	-377 (1261/6935)
M2 17	23	621	89.4	34	784	91.8	0.01297 (3.7)	0.0783 (14.1)	0.04379 (12.0)	83.1 (6.0)	77 (21)	-122 (507/730)
M3 17	36	688	93.7	69	398	91.2	0.01327 (1.1)	0.0823 (4.1)	0.04498 (3.4)	85.0 (1.8)	80.3 (6.3)	-57 (160/177)
M4 3	20	501	85.0	58	196	93.3	0.01264 (1.4)	0.0788 (5.7)	0.04523 (4.9)	81.0 (2.2)	77.0 (8.4)	-43 (224/259)
M5 7	21	961	117	88	232	90.3	0.01310 (0.78)	0.0837 (3.0)	0.04635 (2.6)	83.9 (1.3)	81.6 (4.8)	16 (120/129)
M6 11	27	866	112	69	361	91.0	0.01287 (1.1)	0.0807 (3.8)	0.04549 (3.2)	82.4 (1.7)	78.8 (5.8)	-29 (149/164)
01sis20B												
Z1	152	501	4.3	814	53.0	0.19	0.00907 (0.13)	0.0595 (0.36)	0.04760 (0.27)	58.2 (0.2)	58.7 (0.4)	79 (13)
Z2	56	380	3.3	343	35.9	0.26	0.00897 (0.22)	0.0583 (0.83)	0.04712 (0.70)	57.6 (0.3)	57.5 (0.9)	56 (33)
Z3	90	174	2.0	764	14.4	0.37	0.01124 (0.16)	0.0746 (0.44)	0.04812 (0.36)	72.0 (0.2)	73.0 (0.6)	105 (71)
Z4	229	95	1.2	1120	14.7	0.34	0.01211 (0.17)	0.0797 (0.44)	0.04772 (0.36)	77.6 (0.3)	77.8 (0.7)	85 (17)
01sis150C												
Z1	175	250	7.1	1972	38.8	0.34	0.002836 (0.12)	0.1962 (0.25)	0.05017 (0.15)	180.3 (0.4)	181.9 (0.8)	202.6 (7.1/7.2)
Z3	60	215	6.1	1384	16.3	0.38	0.02834 (0.15)	0.1953 (0.32)	0.04998 (0.23)	180.1 (0.5)	181.1 (1.1)	194 (11)
Z4	27	212	6.4	2050	5.1	0.43	0.02940 (0.12)	0.2035 (0.37)	0.05020 (0.31)	186.8 (0.5)	188.1 (1.3)	204 (14)

[1] All zircon grains selected for analysis were air abraded prior to dissolution. Fraction ID (zircon: Z1, Z2, etc.; titanite: T1, T2, etc.; monazite: M1, M2, etc.; xenotime: X), followed by the number of grains

[2] U blank correction of 1pg ± 20%; U fractionation corrections were measured for each run with a double $^{233-235}U$ spike.

[3] Radiogenic Pb

[4] Measured ratio corrected for spike and Pb fractionation of 0.28-0.37/amu ± 20% (Daly collector) which was determined by repeated analysis of NBS Pb 981 reference material throughout the course of this study.

[5] Total common Pb in analysis based on blank isotopic composition.

[6] Model Th/U derived from radiogenic ^{208}Pb and the $^{207}Pb/^{206}Pb$ age of fraction; for monazites percent radiogenic ^{208}Pb is listed.

[7] Blank and common Pb corrected; Pb procedural blanks were ~1.5-5 pg and U <1 pg. Common Pb concentrations are based on Stacey-Kramers model Pb at the interpreted age of the rock or the $^{207}Pb/^{206}Pb$ age of the fraction (Stacey and Kramers, 1975).

beakers for at least 24 hours at ~130°C. Titanite solutions were again dried to salts and were again redissolved on a hotplate, in the same beakers, in 1 mL of sub-boiled 3.1 M HCl at ~130°C for at least 24 hours, as were the monazites. Separation and purification of Pb and U employed ion exchange column techniques modified slightly from those described by Parrish et al. (1987). Pb and U were sequentially eluted into a single beaker; U from titanite solutions was purified by passing through columns a second time. Elutants were dried in 7 mL screwtop PFA beakers on a hotplate at ~120°C in the presence of 2 μL of ultrapure 1 M phosphoric acid (H3PO4). Samples were then loaded on single, degassed zone refined Re filaments in 5 μL of a silica gel (SiCl4) phosphoric acid emitter. Isotopic ratios were measured using a modified single collector VG-54R thermal ionization mass spectrometer equipped with an analogue Daly photomultiplier. Measurements were done in peak-switching mode on the Daly detector. U and Pb analytical blanks were in the range of 1 pg or less and 2-5 pg, respectively, during the course of this study. U fractionation was determined directly on individual runs using the $^{233\text{-}235}$U tracer, and Pb isotopic ratios were corrected for fractionation of 0.37%/amu, based on replicate analyses of the NBS-981 Pb standard and the values recommended by Thirlwall (2000). Reported precisions for Pb/U and Pb/Pb dates were determined by numerically propagating all analytical uncertainties through the entire age calculation using the technique of Roddick (1987). Concordia diagrams were plotted with and intercept ages and associated errors were calculated with the Isoplot 3.00 software package (Ludwig, 2003). Unless otherwise noted, all errors are quoted at the 2σ level.

U-Pb LA-ICMPS methodology

U-Pb LA-ICPMS data presented in Table AIc. Zircons are separated from their host rocks using conventional mineral separation methods and sectioned in an epoxy grain mount along

Table AIc. U-Pb LA-ICPMS data

Analysis #	$^{207}Pb/^{235}U$	$^{207}Pb/^{235}U$	$^{206}Pb/^{238}U$	$^{206}Pb/^{238}U$	rho	$^{207}Pb/^{206}Pb$	$^{207}Pb/^{206}Pb$	$^{207}Pb/^{235}U$	$^{207}Pb/^{235}U$	$^{206}Pb/^{238}U$	$^{206}Pb/^{238}U$	$^{207}Pb/^{206}Pb$	$^{207}Pb/^{206}Pb$
01-SIS-107													
107S1	0.2433	0.01682	0.0325	0.00071	0.316003	0.05487	0.00357	221.1	13.74	206.2	4.44	407	139.44
107S2	0.23598	0.00875	0.0294	0.00036	0.330234	0.05793	0.00203	215.1	7.19	186.8	2.25	526.9	75.44
107S3	0.21902	0.00552	0.02961	0.00026	0.348401	0.05552	0.00132	201.1	4.59	188.1	1.62	433	51.56
107S4	0.20825	0.00527	0.03001	0.00025	0.329191	0.05119	0.00122	192.1	4.43	190.6	1.58	249.2	54.16
107S5	0.22801	0.0127	0.03063	0.00046	0.269626	0.0531	0.00282	208.6	10.5	194.5	2.9	332.8	115.89
107S6	0.21711	0.00684	0.03016	0.0003	0.315728	0.05279	0.00157	199.5	5.71	191.6	1.89	319.9	66.34
107S7	0.20956	0.00605	0.02981	0.00028	0.325349	0.05137	0.0014	193.2	5.07	189.4	1.76	257.7	61.56
107S8	0.23086	0.00933	0.02909	0.00038	0.323226	0.05688	0.00218	210.9	7.7	184.9	2.39	486.4	82.97
107S9	0.2093	0.00547	0.0292	0.00026	0.340700	0.05304	0.00131	193	4.59	185.6	1.63	330.6	54.93
107S10	0.20314	0.0066	0.02899	0.00029	0.307894	0.05174	0.0016	187.8	5.57	184.2	1.82	273.8	69.49
107S11	0.21636	0.00802	0.0298	0.00035	0.316850	0.05278	0.00187	198.9	6.69	189.3	2.2	319.5	78.53
107S12	0.24037	0.01048	0.03235	0.00047	0.333229	0.05574	0.00226	218.7	8.58	205.2	2.96	441.7	87.78
107S13b	0.19404	0.00753	0.02967	0.00034	0.295296	0.04942	0.00184	180.1	6.4	188.5	2.11	167.7	84.67
107S14	0.2192	0.00481	0.02895	0.00022	0.346314	0.05439	0.00112	201.2	4.01	184	1.39	387.3	45.36
107S15	0.20718	0.00455	0.02865	0.00022	0.349651	0.05349	0.00111	191.2	3.82	182.1	1.38	349.6	46.23
02-SIS-63													
63S1	0.21158	0.0063	0.02862	0.00028	0.328566	0.05481	0.00154	194.9	5.28	181.9	1.74	404.3	61.02
63S2	0.21472	0.0098	0.02768	0.00041	0.324537	0.05955	0.00259	197.5	8.19	176	2.56	587.3	91.79
63S3	0.24778	0.01348	0.02744	0.00049	0.328238	0.06639	0.00344	224.8	10.97	174.5	3.09	818.6	104.59
63S4	0.20108	0.00877	0.02743	0.00038	0.317634	0.05272	0.00218	186	7.41	174.5	2.4	316.8	91.47
63S5	0.21612	0.00849	0.03017	0.00035	0.295311	0.0513	0.00191	198.7	7.09	191.6	2.18	254.5	83.56
63S6	0.2312	0.01182	0.02883	0.00043	0.291739	0.05661	0.00276	211.2	9.75	183.2	2.7	475.8	104.92
63S7a	0.21757	0.01395	0.02967	0.00056	0.294371	0.05432	0.00333	199.9	11.64	188.5	3.52	384.3	131.92
63S8	0.18224	0.0038	0.0251	0.00018	0.343921	0.05378	0.00106	170	3.26	159.8	1.11	361.7	43.76
63S9	0.2284	0.01305	0.02857	0.0005	0.306299	0.05815	0.00315	208.9	10.79	181.6	3.15	534.8	115.02
63S10	0.23324	0.01654	0.02942	0.00059	0.282798	0.05612	0.00379	212.9	13.62	186.9	3.69	456.9	143.71
63S11	0.22732	0.01279	0.02974	0.0005	0.298811	0.05557	0.00298	208	10.58	188.9	3.14	434.9	115.44
63S12	0.20591	0.00745	0.02927	0.00034	0.321053	0.05185	0.00177	190.1	6.27	186	2.14	278.7	76.37
63S13	0.17985	0.00436	0.02554	0.00021	0.339174	0.05181	0.00119	167.9	3.75	162.6	1.31	277.2	51.52
63S14	0.19036	0.0116	0.02873	0.00044	0.251324	0.04921	0.00291	176.9	9.9	182.6	2.75	157.9	133.02
63S15	0.17683	0.0024	0.0254	0.00011	0.319083	0.04952	0.0006	165.3	2.07	161.7	0.71	172.4	27.9
01-SIS-150c													
150SIS1	0.32745	0.02464	0.03368	0.0008	0.315662	0.068	0.00498	287.6	18.85	213.5	4.99	868.5	144.94
150SIS3	0.16937	0.00832	0.02748	0.00042	0.311133	0.04543	0.00222	158.9	7.23	174.8	2.6	0.1	80.74
150SIS4	0.19152	0.00992	0.03047	0.00048	0.304138	0.04579	0.00235	177.9	8.45	193.5	3.02	0.1	106.02
150SIS5	0.24552	0.0187	0.03173	0.00072	0.297926	0.05478	0.00409	222.9	15.24	201.4	4.52	403.1	159.19
150SIS6	0.24062	0.01878	0.03292	0.00081	0.315255	0.05332	0.00409	218.9	15.37	208.8	5.04	342.2	164.56
150SIS7	0.25843	0.01759	0.03001	0.00066	0.323113	0.06204	0.00417	233.4	14.19	190.6	4.11	675.3	137.44
150SIS8	0.30807	0.03941	0.03278	0.00126	0.300472	0.07016	0.00888	272.7	30.59	207.9	7.86	933.2	240.08

continuation of Table AIc. U-Pb LA-ICPMS data

Analysis #	$^{207}Pb/^{235}U$	$^{207}Pb/^{235}U$	$^{206}Pb/^{238}U$	$^{206}Pb/^{238}U$	rho	$^{207}Pb/^{206}Pb$	$^{207}Pb/^{206}Pb$	$^{207}Pb/^{235}U$	$^{207}Pb/^{235}U$	$^{206}Pb/^{238}U$	$^{206}Pb/^{238}U$	$^{207}Pb/^{206}Pb$	$^{207}Pb/^{206}Pb$
150SIS9	0.18914	0.01395	0.02861	0.00064	0.303299	0.04685	0.00342	175.9	11.91	181.8	3.98	41.3	166.31
150SIS10	0.17251	0.0097	0.02863	0.00052	0.323016	0.044	0.00247	161.6	8.4	182	3.24	0.1	22
150SIS11	0.15812	0.01203	0.02934	0.00071	0.318068	0.03922	0.00294	149.1	10.54	186.4	4.43	0.1	0
02-SIS-27c													
27SIS3	0.10174	0.00994	0.02158	0.00068	0.322525	0.03494	0.00344	98.4	9.16	137.6	4.29	0.1	0
27SIS5A	0.11014	0.01048	0.02093	0.00061	0.306298	0.0377	0.00361	106.1	9.58	133.5	3.88	0.1	0
27SIS6	0.11061	0.01119	0.02322	0.00071	0.302246	0.0368	0.00374	106.5	10.23	148	4.44	0.1	0
27SIS7	0.12426	0.01374	0.02156	0.00074	0.310404	0.04323	0.0048	118.9	12.41	137.5	4.64	0.1	100.47
27SIS9	0.09522	0.01148	0.01916	0.00065	0.281387	0.03661	0.00441	92.4	10.64	122.3	4.1	0.1	0
02-SIS-45b													
45SIS3	0.1821	0.0089	0.0224	0.00034	0.310564	0.00294	0.0603	169.9	7.64	142.8	2.17	614.4	101.87
45SIS5	0.27143	0.0173	0.02423	0.00056	0.362615	0.00527	0.08332	243.8	13.81	154.3	3.53	1276.6	118.79
45SIS6	0.13615	0.00583	0.02159	0.00029	0.313686	0.00188	0.04397	129.6	5.21	137.7	1.82	0.1	0
45SIS7	0.11563	0.00566	0.0206	0.0003	0.297514	0.00198	0.0406	111.1	5.15	131.4	1.87	0.1	0
45SIS8	0.12758	0.0061	0.01889	0.00027	0.298940	0.00236	0.04926	121.9	5.49	120.6	1.73	160.2	108.3
02-SIS-110													
110SIS1	0.14632	0.0189	0.02593	0.00092	0.274680	0.04153	0.00533	138.7	16.75	165	5.76	0.1	41.77
110SIS2	0.14498	0.01969	0.0261	0.00095	0.268007	0.04163	0.0056	137.5	17.47	166.1	5.98	0.1	60.46
110SIS3	0.15671	0.02245	0.02538	0.001	0.275035	0.04749	0.00673	147.8	19.71	161.6	6.29	73.2	306.78

with grains of internationally accepted standard zircon (FC-1, a ~1100 Ma zircon standard), and brought to a very high polish. The grains are examined using a stage-mounted cathodoluminescence imaging set-up that makes it possible to detect the presence of altered zones or inherited cores within the zircon. The highest quality portions of each grain, free of alteration, inclusion, or cores are selected for analysis. The surface of the mount is then washed for ~10 minutes with dilute nitric acid and rinsed in ultra clean water. Analyses are carried out using a New Wave 213nm Nd-YAG laser coupled to a Thermo Finnigan Element 2 high resolution ICP-MS. Ablation takes place within a New Wave "Supercell" ablation chamber which is designed to achieve very high efficiency entrainment of aerosols into the carrier gas. Helium is used as the carrier gas for all experiments and gas flow rates, together with other parameters such as torch position, are optimized prior to beginning a series of analyses. Typically a 25 micron spot with 60% laser power is used, and line scans rather than spot analyses were used in order to avoid within-run elemental fractions. Each analysis consists of a 7 second background measurement (laser off) followed by a ~28 second data acquisition period with the laser firing. A typical analytical session consists of four analyses of the standard zircon, followed by four analyses of unknown zircons, two standard analyses, four unkown analyses, etc., and finally four standard analyses. Data are reduced using the GLITTER software package developed by the GEMOC group at Macquarrie University, which subtracts background measurements, propagate analytical errors, and calculates isotopic ratios and ages. This application generates a time-resolved record of each laser shot. Final ages for contiguous populations of relatively young (Phanerozoic) zircons are based on a weighted average of the calculated 206Pb/238U ages for 20-25 individual analyses. For detrital zircon samples 60-100 grains are analysed and displayed on Concordia and probability plots. For the latter 206Pb/238U ages are used for grains less than 1 Ga and 207Pb/206Pb ages for those greater than 1 Ga; these data are filtered at 10% discordance. Plotting of the analytical results employs ISOPLOT 3.00 software (Ludwig, 2003).

$^{40}Ar/^{39}Ar$ methodology

$^{40}Ar/^{39}Ar$ data presented in Table AId. Each sample was crushed and sieved to obtain fragments ranging in the size range from 0.5 to 1 mm. A hand magnet was passed over the samples to remove magnetic minerals and metallic crusher fragments/spall. The samples were washed in deionized water, rinsed and then air-dried at room temperature.

Mineral separates were hand-picked, wrapped in aluminum foil and stacked in an irradiation capsule with similar-aged samples and neutron flux monitors (Fish Canyon Tuff sanidine, 28.02 Ma (Renne et al., 1998); MAC-83 biotite, 24.36, (Sandeman et al., 1999).

The samples were irradiated on October 14 through 16, 2003 at the McMaster Nuclear Reactor in Hamilton, Ontario, for 72 MWH, with a neutron flux of approximately $3x10^{16}$ neutrons/cm^2. Analyses (n=33) of 11 neutron flux monitors irradiated with the samples produced errors of <0.25% in the J value.

The samples were analyzed between March 8 and April 13, 2004, at the Noble Gas Laboratory, Pacific Centre for Isotopic and Geochemical Research, University of British Columbia, Vancouver, BC, Canada. The separates were step-heated at incrementally higher powers in the defocused beam of a 10W CO_2 laser (New Wave Research MIR10) until fused. The gas evolved from each step was analyzed by a VG5400 mass spectrometer equipped with an ion-counting electron multiplier. All measurements were corrected for total system blank, mass spectrometer sensitivity, mass discrimination, radioactive decay during and subsequent to irradiation, as well as interfering Ar from atmospheric contamination and the irradiation of Ca, Cl and K. The

Table AId ^{40}Ar-^{39}Ar age data for hornblende, muscovite and biotite from the Atnarko complex.

Laser[1] Power (%)	Isotope Ratios $^{40}Ar/^{39}Ar$	$^{38}Ar/^{39}Ar$	$^{37}Ar/^{39}Ar$	$^{36}Ar/^{39}Ar$	Ca/K	Cl/K	$\%^{40}Ar$	$\%^{39}Ar$	$^{40}Ar^*/^{39}Ar_K$	Age±2σ
02-SIS-46, hornblende, J = 0.009734±0.000018; volume ^{39}ArK = 274.29 x 10^{-10} cm^3, integrated age 125.33±1.81 Ma (2σ)										
2	349.826±0.028	0.196±0.143	2.884±0.041	0.768±0.058	25.278	0.009	63.91	0.31	126.906±12.149	1451.17±95.44
2.4	132.114 0.032	0.082 0.215	3.872 0.049	0.325 0.084	33.964	0.002	71.16	0.3	38.332 7.739	572.06 98.97
2.6	72.504 0.042	0.060 0.285	3.294 0.047	0.214 0.076	28.88	0.001	85.14	0.49	10.833 4.082	180.86 64.85
2.9	55.582 0.029	0.046 0.242	2.597 0.035	0.144 0.100	22.757	0.001	74.49	0.94	14.245 4.133	234.27 63.74
3.2	26.458 0.014	0.028 0.207	4.040 0.025	0.065 0.047	35.446	0	67.79	2.54	8.572 0.906	144.58 14.69
3.5	9.730 0.012	0.019 0.046	4.505 0.016	0.017 0.032	39.542	0	39.51	12.02	5.921 0.180	101.09 2.98
3.8	8.095 0.016	0.019 0.041	7.191 0.017	0.011 0.049	63.266	0.001	15.02	23.11	6.938 0.198	117.89 3.25
4.1	8.395 0.016	0.021 0.063	8.167 0.018	0.012 0.041	71.91	0.001	17.52	15.81	6.988 0.189	118.73 3.12
4.4	7.472 0.011	0.020 0.049	7.636 0.015	0.009 0.074	67.206	0.001	8.31	15.71	6.911 0.209	117.46 3.44
4.7	12.355 0.017	0.024 0.123	6.058 0.020	0.023 0.119	53.24	0.001	42.72	3.61	7.130 0.836	121.05 13.74
5	7.814 0.010	0.020 0.053	7.126 0.016	0.010 0.072	62.686	0.001	13.05	14.46	6.851 0.222	116.47 3.65
5.3	7.721 0.014	0.020 0.052	7.238 0.018	0.010 0.088	63.681	0.001	12.67	10.69	6.800 0.273	115.63 4.50
01-SIS-20c,hornblende, J =0.005390±0.000006, volume ^{39}ArK = 428.73 x 10^{-10} cm^3, intergrated age 147.16±0.57 Ma (2σ)										
2	303.704±0.014	0.359±0.065	0.409±0.068	0.447±0.039	2.698	0.06	38.59	0.23	188.072±5.730	1262.82±27.67
2.4	264.010 0.011	0.287 0.033	0.280 0.048	0.292 0.024	2.016	0.05	30.75	0.74	182.992 2.831	1238.12 13.86
2.8	88.422 0.009	0.128 0.039	0.178 0.032	0.095 0.023	1.315	0.022	29.39	1.85	61.928 0.850	519.62 6.19
3.2	29.776 0.005	0.190 0.015	0.649 0.019	0.034 0.026	5.045	0.039	29.57	4.08	20.679 0.287	190.65 2.51
3.6	17.116 0.005	0.295 0.011	1.196 0.015	0.011 0.024	9.351	0.065	15.99	19.4	14.308 0.108	134.03 0.98
4	14.312 0.005	0.312 0.011	1.221 0.013	0.008 0.024	9.546	0.069	12.38	37.71	12.501 0.082	117.64 0.75
4.4	14.241 0.006	0.324 0.011	1.192 0.013	0.008 0.020	9.502	0.071	11.5	24.02	12.540 0.088	118.00 0.80
4.8	14.052 0.010	0.299 0.015	1.141 0.019	0.008 0.037	9.094	0.065	10.77	11.97	12.407 0.152	116.79 1.38
02-SIS-107, hornblende, J = 0.009736±0.000020, volume ^{39}ArK = 794.97 x 10^{-10} cm^3, intergrated age 113.51±0.78 (2σ)										
2	164.678±0.021	0.091±0.087	0.354±0.047	0.269±0.062	3.246	0.006	47.68	0.42	86.419±4.989	1101.42±47.59
2.2	42.389 0.013	0.032 0.177	0.195 0.049	0.082 0.059	1.792	0.001	56.3	0.78	18.574 1.427	299.88 21.23
2.4	16.407 0.007	0.022 0.148	0.139 0.036	-0.000 5.668	1.279	0.002	-0.24	1.7	16.488 0.522	268.59 7.91
2.6	11.267 0.013	0.018 0.094	0.138 0.027	0.020 0.068	1.265	0	51.34	2.9	5.494 0.402	94.01 6.70
2.8	9.110 0.011	0.018 0.090	0.199 0.017	0.014 0.068	1.83	0	43.12	3.84	5.193 0.280	88.98 4.68
3	7.688 0.008	0.015 0.058	0.469 0.018	0.009 0.051	4.313	0	34.28	4.67	5.064 0.148	86.83 2.48
3.2	7.425 0.007	0.015 0.026	1.198 0.016	0.007 0.048	11.021	0	22.29	7.86	5.788 0.106	98.90 1.77
3.4	7.053 0.006	0.015 0.034	1.880 0.014	0.004 0.051	17.301	0	10.55	16.71	6.333 0.078	107.94 1.29
3.6	6.931 0.005	0.015 0.034	1.543 0.013	0.004 0.046	14.204	0	9.97	20.29	6.262 0.061	106.77 1.01
3.8	6.829 0.005	0.015 0.038	1.423 0.013	0.004 0.066	12.956	0	9.58	18.71	6.195 0.077	105.66 1.28
4	7.223 0.006	0.015 0.036	1.681 0.014	0.005 0.084	15.312	0	12.98	11.54	6.307 0.125	107.52 2.07
4.2	6.170 0.008	0.014 0.046	1.256 0.015	0.003 0.178	11.435	0	10.34	4.61	5.549 0.183	94.92 3.04
4.6	6.630 0.007	0.015 0.050	1.811 0.014	0.004 0.184	16.5	0	8.44	5.98	6.092 0.201	103.96 3.33
01-SIS-204,hornblende, J =0.009734±0.000018, volume ^{39}ArK = 1283.4 x 10^{-10} cm^3, intergrated age 107.62±0.71 Ma (2σ)										
2	310.868±0.018	0.132±0.057	0.356±0.043	0.497±0.040	3.116	0.006	46.7	0.21	166.197±6.147	1736.11±41.24
2.3	155.701 0.020	0.071 0.122	0.341 0.046	0.244 0.051	2.98	0.003	45.69	0.22	84.812 3.798	1085.86 36.53
2.6	39.979 0.015	0.032 0.154	0.252 0.051	0.082 0.084	2.206	0	59.98	0.44	16.044 2.034	261.80 30.90
2.9	17.319 0.013	0.021 0.078	0.220 0.031	0.032 0.076	1.924	0	53.09	0.97	8.143 0.717	137.62 11.67
3.2	13.633 0.010	0.018 0.104	0.612 0.019	0.021 0.044	5.351	0	44.88	2.45	7.535 0.287	127.70 4.69
3.5	8.573 0.006	0.017 0.028	1.185 0.014	0.010 0.049	10.372	0	29.37	6.77	6.074 0.145	103.62 2.41
3.8	7.205 0.013	0.016 0.034	1.802 0.019	0.005 0.051	15.78	0	12.75	15.61	6.308 0.115	107.52 1.91
4.1	6.150 0.012	0.017 0.033	2.110 0.017	0.003 0.051	18.482	0	7.53	18.66	5.709 0.089	97.57 1.49
4.4	5.696 0.012	0.017 0.026	2.206 0.017	0.003 0.068	19.324	0	4.37	16.98	5.469 0.088	93.56 1.47
4.7	5.704 0.009	0.016 0.033	1.842 0.015	0.003 0.044	16.131	0	4.73	15.07	5.453 0.061	93.31 1.01
5	5.853 0.006	0.016 0.024	1.524 0.013	0.003 0.067	13.45	0	6.87	13.55	5.468 0.063	93.56 1.05
5.3	5.802 0.007	0.016 0.020	1.882 0.014	0.003 0.116	16.625	0	7.5	5.89	5.386 0.117	92.20 1.95
5.6	5.903 0.007	0.015 0.067	1.697 0.015	0.004 0.171	14.992	0	9.9	3.19	5.337 0.183	91.36 3.05
01-SIS-204,biotite, J =0.009729±0.000016, volume ^{39}ArK = 3296.04 x 10^{-10} cm^3, intergrated age 77.01±0.27 Ma (2σ)										
2	52.604±0.012	0.045±0.098	0.036±0.062	0.171±0.024	0.321	0	95.03	0.44	2.619±1.054	45.39±18.04
2.2	10.094 0.006	0.018 0.072	0.010 0.065	0.022 0.068	0.091	0	63.54	1.02	3.685 0.443	63.55 7.50
2.4	5.443 0.006	0.014 0.028	0.005 0.041	0.004 0.042	0.043	0	18.84	7.92	4.425 0.053	76.05 0.88
2.6	5.092 0.008	0.013 0.026	0.004 0.046	0.002 0.044	0.036	0	11.88	8.72	4.494 0.045	77.21 0.76
2.7	4.882 0.006	0.013 0.039	0.003 0.042	0.001 0.073	0.031	0	8.18	8.27	4.491 0.039	77.15 0.66
2.8	4.817 0.005	0.013 0.033	0.004 0.027	0.001 0.077	0.035	0	6.11	7.68	4.530 0.032	77.82 0.54
2.9	4.753 0.005	0.013 0.023	0.004 0.051	0.001 0.084	0.039	0	5.7	7.93	4.490 0.032	77.13 0.53
3	4.799 0.004	0.013 0.035	0.005 0.062	0.001 0.088	0.043	0	5.61	7.08	4.538 0.032	77.94 0.53
3.1	4.801 0.005	0.013 0.019	0.006 0.059	0.001 0.110	0.049	0	5.69	6.3	4.535 0.039	77.90 0.66
3.2	4.787 0.007	0.013 0.031	0.007 0.042	0.001 0.105	0.061	0	6.4	5.33	4.488 0.045	77.11 0.76
3.3	4.824 0.006	0.013 0.023	0.007 0.032	0.001 0.107	0.066	0	6.38	5.29	4.524 0.045	77.71 0.75
3.4	4.810 0.007	0.013 0.031	0.009 0.045	0.001 0.095	0.08	0	6.29	5.08	4.515 0.043	77.56 0.73

continuation of Table AId ^{40}Ar-^{39}Ar age data for hornblende, muscovite and biotite from the Atnarko complex.

3.5	4.788 0.007	0.013 0.017	0.010 0.028	0.001 0.098	0.091	0	6.51	4.52	4.484 0.045	77.03 0.76
3.6	4.750 0.008	0.013 0.023	0.011 0.023	0.001 0.047	0.098	0	5.8	9.43	4.482 0.039	77.00 0.66
3.8	4.760 0.006	0.013 0.026	0.014 0.025	0.001 0.103	0.125	0	5.66	7.68	4.498 0.040	77.27 0.68
4	4.784 0.008	0.013 0.022	0.025 0.031	0.001 0.104	0.222	0	5.83	7.3	4.513 0.048	77.53 0.81
01-SIS-107,biotite, J =0.009734±0.000018, volume ^{39}ArK = 1413.64 x 10^{-10} cm^3, intergrated age69.82±0.50 Ma (2σ)										
2	31.179±0.010	0.030±0.146	0.092±0.029	0.098±0.037	0.828	-0.001	92.15	0.67	2.451±1.057	42.54±18.13
2.3	11.115 0.005	0.018 0.068	0.033 0.039	0.027 0.054	0.296	0	69.54	3.88	3.390 0.427	58.58 7.26
2.6	7.111 0.005	0.015 0.029	0.022 0.021	0.011 0.024	0.2	0	44.72	12.04	3.938 0.081	67.86 1.37
2.8	5.860 0.006	0.014 0.037	0.027 0.029	0.006 0.036	0.239	0	29.93	10.66	4.113 0.069	70.83 1.16
3	5.176 0.006	0.014 0.037	0.030 0.032	0.004 0.060	0.27	0	20.66	10.63	4.114 0.071	70.83 1.20
3.2	5.019 0.006	0.014 0.026	0.026 0.033	0.003 0.059	0.232	0	17.63	10.87	4.141 0.059	71.29 0.99
3.4	4.725 0.006	0.013 0.040	0.025 0.025	0.002 0.076	0.223	0	13.99	11.86	4.071 0.058	70.11 0.98
3.6	4.640 0.006	0.013 0.033	0.026 0.033	0.002 0.082	0.231	0	12.71	8.94	4.057 0.056	69.88 0.94
3.8	4.679 0.006	0.013 0.042	0.029 0.019	0.002 0.074	0.262	0	12.75	10.64	4.090 0.052	70.43 0.89
4.1	4.610 0.005	0.014 0.033	0.046 0.021	0.002 0.127	0.412	0	11.78	8.67	4.073 0.074	70.15 1.26
4.4	4.680 0.007	0.013 0.049	0.070 0.030	0.002 0.082	0.626	0	12.53	7.32	4.101 0.059	70.62 0.99
4.7	4.991 0.009	0.014 0.065	0.131 0.017	0.003 0.167	1.168	0	16.76	3.08	4.162 0.153	71.64 2.58
5	5.912 0.014	0.016 0.109	0.233 0.035	0.000 3.105	2.081	0	0.9	0.73	5.871 0.371	100.27 6.17
01-SIS-181, biotite, J = 0.005386±0.000006, volume ^{39}ArK = 173.71 x 10^{-10} cm^3, intergrated age 70.95±0.47 Ma (2σ)										
2	17.295±0.011	0.054±0.117	0.058±0.099	0.045±0.068	0.094	0.006	49.38	2.14	8.048±0.947	76.55±8.82
2.3	8.646 0.005	0.054 0.028	0.016 0.075	0.006 0.061	0.081	0.009	12.3	17.61	7.365 0.116	70.18 1.08
2.6	8.171 0.005	0.074 0.022	0.018 0.062	0.004 0.051	0.106	0.014	7	21.98	7.406 0.070	70.56 0.65
2.9	7.905 0.005	0.026 0.038	0.016 0.063	0.003 0.073	0.084	0.003	2.49	19.11	7.481 0.075	71.27 0.70
3.2	7.868 0.006	0.026 0.040	0.019 0.066	0.004 0.144	0.086	0.002	0.92	11.91	7.451 0.174	70.99 1.63
3.5	7.872 0.006	0.028 0.051	0.024 0.079	0.005 0.114	0.101	0.003	1.37	8.56	7.303 0.191	69.60 1.79
4	8.071 0.006	0.026 0.048	0.018 0.076	0.004 0.104	0.087	0.002	3.32	14.03	7.512 0.132	71.56 1.24
4.5	8.623 0.007	0.028 0.115	0.035 0.106	0.010 0.087	0.108	0.002	2.58	4.66	7.607 0.268	72.44 2.50
03-SIS-16, biotite, J = 0.009729±0.000016, volume ^{39}ArK = 881.3 x 10^{-10} cm^3, intergrated age 69.86±0.54 Ma (2σ)										
1.8	125.654±0.027	0.074±0.076	0.653±0.048	0.280±0.056	4.508	0.002	65	0.13	44.125±4.242	644.38±52.09
2	86.528 0.011	0.054 0.121	0.710 0.021	0.178 0.054	4.901	0.002	59.83	0.27	34.866 2.838	526.94 37.20
2.2	35.204 0.014	0.023 0.192	0.572 0.036	0.068 0.077	3.948	-0.001	55.91	0.6	15.566 1.534	254.40 23.39
2.4	14.432 0.014	0.018 0.085	0.625 0.027	0.029 0.072	4.312	0	57.17	1.25	6.196 0.605	105.61 10.01
2.6	7.180 0.008	0.014 0.103	0.877 0.016	0.012 0.089	6.052	-0.001	48.35	2.36	3.717 0.330	64.08 5.58
2.8	5.727 0.008	0.015 0.063	1.751 0.016	0.007 0.110	12.092	0	29.67	4.8	4.040 0.231	69.55 3.91
3	4.754 0.005	0.015 0.036	2.115 0.013	0.005 0.068	14.607	0	19.56	7.28	3.836 0.097	66.10 1.64
3.2	4.530 0.005	0.015 0.020	2.424 0.013	0.004 0.038	16.747	0	16	9.87	3.818 0.052	65.80 0.88
3.4	4.316 0.005	0.016 0.029	2.924 0.013	0.003 0.069	20.214	0	9.49	15.94	3.921 0.073	67.54 1.24
3.6	4.154 0.004	0.015 0.019	2.854 0.013	0.003 0.038	19.727	0	8.22	28.97	3.826 0.040	65.94 0.67
3.8	4.367 0.005	0.016 0.046	3.172 0.013	0.004 0.062	22.116	0	11.05	15.26	3.899 0.074	67.17 1.26
4	3.966 0.006	0.014 0.051	1.927 0.013	0.003 0.062	13.422	0	9.04	8.71	3.618 0.052	62.41 0.89
4.2	3.993 0.006	0.015 0.055	2.003 0.013	0.004 0.078	13.96	0	16.2	4.55	3.356 0.087	57.96 1.48
01-SIS-69, hornblende, J = 0.005387±0.000006; volume ^{39}ArK = 605.44 x 10^{-10} cm^3, integrated age 129.27 ± 0.49 Ma (2σ)										
2	887.553±0.030	2.568±0.045	0.461±0.073	1.266±0.036	2.079	0.682	39.01	0.09	692.519±29.238	2803.65±60.07
2.3	366.111 0.013	1.124 0.019	0.244 0.042	0.434 0.022	1.564	0.248	33.35	0.49	255.000 4.299	1559.53 17.60
2.6	88.316 0.007	0.268 0.027	0.205 0.037	0.111 0.020	1.467	0.054	33.97	1.17	58.836 0.803	496.70 5.93
2.9	22.510 0.012	0.357 0.016	0.757 0.025	0.025 0.028	6.012	0.078	27.55	4.27	16.183 0.284	150.79 2.54
3.2	13.407 0.006	0.416 0.011	0.877 0.015	0.008 0.022	6.986	0.093	12.74	12.62	11.624 0.088	109.57 0.80
3.5	12.660 0.011	0.404 0.014	0.866 0.016	0.006 0.036	6.898	0.09	10.11	15.51	11.312 0.148	106.72 1.36
3.8	12.431 0.005	0.470 0.010	0.934 0.014	0.006 0.020	7.442	0.105	9.21	26.42	11.242 0.063	106.08 0.58
4.1	11.975 0.006	0.431 0.010	0.837 0.014	0.005 0.043	6.667	0.096	8.07	19.06	10.947 0.094	103.38 0.86
4.4	11.665 0.009	0.407 0.012	0.790 0.015	0.004 0.036	6.286	0.091	5.6	13.89	10.930 0.112	103.22 1.03
4.8	12.381 0.006	0.445 0.013	0.871 0.017	0.006 0.043	6.932	0.099	6.91	6.48	11.378 0.105	107.32 0.96
02-SIS-45B, muscovite, J = 0.009737±0.000020, volume ^{39}ArK = 472.09 x 10^{-10} cm^3, intergrated age 109.26 ± 0.85 Ma (2σ)										
2	10.191±0.016	0.015±0.129	0.010±0.286	0.019±0.096	0.088	-0.001	54.61	1.72	4.634±0.545	79.62±9.16
2.2	7.358 0.008	0.013 0.080	0.004 0.260	0.005 0.100	0.041	0	18.03	5.79	6.044 0.143	103.16 2.37
2.4	7.227 0.008	0.014 0.062	0.001 0.454	0.004 0.174	0.009	0	15.1	8.01	6.148 0.199	104.89 3.29
2.6	7.586 0.005	0.013 0.039	0.001 0.262	0.002 0.078	0.009	0	8.8	17.62	6.933 0.066	117.86 1.09
2.7	6.367 0.006	0.013 0.048	0.001 0.413	0.002 0.272	0.009	0	8.72	11.74	5.823 0.157	99.50 2.61
2.9	7.089 0.007	0.013 0.107	0.001 0.258	0.002 0.171	0.011	0	9.07	11.72	6.459 0.121	110.04 2.01
3.1	7.156 0.006	0.012 0.034	0.001 0.282	0.002 0.212	0.005	0	8.98	16.09	6.527 0.145	111.16 2.39
3.3	7.126 0.007	0.014 0.080	0.002 0.239	0.002 0.264	0.014	0	7.89	8.47	6.577 0.159	111.99 2.62
3.5	8.007 0.018	0.012 0.356	0.005 0.605	0.005 0.318	0.042	-0.001	19.5	2	6.459 0.518	110.04 8.55
3.8	6.892 0.006	0.013 0.079	0.001 0.449	0.001 0.283	0.007	0	6.18	16.83	6.479 0.128	110.37 2.12
03-SIS-29,biotite, J = 0.009729±0.000016, volume ^{39}ArK = 866.79 x 10^{-10} cm^3, intergrated age 180.68 ± 0.54 Ma (2σ)										
2	22.889±0.012	0.024±0.146	0.018±0.114	0.063±0.038	0.162	-0.001	80.08	1.82	4.567±0.689	78.42±11.58
2.2	8.504 0.006	0.016 0.048	0.009 0.095	0.014 0.045	0.079	0	48.39	5.86	4.396 0.192	75.56 3.23

continuation of Table AId ^{40}Ar-^{39}Ar age data for hornblende, muscovite and biotite from the Atnarko complex.

2.4	6.181	0.005	0.014	0.053	0.005	0.091	0.005	0.059	0.045	0	23.77	10.15	4.720	0.091	81.01	1.53
2.6	5.427	0.005	0.013	0.030	0.006	0.048	0.002	0.102	0.05	0	13.29	14.07	4.715	0.079	80.91	1.32
2.8	5.155	0.005	0.013	0.019	0.004	0.059	0.002	0.070	0.033	0	8.58	16.15	4.721	0.040	81.02	0.66
3	5.182	0.005	0.013	0.039	0.004	0.063	0.002	0.092	0.033	0	8.64	14.5	4.743	0.048	81.39	0.81
3.2	5.366	0.007	0.013	0.069	0.007	0.072	0.002	0.172	0.059	0	11.81	7.74	4.741	0.116	81.36	1.95
3.4	5.469	0.007	0.013	0.082	0.008	0.070	0.003	0.096	0.072	0	13.61	6.65	4.733	0.081	81.21	1.36
3.6	5.544	0.005	0.014	0.076	0.014	0.064	0.003	0.085	0.12	0	15.04	6.93	4.719	0.077	80.98	1.29
3.9	5.423	0.006	0.013	0.047	0.014	0.065	0.002	0.161	0.126	0	12.22	9.65	4.769	0.113	81.82	1.90
4.2	5.209	0.006	0.013	0.060	0.025	0.041	0.002	0.183	0.22	0	11.73	6.48	4.606	0.118	79.09	1.99

[1] "<" indicates step used in plateau age calculations, ">'" indicates step used in inverse correlation calculations.

Neutron flux monitors: 24.36 Ma MAC-83 biotite (Sandeman et al. 1999); 28.02 Ma FCs (Renne et al., 1998)

Isotope production ratios: $(^{40}Ar/^{39}Ar)_K$=0.0302, $(^{37}Ar/^{39}Ar)_{Ca}$=1416.4306, $(^{36}Ar/^{39}Ar)_{Ca}$=0.3952, Ca/K=1.83$(^{37}Ar_{Ca}/^{39}Ar_K)$.

plateau and correlation ages were calculated using Isoplot ver.3.09 (Ludwig, 2003). Errors are quoted at the 2-sigma (95% confidence) level and are propagated from all sources except mass spectrometer sensitivity and age of the flux monitor

REFERENCES

Krogh, T. E., 1982, Improved accuracy of U-Pb zircon ages by the creation of more concordant systems using an air abrasion technique: Geochimica et Cosmochimica Acta, v. 46, p. 637-649.

Ludwig, K. R., 2003, Isoplot 3.0, A geochronological toolkit for Microsoft Excel, University of California at Berkley.

Parrish, R. R., Roddick, J. A., Loveridge, W. D., and Sullivan, R. W., 1987, Uranium-lead analytical techniques at the geochronology laboratory, Geological Survey of Canada, In Radiogenic Age and Isotopic Studies, Report 1, Geological Survey of Canada, Paper 87-2, p. 3-7.

Renne, P. R., Swisher, C. C., III, Deino, A. L., Karner, D. B., Owens, T. J., and DePaolo, D. J., 1998, Intercalibration of standards, absolute ages and unertanties in 40Ar/39Ar dating: Chemical Geology, v. 145, no. 1-2, p. 117-152.

Roddick, J. A., 1987, Generalized numerical error analysis with application to geochronology and thermodynamics: Geochemica et Cosmochimica Acta, v. 51, p. 2129-2135.

Sandeman, H. A., Archibald, D. A., Grant, J. W., Villeneuve, M. E., and Ford, F. D., 1999, Characterization of the chemical composition and 40Ar/39Ar systematics of intralaboratory standard MAC-83-biotite, Radiogenic age and isotopic studies: Report 12; Geological Survey of Canada, Current Research, 1999-F, p. 13-26.

Thirlwall, M. F., 2000, Inter-laboratory and other errors in Pb isotope analyses investigated using a ^{207}Pb-^{204}Pb double spike: Chemical Geology, v. 163, p. 299-322.

APPENDIX II

GEOCHEMISTRY

Geochemical data for metabasalts and migmatitic gneisses are found in Table AIIa. Analyses preparation and analyses were performed by ALS Chemex in Vancouver, B.C. Whole rock major element analyses by XRF. Rare Earth elements by ICP-MS.

Table AIIa. **Chemical compositions of samples of metabasalt based on XRF analysis for major element contents (wt%) and ICP-MS analysis for REE concentraions (ppm)**

SAMPLE	01-SIS-45A	01-SIS-36	01-SIS-61A	02-SIS-27A	02-SIS-77	02-SIS-112	02-SIS-28
SiO2	67	61.52	62.5	51.05	53.41	66.47	56.4
Al2O3	16.24	16.78	14.87	18.14	17.84	14.55	16.28
Fe2O3 (T)	3.67	6.34	6.78	10.3	11.4	3.91	10.93
FeO	3.30	5.70	6.10	9.27	10.26	3.52	9.83
CaO	4.3	6.12	5.51	5.05	4.6	4.29	7.6
MgO	1.48	2.86	2.48	5.82	3.62	1.88	3.35
Na2O	3.9	3.02	2.81	1.28	3.38	3.26	2.67
K2O	1	0.95	1.12	1.45	1.74	1.29	0.43
Cr2O3	0.01	0.04	0.02	0.03	<0.01	0.02	0.02
TiO2	0.53	0.51	0.94	1.18	1.05	0.42	1.05
MnO	0.03	0.1	0.12	0.26	0.17	0.05	0.21
P2O5	0.17	0.13	0.23	0.26	0.16	0.15	0.22
SrO	0.07	0.05	0.04	0.04	0.03	0.07	0.04
BaO	0.05	0.06	0.05	0.18	0.11	0.07	0.04
LOI	1.13	0.91	1.43	4.17	1.74	3.15	0.59
Total	99.58	99.37	98.9	99.22	99.26	99.56	99.84
Rare Earth Element compositions							
Ce	24	17.9	24.2	32.3	11.2	42.6	19.2
Dy	1.1	1.9	6.1	4.7	3.9	1.3	4.5
Er	0.8	1.2	4	3	2.5	0.7	2.8
Eu	0.6	0.7	1.3	1.4	1.1	0.9	1.3
Gd	1.6	2	5.1	4.6	3.4	2.5	4
Ho	0.2	0.4	1.3	0.9	0.8	0.2	0.9
La	12.6	9.3	9.9	14.1	5.4	21.5	8.6
Lu	0.1	0.2	0.6	0.4	0.4	0.1	0.4
Nd	10.2	9.2	17.6	20.3	9.8	19.7	13.8
Pr	2.7	2.3	3.8	4.4	2	5.3	2.8
Sm	1.7	2.1	5	4.8	3.1	3.1	3.7
Tb	0.2	0.3	0.9	0.8	0.6	0.3	0.7
Th	3	2	2	2	<1	3	1
Tm	0.1	0.2	0.6	0.4	0.4	0.1	0.4
U	1.5	1.2	1	0.9	<0.5	0.7	0.5
Y	7.1	11.3	35.1	27.7	22.5	6.8	26.9
Yb	0.8	1.2	3.9	2.7	2.4	0.6	2.8
Cr	168	302	181	210	74	193	149
Nb	3	2	2	4	2	3	2
Ni	<10	<10	<10	70	<10	20	<10
Zr	228	60	145	153	50	103	67
V	76	129	128	186	360	76	224

Table AIIb. **Chemical compositions of samples of Gneisses based on XRF analysis for major element contents (wt%) and ICP-MS analysis for REE concentraions (ppm)**

SAMPLE	02-SIS-157A	02-SIS-158	01-SIS-135A	01-SIS-137A	01-SIS-101C	02-SIS-128B	02-SIS-45C	02-SIS-45D	02-SIS-85	01-SIS-107
SiO2	65.89	63.61	68.18	70.68	66	70.46	74.51	48.77	62.41	63.01
Al2O3	16.29	15.9	16.31	15.75	15.49	15.09	15.4	17.52	14.92	16.55
Fe2O3 (T)	4.77	5.54	3.18	3.2	4.92	3.61	1.24	12.4	6.65	5.44
FeO	4.29	4.98	2.86	2.88	4.43	3.25	1.12	11.16	5.98	4.89
CaO	4.31	4.76	4.69	2.8	4.33	4.78	2.06	9.96	5.57	5.42
MgO	1.83	2.16	0.55	1.07	1.79	1.25	0.2	5.03	2.46	2.3
Na2O	3.71	3.2	3.63	4.16	3.34	3.09	4.2	2.11	2.42	3.15
K2O	1.45	1.83	1.66	1.16	1.16	0.48	1.15	0.71	2.06	1.22
Cr2O3	<0.01	0.01	0.01	0.02	0.04	0.02	0.02	0.01	0.01	0.01
TiO2	0.49	0.62	0.33	0.24	0.44	0.53	0.08	1.02	0.67	0.48
MnO	0.1	0.1	0.04	0.03	0.08	0.04	0.02	0.27	0.13	0.1
P2O5	0.15	0.15	0.13	0.03	0.12	0.06	0.02	0.09	0.15	0.16
SrO	0.04	0.07	0.09	0.06	0.05	0.07	0.06	0.04	0.04	0.05
BaO	0.06	0.09	0.08	0.11	0.07	0.02	0.14	0.04	0.05	0.08
LOI	0.31	0.59	0.96	0.65	1.9	0.31	0.69	1.59	0.94	1.25
Total	99.41	98.64	99.85	99.97	99.73	99.81	99.81	99.54	98.48	99.22
Rare Earth Element compositions										
Ce	28.2	24	24.7	73.6	35.4	7.1	14.4	7.1	25.2	21.5
Dy	3.1	3	1.1	0.8	3	1.1	0.4	2.6	3.4	2.8
Er	2	1.8	0.5	0.4	1.9	0.7	0.2	1.7	2.1	1.8
Eu	0.9	0.9	0.8	0.8	1	0.5	0.4	0.8	1	0.9
Gd	3.2	3.3	2	3.1	3.5	1.2	0.8	2.1	3.3	2.8
Ho	0.6	0.6	0.2	0.1	0.6	0.2	0.1	0.5	0.7	0.6
La	13.6	11.2	12	36.5	17.2	3.8	7.8	3.8	12.4	10.2
Lu	0.3	0.2	0.1	0.1	0.3	0.1	<0.1	0.2	0.3	0.2
Nd	15.2	15.4	13.6	33.8	19.8	4.7	6.8	5.8	14.5	11.9
Pr	3.7	3.4	3.3	9.2	4.7	1	1.8	1.1	3.3	2.8
Sm	3.3	3.6	2.8	4.3	4.1	1.2	1.1	1.9	3.4	2.7
Tb	0.5	0.5	0.2	0.3	0.5	0.2	0.1	0.4	0.5	0.5
Th	3	2	2	4	3	<1	<1	<1	3	2
Tm	0.3	0.2	0.1	<0.1	0.3	0.1	<0.1	0.2	0.3	0.3
U	1.7	1.5	1.3	<0.5	0.6	<0.5	<0.5	<0.5	1.5	0.5
Y	19.1	17.4	5.9	3.7	17.4	6.7	2.5	15.4	20.2	17.7
Yb	2	1.7	0.5	0.3	1.8	0.7	0.3	1.6	2.1	1.7
Cr	111	112	174	219	367	177	232	120	131	102
Nb	4	3	2	2	2	2	3	3	2	3
Ni	<10	<10	<10	10	<10	<10	<10	<10	<10	<10
Zr	83	67	87	67	101	172	45	27	102	74
V	87	121	72	29	77	39	10	377	170	113

APPENDIX III

Appendix III contains two 1:50 000-scale bedrock geology maps of the Atnarko complex and surrounding area.

Natural Resources Canada / Ressources naturelles Canada

GEOLOGICAL SURVEY OF CANADA / COMMISSION GÉOLOGIQUE DU CANADA

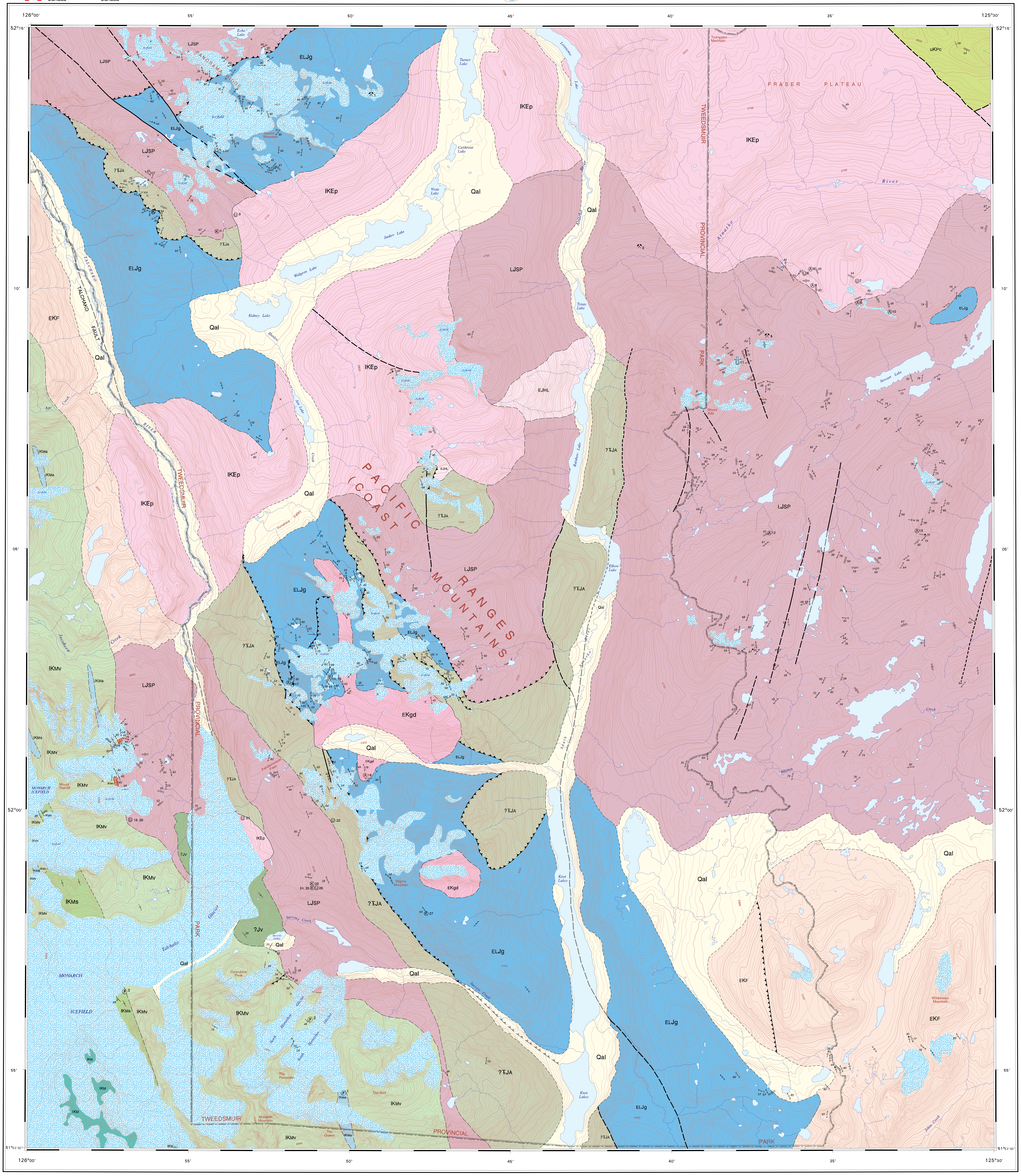

LEGEND

STRATIFIED ROCKS

QUATERNARY

Qal — *Recent alluvium, till, colluvium*

UPPER CRETACEOUS

POWELL CREEK FORMATION

uKPC — *Green, purple, maroon and grey, subaerial andesitic agglomerate and breccia, lapilli tuff, rare flows; minor intercalated calcareous siltstone and sandstone*

LOWER CRETACEOUS

?VALANGINIAN, HAUTERIVIAN TO BARREMIAN

MONARCH ASSEMBLAGE

lKM — *Dominantly interstratified basalt and basaltic andesite, tuff, tuff breccia, and volcanic breccia; lesser feldspathic sandstone, locally calcareous; siltstone; contains distinct laterally continuous intervals (1-10 m thick) of black argillite and slate*

Volcanic Facies

lKMv — *Dominantly volcanic rocks; amorphous olive green amygdaloidal basalt and basaltic andesite and associated breccia, tuff and tuff breccia; locally intercalated with thinly bedded siltstone, black argillite to slate; complexly interfingered with* lKMs

Sedimentary Facies

lKMs — *Dominantly sedimentary rocks; feldspathic sandstone and siltstone; black argillite, locally with thin cross-stratified calcareous sandstone to sandy limestone containing shallow water marine fauna; pebble to cobble conglomerate; lapilli tuff and welded ash-flow tuff; lesser basaltic andesite and basalt flows and breccias; rare intraformational conglomerate within sedimentary sequences; complexly interfingered with* lKMv

Argillite Facies

lKMa — *Black argillite, locally with thin cross-stratified siltstone and sandstone; pebble to cobble conglomerate*

Conglomerate Facies

lKMc — *Pebble to boulder conglomerate, typically of granitoid composition*

?JURASSIC

?Jv — *Undifferentiated intermediate to felsic volcanic rocks intercalated with fine-grained siltstone and quartz-sandstone; medium-to-coarse-grained sandstone with granitic clasts locally observed; some flows may be sub-volcanic dykes*

LOWER TO UPPER JURASSIC

ELJg — *Middle to upper amphibolite facies undifferentiated orthogneiss and migmatitic gneiss; black fine-grained amphibolite with stromatic, tonalite leucosomes; could be in part metamorphosed equivalents of* ?TJA, LJSP *and* EJHL

?TRIASSIC TO LOWER JURASSIC

ATNARKO ASSEMBLAGE

?TJA — *Upper greenschist facies dark green, fine-grained basaltic metavolcanic rocks interlayered with fine-grained metasedimentary rocks, rare interbeds of meta-rhyolite within metavolcanic rocks; strongly foliated and internally folded*

INTRUSIVE ROCKS

LATE CRETACEOUS TO EOCENE

LKEp — *Undifferentiated granitic plutons; hornblende-biotite tonalite to granite; fine- to medium-grained, equigranular*

EARLY CRETACEOUS

EKgd — *(U/Pb ca. 117-103 Ma): Undifferentiated granodiorite to quartz-diorite and tonalite, locally garnet bearing; medium- to coarse-grained, strongly foliated to gneissic textures developed locally*

FIRVALE PLUTONIC SUITE (U/Pb ca. 132-141 Ma)

EKF — *Hornblende-biotite diorite and granodiorite to granite; medium- to coarse-grained; light pink to light green colour from incipient chlorite alteration; strongly foliated to gneissic textures*

LATE JURASSIC

STICK PASS PLUTONIC SUITE (U/Pb ca. 148-164 Ma)

LJSP — *Hornblende-biotite quartz monzodiorite to granite; medium- to coarse-grained, equigranular to inequigranular; abundant epidote veining; mylonitic to gneissic textures developed locally*

EARLY JURASSIC

HOWE LAKE PLUTONIC SUITE (U/Pb ca. 181-189 Ma)

EJHL — *Fine- to coarse-grained pyroxene-hornblende diorite to quartz diorite and medium- to coarse-grained biotite-hornblende tonalite; abundant metavolcanic screens and mafic xenoliths, commonly amphibolitic; common magmatic and tectonic foliation; may be subvolcanic to Hazelton Group strata*

SYMBOLS

Geological contact (defined, approximate, assumed)

Fault (defined, approximate, assumed; shaded under Qal and water)

Fault, compressional, defined, approximate, assumed (teeth on upthrust side)

Shear zone (inclined, vertical)

Anticline (defined and approximate)

Syncline (defined and approximate)

Fold axis

Bedding (tops unknown inclined, overturned, tops known inclined, vertical)

Foliation (inclined, vertical)

Mineral lineation

Stretching lineation

Lineation (undivided)

Dyke (inclined, vertical)

Fault

Field Station location where not indicated by other symbol (foliation, etc.)

*Fossil locality with ID number**

Ar-Ar age determination locality with ID number

K-Ar age determination locality with ID number

U-Pb age determination locality with ID number

MINFILE occurrence with ID number

Park Boundary

MINFILE*

MAP #	MINFILE #	NAME	STATUS	COMMODITIES
1	093C 008	PANORAMA RIDGE EAST	Showing	Copper, Silver
2	093C 003	LONESOME LAKE EAST	Showing	Copper
3	093C 005	ADA	Showing	Copper

* Data from British Columbia Geological Survey Branch MINFILE Mineral Inventory

GEOCHRONOLOGY

MAP #	FIELD #	AGE (Ma)	MINERAL	METHOD	REFERENCE
1	01-SIS-107	70.5 ± 0.5	Biotite	Ar-Ar	1
2	01-SIS-107	106.9 ± 0.8	Hornblende	Ar-Ar	1
3	V89-61-1	65.2 ± 0.3	Zircon	U-Pb	2
4	V89-62-4	148.9 ± 6.3	Hornblende	K-Ar	2
5	A92-180	57.7 ± 0.8	Biotite	Ar-Ar	3
6	A92-179	58.5 ± 1.0	Zircon	U-Pb	3
7	A92-175	58.5 ± 1.0	Zircon	U-Pb	3
8	A92-177	75.1 ± 2.4	Hornblende	Ar-Ar	3
9	A92-170b	91.5 ± 1.5	Hornblende	Ar-Ar	3
10	A92-167	131.2 ± 1.4	Hornblende	Ar-Ar	3
11	A92-229	151 ± 1	Zircon	U-Pb	3
12	J92-29b	128.3 ± 1.2	Biotite	Ar-Ar	3
13	A92-134	58.3 ± 0.9	Biotite	Ar-Ar	3
14	01-SIS-204	77.5 ± 0.4	Biotite	Ar-Ar	1
15	01-SIS-204	93.3 ± 0.8	Hornblende	Ar-Ar	1
16	02-SIS-45B	110.7 ± 1.2	Muscovite	Ar-Ar	1
17	02-SIS-46	117.5 ± 1.7	Hornblende	Ar-Ar	1
18	03-SIS-29	81.2 ± 0.6	Biotite	Ar-Ar	1
19	V89-137	155.42 ± 0.24	Zircon	U-Pb	2
20	V89-137	153.4 ± 0.8	Titanite	U-Pb	2
21	V89-117-1	63.3 ± 0.3	Zircon	U-Pb	2
22	V89-115-1	158.8 ± 0.3	Zircon	U-Pb	2
23	V89-113-3	62.2 ± 4.8	Whole Rock	K-Ar	2
24	V89-111	128 ± 8	Hornblende	K-Ar	2
25	V89-111	96.8 ± 7.2	Biotite	K-Ar	2
26	V89-112-3	157 ± 11	Zircon	U-Pb	2
27	V89-134	113 ± 8	Muscovite	K-Ar	2

[1] This report; all analyses performed at University of British Columbia

[2] van der Heyden, P. 2004. Uranium-lead and potassium-argon ages from eastern Bella Coola and adjacent parts of Anahim Lake and Mount Waddington map areas, west-central British Columbia. Geological Survey of Canada, Current Research 2004-A2, 14 pp.

[3] van der Heyden, P., Calderwood, A., and Huntley, D.H. 1994. Preliminary geological map, Charlotte Lake - Junker Lake (east half), British Columbia. Geological Survey of Canada, Open File 2984, scale 1:50 000; P. van der Heyden, unpublished data

PALEONTOLOGY*

MAP #	GSC #	COLLECTOR	DATE	FOSSILS	AGE	IDENTIFIER	REPORT # **
1	79712⁺	H.W. Tipper	1967	*Quoieocchia* ex gr. *aliciae*, *Yaadia* ex gr. *lewisagassizi*, *Pleuromya* sp. indet., *Arctica* ? sp. indet., bivalves indet., gastropods indet.	Early Cretaceous (Hauterivian-Barremian)	J.A. Jeletzky	Km-12-1967-JAJ
2	C-307515	S. Israel	11-08-2001	Belemnites, gen. et sp. indet.	Jurassic to Cretaceous (pre-Albian)	J.W. Haggart	This report
3	n.a.	G.J. Woodsworth	1982	Plant matter	Indeterminate	G.J. Woodsworth	This report

* compiled by J.W. Haggart

** unpublished G.S.C Paleontological Report numbers

⁺ precise location unknown

n.a. = not available


LOCATION MAP

Geology by S. Israel (2001-2003), J.W. Haggart (2003-2004), G.J. Woodsworth (1976,1979, 2003-2004), P. van der Heyden (1989-1991), H.W. Tipper (1954-1967), J.A. Roddick (1976, 1978, 1979), W.W. Hutchison (1967)

Geological compilation by S. Israel, P. van der Heyden, J.W. Haggart and G.J. Woodsworth

Digital cartography by N.L. Hastings and M. Coh, Geological Survey of Canada

Contribution of Bella Coola Targeted Geoscience Initiative, Cordilleran Energy and Minerals Project Number Y15

OPEN FILE 5388

GEOLOGY

JUNKER LAKE AND PART OF KNOT LAKES (93C/04 AND 92N/13)

BRITISH COLUMBIA

Scale 1:50 000/Échelle 1/50 000

Universal Transverse Mercator Projection / North American Datum 1983

Projection transverse universelle de Mercator / Système de référence géodésique nord-américain, 1983

Any revisions or additional geological information known to the user would be welcomed by the Geological Survey of Canada

Digital base map from data compiled by Geomatics Canada modified by Geological Survey of Canada

Mean magnetic declination 2006, 19°51' E, decreasing 14.0' annually. Readings vary from 19°58' E in the northwest to 19°44' E in the southeast corner of the map

Elevations in feet above mean sea level

Contour interval 100 feet

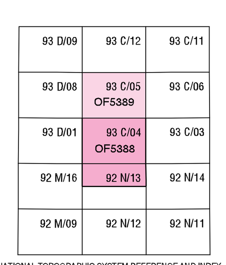
NATIONAL TOPOGRAPHIC SYSTEM REFERENCE AND INDEX TO ADJOINING GEOLOGICAL SURVEY OF CANADA MAPS

OPEN FILE / DOSSIER PUBLIC

5388

GEOLOGICAL SURVEY OF CANADA / COMMISSION GÉOLOGIQUE DU CANADA

2006

Open files are products that have not gone through the GSC formal publication process.

Les dossiers publics sont des produits qui n'ont pas été soumis au processus officiel de publication de la CGC.

Recommended citation:
Israel, S., van der Heyden, P., Haggart, J.W., and Woodsworth, G.J. 2006: Geology, Junker Lake and part of Knot Lakes (93C/04 and 92N/13), British Columbia; Geological Survey of Canada, Open File 5388, scale 1:50 000.

Canada

Natural Resources Canada / Ressources naturelles Canada

GEOLOGICAL SURVEY OF CANADA / COMMISSION GÉOLOGIQUE DU CANADA

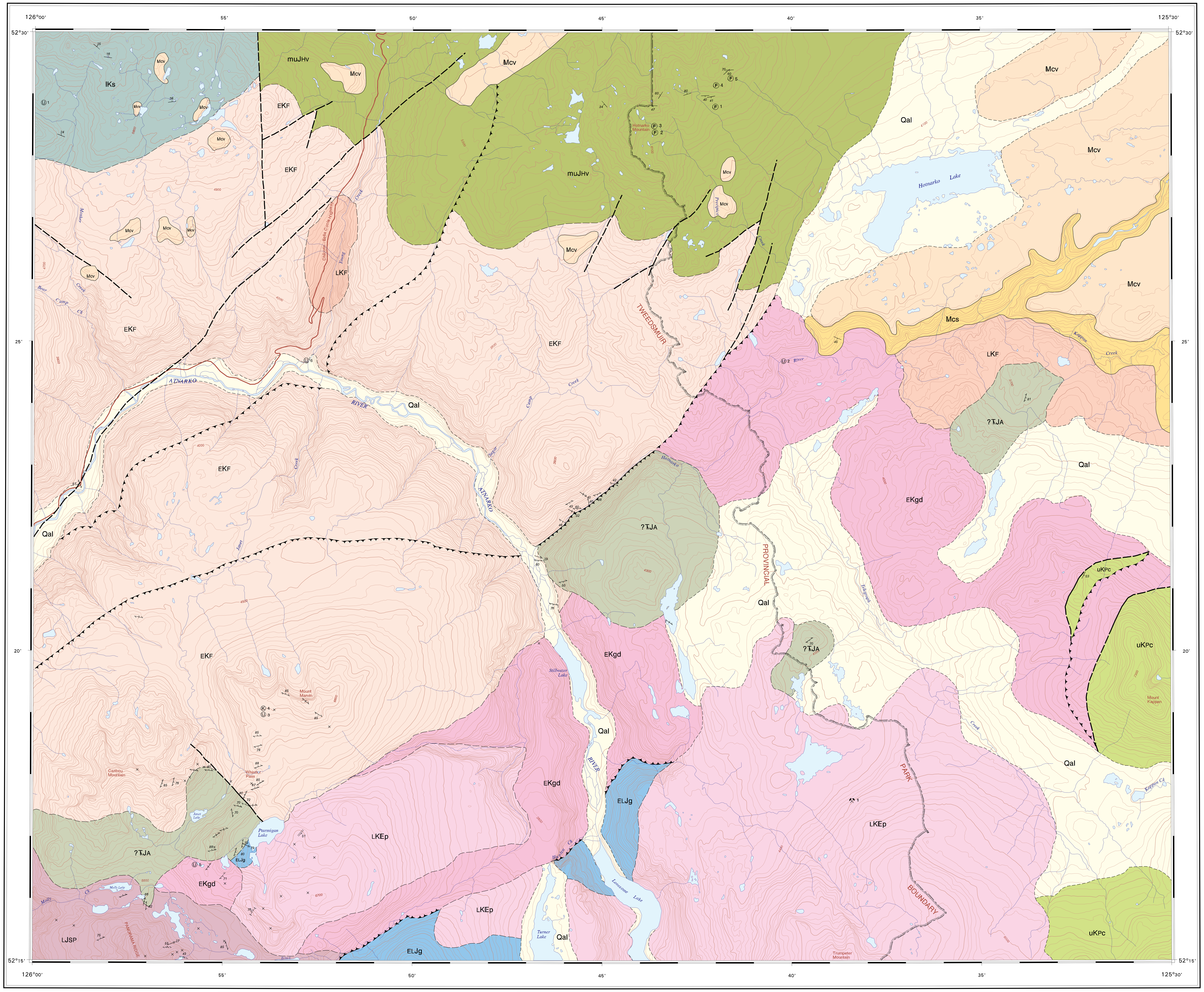

LEGEND

STRATIFIED ROCKS

QUATERNARY

Qal	*Recent alluvium, till*

NEOGENE
MIOCENE
CHILCOTIN GROUP

Mcv	*Vesicular and amygdaloidal basalt, fine-grained to porphyritic black, brown and grey olivine basalt; breccia, tuff; columnar jointing common*
Mcs	*Poorly consolidated conglomerate, breccia, fine-grained siltstone; angular clasts of vesicular olivine basalt and plutonic rocks in fine grained sandy matrix; buff weathering siltstone*

UPPER CRETACEOUS
POWELL CREEK FORMATION

uKPC	*Green, purple, maroon and grey, subaerial andesitic agglomerate and breccia, lapilli tuff, rare flows; minor intercalated calcareous siltstone and sandstone*

LOWER CRETACEOUS
?APTIAN-ALBIAN
SALLOOMT ASSEMBLAGE (U/Pb ca. 112 Ma)

lKs	*Amygdaloidal basalt +/- hornblende-augite-plagioclase andesite porphyry; local reworked volcanic breccias; rare columnar jointing; lesser andesitic to rhyolitic lapilli tuff, maroon to green to white; fine- to medium-grained feldspathic sandstone, locally cross-stratified and calcareous, with shale rip-up clasts; siltstone; black mudstone to argillite*

MIDDLE TO UPPER JURASSIC
CALLOVIAN-OXFORDIAN
HOTNARKO VOLCANICS

muJHv	*Green and maroon dacite and andesite flows; flow-banded rhyolite, crystal-lithic tuffs and volcanic breccias with plagioclase phenocrysts; minor shale and siltstone; can be mistaken for* lKMv

LOWER TO UPPER JURASSIC

ELJg	*Middle to upper amphibolite facies undifferentiated orthogneiss and migmatitic gneisses; black fine-grained amphibolite with stromatic, tonalite leucosomes; could be in part metamorphosed equivalents of* ?TJA *and* LJSP

?TRIASSIC TO LOWER JURASSIC
ATNARKO ASSEMBLAGE

?TJA	*Upper greenschist facies dark green, fine-grained basaltic metavolcanic rocks interlayered with fine-grained metasedimentary rocks, rare interbeds of meta-rhyolite within metavolcanic rocks; strongly foliated and internally folded*

INTRUSIVE ROCKS

LATE CRETACEOUS TO EOCENE

LKEp	*Undifferentiated granitic plutons; hornblende-biotite tonalite to granite; fine-to medium-grained, equigranular*

LATE CRETACEOUS
FOUGNER PLUTONIC SUITE (U/Pb ca. 63-68 Ma)

LKF	*±Pyroxene-hornblende-biotite quartz diorite to granodiorite; medium- to coarse-grained, equigranular to locally inequigranular with potassium feldspar megacrysts, homogeneous; distinct salt-and-pepper fresh appearance with conspicuous sphene*

EARLY CRETACEOUS

EKgd	*(U/Pb ca. 114-103 Ma): Undifferentiated granodiorite to quartz-diorite and tonalite, locally garnet bearing; medium- to coarse-grained, strongly foliated to gneissic textures developed locally*

FIRVALE PLUTONIC SUITE (U/Pb ca. 132-141 Ma)

EKF	*Hornblende-biotite diorite and granodiorite to granite; medium- to coarse-grained; light pink to light green colour from incipient chlorite alteration; strongly foliated to gneissic textures*

LATE JURASSIC
STICK PASS PLUTONIC SUITE (U/Pb ca. 148-156 Ma)

LJSP	*Hornblende-biotite quartz monzodiorite to granite; medium-to coarse-grained, equigranular to inequigranular; abundant epidote veining; mylonitic to gneissic textures developed locally*

SYMBOLS

Geological contact (defined, approximate, assumed)
Fault (defined, approximate, assumed; shaded under Qal and water)
Fault, compressional, defined, approximate, assumed (teeth on upthrust side)
Shear zone (inclined) 35
Fold axis 45
Bedding (tops unknown inclined) 45
Foliation (inclined, vertical) 15
Stretching lineation 42
Lineation (undivided) 13
Dyke (inclined) 45
Fault 45
Field Station location where not indicated by other symbol (foliation, etc.)
Fossil locality with ID number 5
Kr-Ar age determination locality with ID number 4
U-Pb age determination locality with ID number 6
MINFILE occurrence with ID number 4
Park Boundary

GEOCHRONOLOGY

MAP #	FIELD #	AGE (Ma)	MINERAL	METHOD	REFERENCE
1	V90-30-1	112.2 ± 0.6	Zircon	U-Pb	1
2	V90-79	117.1 ± 0.3	Zircon	U-Pb	2
3	V89-72	129.8 ± 0.5	Zircon	U-Pb	1
4	V89-72	99.4 ± 6.2	Biotite	K-Ar	1
5	V89-70	114.9 ± 0.3	Zircon	U-Pb	1
6	V89-42	ca. 132.4	Zircon	U-Pb	1

[1] van der Heyden, P. 2004. Uranium-lead and potassium-argon ages from eastern Bella Coola and adjacent parts of Anahim Lake and Mount Waddington map areas, west-central British Columbia. Geological Survey of Canada, Current Research 2004-A2, 14 pp.
[2] van der Heyden, P. Unpublished data.

MINFILE*

MAP #	MINFILNO	NAME	STATUS	COMMODITY
1	093C 012	TEL	Showing	Molybdenum

* Data from British Columbia Geological Survey Branch MINFILE Mineral Inventory

PALEONTOLOGY*

MAP #	GSC #	FIELD #	COLLECTOR	DATE	FOSSILS	AGE	IDENTIFIER	REPORT #**
1	79739	F-An-100-TD	H.W. Tipper	1957	*Pleuromya* sp. indet.; cf. *Lopha* sp. indet.; *Haidaia*? ex aff. *packardi*; bivalves indet.	Probably Bathonian to Early Oxfordian	J.A. Jeletzky T.P. Poulton	Km-12-1967-JAJ J-9-1990-TTP J-5-1992-TPP
2+	28316	F56-1-TD	H.W. Tipper	1956	hexacorals indet.; trigoniid ? bivalve fragments	Late Triassic?	E.T. Tozer	Tr-10-1956/57-ETT
3+	28317	FTG-27-TD	H.W. Tipper	1956	bivalve fragments; belemnite fragments	Late Triassic?	E.T. Tozer	Tr-10-1956/57-ETT
4	C-156336	HHB-V89-29	P. van der Heyden	1989	*Gryphaea* (?) sp.; *Pleuromya* sp.; *Myophyorella* sp.aff. *packardi*; *Anditrigonia* sp.aff. *plumasensis*; *Myophorella* sp.; *Astarte* sp.; '*Lucina*' sp.; belemnites(?) indet.; echinoderm fragments	Probably Callovian; perhaps early or Middle Oxfordian	T.P. Poulton	J5-1992-TPP
5	C-156337	HHB-V89-84	P. van der Heyden	1989	corals, indet.; belemnites(?) indet.	Middle or Late Jurassic	T.P. Poulton	J5-1992-TPP

* compiled by J.W. Haggart
** unpublished G.S.C Paleontological Report numbers
+ precise location unknown

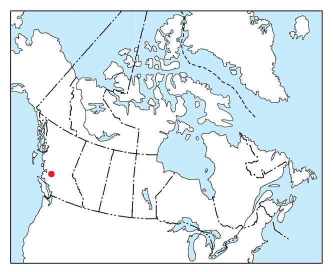

LOCATION MAP

Geology by S. Israel (2001-2002), P. van der Heyden (1989-1991), H.W. Tipper (1954-1957)

Geological compilation by S. Israel

Digital cartography by N.L. Hastings and M. Ceh, Geological Survey of Canada

Contribution of Bella Coola Targeted Geoscience Initiative, Cordilleran Energy and Minerals Project Number Y15

Any revisions or additional geological information known to the user would be welcomed by the Geological Survey of Canada

OPEN FILE 5389

GEOLOGY

ATNARKO (93C/05)

BRITISH COLUMBIA

Scale 1:50 000/Échelle 1/50 000

kilometres 1 0 1 2 3 4 kilomètres

Universal Transverse Mercator Projection
North American Datum 1983

Projection transverse universelle de Mercator
Système de référence géodésique nord-américain, 1983

Digital base map from data compiled by Geomatics Canada modified by Geological Survey of Canada

Mean magnetic declination 2006, 19° 59´ E, decreasing 15.0´ annually. Readings vary from 20° 05´ E in the northwest to 19° 53´ E in the southeast corner of the map

Elevations in feet above mean sea level

Contour interval 100 feet

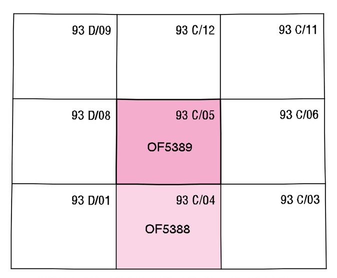

NATIONAL TOPOGRAPHIC SYSTEM REFERENCE AND INDEX TO ADJOINING GEOLOGICAL SURVEY OF CANADA MAPS

OPEN FILE
DOSSIER PUBLIC
5389
GEOLOGICAL SURVEY OF CANADA
COMMISSION GÉOLOGIQUE DU CANADA
2006

Open files are products that have not gone through the GSC formal publication process.

Les dossiers publics sont des produits qui n'ont pas été soumis au processus officiel de publication de la CGC.

Recommended citation:
Israel, S and van der Heyden, P.
2006: Geology, Atnarko (93C/05), British Columbia; Geological Survey of Canada, Open File 5389, scale 1:50 000.

Canada